UNIVERSITY OF READING

Department of Geography & Environmental Science

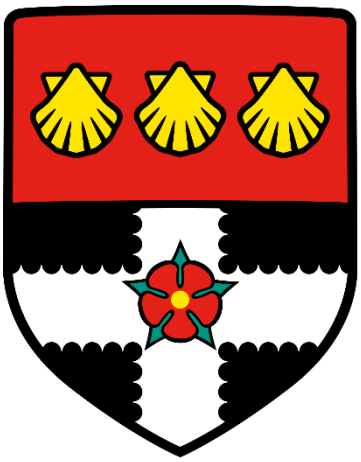

# Climate variability and extended-range flood forecasting for the Amazon basin

Jamie Towner

A thesis submitted for the degree of Doctor of Philosophy

February 2021

# Declaration

I can confirm that this is my own work and the use of all material from other sources has been properly and fully acknowledged.

Jamie Towner

# Abstract

The aim of this research is to investigate how large-scale climate variability affects flooding in the Amazon basin, using this assessment to demonstrate the potential predictability that these modes can provide to enable earlier warning of impactful floods. To address this a multi-stage approach is adopted; first to understand the gaps and confidence in the state of current knowledge on how climate variability affects both rainfall and river discharge in the Amazon basin, secondly, to understand the skill of global hydrological models for undertaking further assessment, and thirdly to undertake a robust assessment of the impact of climate variability on different flood characteristics while considering different methodological approaches in more detail.

An assessment of the robustness in the results of previous studies suggests the need to explore in detail the physical mechanisms leading to flood events on an individual basis. While composite analysis of several floods identified a particular response associated with La Niña conditions, investigation into individual events show it is unknown if the same response would be identified for all events individually. The performance of eight large-scale hydrological models are evaluated for their ability to capture previous peak river flows. The choice of precipitation input is found to be the dominant component of the hydrometeorological modelling chain, with improvement found when ERA5 is the chosen meteorological forcing. Calibration of the Lisflood routing model is identified to have no impact on the ability to capture flood peaks, stressing the need to use an objective function that fits the purpose of the model. Examination of how climate variability impacts flood characteristics in the Amazon basin identified significant changes for both flood magnitude and duration during the negative ENSO phase, particularly in the north-eastern Amazon. This response was not identified for eastern Pacific ENSO events, highlighting how results can differ between ENSO types, while no notable impact or pattern is observed for flood timing.

This thesis has provided important information on how climate variability impacts less studied flood characteristics (flood timing and duration) which are associated with important flood types (e.g. early or long floods). Future work should focus on the improvement of climate reanalysis to produce a longer-term dataset consistent with observations to extend climate analysis. This would allow the examination on the impact of climate phases at a more granular scale (e.g. analysing the strength or combination of climate phases).

# Acknowledgments

A great deal of thanks goes to my supervisors, Liz Stephens, and Hannah Cloke. Their support, advice, and encouragement throughout my PhD has been first class and they have allowed me to take on countless opportunities to which I am very grateful. Further thanks go to my external supervisors Juan Bazo and Erin Coughlan de Perez who have provided useful advice throughout the project and were particularly helpful during my eventful trip to Peru! Additionally, a great deal of gratitude goes towards Andrea Ficchí who always made himself available to speak through various methods and results and provided useful advice in our collaboration on a research article.

Specific thanks also go to Ervin Zsoter for continuously extracting datasets to which this thesis would not have been possible without. I would also like to extend my gratitude to friends and colleagues in the Water@Reading research group and in the Environmental Forecast team at ECMWF, for making me feel welcome and providing continuous support and advice over the five years. Thanks also goes to Andrew Wade, for overseeing the progress of my PhD and ensuring that I was always heading in the right direction and to my examiners Mark Trigg and Anne Verhoef for an enjoyable and interesting discussion during my viva.

I would also like to acknowledge William Santini and Waldo Lavado Casimiro who provided expert advice on Amazon hydrometeorology and for their efforts on our research collaborations.

I am incredible grateful to my wonderful family for whom have supported, encouraged, and persisted throughout my academic journey.

Finally, a huge thanks goes to my incredible other half, Gemma, who has been so supportive, making what is one of the hardest times the most pleasurable. The consistent supply of baked goods really was the icing on the cake (pun intended).

# Contents

# Chapter 1

# Introduction

## 1.1 Motivation

Flooding is a fundamental part of life for those living within the Amazon basin, where communities have long adapted to live with the annual rise and fall of the Amazon River. However, recent population growth combined with inadequate urban planning has resulted in increased risk to vulnerable communities living within the main Amazon floodplain (Davidson et al., 2012; Filizola et al., 2014). Flood risk can be considered as a combination of the probability of a flood occurring and the consequences (i.e. impacts) of its occurrence to areas exposed. Since 1990, there has been a hypothesised intensification of the hydrological cycle, in which the Amazon has become substantially wetter, with an increase in the frequency and severity of flood events (Gloor et al., 2013). This has been supported in recent years with severe high-water levels observed in 2009, 2012, 2014 and 2015 in several regions across the basin (Marengo and Espinoza, 2016). These events have had devastating impacts on local communities, consistently resulting in the displacement of populations, but also affecting the health and wellbeing of individuals more broadly through a deficit of safe drinking water and sanitation (Costa and Brondizio, 2011; Mansur et al., 2018).

Flood preparedness and monitoring is one effective way to mitigate risk (Alfieri et al., 2018), with the implementation of Early Warning Systems (EWS), based on hydrometeorological forecasts becoming increasing popular for various sectors (e.g. humanitarian, agriculture, transportation) on the global scale (Emerton et al., 2016). An EWS is a procedure which utilises climate forecasts and observations to predict and provide early warning information of natural hazards before they materialise, allowing the implementation of humanitarian actions (e.g. distribution of water purification tablets and medical supplies) before rather than after an event having occurred (Coughlan de Perez et al., 2015). Early warnings are often disseminated from disaster managers and teams from organisations such as the Red Cross Climate Centre based on scientific advice and information on the ground and can characterise risk throughout several timescales from hours to years ahead of hazards occurring (Coughlan de Perez et al., 2014). This means the actions can vary from the very short term (e.g. evacuation) to the very long term (e.g. building drainage channels to prevent long term flooding).

Suitable forecasts of flood hazard have only been made possible in recent years due to the progressive development of Numerical Weather Predictions (NWP), which has benefited from the expansion of satellite data and assimilation techniques (English et al., 2013), increased computing power (~increases of one order of magnitude every 5 years since 1980; Bauer et al., 2015), advancements in numerical modelling techniques (Yamazaki et al., 2011), incorporation of ensemble modelling (Cloke and Pappenberger, 2009), improvements in precipitation datasets (Novak et al., 2013), and further efforts for collaborative flood risk research through the Global Flood Partnership (GFP; see De Groeve et al., 2015).

A common problem for many EWS however is that the length and accuracy of lead-times that these models can provide may not be sufficient in certain locations. The timescales needed for some humanitarian actions can be long (e.g. weeks to months ahead to reinforce houses) and are currently beyond the capabilities of many flood forecasting systems. However, it is assumed that accurate seasonal forecasts (i.e. months ahead) of hydrometeorology may be feasible in many locations of the world, with slowly varying components of the climate system (e.g. SSTs, soil moisture and sea ice) influencing hydrological forecast skill and possibly impacting peak river flow characteristics (e.g. the timing, duration and magnitude of flows) (Palmer, 1993; Barnston, 1994; Schöngart and Junk, 2007).

Slowly varying climate variables such as SSTs can be described as climatic drivers or modes of climate variability whereby a climatic variable deviates around a long-term mean resulting in changes to hydrometeorological variables (e.g. rainfall and streamflow) and the likelihood of natural hazards occurring. In the Amazon for instance, extreme flooding (droughts) has been associated with colder (warmer) than usual SSTs in the tropical Pacific region (Espinoza et al., 2013; Ronchail et al., 2005b; Marengo and Espinoza, 2016). This is owing to variations of SSTs changing the location and magnitude of convective activity which in turn modifies the atmospheric circulation (e.g. Walker circulation; Barichivich et al., 2018) and thus patterns of rainfall.

Whilst the magnitude of river flows/water levels in the Amazon basin are often linked with climate anomalies (Ronchail et al., 2005b; Espinoza et al., 2009a), studies examining the relationship with the timing and duration of river discharge are less common. This is despite the length of the wet season and timing of peak river flows in coinciding tributaries playing a major role in the dampening or super positioning of the travelling Amazon flood wave

(Tomasella et al., 2010), and having been previously associated with extreme flood events (e.g. 2009 in the Brazilian Amazon; Marengo et al., 2012).

Additionally, although previous extreme flood events have been attributed to particular climate modes of variability, the usefulness of this information within a flood prediction capacity is still limited and the mechanisms in the build up to these events are not fully understood. For instance, cooler than usual SSTs in the equatorial Pacific Ocean have been identified to provide the atmospheric conditions that maintains a strong humidity flux over the basin and consequently produces increased rainfall and flooding (Espinoza et al., 2013). However, it is not understood, if a particular magnitude of SST anomaly is required or how the spatial extent of SST anomalies would impact the atmospheric response.

Throughout the scientific literature an array of terminology is used interchangeably when describing flooding from a particular magnitude of river discharge to overbank flow and levels of inundation. Though all are suitable terminologies, it is important that they are used within the correct context. For instance, when evaluating floods in terms of risk to an area, flood inundation maps related to particular return periods of river discharge would provide more valuable information and would be a better description of flooding to disaster response teams and communities. A similar case would be for those interested in urban development where project managers and engineers would be interested in understanding what exact areas would be exposed to a particular magnitude of flooding. While in this thesis, more indirect indicators of flood hazard, such as river discharge and water levels are used to evaluate the relationship of these variables to climate variability. Though, maps of flood inundation are available to be used in climate-related analysis, river discharge is more widely available across the Amazon Basin with records going back longer in time.

## 1.2 Aim and Objectives

The aim of this research is to investigate how different modes of large-scale climate variability (e.g. the El Niño Southern Oscillation; ENSO) affects flooding in the Amazon basin and to demonstrate the potential predictability that these modes can provide to enable earlier warning of impactful floods. The work undertaken is in close collaboration with the Red Cross Red Crescent Climate Centre, SENAMHI, and Cruz Roja Purana to ensure the relevance and usefulness of the results.

To achieve the aforementioned aim, this thesis will address the following research objectives:

1. To provide an up-to-date depiction on what we currently know and do not know about how large-scale variability influences precipitation and river discharge regimes in the Amazon basin, and thus flooding.
2. To determine whether river flow simulations from global or large-scale hydrological models are sufficient for linking large-scale climate patterns and teleconnections to anomalously high river flows.
3. To investigate whether warm or cold phases of different hydroclimatic drivers significantly alter the characteristics of river flows throughout the Amazon basin (e.g. the magnitude, timing, and duration of river flows) relative to neutral conditions.
4. To discuss whether statistical methods provide sufficient information to support extended-range forecasting in the Amazon Basin, and what could potentially be offered by methods that address the physical mechanisms.

The results of this thesis will provide evidence on the usefulness of large-scale hydroclimatic drivers (e.g. ENSO) for extended flood predictability (i.e. seasonal) in the Amazon basin. This information has the potential to help inform stakeholders within a range of sectors from humanitarian aid workers to agricultural businesses.

## 1.3 Structure of thesis

The thesis is structured around a review article, two research papers, and a reflections chapter.

**Chapter 2** is the first paper presented in this thesis and provides an in-depth review of several hydroclimatic drivers and their influence on rainfall and river discharge regimes independently. The links between variations in climate patterns and flooding in the Amazon is assessed for 34 previous flood events since 1953, based on previous studies. Conclusions provide five key areas in which to focus research efforts to better understand how climate variability impacts flood risk in the Amazon basin. These areas form the motivation for the rest of this thesis.

**Chapter 3** is the second paper and addresses the second objective of this thesis. Chapter 3 assesses the performance of eight Global Hydrological Models (GHMs) in their ability to capture annual maximum river flows in the Amazon basin. Results provide an indication of the usefulness of data provided by global or large-scale hydrological models for hydrological and climate research purposes.

**Chapter 4** sets out to answer the third objective of this thesis and presents the third paper. Chapter 4 investigates how SST anomalies for several well-established climate indices (e.g. El Niño 3.4) impact flood characteristics in the Amazon basin. Positive and negative phases for each index are compared against neutral conditions to provide an evaluation of how SST anomalies can alter the timing, magnitude, and duration of peak river flows and thus their potential usefulness for extended flood predictability (e.g. by knowing whether or not La Niña conditions can result in earlier flood peaks and/or longer higher water periods).

**Chapter 5** compares the value of statistical, physically based mechanisms and machine learning approaches for accurate flood prediction. This chapter arises based on discussions between the reviewers and authors of chapter 4.

**Chapter 6** summarises the key findings, scientific advancements, and the wider scope of this thesis, in addition to exploring avenues for future work.

The three papers presented in this thesis have been reformatted as chapters and have not been modified in any way. The published versions of Chapters 2, and 3 are provided in the Appendix. At the time of submission, Chapter 4 was still in the reviewing stages of publication, but the online discussion paper and reviewer comments can be found in the Appendix. Statements of author contributions are given at the start of each of the relevant chapters.

# Chapter 2

# The attribution of Amazon floods to modes of climate variability: A review

Shortly after beginning the PhD program it quickly became apparent the breadth of knowledge needed to understand how climate variability affects flooding across the world's largest hydrological basin. From the climate patterns and atmospheric circulation to the hydrological mechanisms controlling the connecting flood waves. Thus, the first question raised was simply, what do we currently know and do not know about how large-scale climate variability affects flooding in the Amazon basin.

This paper has been published as a review paper in Wiley, the journal of Meteorological Applications, with the following reference:

Towner, J., Cloke, H. L., Lavado, W., Santini, W., Bazo, J., Coughlan de Perez, E., and Stephens, E. M.: Attribution of Amazon floods to modes of climate variability: A review. Meteorol. Appl., *27*, e1949, https://doi.org/10.1002/met.1949, 2020.



The contributions of the authors of this paper are as follows: J.T conducted the literature review, undertook the small analysis, and wrote the paper, with guidance from E.M.S, H.L.C, W.L, W.S, J.B, and E.C.P. W.S also provided river discharge data for the analysis. All authors commented on the manuscript. Overall, 80% of the writing was undertaken by J.T.

**Abstract.** Anomalous conditions in the oceans and atmosphere have the potential to be used to enhance the predictability of flood events, enabling earlier warnings to reduce risk. In the Amazon basin, extreme flooding is consistently attributed to warmer or cooler conditions in the tropical Pacific and Atlantic oceans, with some evidence linking floods to other hydroclimatic drivers such as the Madden–Julian Oscillation (MJO). This review evaluates the impact of several hydroclimatic drivers on rainfall and river discharge regimes independently, aggregating all the information of previous studies to provide an up-to-date depiction of what we currently know and do not know about how variations in climate impact flooding in the

Amazon. Additionally, 34 major flood events that have occurred since 1950 in the Amazon and their attribution to climate anomalies are documented and evaluated. This review finds that despite common agreement within the literature describing the relationship between phases of climate indices and hydrometeorological variables, results linking climate anomalies and flood hazard are often limited to correlation rather than to causation, while the understanding of their usefulness for flood forecasting is weak. There is a need to understand better the ocean–atmosphere response mechanisms that led to previous flood events. In particular, examining the oceanic and atmospheric conditions preceding individual hydrological extremes, as opposed to composite analysis, could provide insightful information into the magnitude and spatial distribution of anomalous sea surface temperatures required to produce extreme floods. Importantly, such an analysis could provide meaningful thresholds on which to base seasonal flood forecasts.

## 2.1 Introduction

River records highlight that, on average, the Amazon typically experiences an extreme hydrological event (i.e. flood or drought) once per decade (Marengo et al., 2011). Yet, since approximately 1990, the flood risk to communities living within the Amazon floodplain is thought to have increased due to a combination of population growth, rapid urban expansion, hydrometeorological change and a possible strengthening of the hydrological cycle (Davidson et al., 2012; Gloor et al., 2013; Filizola et al., 2014; Nobre et al., 2016). Record-breaking floods (e.g. in 2009, 2012, 2014 and 2015) and two “once in a century” droughts recorded in 2005 and 2010 (Marengo and Espinoza, 2016) have demonstrated the significant impact that these events can have on both human and natural systems (Espinoza et al., 2013; Marengo et al., 2013b). The 2012 floods alone affected a reported 202,676 people in Loreto, Peru, with large losses of cropland (about 2,000 ha), an example of the damage inflicted upon livelihoods (IRFC, 2012).

### 2.1.1 Limits and sources of predictability

To provide early flood warnings and consequently reduce risk, the probability of exceeding flood warning thresholds, based on estimates of river discharge produced from global hydrological models (GHMs), can be used (Alfieri et al., 2018). For example, in the Peruvian Amazon, Forecast-based-Financing (FbF), an initiative of the German Red Cross, is being implemented by disaster managers in order to take early action (FbF, 2019). The FbF is a

protocol that uses automatic trigger actions (e.g. the delivery of mosquito nets and first-aid kits when a particular magnitude of river discharge is reached) based on probabilistic hydrometeorological forecasts, whereby actions are taken before a flood in order to reduce flood risk (Coughlan de Perez et al., 2015). Currently, the available lead time for skilful forecasts (both weather and hydrological) leaves little time in which to act, particularly when many humanitarian actions require long timescales, such as several weeks ahead to reinforce and modify houses to make them more flood resilient. The ability to predict floods weeks in advance is mainly determined by how the uncertainties in the initial state of the atmosphere and oceans evolve over time (Palmer, 1996). Due to the chaotic nature of the atmosphere, precipitation forecasts that many hydrological models rely upon are typically restricted to lead times up to 15 days ahead (Cloke and Pappenberger, 2009). To overcome this many operational flood forecasting systems (e.g. the Global Flood Awareness System; Alfieri et al., 2013), which provide hydrological forecasts within the Amazon basin, now use ensemble numerical weather predictions (NWPs), commonly referred to as an ensemble prediction system (EPS). Here, the uncertainties in the initial conditions of the deterministic meteorological forecast are represented by perturbing them to produce a range of initial states (commonly between 10 and 51; Emerton et al., 2016). The EPS is then used as an input into a hydrological model to produce a range of river discharge predictions, which are equally probable. Such models typically produce sub-seasonal forecasts (usually up to 30 days ahead). Monthly and seasonal hydrological forecasts can be achieved in some regions, with several factors influencing the likelihood of a particular atmospheric behaviour occurring (e.g. increased or decreased zonal trade wind speeds). Such factors include anomalous sea surface temperatures (SSTs) (Palmer, 1993; Barnston et al., 1994), vegetation effects (e.g. biotic pump hypothesis; Makarieva and Gorshkov, 2007), land surface anomalies such as soil moisture, surface and groundwater states (Paiva et al., 2012), stratospheric variability (Sigmond et al., 2013), sea-ice and major volcanic events (Robock, 2000).

### 2.1.2 Intensification of the hydrological cycle

When analysing floods, it is important to consider that their frequency and attribution could be related to both the long-term climate signal (e.g. decadal to multi-decadal patterns) and to short-term climate variability (e.g. interannual and intra-seasonal patterns). The reported intensification of the hydrological cycle in the Amazon basin with a tendency towards extreme flooding has been associated with a coinciding increasing decadal trend in SSTs in the tropical Atlantic Ocean (+0.7°C between 1990 and 2010; Gloor et al., 2013). Precipitation and

consequently river discharge have been found to increase, particularly during the wet season, driving greater difference between peak and minimum flows. Although trends are more dominant in certain regions (e.g. north-western Amazonia), this intensification is considered for the average trend throughout the entire Amazon, with a greater diversity found in trends of discharge across sub-basins and a large variability is acknowledged in spatial extremes. For example, drying trends are acknowledged in the southern Amazon basin (Espinoza et al., 2009a), with a significant increase in dry day frequency (days with < 1 mm of rainfall; Espinoza et al., 2019). This recent shift in discharge extremes since approximately 1990 is expected to continue in the long term under further atmospheric warming, based on the latest climate projections (Hirabayashi et al., 2013; Langerwisch et al., 2013; Sorribas et al., 2016; Zulkafli et al., 2016; Alfieri et al., 2017). It is important to consider that any trends and shifts in extremes could be associated with multidecadal natural variability and that projections of future extremes can vary enormously based on different greenhouse gas scenarios, levels of deforestation and other land-use changes, insufficient knowledge on initial and boundary conditions, and model deficiencies in relevant physical processes (Gloor et al., 2013; Torres and Marengo, 2013; Marengo et al., 2018).

### 2.1.3 Hydroclimatic drivers

Climatic or hydroclimatic drivers can be defined as modes of large-scale climate variability around a long-term trend that has the potential to drive spatial and temporal changes in hydrometeorological variables (i.e. precipitation and river discharge; Nobre et al., 2017). To explore such drivers, we first identify using the scientific literature those responsible for impacting atmospheric circulation, moisture transport and thus hydrometeorological variables in and around South America (Table 1). For the Amazon, increased rainfall and river discharge are consistently attributed to lower and upper atmospheric circulation anomalies as a consequence of anomalous SST conditions in the tropical Atlantic and Pacific oceans (Richey et al., 1989; Yoon and Zeng, 2010; Davidson et al., 2012; Marengo and Espinoza, 2016). Other, less studied, climate drivers have also been related to flooding in the Amazon (e.g. the Madden–Julian Oscillation—MJO; Shimizu et al., 2017), with climate variations operating at lower frequencies (e.g. Pacific Decadal Oscillation—PDO; and Atlantic Multidecadal Oscillation—AMO; Barichivich et al., 2018) also linked to wetter and drier conditions. An overview of each driver and their mechanisms are provided in Table 1. Here, general definitions are provided, with their influence on the spatial pattern of Amazon rainfall and river discharge discussed in Section 2.4.

**Table 1.** Hydroclimatic drivers of Amazon flooding, their description, mechanisms, and key authors.

| Hydroclimatic Driver | Abbreviation | Description | Timescale | Mechanism | Author(s) |
|---|---|---|---|---|---|
| **El Niño Southern Oscillation** | ENSO | Set of indices measuring the interannual variability of SSTs in the equatorial Pacific Ocean (5N-5S, 170W-120W), with oscillating phases of warmer or cooler than usual conditions generated by coupled atmosphere and oceanic interactions. Anonymously warm or cold SSTs are termed El Niño and La Niña events respectively. | Interannual | During El Niño the lower equatorial easterly trade winds and surface zonal currents become weaker owing to surface air pressure over the tropical western Pacific becoming higher than in the tropical eastern Pacific relative to mean conditions. Consequently, the upwelling of cold water in the eastern Pacific is reduced, leading to a deeper thermocline and a shift of warmer SSTs into the eastern and central tropical Pacific. As a result, the Pacific Walker circulation, and hence convective rainfall also shifts eastwards, impacting rainfall and discharge patterns in the surrounding continents (Yeh et al., 2018).<br><br>During La Niña, the easterly trade winds are enhanced, leading to increased upwelling of cold Pacific waters off the coast of Peru and colder than usual SSTs in the eastern and central tropical Pacific. Rainfall patterns are consequently displaced further west compared to neutral conditions. | Bjerknes (1969); Trenberth (1997); Trenberth et al. (2001) |
| **Tropical North Atlantic** | TNA | Patterns of average SST variability in the TNA ($5.5^0$ N to $23.5^0$ N and $15^0$ W to $57.5^0$ W). Couples with the variability in the TSA, influencing the | Interannual | When the TNA is abnormally warmer (cooler) than usual, the Inter Tropical Convergence Zone (ITCZ) is found to migrate anomalously north (south), bringing changes to low-level atmospheric circulation and spatial rainfall patterns. These patterns are associated with a weakening (intensification) of the north-eastern trade winds and moisture flux from the | Enfield (1996); Enfield et al. (1999) |

| | | | | | |
|---|---|---|---|---|---|
| | | migration pattern of the ITCZ. | | Atlantic basin (Enfield 1996; Nobre and Shukla, 1996; Panisset et al., 2018). | |
| **Tropical South Atlantic** | TSA | Patterns of averaged SST variability in the TSA (Eq to $20^0$ S and $10^0$ E to $30^0$ W). Couples with the variability in the TNA, influencing the migration pattern of the ITCZ. | Interannual | When the TSA is warmer (cooler) than usual, the ITCZ shifts further south (north), weakening (strengthening) the south-east trade winds (Utida et al., 2019). Consequently, this changes the location of maximum tropical convection and precipitation, influencing upper and lower flows. The ITCZ commonly reaches its most southernmost position during austral autumn (MAM), when TSA SSTs are at their highest. In contrast, coolest temperatures and a northern migration of the ITCZ are common during austral winter (JJA). | Enfield (1996); Enfield et al. (1999) |
| **Madden-Julian Oscillation** | MJO | The dominant component of the intraseasonal (30–60 days) variability in the tropical atmosphere. The MJO is a moving pattern, propagating eastward through the atmosphere above warm portions of the Indian and Pacific oceans. | Intraseasonal (~30-60 days) | The MJO consists of simultaneous convective and supressed rainfall phases which operate in a dipole structure. The locations of convection are often grouped into eight stages, based on the geographical location (see Figure 1 in Pohl & Matthews, 2007). Events of MJO force a thermodynamic response in the upper layers of the ocean. When active the MJO modifies extratropical circulation via a Rossby wave response to latent heat release, related to tropical convection (Matthews et al., 2004). An enhanced (supressed) convective phase leads to a reduction (increase) in latent heat fluxes and thus cooling (warming) of SSTs, prompting an eastward propagation (see Webber et al., 2010). In regions of anomalously warm SSTs, there is increased large-scale ascent and upper tropospheric divergence. In contrast, in locations which lack convective activity, increased descent and upper-tropospheric convergent inflow is witnessed (Matthews et al., 2004). | Madden and Julian (1971, 1972); Madden and Julian (1994); Zhang (2005) |

| | | | | | |
|---|---|---|---|---|---|
| **Pacific Decadal Oscillation** | PDO | Empirical Orthogonal Function (EOF) of monthly anomalies of SST in the north Pacific Ocean, poleward of $20^0$ N. | Decadal (~16-20 & 50-70 years) | The physical mechanisms driving the PDO and its variability remain unclear (Mantua and Hare, 2002; Geng et al., 2019). Possible explanations argue that oceanic Rossby waves driven by atmospheric forcing are pivotal in maintaining and setting the timescale of PDO variability (Geng et al., 2019). While Newman et al. (2016) describe the mechanisms of PDO as a set of atmospheric-oceanic processes rather than a single mode of climate variability, meaning PDO impacts stated in the literature may instead represent correlation to processes driving variations in both the PDO and impact variables. The impact of PDO variability on hydrometeorological variables, is locally specific, generally producing similar responses to ENSO (e.g. warm PDO impacts are similar to the response to El Niño conditions). | Mantua et al. (1997); Zhang (1997) |
| **Atlantic Multidecadal Oscillation** | AMO | Oscillation of SSTs in the North Atlantic Ocean, typically within a $0.4^0$ C range. | Multidecadal (~50-70 years) | Similarly, to the PDO, owing to the relatively short observational record and timescale at which the driver operates, the mechanisms and variability of the AMO are still debated (Wills et al., 2019). Previous studies have shown the AMO to be related to heat transport by the Atlantic Meridional Overturning Circulation (AMOC; Zhang and Wang, 2013), to the variability of aerosol forcing on surface shortwave radiation (Booth et al., 2012) and due to low frequency forcing of SSTs, driven by ocean circulation variability (O'Reilly et al., 2016). In the positive (negative) phase, SSTs are warmer (cooler) in the North Atlantic, whilst being cooler (warmer) in the equatorial Atlantic (Martin-Rey et al., 2018). Consequently, the mean oceanic and atmospheric state has been found to be significantly different between positive and negative periods (Jones and Carvalho, 2018). | Kerr (2000) |

### 2.1.4 Attribution

Attribution studies attempt to understand to what extent can certain factors (e.g. land cover change, SST anomalies) explain changes in certain variables (e.g. streamflow) or the likelihood or indeed the strength of hydrometeorological events taking place. Attribution encompasses a range of different kinds of studies (e.g. the influence of land-cover changes on streamflow, Slater and Villarini, 2017; urbanisation influence on flooding intensity, Zhang et al., 2018), though two types are particularly common for extreme event attribution. The first type attempts to establish an association between an event and climatological patterns (e.g. floods caused by El Niño). The second type assesses the role of human-induced activities and climate change (e.g. through increased greenhouse gas emissions) on a particular event (Trenberth et al., 2015). In this review we focus on the former. To relate an event to a specific climate pattern, common methods vary from basic correlation analysis, partially linking events and climatic drivers, to the use of climate models and ensemble forecasts to predict the response of the climate to different atmospheric and oceanic forcings (Coumou and Rahmstorf, 2012).

### 2.1.5 From sources of predictability to early warning

Many studies have identified the impacts that different sources of predictability (e.g. SST anomalies) can have on hydrometeorological variables in the Amazon (e.g. Richey et al., 1989; Ronchail et al., 2002; Yoon, 2016; Sulca et al., 2018). Fewer studies, however, demonstrate how knowledge about these relationships can translate into improved flood prediction and risk reduction using early warning systems (EWS). An EWS is a protocol that uses information of potential upcoming natural hazards (e.g. floods), from climate models forced by seasonal forecasts of the SST and other sources of predictability. Such information is then used to help inform decision-making (e.g. whether to distribute water purification tablets or evacuate a particular community) in an attempt to reduce risk before an event taking place (Coughlan de Perez et al., 2015). The EWS combine several disciplines and can generally be described as a chain consisting of four main categories: (1) risk knowledge, (2) monitoring, forecasting and warning, (3) communication of early warning and (4) response capability (Cools et al., 2016). Though many challenges remain to achieve the full benefits of an EWS, particularly with regards to categories 3 and 4 and understanding the feedbacks and interactions between the physical and social systems (Lopez et al., 2017), the evidence required for the forecasting

component of the chain remains essential for effective alerts and the communication of early risk information.

Currently, the available evidence demonstrating the potential usefulness of the SST anomalies as predictors for forecasting flood variables in the Amazon comes mainly from statistical modelling, with simulations forced using SST data. For instance, Schöngart and Junk (2007) developed a retrospective forecast model that showed that water levels in central Amazonia were an integrator of Pacific SSTs, with forecasts of water levels achievable up to four months in advance when modelled results were compared with observations for the period 1903–2004. Other studies include the use of a series of statistical models forced by lagged spatial averages of central and tropical North Atlantic SSTs to explain variability in terrestrial water storage anomalies (De Linage, Famiglietti, & Randerson, 2014) and a statistical model that showed that northern (southern) sub-basins in the Amazon basin are better forecasted when using Pacific (Atlantic) SSTs (Uvo and Graham, 1998).

### 2.1.6 Objective and framework

Having first identified the main hydroclimatic drivers that influence the atmospheric circulation and moisture transport in and around South America (Table 1), the objective of this review is to draw together knowledge of the current understanding of how each driver impacts the characteristics of rainfall and river discharge regimes and their links to extreme flooding in the Amazon basin. Due to the non-linearity between rainfall and river discharge (Stephens et al., 2015), and significant differences previously identified between the mean states of the two variables in response to phases of climatic indices (Dettinger and Diaz, 2000), it is important to consider the effect of large-scale climate variability for each independently. Therefore, the framework of this review is structured based on the discussion of how hydroclimatic drivers influence rainfall variability, river discharge variability and the relationship between previous extreme flood occurrences and different climate phases; thereby scoping out the potential for earlier flood warning in the Amazon basin.

## 2.2 Methods and data

Using the published literature, the impact of the SST anomalies from different ocean basins on rainfall and river discharge regimes are evaluated across different regions of the Amazon basin. The evaluation is broken down for rainfall and discharge independently and consists of

combining the results from previous studies to provide an up-to-date depiction of the current knowledge in the form of composite maps (in Section 2.4).

To evaluate the relationship between climate phases and extreme flood events, we have constructed a table of major floods as sourced from the scientific literature, humanitarian reports and flood databases (i.e. the Dartmouth Flood Observatory) throughout the Brazilian, Bolivian and Peruvian Amazon since 1950 (Table 2) (see Section 2.5). While reports of flooding in the Amazon basin date to the mid-19th century (e.g. 1859; Le Cointe, 1935), earlier records are often assembled from qualitative data such as newspapers, humanitarian records and verbal information from communities (Sutcliffe, 1987). In addition, the reliability and quantity of pressure and SST observations are considered questionable before 1950 (Bunge and Clarke, 2009), and thus we only consider events that have occurred after this period.

Table 2 extends the work of Marengo and Espinoza (2016) to include areas of the Bolivian Amazon, further flooding in the Peruvian and Brazilian Amazon, and an indication of how strong are the links between floods and climate anomalies. The strength of evidence is evaluated as either very low, low, medium or high and considers the magnitude of the SST anomalies, peak river flows, the timing and duration of flood events, how each flood is classified by the authors (e.g. events could be determined by a specific streamflow exceedance), and by the type of analysis performed (e.g. correlation or composite analysis).

A very low rating may be given when observed SST anomalies disagree with the phase of climate variability attributed (e.g. observed positive SST anomalies in the Pacific with a La Niña attribution). A low to medium rating is when SST anomalies are in agreement, but where no atmospheric analysis (e.g. atmospheric response to abnormal SST anomalies) has been performed. Finally, a high rating is when SSTs are highly abnormal, the level of flooding is highly anomalous and the atmospheric response during the event has been inspected for that given year. We consider all major flood events as determined by the reference(s). The stated climate driver for each event and type of analysis performed is obtained from the authors highlighted in bold in Table 2.

### 2.2.1 River discharge data

Peak river flows for floods are obtained from the time series of seven hydrological gauges provided by the national meteorological and hydrological services of the respective countries situated in the Amazon basin and from the Institute of Research for Development (IRD). These include: the Agência Nacional de Águas (Water National Office—ANA, Brazil) and the Servicio

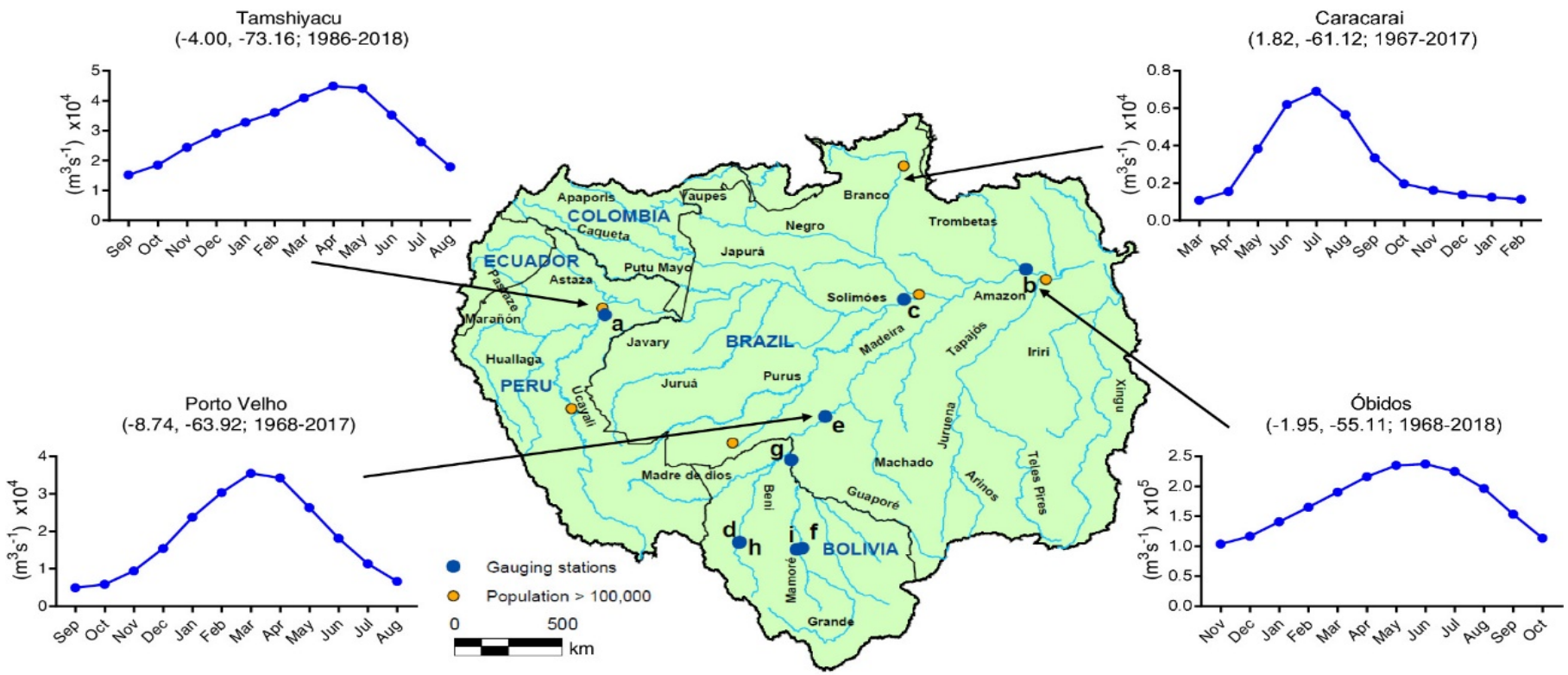


**Figure 1.** *River network and hydrographs at key gauging stations within the Amazon basin. Hydrographs show observed mean monthly river flows. The hydrological years for each hydrograph start from the lowest monthly discharge and thus differ depending on the specific station. Letters correspond to the gauging stations used for the classifications of flood events in Table 2 (Section 2.5) and are referred to throughout the main text. City population data are sourced from Esri (https://hub.arcgis.com/).*

Nacional de Meteorología e Hidrología (National Meteorology and Hydrology Service—SENAMHI, Peru and Bolivia). Data are sourced through the SO-HYBAM observational service (see https://hybam.obs-mip.fr/). The locations of stations are displayed in Figure 1, with letters corresponding to each station highlighted throughout the main text to allow for easier interpretation and navigation. The Puerto Varador (f) and Puerto Almacen gauging stations (i) are no longer operational with previous data suffering from uncertainty due to the backwater effect (Meade et al., 1991). Therefore, we have excluded discharge information for these stations in Table 2.

### 2.2.2 SST data

Equatorial Pacific SST data are provided by the National Oceanic and Atmospheric Administration's (NOAA) Climate Prediction Centre (CPC), using the monthly ERSSTv5 (centred base periods) Niño 3.4 (5° N–5° S, 170–120° W) data set, which is used as input to the Oceanic Niño Index (ONI). Atlantic SSTs are provided by the Tropical North (5.5–23.5° N and 15–57.5° W) and South (Equator–20° S and 10° E–30° W) Atlantic indices (climatology is 1971–2000; Enfield et al., 1999).

The latest version of the Multivariate El Niño Southern Oscillation index (MEI v2), based on five variables (sea level pressure (SLP), SST, surface zonal winds (U), surface meridional winds (V) and outgoing long wave radiation (OLR)) is used to provide an index based on both oceanic and atmospheric conditions from 1979 onwards. It builds on the original MEI index (Wolter and Timlin, 1993) using the JRA-55 global reanalysis (Kobayashi et al., 2015). Here, monthly values are based on bimonthly means; for example, August 2018 is calculated from July–August 2018 SST data. In Table 2, MEI values are averaged for three consecutive bimonthly readings. For example, for October–December considering a flood event in 2012, the average is taken from bimonthly values in September–October, October–November and November–December 2011.

The monthly PDO time series, defined as the leading principal component (PC) of monthly anomalies in the North Pacific Ocean, poleward of 20° N (1854–present) is provided by the National Centre for Environmental Information (NCEI). The NCEI PDO index is based on NOAA's extended reconstruction of the SSTs (ERSSTv4). Finally, monthly detrended AMO data are provided by NOAA's ESRL based on the unsmoothed Kaplan SST V2 data set (Enfield et al., 2001). The PDO and AMO data in Table 2 are averaged for the calendar year.

## 2.3 The Amazon basin

The Amazon (Figure 1) is the world's largest river basin, draining an area of approximately 6 million $km^2$. Its river network consists of over 1,000 tributaries with the main stem discharging an average of about 209,000 $m^3s^{-1}$ of freshwater into the Atlantic Ocean per annum (Molinier et al., 1996; Callède et al., 2010). The basin extends between 5° N and 20° S, covering seven countries: Brazil (63%), Peru (16%), Bolivia (12%), Colombia (6%), Ecuador (2%), and Venezuela and Guyana (1%) (Espinoza et al., 2009b). In terms of climate, the Amazon basin witnesses a large interannual variability of rainfall with distinct spatial variations (see Laraque et al., 2007 for Ecuador; Ronchail and Gallaire, 2006 for Bolivia; Lavado et al., 2012, 2013, for Peru; Figueroa and Nobre, 1990; Ronchail et al., 2002, and Espinoza et al., 2009b, for the entire Amazon). On average, locations within the Amazon receive around 2,000–2,200 mm of rainfall annually (Marengo and Nobre, 2001), sourced from local evapotranspiration and via water transport provided by the easterly trade winds from the Northern Hemisphere (Salati et al., 1979; Salati and Vose, 1984). A climatic gradient can be identified from the wet northwest to the dry southern and eastern borders, which experiences a long dry season, and where deforestation from tropical forest to pasture and cropland is at its greatest (Davidson et al., 2012).

Owing to the size and location of the basin, both precipitation and discharge regimes differ depending on location. In general, the wet season in the Amazon is from December to April, while its dry period is between June and October (Yoon and Zeng, 2010). More specifically, in the north of the basin, around the Branco catchment (Figure 1), peak rainfall is noted during June–August and is predominately controlled by large-scale convection, modulated by the migration pattern of the intertropical convergence zone (ITCZ) (Ronchail et al., 2002). Rainfall totals are greatest near the mouth of the Amazon River within regions of the Amazon Delta and in the northwest towards the Colombian Amazon (Espinoza et al., 2009b). In these regions, wetter conditions are prevalent between December and May, though less seasonal variability exists in western catchments (Figueroa and Nobre, 1990; Ronchail et al., 2002). Rainfall in the south is heavily influenced by organised convection from the South Atlantic convergence zone (SACZ) and precedes northern regions by approximately six months, peaking in December–February (Ronchail et al., 2002; Tomasella et al., 2011). Consequently, river discharge in northern, southern, and central tributaries also adheres to an asynchronous pattern in peak river flows, providing a dampening effect on the main flood wave travelling down the central Amazon River (Ronchail et al., 2006; Espinoza et al., 2009a). The rainfall–

runoff relationship displays a large lag between peaks in rainfall and peaks in river discharge in large parts of the basin, with river flows showing a stronger response to seasonal rainfall patterns as opposed to single rainfall events (Trigg, 2010). This lag can be related to (1) the size and length of many Amazonian rivers; (2) floodplain storage and interactions; and (3) rivers generally having a shallow bed and topographical slopes, with relatively slow moving waters (Trigg et al., 2009; Yamazaki et al., 2012), though rivers located in upstream catchments, particularly those of Andean origin, are prone to flash flooding and are highly sensitive to extreme rainfall (Laraque et al., 2009). On average, the highest water levels are found two to three months earlier in the largest southern tributary (Madeira River) than its northern counterpart (Rio Negro) and larger tributaries follow a monomodal pattern (i.e. one annual flood wave) (Ronchail et al., 2006; Espinoza et al., 2009a).

## 2.4 Influence of hydroclimatic drivers

### 2.4.1 Rainfall variability

#### 2.4.1.1 Pacific influence

The SST variability in the Equatorial tropical Pacific (i.e. the El Niño Southern Oscillation—ENSO) is arguably the most well-known mechanism responsible for the interannual and spatial variability of Amazon rainfall (Marengo, 1992; Nobre and Shukla, 1996; Foley et al., 2002; Espinoza et al., 2009b) and indeed worldwide (Cai et al., 2015). Figure 2 summarises the relationship between the two phases of the ENSO and Amazon rainfall based on results identified in previous studies. In general, when El Niño (i.e. the warm phase of the ENSO) conditions are prevalent, a deficit in rainfall is common throughout much of the Amazon Basin, whilst the opposite is true for La Niña events (Ronchail et al., 2002; Yoon and Zeng, 2010) (Figure 2a,d). This is also evident when examining extreme precipitation frequency, whereby Grimm and Tedeschi (2009) note decreased (increased) activity associated with El Niño (La Niña) conditions over the entire Amazon basin relative to neutral conditions in the austral autumn (March–May). By categorising the wet and dry seasons into dry, very dry, wet and very wet years, based on monthly observed rainfall data (1931–1996), Andreoli et al. (2012) showed that dry and very dry rainy seasons are associated with weak and intense El Niño events, respectively. In contrast, very wet rainy and very wet dry seasons are associated with intense La Niña and La Niña conditions.

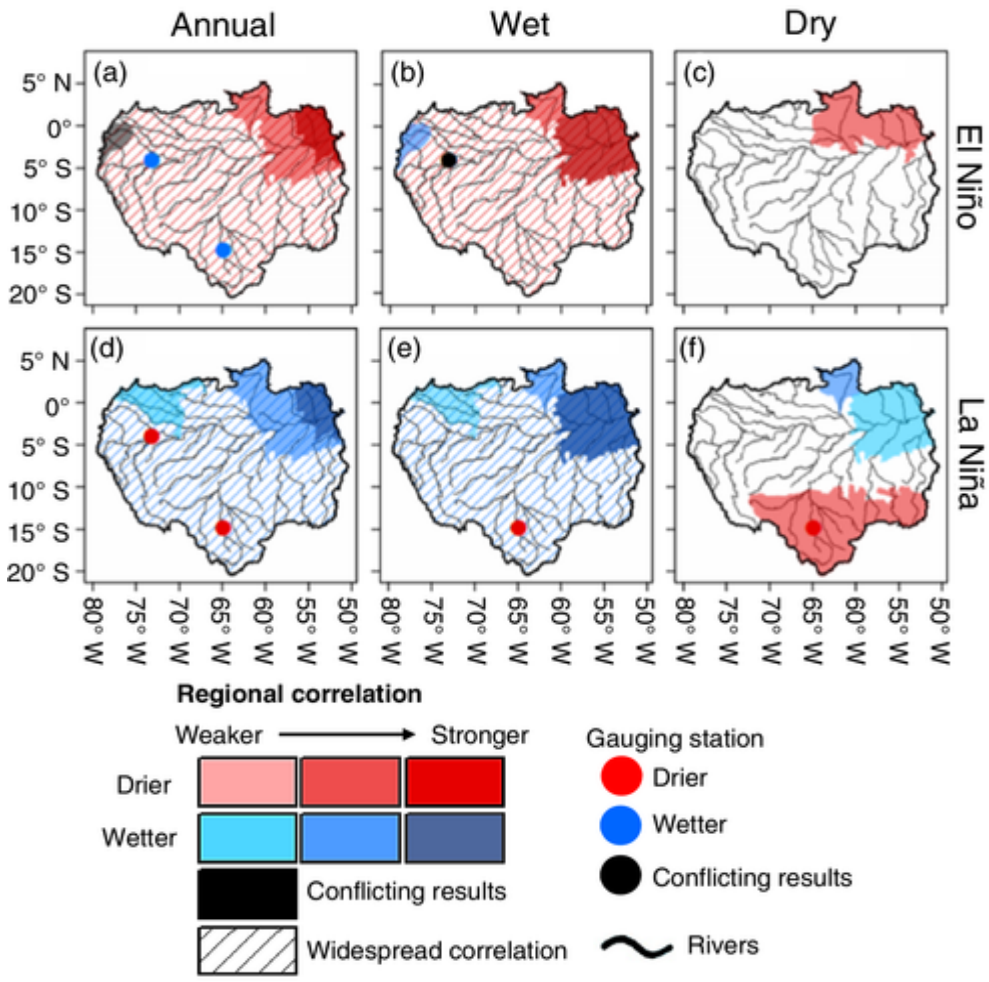


**Figure 2.** *Influence of the El Niño Southern Oscillation (ENSO) on rainfall throughout the Amazon basin, based on results identified within the literature: (a, d) the entire year; (b, e) the Amazon wet season (December–April); and (c, f) the Amazon dry season (June–October). Blue circles and shading indicate wetter than usual conditions; red represents drier conditions; black circles or shading are used where conflicting results are found between different authors; darker shading depicts locations where the correlation is considered stronger; regions in white indicate that no correlation exists or that there is currently no information available. Hatched markings highlight when correlations are widespread throughout the majority of the basin. It is important to highlight where widespread correlation is shown, the correlation is not uniform and can be higher or lower for different regions. For full details of the reference(s), type of analysis used and strength of the relationships, see Tables S1–S6 in the additional supporting information.*

Rainfall anomalies associated with the ENSO are strongest during the austral summer (December–February) and autumn (March–May), aligning with the peak rainy season in South America (Sulca et al., 2018). This is highlighted in Figure 2b,e, where Pacific SST anomalies are

found to have a similar influence on annual and wet season (December–April) rainfall patterns. The influence on the dry season (June–October) is more limited, with impacts mainly observed in northern and eastern areas (Figure 2c,f) when using gauge-based rainfall estimation products (Yoon and Zeng, 2010). Investigations performed solely using precipitation observations show contrasting rainfall anomalies between the northern Branco basin and in the southern Amazon during June–August (Ronchail et al., 2002) (Figure 2f). During La Niña years, drier-than-usual conditions are more common in the southern Amazon, with wetter conditions in the far north. Here, it is worth reiterating that rainfall in the northern Branco basin generally peaks later (June–August) relative to the rest of the Amazon.

In northern and north-eastern catchments of the Brazilian Amazon, the ENSO–rainfall relationship is strong, particularly around the Amazon River towards its mouth on the Atlantic on both annual and seasonal timescales (Liebmann and Marengo, 2001; Ronchail et al., 2002; Zeng et al., 2008; Yoon and Zeng, 2010). A deficit (increase) in rainfall is recorded at the majority of meteorological stations during El Niño (La Niña) events with a reduction in signal towards southern areas (Ronchail et al., 2002; Espinoza et al., 2009b). This signal is also identifiable on the western side of the Colombian Andes and Amazon basin, albeit weaker, where abundant rainfall is associated with La Niña conditions (Poveda and Mesa, 1993; Poveda et al., 2011; Espinoza et al., 2009b) (Figure 2d,e).

For the Peruvian Amazon, particularly areas around Iquitos (a), lower (greater) than usual rainfall is generally associated with El Niño (La Niña) events (Lavado et al., 2013; Sulca et al., 2018). However, correlations at this station are often weak, with certain analysis having identified both a wet and a dry signal during the warm phase of the ENSO (Ronchail et al., 2002; Lagos et al., 2008) (Figure 2b). The association between rainfall and the ENSO in the Ecuadorian Amazon is much less well understood owing to its remoteness. Previous studies have mainly focused on the ENSO connection in coastal and Andean locations of Ecuador (Rossel, 1997), with research most likely limited for the Ecuadorian Amazon owing to its remote location and sparse population (Laraque et al., 2007). Evidence is conflicting between studies with above-normal rainfall identified during phases of El Niño in the Ecuadorian lowlands and on the eastern slope of the Andes for Ronchail et al. (2002), while a deficit in rainfall is acknowledged by Vuille et al. (2000), and no significant effect was identified by Tobar and Wyseure (2018) (Figure 2a). The wet signal identified by Ronchail et al. (2002) is deemed more significant during the wet season (March–May) (Figure 2b).

The relationship can be complex, particularly when investigating the influence of the ENSO at smaller scales in which distinct spatial differences can be identified. For instance, in Bolivia, correlations are often dependent on altitude and topography (Ronchail and Gallaire, 2006). Less rainfall is reported during the peak of the wet season (February) in the lowlands of the central Bolivian Amazon when La Niña conditions prevail (Trinidad station) (Figure 2e). In contrast, on the slopes of the Zongo Valley, in which the Zongo River empties into the Beni River, an Amazon tributary, drier conditions are reported during El Niño events on an annual time scale, with a La Niña/wet signal evident for February (Ronchail and Gallaire, 2006). This is supported by increased sedimentation within the Beni River during La Niña events (Aalto et al., 2003). These findings demonstrate the need to consider the hydrological response to climate anomalies not only at the location of interest but also at locations further upstream owing to increases in river flow in upstream tributaries having the potential to cause flooding further downstream.

Several studies have highlighted the importance of considering the diversity of the ENSO events, with the location and intensity of the SST anomalies in the tropical Pacific found to cause significant differences in rainfall anomalies over South America (Hill et al., 2009; Sulca et al., 2018; Cai et al., 2020). This is a consequence of modifications to the Walker Circulation owing to whether the centre of warming or cooling of the SST anomalies was located in the central or eastern Pacific Ocean (Cai et al., 2020). For instance, Sulca et al. (2018) identified that a warm eastern Pacific ENSO index results in significant dry anomalies over the Peruvian Amazon, along the Peru–Brazil boundary. These signals were deemed insignificant when the extreme 1983 and 1998 El Niño years were removed, while the dry anomalies were still significant after the removal of these years for the central Pacific index. Such results highlight the need to consider both the SST magnitude and location when attempting to understand the relationship between the ENSO phases and the response of rainfall in different regions of the Amazon basin.

#### 2.4.1.2 Atlantic influence

In the early 1990s, Marengo (1992) identified that an increase in rainfall over the Amazon basin was associated with an increase in water vapour fluxes from the Atlantic Ocean. At the time, little attention had been paid to the relationship between the tropical SSTs in the Atlantic and Amazon rainfall. Previous studies mainly focused on the role of Atlantic SSTs in determining rainfall variability over South America, particularly in north-eastern Brazil (Moura

and Shukla, 1981; Nobre and Shukla, 1996). At the turn of the millennium, Liebmann and Marengo (2001) and Ronchail et al. (2002) began to assess the importance of the tropical Atlantic SSTs for the Amazon. However, it was not until after the record-breaking drought event witnessed in 2005 that the tropical Atlantic was considered as a climatic driver, with numerous studies then highlighting the importance of the SST abnormalities in determining the Amazon's water budget (Marengo et al., 2008; Zeng et al., 2008; Yoon and Zeng, 2010). Generally, more (less) rainfall in the Amazon basin is correlated to anomalously cold (warm) SST conditions in the Tropical North Atlantic (TNA), coupled with warm (cold) SST anomalies in the Tropical South Atlantic (TSA) (Yoon, 2016), associated with the north–south migration pattern of the ITCZ (Enfield, 1996). This is supported by Andreoli et al. (2012) who identified that years that are considered to have a drier rainy season are associated with positive (negative) TNA (TSA) SST anomalies. In contrast, a very wet rainy season and wet dry season were associated with the opposite dipole pattern (i.e. a cold TNA and a warm TSA).

Figure 3 provides a summary of how anomalous SSTs in the TNA and TSA affect precipitation variability over the Amazon basin. For the TNA, significant correlations exist over much of the Amazon with a stronger relationship found in the southern Amazon (Zeng et al., 2008; Yoon and Zeng, 2010) (Figure 3a–c). Here, lower than usual precipitation is a persistent response to the warm TNA SST anomalies throughout most of the Amazon basin and is related to a weakening of the northeast trade winds and moisture fluxes towards the basin. This weakening is a result of a northward displacement of the ITCZ, which consequently produces atmospheric subsidence over the Amazon basin (Cox et al., 2008; Marengo et al., 2016). These findings were replicated by Yoon (2016) in an idealised analysis using five atmospheric global climate models (AGCMs). All models were found to simulate drier (wetter) conditions during the dry season in the southern Amazon when SSTs in the north Atlantic were warmer (cooler) than usual. Yoon (2016) highlighted the importance of models accurately representing climatological seasonal rainfall totals in order better simulate the response to anomalous SSTs. Models that simulated too little rainfall during the Amazon dry season tended to underestimate the response to changes to the Atlantic SSTs. When focusing on two of the strongest warm TNA events (2005 and 2010), a contrast in rainfall anomalies is found during March–May, with wetter conditions in the north and drier conditions over the southern Amazon (Jimenez et al., 2019). In the case of 2010, an El Niño event occurred previous to the warm TNA event in March–May, and widespread precipitation deficits were observed over northern Amazonia during December–February, highlighting the need to consider the effects of a combination of climatic phases occurring within a small timeframe.

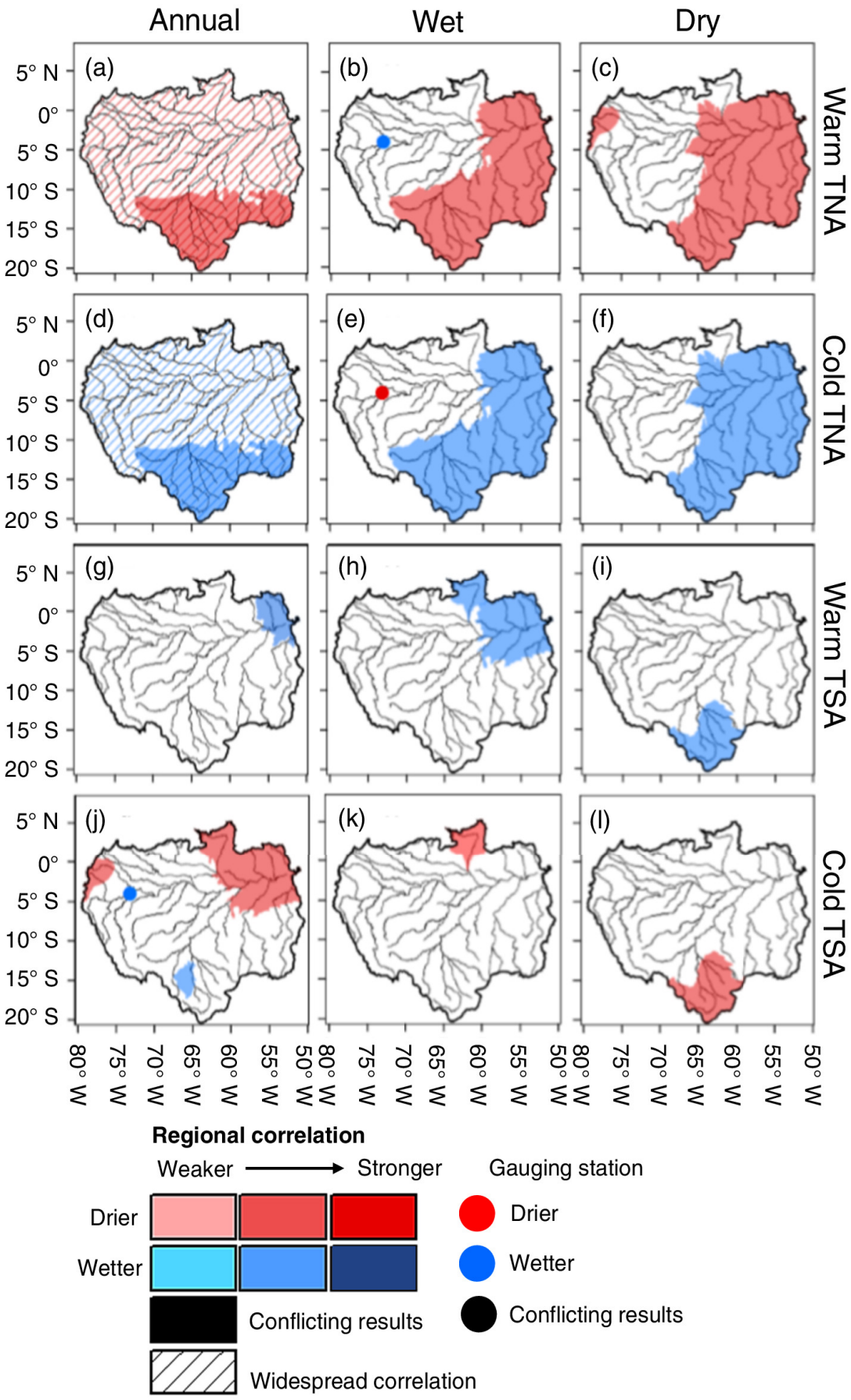
Annual
Wet
Dry
Warm TNA
Cold TNA
Warm TSA
Cold TSA
(a)
(b)
(c)
(d)
(e)
(f)
(g)
(h)
(i)
(j)
(k)
(l)
5° N
0°
5° S
10° S
15° S
20° S
80° W
75° W
70° W
65° W
60° W
55° W
50° W
Regional correlation
Weaker
Stronger
Drier
Wetter
Conflicting results
Widespread correlation
Gauging station
Drier
Wetter
Conflicting results

**Figure 3.** *Influence of tropical Atlantic sea surface temperatures (SSTs) on rainfall throughout the Amazon basin based on results identified within the literature: (a–c) a warm Tropical North Atlantic (TNA), (d–f) a cold TNA, (g–i) a warm Tropical South Atlantic (TSA) and (j–l) a cold TSA. The legend is the same as for Figure 2. For full details of the reference(s), type of analysis used and strength of the relationships, see Tables S7–S18 in the additional supporting information.*

The TSA, on the other hand, is considered less influential (Figure 3g–l), with its effect more pronounced on the southern edge of the Amazon between June and October (Figure 3l) and during the transitional phase in between the wet and dry seasons (Yoon and Zeng, 2010). Significant correlations do exist between rainfall anomalies and the SSTs in the TSA when analysing correlations against observed rainfall data (Ronchail et al., 2002). For example, when the TSA is warmer than usual, there is a corresponding increase in rainfall at stations located in the north-eastern Amazon (Figure 3g).

#### 2.4.1.3 The Madden-Julian oscillation (MJO)

Unlike the ENSO and tropical Atlantic indices, which typically occur on an interannual timescale, the MJO is an intra-seasonal oscillation, meaning it can occur between seasons in a single year, and it has the potential to provide predictability of rainfall and river discharge for the upcoming season. On a global scale, the MJO is considered the greatest modulator of regional rainfall on an intra-seasonal timescale, and is particularly influential in parts of the eastern Amazon (De Souza and Ambrizzi, 2006). Jones et al. (2004) identified that when convective activity was enhanced over the western Indian Ocean, there was an increase in the frequency of precipitation extremes in the eastern part of South America. The reasoning behind this increase has been associated with increased activity and rainfall within the SACZ, whereby intense SACZ events are modulated by the MJO (Carvalho et al., 2004). Composite analysis performed by Liebmann et al. (2004) supports these findings, revealing statistically significant variations in precipitation both downstream of the South American low-level jet (SALLJ) and within the SACZ depending on the phase of the oscillation. The MJO activity was found to be influential in enhancing upper level cyclonic and low-level anti-cyclonic anomalies, which are both features of a strengthened SALLJ.

Shimizu et al. (2017) explored the relationship between extreme precipitation events in the Amazon basin and phases of the MJO and ENSO activity. Extreme wet events in the Amazon were found to be more frequent when the MJO was active, particularly when tropical convection was strongest over the Indian Ocean (phases 1 and 2) and during phases 7 and 8

when convective activity is reduced over Australia. Shimizu et al. (2017) also note that despite the frequency of wet events being at its highest during phase 7 of the MJO cycle, considering cases for only the MJO events (i.e. not accounting for the ENSO), precipitation and convective motion were strongest in phase 2, indicating that events may become more extreme when the MJO is positioned over the Indian Ocean.

#### 2.4.1.4 Pacific decadal and Atlantic multidecadal oscillations

Studies analysing the impact of the PDO and AMO on rainfall variability tend to explore the relationship indirectly, focusing on how the PDO/AMO phases modulate the ENSO characteristics (e.g. Wang et al., 2014; García-García and Ummenhofer, 2015). For instance, the frequency and intensity of the ENSO anomalies have been found to be controlled by the phase of the PDO, with an intensification of wet/dry anomalies identified when the ENSO and PDO are in phase (e.g. a warm PDO and El Niño; Wang et al., 2014). Moreover, when the ENSO and PDO are out of phase, typical the ENSO and climate relationships were found to weaken or even disappear. For instance, during the cold phase of the PDO, precipitation anomalies associated with El Niño conditions are weakened over northern South America, including within parts of the Brazilian Amazon basin (Wang et al., 2014). These results were previously identified by Kayano and Andreoli (2007) who concluded that the strength of the ENSO teleconnections is potentially related to the phase of the PDO, with composites of rainfall for El Niño and La Niña years over South America substantially different between the PDO phases.

For the AMO, an opposing relationship emerges, with cold (warm) AMO regimes associated with stronger (weaker) ENSO variability (Timmermann et al., 2007; García-García and Ummenhofer, 2015). In other words, the ENSO events, in general, tend to be stronger when the two indices of the SSTs are out of phase (e.g. El Niño and a cold AMO regime), with the positive AMO regime characterised by anomalous easterly winds over the central and western Pacific that deepen the thermocline in the west Pacific (García-García and Ummenhofer, 2015). Over South America, anomalous precipitation composites showed more (less) organised patterns of rainfall, with significant anomalies occupying more (less) land area when the ENSO and AMO are in the opposite (same) phase (Kayano and Capistrano, 2013). Direct studies between the AMO and Amazon rainfall have shown positive phases of the AMO are linked to increased drought frequency (Barichivich et al., 2018) and the shortage of rainfall during the 2005 and 2010 mega-droughts (Aragão et al., 2018). A recent study by Kayano et al. (2019) explored the concomitant influence of the AMO and PDO phases on La Niña

teleconnections over South America. The highest (lowest) number of La Niña events occurred during periods in which warm AMO/cold PDO (cold AMO/warm PDO) persisted, consistent with what is expected based on the previous literature (e.g. Kayano and Capistrano, 2013; Wang et al., 2014; García-García and Ummenhofer, 2015). Considering other backgrounds, a combination of a cold AMO/cold PDO represented a larger percentage of La Niña events relative to a warm AMO/warm PDO, suggesting the importance of the cold PDO phase in favouring La Niña SST anomalies in the Equatorial Pacific.

### 2.4.2 River discharge variability

#### 2.4.2.1 Pacific influence

Marengo et al. (1993) identified using observations and simulations that the variability of river flows in the Amazon can differ on the order of two standard deviations between El Niño and non-El Niño years. More recently, Emerton et al. (2017) produced historical probabilities of the chances of observing abnormally high or low streamflow for the entire globe in response to El Niño and La Niña events for both the year in which an event peaks and for when it decays. For the Amazon, regions south of the Amazon River, particularly towards the western side of the basin are likely to observe higher than usual river flows during August and September for El Niño years during the initial stages of an ENSO event (40–60% probability) (Figure 4c). The signal reverses in the Brazilian Amazon for months closer to boreal winter, when El Niño typically reaches its peak. From November, lower than usual flows dominate the Brazilian Amazon with the signal strongest during December and between May and July during the decaying phase (Figure 4b,c). Drier conditions are dominant in the north-eastern Amazon throughout both the wet and dry seasons, which occur slightly later than those noted for rainfall due to the large lag between rainfall and discharge peaks (Figure 4b,c).

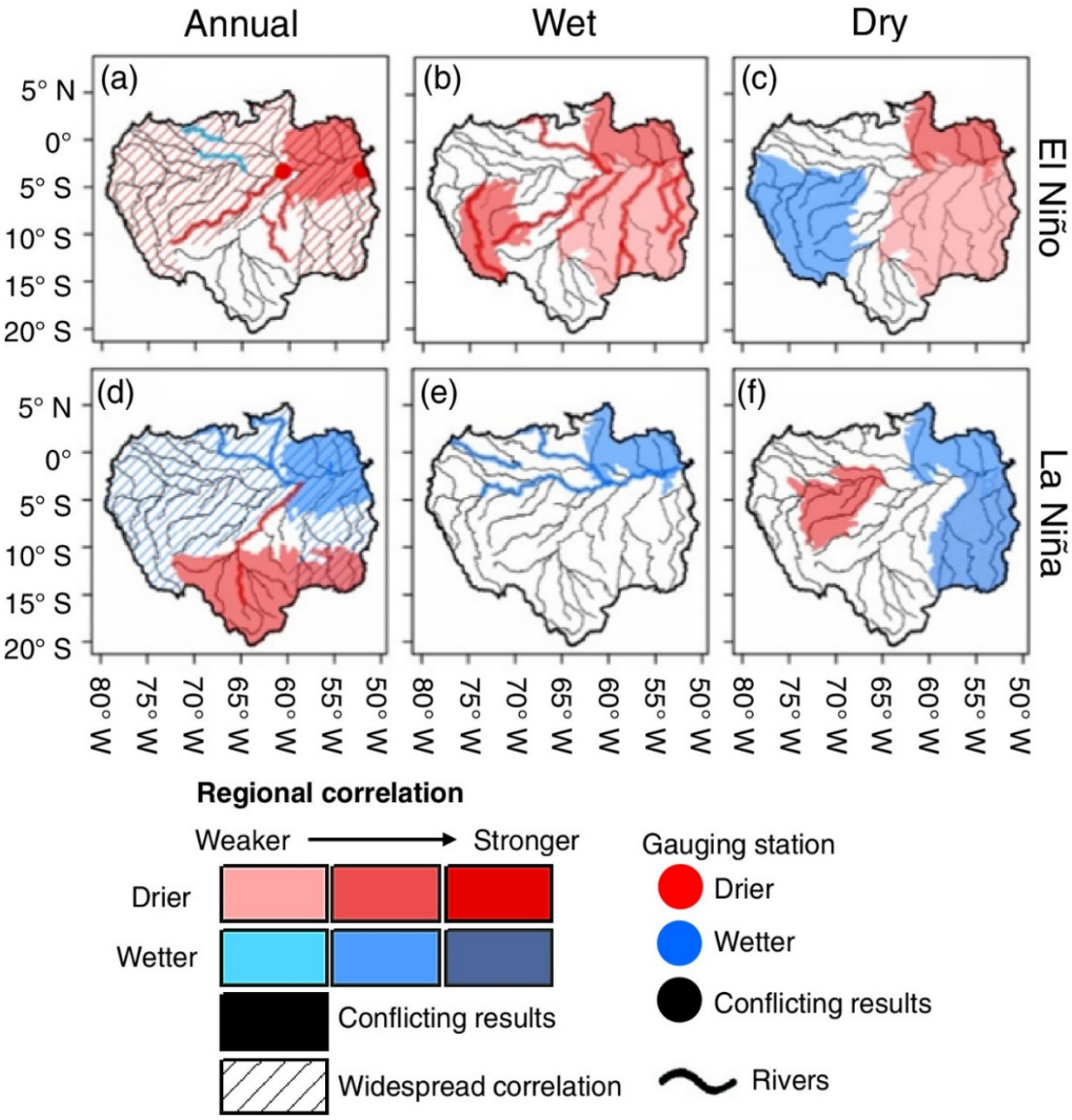


**Figure 4.** *Influence of El Niño Southern Oscillation (ENSO) conditions on river discharge in the Amazon basin based on results identified within the literature: (a, d) the entire year; (b, e) the Amazon wet season (February–June); and (c, f) the Amazon dry season (August–December). The legend is the same as for Figure 2. For full details of the reference(s), type of analysis used and strength of the relationships, see Tables S19–S24 in the additional supporting information.*

For La Niña years (i.e. the cold phase of the ENSO), the signal is generally weaker across the basin. Towards the northwest, around the confluence point of the Solimões River, where the headwaters of the Marañón and Ucayali rivers meet and in the western Brazilian Amazon, drier-than-usual flows are more likely in September and December (Figure 4f). In contrast, increased river flows are more likely in the north-eastern Amazon above the Amazon River from as early as July and lasting until around the following July. This signal is strongest during

February and March as La Niña begins to decay and extends into the southern Amazon during December (Figure 4e,f).

Analysis using observed river discharge data have identified similar signals for mean annual river flows, with lower (higher) levels of discharge during El Niño (La Niña) years found in all river basins with the exception of the southern Madeira basin (Espinoza et al., 2009a), consistent with results of Ronchail et al. (2005b) (Figure 4a,d). Major negative anomalies during El Niño are observed in tributaries in the north-eastern Amazon, similar to the response for rainfall (Figure 2a) and at Altamira station, located downstream of the southern Xingu River (Figure 4a) (Ronchail et al., 2005b). The signal in the north is replicated in several further studies (e.g. Uvo and Graham, 1998; Foley et al., 2002; Schöngart and Junk, 2007) with improved skill at forecasting discharge in northern sub-basins when using the Pacific SSTs (Uvo and Graham, 1998; Uvo et al., 2000). River flows in the Negro River were found to be significantly lower during El Niño years relative neutral conditions, whilst the opposite is true for La Niña (Figure 4b,e) (Schöngart and Junk, 2007).

Other notable regions include tributaries positioned to the east of the Madeira River (Ji-Parana, Aripuana, and Sucunduri), which witness up to a 25% decrease in discharge during El Niño phases (Ronchail et al., 2005b). An opposing signal (i.e. higher than normal river flow) was evident in the Japura River towards the Colombian Amazon and in the upper Negro basin (Figure 4a). Positive anomalies during La Niña events are predominately observed towards the north-eastern Amazon and along the Branco River, with lower than usual river flows more common in southern tributaries, particularly in the Mamoré and Madeira rivers (Figure 4d).

These studies support the global analysis of Ward et al. (2010), who investigate the sensitivity of annual mean, one and seven day maximum river discharge to the ENSO. They observed a positive relationship (i.e. drier conditions during El Niño) at all stations within the tropics, associated with the anomalous displacement of the Walker circulation. No statistical differences were found in the sensitivity to the Southern Oscillation Index (SOI) between mean and maximum discharges. This means the impacts of the ENSO were not found to be stronger for high flows compared with mean conditions, as is observed in many areas of the world.

#### 2.4.2.2 Atlantic influence

Espinoza et al. (2009a) find that for the TNA discharge variability in Amazonian rivers responds similarly to the ENSO. A negative correlation is identified between the TNA SSTs and mean and annual maximum river flows, indicating that when the TNA is warmer than usual, river

discharge decreases (Figure 5a), highlighting the same response to rainfall (i.e. a decrease in rainfall). This similar response to both the ENSO and TNA SSTs can be explained by positive correlations between the two indices. Several studies have highlighted the impact of the ENSO on the tropical Atlantic SSTs (Enfield and Mayer, 1997; García-Serrano et al., 2017) and its reversal through the induction of low-level cyclonic atmospheric flow due to the warming of TNA SSTs in boreal spring (Ham et al., 2013).

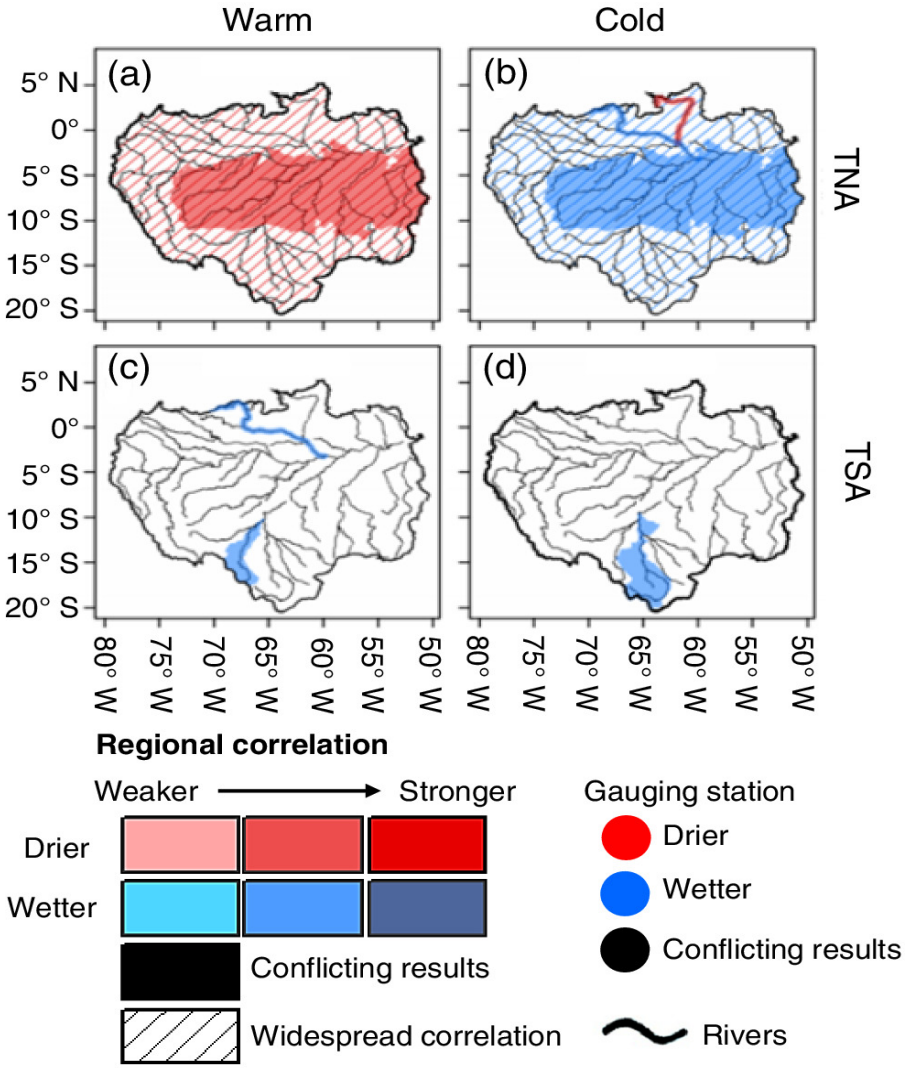


**Figure 5.** *Influence of tropical Atlantic sea surface temperatures (SSTs) on river discharge in the Amazon basin based on results identified within the literature: (a) a warm Tropical North Atlantic (TNA), (b) a cold TNA, (c) a warm Tropical South Atlantic (TSA) and (d) a cold TSA. Results are only shown for the entire year owing to the limited number of studies that have seasonal results. The legend is the same as for Figure 2. For full details of the reference(s), type of analysis used and strength of the relationships, see Tables S25–S28 in the additional supporting information.*

This relationship for lower than usual river flows was observed in most sub-basins except for the southern Madeira and northern Branco rivers, with the colder than usual TNA SSTs found to produce the opposite effect (Espinoza et al., 2009a) (Figure 5b). Marengo (1992) identified when the anomalously cold SSTs in the TNA occur concurrently with a warmer than usual TSA, water levels in the Negro River are generally higher (Figure 5b,c). These results are consistent with those produced by Ronchail et al. (2005b) for most regions of the Amazon. Stations situated between the Amazon River and 10° S showed higher than usual low and mean flows when the TNA is colder than usual, though an inverse relationship was observed in the Branco River basin in the far north (Figure 5b).

Considering the TSA, identified as being less important for Amazon rainfall (Yoon and Zeng, 2010), the relationship with discharge is more complex and is considered time dependent (Ronchail et al., 2005b). For instance, between 1974 and 1994, a warm TSA was linked with higher river flow in the Beni River basin (Figure 5c). In contrast, the Mamoré-Madeira basin, located just east of the Beni and Madeira rivers, increased discharges that corresponded to anomalously cold conditions (1988–2001) (Figure 5d). This relationship in the southern Amazon highlights the problems that could arise when using SST anomalies for potential flood prediction, with wetter conditions found in neighbouring sub-basins for opposing SST anomalies.

#### 2.4.2.3 Other drivers

There is an absence of literature focusing on the influence of the MJO, PDO and AMO on river flows in the Amazon basin relative to indices on shorter timescales (e.g. the ENSO). For several indices of longer term Atlantic and Pacific variability, only the AMO and the cross-equatorial Atlantic SST (Deser et al., 2010) indices were significantly and negatively correlated with variations in minimum dry season water levels at Manaus gauging site (Barichivich et al., 2018). Lee et al. (2018) observe the same negative correlation with seasonal peak flows in central South America providing “fair” predictions of seasonal flows based on a global scale prediction model evaluated using the categorical Gerrity skill score (GSS). These results are consistent with the typical relationship found between rainfall, river discharge and warmer conditions in the north Atlantic, with drier conditions dominating throughout much of the Amazon owing to the northward displacement of the ITCZ. This highlights the dominant role of the tropical Atlantic in modulating drought frequency in the Amazon and thus the ability to predict periods of dry spells.

The modulation of flooding or periods of abnormally high flows at longer timescales is much less understood (Barichivich et al., 2018). Recent studies have shown some predictability with regards to the strengthening of the Walker Circulation and associated enhancement of the Equatorial trade winds in the Pacific Ocean, which may offer multiyear predictability in some parts of the world (McGregor et al., 2014; Espinoza et al., 2016). In the Amazon, variations in maximum water levels at Manaus gauging station are consistently correlated with the strength of the Pacific trade winds (averaged 10 m zonal winds; Barichivich et al., 2018) and the SST gradients between the Atlantic and Pacific oceans basins (Chikamoto et al., 2015). The mechanisms behind this strengthening can be related to the dynamics of trans-basin variability (TBV), which is defined as the difference between the area-averaged Atlantic and Pacific SSTs. McGregor et al. (2014) implemented a basin-scale TBV index, defined as the monthly mean difference of the Atlantic–Pacific SST anomalies. They show how the TBV index is heavily influenced by the strength of the trade winds and operates on a frequency of roughly five years. Around 1991, cool Atlantic conditions featured alongside a relatively warm eastern Pacific, resulting in a negative TBV phase where Pacific trade winds were anomalously weaker. Since the late 1990s, rapid warming in the Atlantic Ocean (Gloor et al., 2013) combined with subsequent cooling in the eastern Pacific led to a reversal in the TBV index, whereby the Equatorial trade winds were enhanced due to anomalous low (high) pressure over the Atlantic (Pacific) oceans. This enhancement is found to coincide with a 55% increase in wet-day frequency (> 10 mm·day–1) in the western Amazon (Espinoza et al., 2016).

Indices that operate at lower frequencies (e.g. the TBV, PDO and AMO) could translate into useful information for the risk assessment for various sectors operating in the Amazon (e.g. agriculture). However, unlike for the relationship between droughts and warmer than usual North Atlantic SSTs, the mechanisms behind flooding at longer timescales still require further research.

### 2.4.3 Rainfall vs river discharge

Overall a similar relationship is clear between the phases of the ENSO and the trends seen in both rainfall and river discharge, particularly on annual timescales (Figures 2 and 4). During El Niño events, drier conditions are prevalent, while increased rainfall and river discharge are generally found throughout the basin during La Niña. Changes in association to the ENSO are strongest in the north-eastern Amazon for both variables. Some discrepancies appear during

the dry season for La Niña years, with less rainfall noted in the southern Amazon (Figure 2f), while a reduction of discharge is only observed in parts of the north-western Amazon (Figure 4f). It should be noted that the dry season typically overlaps when ENSO is in its initial building or decaying phase, with a stronger association generally acknowledged during December–February when the ENSO reaches its peak. For the Atlantic, rainfall and discharge respond similarly, with a reduction in rainfall and discharge when the TNA is anomalously warm and an increase when the TNA is colder than usual. The TSA is found to be less influential for both variables (Figures 3 and 5).

In addition to magnitude, the SST variability has been shown to affect the onset and withdrawal timings of the wet season. In the central Amazon, the average onset date was determined to be around September 25 when constructing five-day rainfall averages (pentads), and is associated with anomalous anticyclone activity and enhanced trade winds in the Atlantic (Marengo et al., 2001). The combination of the cold Atlantic and warm Pacific SST anomalies is linked with a delayed onset and early withdrawal of wet season rainfall. For this particular configuration of the SSTs, there is an observed delay in the seasonal migration of peak convection from the Northern to the Southern hemisphere, owing to the delay of planetary boundary layer (PBL) moisture. This build up of the PBL moisture is responsible for the onset of convection, with regions closer to the Equator more sensitive to small changes in the thermodynamic and dynamical structure of the atmosphere relative to the southern Amazon (Fu et al., 1999). Thus, central and northern catchments are likely to be more sensitive to changes in the SSTs in the adjacent oceans.

So far, the aforementioned studies have described the role of the tropical Atlantic and Pacific oceans in determining precipitation variability in the Amazon basin. However, Builes-Jaramillo et al. (2018) hypothesise that the interaction between the SSTs in the Atlantic and the hydrology of the Amazon are more complex, proposing a two-way feedback system. They identify that shifts in the hydrology of the Amazon can influence future states of the TNA SSTs up to two months in advance. When the Amazon is particularly dry (wet), atmospheric surface pressure over the Amazon increases (decreases). Consequently, the atmospheric surface pressure between the TNA and the Amazon is reduced (increased), which in turn reduces (enhances) the zonal trade winds. As the zonal trade winds weaken (strengthen) over the TNA, there is reduced (increased) evaporative cooling leading to an increase (decrease) in the TNA SSTs.

It is important to highlight the fact that the majority of correlations described in Section 2.4 are often considered for larger catchment areas and/or for a small number of meteorological/hydrological stations. This is particularly true for precipitation in smaller sub-basins, which suffers from poor spatial coverage (Paccini et al., 2018). Consequently, the relationship between rainfall and climate drivers can be difficult to assess.

## 2.5 Hydroclimatic drivers and extreme floods

Figure 6 shows all the flood events outlined in Table 2 plotted onto the times series of the SST anomalies for the El Niño 3.4, TSA and TNA regions. It should be noted that these floods were based on what was identified within the literature and flood databases, and so it is biased towards regions where more research and flood recordings take place. The southwestern Amazon, for example, shows more floods through time, but this could be due to flood events being recorded and analysed more frequently in these locations. In addition, southwestern regions have several gauging stations where floods tend to be analysed (d–i), whereas floods in the Peruvian Amazon are generally based on water levels at Tamshiyacu gauging station (a). Figure 6 also highlights that flood events can occur in several regions of the basin regardless of whether the SST anomalies are in their positive, neutral or negative phases. This implies that although flooding in a certain location may be linked to a particular phase of climate (e.g. La Niña), floods are not restricted to this particular phase and demonstrates the complexities that exist when making any association with a particular hydroclimatic driver.

**Table 2.** Characteristics of flood events in the Amazon basin and their links to hydroclimatic drivers. The attributed flood driver and method of analysis for each event are taken from the author(s) highlighted in bold. Superscripted letters correspond to the gauging stations at which the flood was recorded. SSTs provided are anomalies.

| Year and Location Affected | Peak Discharge Timing | Peak Discharge ($m^3s^{-1}$) | Days over 90th Percentile of Flow | Attributed Flood Driver | EN 3.4 $^0$C (OND/DJF) | MEI .v2 EN $^0$C (OND/DJF) | TNA $^0$C (MAM) | TSA $^0$C (MAM) | Phase of PDO/AMO $^0$C | Method of Analysis | Strength of Evidence | Author(s) |
|---|---|---|---|---|---|---|---|---|---|---|---|---|
| **1953** Eastern Amazon[b] | /[b] | /[b] | /[b] | Warm TSA | 0.05/0.40 | / | 0.08 | -0.14 | Cold (-0.57)/ Warm (0.26) | - None | Very low | **Marengo et al. (2013a)** Satyamurty et al. (2013) Rodier & Roche (1984) O'Connor & Costa (2004) Callède et al. (2004) |
| **1956** South-west[f] | /[f] | /[f] | /[f] | LN | -1.67/-1.11 | / | -0.11 | -0.58 | Cold (-1.82)/ Warm (-0.03) | - Correlation analysis between rainfall, inundation and SST | Low | **Ronchail et al. (2005a)** |
| **1958** South-west[f] | /[f] | /[f] | /[f] | EN | 1.53/1.80 | / | 0.85 | -0.76 | Cold (0.92)/ Warm (0.20) | - See 1956 | Low | **Ronchail et al. (2005a)** |
| **1963** Eastern Amazon[b] | /[b] | 250000*[b] | /[b] | Not defined | -0.30/-0.40 | / | 0.30 | 0.30 | Cold (-0.28)/ Warm (-0.01) | - No link to hydroclimate drivers | / | Rodier & Roche (1984) O'Connor & Costa (2004) |
| **1966** South-west[f] | /[f] | /[f] | /[f] | EN | 1.97/1.37 | / | 0.44 | -0.06 | Cold (-0.50)/ Cold (0.00) | - See 1956 | Low | **Ronchail et al. (2005a)** |
| **1968** South-west[d,h] | 25/02/1968[d] 25/02/1968[h] | 17490[d] 17490[h] | 22[d] 22[h] | Non-ENSO | -0.34/-0.63 | / | -0.09 | -0.09 | Cold (-0.19)/ Cold (-0.18) | - Discharge > 6000 $m^3s^{-1}$ at Rurrenbaque gauging station compared to ONI ENSO classification | / | **Vauchel et al. (2017)** Gautier et al. (2006) |

| Year and Location Affected | Peak Discharge Timing | Peak Discharge ($m^3s^{-1}$) | Days over 95th Percentile of Flow | Attributed Flood Driver | EN 3.4 $^0$ C (OND/DJF) | MEI .v2 EN $^0$ C (OND/DJF) | TNA $^0$ C (MAM) | TSA $^0$ C (MAM) | Phase of PDO/AMO $^0$ C | Method of Analysis | Strength of Evidence | Author(s) |
|---|---|---|---|---|---|---|---|---|---|---|---|---|
| **1971** South-west[d,h] | 26/02/1971[d]<br>26/02/1971[h] | 17340[d]<br>17340[h] | 57[d]<br>56[h] | LN | -0.86/-1.36 | / | -0.33 | 0.09 | Cold (-1.34)/ Cold (-0.32) | - Discharge > 15000 $m^3s^{-1}$ at Rurrenbaque gauging station compared to ONI ENSO classification | Low | **Espinoza et al. (2014)**<br>Vauchel et al. (2017)<br>Gautier et al. (2006) |
| **1972** South-west[h] | 22/01/1972[h] | 14850[h] | 16[h] | Not defined | -0.96/-0.70 | / | -0.42 | -0.06 | Cold (-1.17)/ Cold (-0.37) | - No link to hydroclimate drivers | / | Gautier et al. (2006) |
| **1973** Eastern Amazon[c] South-west[d,f] | 21/06/1973[c]<br>29/01/1973[d]<br>/[f] | 146800[c]<br>12560[d]<br>/[f] | 0[c]<br>41[d]<br>/[f] | EN | 2.09/1.85 | / | -0.16 | 0.76 | Cold (-1.18)/ Cold (-0.23) | - See 1956 | Low | **Ronchail et al. (2005a)**<br>Vauchel et al. (2017)<br>Richey et al. (1989) |
| **1974** South-west[d,f,h] | 16/01/1974[d]<br>/[f]<br>16/01/1974[h] | 13290[d]<br>/[f]<br>13290[h] | 42[d]<br>/[f]<br>42[h] | LN | -1.95/-1.84 | / | -0.90 | 0.33 | Cold (-0.38)/ Cold (-0.43) | - See 1956 | Low | **Ronchail et al. (2005a)**<br>Vauchel et al. (2017)<br>Gautier et al. (2006) |
| **1975** South-west[f] | /[f] | /[f] | /[f] | LN | -0.75/-0.54 | / | -0.55 | -0.07 | Cold (-1.46)/ Cold (-0.31) | - See 1956 | Low | **Ronchail et al. (2005a)** |
| **1976** Eastern Amazon[b,c] | 20/05/1976[b]<br>26/06/1976[c] | 269400[b]<br>145600[c] | 81[b]<br>0[c] | LN | -1.55/-1.55 | / | -0.75 | -0.62 | Cold (-0.18)/ Cold (-0.39) | - Composite analysis of SST anomalies and moisture flux (Oct-Apr), for five highest flood years prior to 2012 (1953,1976,1989,1999 and 2009) | Medium | **Satyamurty et al. (2013)**<br>Rodier & Roche (1984)<br>Richey et al. (1989)<br>O'Connor & Costa (2004) |

| Year and Location Affected | Peak Discharge Timing | Peak Discharge ($m^3s^{-1}$) | Days over 95th Percentile of Flow | Attributed Flood Driver | EN 3.4 $^0$ C (OND/DJF) | MEI .v2 EN $^0$ C (OND/DJF) | TNA $^0$ C (MAM) | TSA $^0$ C (MAM) | Phase of PDO/AMO $^0$ C | Method of Analysis | Strength of Evidence | Author(s) |
|---|---|---|---|---|---|---|---|---|---|---|---|---|
| **1977** South-west[f] | /[f] | /[f] | /[f] | EN | 0.86/0.71 | / | -0.09 | -0.03 | Warm (0.02)/ Cold (-0.20) | - See 1956 | Low | **Ronchail et al. (2005a)** |
| **1978** South-west[d,f,h] | 05/02/1978[d] /[f] 05/02/1978[h] | 19730[d] /[f] 19730[h] | 21[d] /[f] 19[h] | Warm SSA Negative TSA-SSA gradient EN | 0.81/0.69 | / | 0.20 | -0.58 | Warm (0.01)/ Cold (-0.19) | - Composite analysis of SST, 850-hPa geopotential height and humidity flux anomalies for non-La Niña floods (1978, 1982, 2001 and 2014)<br><br>- See 1956 | Medium | **Espinoza et al. (2014)** **Ronchail et al. (2005a)** Gautier et al. (2006) |
| **1982** South-west[d,f,h] | 06/03/1982[d] /[f] 06/03/1982[h] | 16720[d] /[f] 16720[h] | 23[d] /[f] 22[h] | Warm SSA Negative TSA-SSA gradient | -0.15/-0.05 | -0.17/-0.34 | -0.09 | -0.31 | Warm (-0.25)/ Cold (-0.23) | - See 1978 | Medium | **Espinoza et al. (2014)** Gautier et al. (2006) |
| **1983** South-west[f,h] | /[f] 18/02/1983[h] | /[f] 12700[h] | /[f] 8[h] | EN | 2.18/2.18 | 2.23/2.60 | 0.35 | 0.18 | Warm (1.19)/ Cold (-0.09) | - See 1956 | Low | **Ronchail et al. (2005a)** Gautier et al. (2006) |
| **1984** South-west[d,h] | 02/03/1984[d] 02/03/1984[h] | 13100[d] 13100[h] | 64[d] 54[h] | Non-ENSO | -1.00/-0.60 | -0.43/-0.49 | -0.15 | 0.52 | Warm (0.59)/ Cold (-0.22) | - See 1968 | Low | **Vauchel et al. (2017)** Gautier et al. (2006) |
| **1986** Peruvian Amazon[a] | 08/05/1986[a] | 53920[a] | 54[a] | LN | -0.27/-0.49 | -0.14/-0.34 | -0.60 | 0.31 | Warm (0.96)/ Cold (-0.30) | - Composite analysis of SST, 850-hPa geopotential height and humidity flux anomalies for OND 1985, 1992, 1998 and 2011 | Low | **Espinoza et al. (2013)** |

| Year and Location Affected | Peak Discharge Timing | Peak Discharge ($m^3s^{-1}$) | Days over 95th Percentile of Flow | Attributed Flood Driver | EN 3.4 $^0$ C (OND/DJF) | MEI .v2 EN $^0$ C (OND/DJF) | TNA $^0$ C (MAM) | TSA $^0$ C (MAM) | Phase of PDO/AMO $^0$ C | Method of Analysis | Strength of Evidence | Author(s) |
|---|---|---|---|---|---|---|---|---|---|---|---|---|
| **1989** Peruvian Amazon[a] Eastern Amazon[b] | 09/05/1989[a] 06/06/1989[b] | 48220[a] 274400[b] | 3[a] 96[b] | LN | -1.80/-1.69 | -1.55/-1.21 | -0.74 | 0.32 | Warm (-0.55)/ Cold (-0.10) | - Comparison of 1989, 1999 and 2009 floods comparing atmospheric and SST anomalies and further hydrological analysis (e.g. mean and max Q/timing of Q) | Medium | **Marengo et al. (2012)** Satyamurty et al. (2013) |
| **1992** South-west[f] | /[f] | /[f] | /[f] | MEI EN | 1.21/1.71 | 1.18/1.53 | -0.22 | -0.54 | Warm (0.70)/ Cold (-0.23) | - See 1956 | Low | **Ronchail et al. (2005a)** Bourrel et al. (2009) |
| **1993** Peruvian Amazon[a] Eastern Amazon[b] South-west[f] | 11/05/1993[a] 23/05/1993[b] /[f] | 51740[a] 246000[b] /[f] | 64[a] 61[b] /[f] | LN MEI EN | -0.28/0.09 | 0.75/0.83 | -0.11 | 0.05 | Warm (0.97)/ Cold (-0.23) | - See 1986 - See 1956 | Low | **Espinoza et al. (2013)** **Ronchail et al. (2005a)** Bourrel et al. (2009) |
| **1994** South-west[i] | /[i] | /[i] | /[i] | Not defined | 0.04/0.06 | 0.63/0.04 | -0.52 | 0.18 | Warm (-0.53)/ Cold (-0.19) | - Hydrological and remote sensing analysis (discharge and flood imagery) No connection to hydroclimate drivers stated or analysed | / | Bourrel et al. (2009) |
| **1995** South-west[i] | /[i] | /[i] | /[i] | Not defined | 1.00/0.96 | 1.10/0.70 | 0.12 | 0.65 | Warm (0.32)/ Warm (0.12) | - See 1994 | / | Bourrel et al. (2009) |
| **1997** South-west[f,i] | /[f] /[i] | /[f] /[i] | /[f] /[i] | Not defined | -0.45/-0.50 | -0.37/-0.61 | 0.28 | -0.50 | Warm (1.22)/ Warm (0.03) | - See 1994 | / | Bourrel et al. (2009) |

| Year and Location Affected | Peak Discharge Timing | Peak Discharge ($m^3s^{-1}$) | Days over 95th Percentile of Flow | Attributed Flood Driver | EN 3.4 $^0$ C (OND/DJF) | MEI .v2 EN $^0$ C (OND/DJF) | TNA $^0$ C (MAM) | TSA $^0$ C (MAM) | Phase of PDO/AMO $^0$ C | Method of Analysis | Strength of Evidence | Author(s) |
|---|---|---|---|---|---|---|---|---|---|---|---|---|
| **1998** South-west[i] | /[i] | /[i] | /[i] | Not defined | 2.40/2.24 | 2.06/2.24 | 0.64 | 0.59 | Cold (-0.45)/ Warm (0.36) | - See 1994 | / | Bourrel et al. (2009) |
| **1999** Peruvian Amazon[a] Eastern Amazon[b] South-west[d,h] | 21/05/1999[a] 02/06/1999[b] 20/03/1999[d] 20/03/1999[h] | 53020[a] 268200[b] 22330[d] /[h] | 54[a] 57[b] 36[d] /[h] | LN | -1.48/-1.55 | -1.24/-1.22 | -0.08 | 0.44 | Cold (-1.78)/ Warm (0.10) | - See 1986<br>- See 1989 | Medium | **Espinoza et al. (2013)** **Marengo et al. (2012)** Marengo & Espinoza (2016) Gautier et al. (2006) Dartmouth Flood Observatory (2018) Vauchel et al. (2017) |
| **2001** South-west[d,h] | 13/01/2001[d] 13/01/2001[h] | 16950[d] /[h] | 40[d] /[h] | Warm SSA | -0.75/-0.68 | -0.76/-0.83 | 0.09 | 0.38 | Cold (-1.13)/ Warm (0.10) | - See 1978 | Medium | **Espinoza et al. (2014)** Gautier et al. (2006) Vauchel et al. (2017) |
| **2007** South-west[g] | 28/04/2007[g] | 18950[g] | 40[g] | EN | 0.90/0.71 | 0.73/0.53 | 0.31 | 0.19 | Cold (-0.78)/ Warm (0.13) | -Hydrological comparison of the 2007, 2008 and 2014 floods (e.g. monthly rainfall and discharge, flood timing, total flooded area based on remote sensing imagery<br><br>No atmospheric analysis performed | Low | **Ovando et al. (2016)** CEPAL (2008) Dartmouth Flood Observatory (2018) |

| Year and Location Affected | Peak Discharge Timing | Peak Discharge ($m^3s^{-1}$) | Days over 95th Percentile of Flow | Attributed Flood Driver | EN 3.4 $^0$C (OND/DJF) | MEI .v2 EN $^0$C (OND/DJF) | TNA $^0$C (MAM) | TSA $^0$C (MAM) | Phase of PDO/AMO $^0$C | Method of Analysis | Strength of Evidence | Author(s) |
|---|---|---|---|---|---|---|---|---|---|---|---|---|
| **2008** South-west[g] | 18/04/2008[g] | 22620[g] | 59[g] | LN | -1.55/-1.59 | -1.16/-1.19 | 0.21 | 0.69 | Cold (-1.75)/ Warm (0.12) | - See 2007 | Low | **Ovando et al. (2016)** CEPAL (2008) Dartmouth Flood Observatory (2018) |
| **2009** Eastern Amazon[b] | 05/08/2009[b] | 262400[b] | 50[b] | Warm TSA | -0.60/-0.80 | -1.06/-0.97 | -0.29 | 0.62 | Cold (-1.09)/ Warm (0.02) | - See 1989 | Medium | **Marengo et al. (2012)** Sena et al. (2012) Filizola et al. (2014) |
| **2011** South-west[d] | 23/02/2011[d] | 20250[d] | 38[d] | LN | -1.69/-1.36 | -2.03/-1.78 | 0.38 | 0.50 | Cold (-1.91)/ Warm (0.09) | - See 1971 | Medium | **Espinoza et al. (2014)** Vauchel et al. (2017) |
| **2012** Peruvian Amazon[a] Eastern Amazon[b] | 20/04/2012[a] 18/07/2012[b] | 55400[a] 260100[b] | 70[a] 50[b] | LN + warm TSA | -1.14/-0.82 | -1.26/-0.99 | -0.11 | -0.15 | Cold (-1.66)/ Warm (0.20) | - See 1986 Anomalies also calculated solely for the 2012 event | High | **Espinoza et al. (2013)** Marengo & Espinoza (2016) Satyamurty et al. (2013) |
| **2014** South-west[d,e,g] | 12/02/2014[d] 30/03/2014[e] 05/04/2014[g] | 25060[d] 59080[e] 29090[g] | 53[d] 111[e] 85[g] | Warm IP & SSA Negative TSA-SSA gradient | -0.22/-0.37 | -0.23/-0.43 | -0.21 | 0.31 | Warm (0.48)/ Warm (0.09) | - See 1978 Anomalies also calculated solely for the 2014 event | High | **Espinoza et al. (2014)** Espinoza et al. (2012) Ovando et al. (2016) |
| **2015** Peruvian Amazon[a] | 25/04/2015[a] | 53880[a] | 91[a] | Not defined | 0.59/0.60 | 0.25/0.2 | -0.09 | 0.35 | Warm (0.92)/ Warm (0.10) | - None | / | SO-HYBAM (2015) |

Extended table from Marengo and Espinoza (2016). LN = La Niña; TSA = Tropical South Atlantic; IP = Indo-Pacific Ocean; and SSA = Subtropical South Atlantic. Peak discharge values marked with an asterisk (*) are based on those provided by Rodier & Roche (1984).

[a] Tamshiyacu, Solimões River (1986-2017)

[b] Óbidos, Amazon River (1968-2018)

[c] Manacapurú, Solimões river (1968-2017)

[d] Rurrenbaque, Beni river (1968-2016)

[e] Porto Velho, Madeira river (1968-2017)

[f] Puerto Varador, Mamoré river (Data not available)

[g] Guajara-Mirim, Mamoré river (1971-2014)

[h] Angosto del Bala, Beni river (1968-1994)

[i] Puerto Almacen, Ibaré river (Data not available)

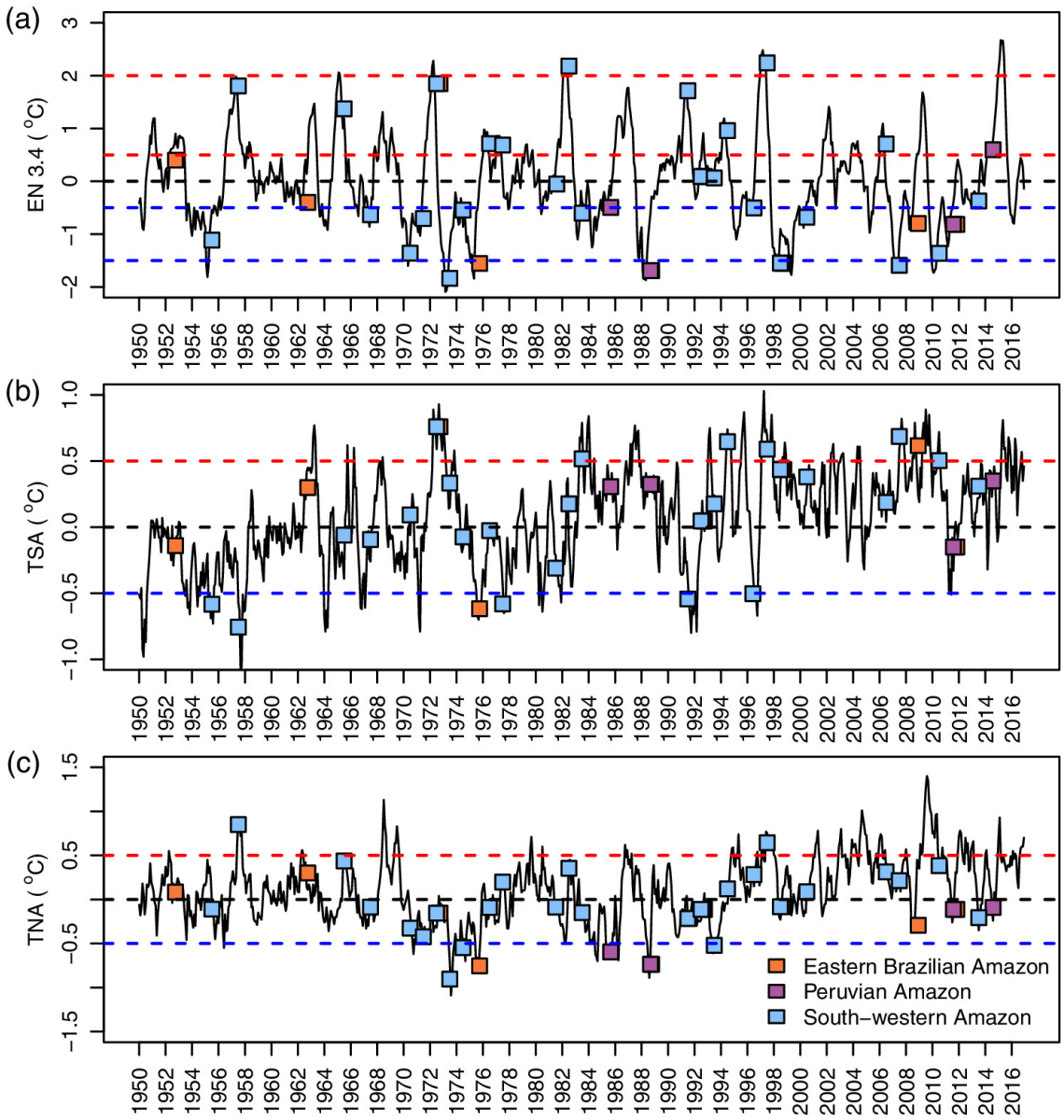


**Figure 6.** *Amazon flood events from Table 2 plotted onto the time series of the sea surface temperature (SST) anomalies in the tropical Pacific and Atlantic oceans: (a) El Niño 3.4 region,*

*(b) Tropical South Atlantic (TSA) and (c) Tropical North Atlantic (TNA). Floods are based on the gauging stations that match those shown in Table 2, with colours representing the region in which the flood occurred. Circles are positioned during the month of occurrence (i.e.* x*-axis) with the height (i.e.* y*-axis) determined by the preceding October–December (March–May) mean SST anomaly for the El Niño 3.4 (TNA and TSA) regions. Dashed blue and red lines depict the threshold for the respected warm and cold phases of each index (e.g. – 0.50°C for a weak La Niña event and 2.0°C for a very strong El Niño, as classified for the Oceanic Niño Index (ONI).*

### 2.5.1 Attribution of drivers

#### 2.5.1.1 Lower confidence attribution case: The 1993 Peruvian Amazon event

Indices of hydroclimate drivers are of interest for flood forecasters and humanitarian organisations alike due to the potential for their use in increasing the predictability of upcoming floods. However, in some cases, the links between floods and hydroclimate drivers are not clear. Figure 6 plots each flood event identified in Table 2 over the time series of the SST anomalies in the tropical Pacific and Atlantic oceans. Some floods, such as those observed at Tamshiyacu (a), in 1993, have previously been associated with La Niña conditions during the preceding austral spring and summer (Espinoza et al., 2013). Considering the region (5° N–5° S, 120–170° W), the SST anomalies in the central Pacific in the build up to this event did not in fact reach the typical ONI −0.5°C threshold (weak La Niña) for any three-month period (preceding October–December mean = −0.28°C) (Figure 6a), with the positive SST anomalies observed from January 1993 onwards. Similarly, the 1986 event, also attributed to La Niña conditions (Espinoza et al., 2013), never broke the −0.5°C threshold during austral spring and summer, though the negative SST anomalies were persistent throughout the period. This means it is unlikely that these floods were due to La Niña conditions and that a different response mechanism could be responsible.

Analysis for these events was centred around a composite of the SSTs, geopotential height and vertical integrated humidity flux anomalies for the four strongest flood years at Tamshiyacu gauging site (a) (1993, 1986, 1999 and 2012) for the preceding October–December season (Espinoza et al., 2013). Atmospheric anomalies were identified and found to be responsible for increased moisture convergence over the north-western Amazon. This analysis was performed for the mean of the four years, which included the stronger La Niña conditions observed in austral summer during 1998 and 2011, with the atmospheric response to individual events only mentioned for 2012. It is therefore currently unknown if the oceanic conditions in the

Pacific in the build up to the 1993, 1986 and 1999 floods were capable of reproducing the same or a similar atmospheric response that could be determined as the cause for those events. Further investigation of the SST anomalies and atmospheric response to each individual event (as performed for the 2012 flood) rather than as a composite could form a useful task in identifying the relationship between the magnitude and location of cooling in the central equatorial Pacific and the level of humidity flux convergence over the Amazon basin. Such an analysis could allow more confidence in the understanding of the magnitude of the SSTs required to favour an atmospheric response that commonly produces severe flooding.

Other cases also exist, for instance, for the 1953 floods at Óbidos (b), Brazil (Table 2). Here, the link to climate is often not directly stated (e.g. Marengo and Espinoza, 2016) (Table 1), whereas in other works (Marengo et al., 2013a), it has been connected to a warmer than usual TSA in the absence of La Niña. Though, as shown in Table 2 and Figure 6b, the SST anomalies in the TSA are mostly negative throughout the entire preceding year to the event with a minimum temperature anomaly of −0.29 in April 1953.

#### 2.5.1.2 Higher confidence attribution case: The 2014 Brazilian Amazon event

The 2014 extreme floods affected many locations within the southwestern Amazon, particularly in the Madeira basin with river discharge reaching a record breaking 58,000 $m^3s^{-1}$ at Porto Velho gauging station (e) (Table 2). Espinoza et al. (2014) first identified anomalies in hydrological conditions, with higher than normal rainfall observed as early as September 2013, peaking towards the end of January 2014. Examining large-climatological features in the build up to the event (i.e. the wet season from December to March), a negative TSA–SSA gradient was attributed to the event with the exceptionally warm SSTs in the SSA present from January 2014.

These conditions were associated with a change in atmospheric circulation from January to March 2014. Positive 850 hPa geopotential height anomalies were found to produce anomalous anticyclonic circulation, which extended from the SSA into South America and was responsible for a weakening of the SACZ activity and an enhancement of the SALLJ bringing anomalous rainfall. Moreover, vertically integrated vapour transport anomaly fields from December 2013 to March 2014 showed an intense incursion from the TNA to the southern Amazon (Espinoza et al., 2014).

Further analysis involved using a composite analysis to investigate floods in the region which were not associated with La Niña. As in Espinoza et al. (2013), the climatological conditions were averaged for four flood years (1978, 1982, 2001 and 2014), producing an TSA–SSA SST gradient and a positive 850 hPa in the SSA region. However, humidity composites were then compared with those solely for the 2014 event and revealed that the incursion of the humidity flux from the tropical Atlantic was more intense for this specific event.

As climatological conditions (i.e. the SST anomalies, geopotential height anomalies and humidity fluxes) were analysed solely for conditions witnessed in the build up to the 2014 event (i.e. December 2013—March 2014), greater confidence can be obtained in the attribution of the flood compared with years in which conditions were only presented for averaged conditions (i.e. 1978, 1982 and 2001). This is the same case for the 2012 Peruvian Amazon flood (Espinoza et al., 2013), whereby a single flood year is analysed in addition to a composite of years. It is important to recognise that this does not imply that the other flood events within the composite are not associated with atmospheric circulation patterns sourced from a strengthened TSA–SSA gradient, but rather the specific climatological response for each individual event is less known. Further numerical modelling analysis investigating the ocean–atmosphere mechanisms behind flooding is still required. Comparisons between conditions of similar events may help explain differences in intensity and persistence (Espinoza et al., 2014), and provide useful information to provide early warnings for future floods.

### 2.5.2 Classification of a flood

Most of the large Amazonian rivers experience a single flood period with overbank flow in a "normal" year. This is why, when reviewing the literature, discrepancies appear in the classification of a flood event. Should a flood be classified based on a threshold of streamflow exceedance, the number of days above threshold, the extent of inundation, by riverbank exceedance or by socioeconomic impact? In the introduction to Vauchel et al. (2017), a discharge > 6,000 $m^3s^{-1}$ at Rurrenbaque gauging station (d) (Beni River) is determined as a flood event based on the average high flood level when evaluating floods against the ENSO frequency. However, this level is exceeded almost every year, making any association with the ENSO phases difficult.

Another example includes the 250,000 $m^3s^{-1}$ discharge threshold used by some authors (e.g. Callède et al., 2004; Ronchail et al., 2006) at Óbidos (b). Though this value represents the water level at which the town begins to inundate (Callède et al., 2004), streamflow

observations for this station show this level is regularly exceeded, despite no significant impacts or reports of extreme flooding being registered every time (e.g. between May and July 2010). Thus, thresholds used for decision-making, flood warnings and forecasting research could be better chosen to reflect the risk to communities in a particular reach of a river as opposed to a magnitude of river flow that causes a river to exceed its banks.

### 2.5.3 "Normal" vs "extreme" floods

It is also important to understand how a "normal" flood is distinguished from an "extreme" flood. A case is presented in the upper Madeira basin, where in 2007 and 2008 rainfall was higher than the climatological average producing flooding along the Mamoré (g) and Guaporé rivers (Table 2). Ovando et al. (2016) state that in terms of river discharge, the floods would be better classified as "above normal", but argue they should be considered "extreme" due to their socioeconomic impact. The two floods combined reportedly affected > 250,000 people, resulting in 49 fatalities (CEPAL, 2008).

For better classification, both flood hazard and flood risk should be considered. For instance, when assessing how climate variability affects flood hazard, it is important to use measures of flooding that are hazard related (e.g. streamflow, water level and flood extent). Whereas for the EWS and humanitarian protocols (e.g. FbF; Coughlan de Perez et al., 2015) it is the flood risk that becomes more important; thus, statistics and information including economic cost, the number of people exposed or implications for local populations (e.g. food provisions) are a more suited measure of flood severity. It is therefore necessary to recognise both, as in Langill and Abizaid (2019), as a flood-type analysis for a village located along the Ucayali River in Peru. In their analysis, the authors used a combination of hydrograph (i.e. water level, high-water period and onset dates) and field data (i.e. interviews with community members) to help distinguish what makes a "bad" or "extreme" flood. Four flood types (high, long, early and late) are classified, the authors concluding that while high floods are the most common, long and early floods occur on a similar frequency and tend to have more severe implications for people.

### 2.5.4 Flood mechanisms during La Niña

Figure 7 displays a schematic of the step-by-step processes in which the abnormal SST conditions can drive atmospheric behaviour and consequently cause excessive rainfall and flooding in the north-western Amazon. It is important to highlight that the mechanisms behind

flood events often differ depending on the exact location within the basin (e.g. upstream in the northwest versus downstream in the Brazilian Amazon; Espinoza et al., 2013). These processes have been determined by the occurrences of events in the build up to previous floods from studies in the literature:

- During typical conditions, the equatorial trade winds blow east to west (i.e. easterly trade winds). Consequently, warmer surface waters in the central Pacific are pushed west towards Indonesia, raising the water levels in the region relative to those found off the coast of Peru. To compensate, deep colder waters rise off the coast of Peru (i.e. cold-water upwelling) in order to replace the warmer waters that have been transported by the surface winds. During La Niña, the easterly trade winds that carry large quantities of moisture are enhanced (Figure 7a) owing to decreases in pressure in the Indonesian continent relative to the central and eastern Pacific.
- This results in warmer surface waters in the central Pacific being pushed further west, increasing the upwelling of cold water and causing cooler than usual SSTs in the central to eastern Pacific. The ENSO events typically reach their peak during the boreal winter (Emerton et al., 2017), with previous Amazon floods associated with colder than usual SSTs from October–December onwards (Espinoza et al., 2013). During La Niña, the negative SST anomalies dominate the central equatorial Pacific, usually on the order of −1 and −2°C during strong events. The positive SST anomalies are often observed over the northern and southern Pacific and Atlantic oceans (either side of the negative anomalies), whilst cooler than usual waters are found off the coast of Brazil in the Atlantic Ocean (about 20° S) (Satyamurty et al., 2013).
- This pattern of the SSTs favours positive 850 hPa geopotential height anomalies over both the northern and southern Pacific and Atlantic oceans, with the stronger positive SSTs in the northern and southern Pacific resulting in stronger positive 850 hPa geopotential height anomalies (Espinoza et al., 2013) (Figure 7b). Negative 850 hPa anomalies are also observed between the positive anomalies (about 125° W).
- The succession of positive and negative 850 hPa geopotential height anomalies, features a Rossby wave response from October to December, in which warm air is transported from the Equator towards the Poles in an attempt to restore the atmospheric energy balance. These geopotential height patterns are shown to favour the enhancement of moisture convergence towards the Amazon basin via two mechanisms (Espinoza et al., 2013):

1. The easterly humidity flux is intensified over the North Atlantic and is directed towards the Caribbean Sea by the positive geopotential height anomaly situated in the North Atlantic before moving southwards towards the north-western Amazon (Figure 7b).
2. The southward positive geopotential height anomaly in the Atlantic is responsible for generating humidity fluxes that progress northwards near the Andes, reducing the monsoon flux towards the La Plata basin and the strength of the SLLJ which is responsible for transporting large amounts of moisture from the Amazon basin to the subtropics (Montini et al., 2019), and thus helping to maintain higher levels of humidity over the Amazon basin.

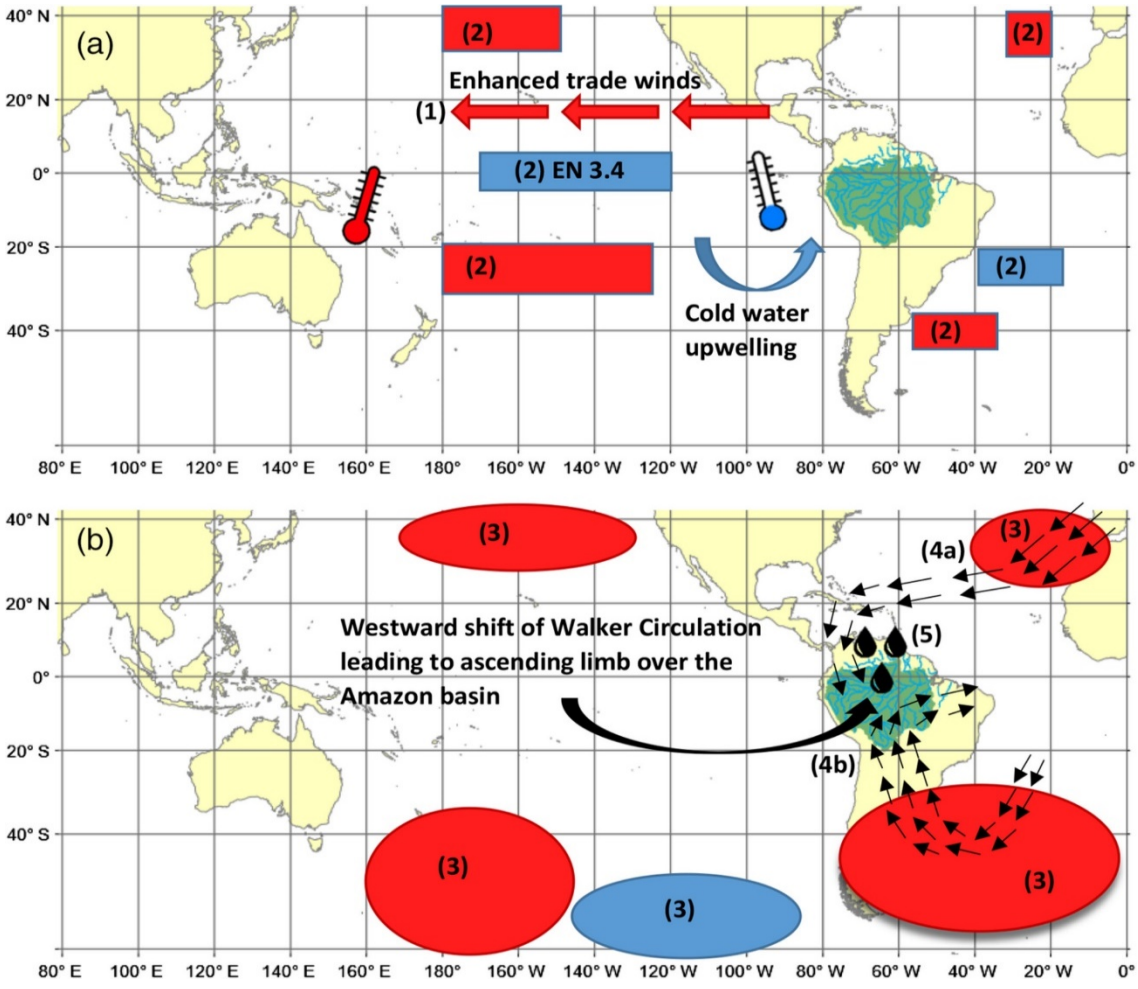


**Figure 7.** *Step-by-step climatic features associated with floods attributed to La Niña: (a) enhanced trade winds, cold water upwelling and sea surface temperature (SST) anomalies; and (b) 850 hPa geopotential height anomalies and humidity transport fluxes. Red (blue) colours represent positive (negative) anomalies of the SST and 850 hPa geopotential height; circles represent geopotential heights anomalies; squares/rectangles denote SST anomalies; and numbers refer to the specific processes explained in Section 2.5.4.*

- In addition to these two humidity fluxes, the SST pattern associated with La Niña results in the Walker Circulation shifting farther west, whereby the ascending limbs of moist air are situated over both the maritime continent and South America resulting in positive rainfall anomalies (Yeh et al., 2018)

Owing to the mechanisms described by Espinoza et al. (2013) for moisture convergence, it seems the intensity and locations of the 850 hPa geopotential height anomalies are pivotal to create the required atmospheric circulation for maintaining the convergence of humidity fluxes over the Amazon basin. As mentioned, these geopotential height anomalies are positioned where warmer than usual SSTs are situated in the northern and southern Pacific and Atlantic oceans and are stronger as the SSTs increase. Therefore, though the typical ENSO 3.4 region in the central Pacific is often used as the index to predict flooding through its role in shifting the Walker Circulation, these other zones of the SST variability could be influential in the prediction of upcoming events and deserve further investigation.

## 2.6 Conclusions

This review discusses out what is currently known about how climate variability influences rainfall, river discharge and flooding in the Amazon basin. This information is a key component in aiding flood prediction, providing potential sources of predictability at interannual to decadal timescales to enable the possible implementation of early warning systems (EWS). Based on evidence from studies in the published literature, it is clear that dry spells in the Amazon are driven by the warm phase of the El Niño Southern Oscillation (ENSO) and warmer than usual sea surface temperatures (SSTs) in the Tropical North Atlantic (TNA), particularly affecting the southern Amazon. While wetter conditions and flooding are often associated with the cold phase of the ENSO and to a combination of warm (cold) SST anomalies in the Tropical South Atlantic (TSA) (TNA). However, the meteorological and hydrological response in association with climate patterns such as La Niña are still not fully understood, and evidence for their usefulness for flood forecasting remains weak. Though there is a clear link between hydrometeorological variables and certain phases of climate, more research is required in calculating the probabilities of flood risk during certain climate patterns, particularly for years in which multiple climate variations feature simultaneously (e.g. a warm TSA and La Niña), and then communicating this information in an informative way to aid decision-making. Here, we identify five areas in which to focus research efforts to better understand how climate variability impacts flood risk in the Amazon basin.

### 2.6.1 Uncertainties and lack of evidence

The relationship between climate indices and hydrometeorological variables (i.e. rainfall and river discharge) can be highly uncertain owing to a range of factors. First, though strong correlations do exist between the ENSO and hydrometeorological variables, no two ENSO events are exactly alike (e.g. different temporal evolutions, spatial and magnitude differences of the SST anomalies), with asymmetrical differences found between the cold and warm phases (Cai et al., 2020). This is highlighted by several authors (Hill et al., 2009, 2011; Rodrigues and McPhaden, 2014) who have identified different or even opposing rainfall anomalies in different regions of the world depending on whether the centre of cooling or warming in the equatorial Pacific Ocean was central or eastern specific. Such differences are associated with the location of the SST anomalies modifying the Walker Circulation and, hence, upward convection and rainfall locations (Hill et al., 2009). Further evidence is required to understand the hydrological response in basins to the diversity of possible climatic events.

The back-water effect (Meade et al., 1991) and autocorrelation could also have an impact on correlations between climate phases and river flow as some commonly used statistical tests (e.g. Mann–Kendall and linear regression) may not be suitable for certain regions and rivers that have a large-basin memory (Marengo et al., 1998). Where autocorrelation exists, correlations may be overestimated and identify significant relationships where they do not exist, consequently leading to misleading significance. It is therefore an important reminder to consider running suitability checks on data before any climate analysis is undertaken. Such checks include plotting river flow using a correlogram (i.e. correlation of series data with itself), running a Durbin–Watson test and checking for trends and correlations for both rainfall and river discharge where possible owing to autocorrelation issues being less likely in rainfall data (Marengo et al., 1998).

The robustness in changes to hydrological variables are also debatable due to the observational records in both hydroclimatic drivers (e.g. the ENSO) and individual hydrological time series being limited in time (Wittenberg, 2009; Marengo and Espinoza, 2016; Marengo et al., 2018; Yeh et al., 2018). For instance, in the southern Amazon, the effect of the anomalous SSTs in the Atlantic Ocean on river discharge is dependent on the time period investigated, with an opposing response to the SST anomalies identified in neighbouring basins (Ronchail et al., 2005b). In this and similar works, the period of investigation is often limited to between 10 and 20 years, where few climate events (e.g. El Niño) feature, preventing strong conclusions to be made. This is particularly problematic when considering the relationship for lower

frequency climatic drivers (e.g. the PDO and AMO) that operate on decadal to multi-decadal timescales, as many station time series may only exist during one particular phase. Newly developed climate reanalysis and hydrological models can produce data sets that can extend the analysis back to 1950 (e.g. ERA-5; Zsoter et al., 2019), though the accuracy of simulated streamflow data requires robust evaluation. A model run incorporating ERA-5 as the meteorological input into a hydrological model was found to improve the ability to simulate annual peak river flows in the Amazon basin, particularly at stations situated within the Peruvian Amazon (Towner et al., 2019). The ERA-5 is now fully accessible back to 1950, and with the release of ERA-5 land, which incorporates the evolution of land surface variables (e.g. soil temperature) over several decades at an enhanced resolution compared with ERA-5 (ECMWF, 2020), and thus further investigation is required.

### 2.6.2 Understanding flood mechanisms

To enhance the predictability of flooding in the Amazon basin, more focus is needed to understand the mechanisms behind individual events and their potential to provide predictability. Two of the most extreme flood events (2012 in Iquitos and 2014 in the Madeira basin) were assessed individually (Espinoza et al., 2013, 2014), highlighting the mechanisms and atmospheric response associated behind each flood event in response to climate anomalies present in the atmosphere and surrounding oceans. However, other devastating, but less extreme, floods such as those observed in 1989, 1993 and 1999 are currently restricted to composite analysis in which the climatic conditions are smoothed across multiple events. Although the average conditions have been shown to produce atmospheric conditions responsible for flooding (e.g. Espinoza et al., 2013), it is unknown if the climate anomalies, which are weaker for certain events, would result in the same atmospheric response. Numerical analysis and modelling of the ocean–atmospheric response to each event individually could allow further evidence to be obtained in understanding the characteristics of the SST anomalies required to produce flooding across the basin (e.g. the spatial distribution and magnitude of the SSTs). Although complicated by the non-linearity in the response to climate phases such as the ENSO (Frauen et al., 2014) and by the limited number of observed events, such an analysis could provide useful information to flood forecasters and decision-makers within humanitarian sectors.

### 2.6.3 Flood timing and additional indices

In March 2018, the Red Cross led an inter-agency assessment mission to assess how communities in the Peruvian Amazon were affected during particularly strong flood events, such as those observed in 2012 and 2015 to aid decision-making. Problems associated with the duration of the wet season rather than solely the magnitude of extreme flooding was highlighted by residents living within the floodplain (Bazo, 2018). Several authors (Ronchail et al., 2006; Tomasella et al., 2011; Marengo et al., 2012; Espinoza et al., 2013; Langill and Abizaid, 2019) highlight the importance of flood timing in major Amazonian tributaries in the dampening or superposition of the travelling Amazon flood wave along the main stem. Therefore, we encourage more authors to consider both flood timing and duration in addition to flood magnitude when investigating the influence of different phases of large-scale climate variability. In addition, many studies focus on the conventional SST and sea-surface pressure definitions of the ENSO events, disregarding atmospheric variables such as outgoing long wave radiation (OLR) and zonal wind speeds, which have been proven to show to improved predictability in certain regions of the world (Chiodi and Harrison, 2013, 2015; Barichivich et al., 2018). Future analysis would be useful in understanding the response of hydrometeorological parameters to the different ENSO types in the Amazon basin through an intercomparison analysis. Ideally this would incorporate both spatially defined (e.g. East Pacific and central Pacific El Niños) and variable specific indices such as the OLR defined events. Such work has already begun for extreme precipitation events in South America (Tedeschi et al., 2016), summer rainfall over Peru (Sulca et al., 2018) and recent droughts in the Amazon basin (Jimenez et al., 2019).

### 2.6.4 Impact of indices on forecast skill

Understanding how different modes of climate variability affect rainfall and river discharge in the Amazon basin could indicate that a realistic representation of these modes is an important component for a climate model that aims to simulate flooding in the Amazon. Hence, it is important to know how well models can capture particular climate features, in addition to knowing by how much does the inclusion of capturing climate features (e.g. phases of MJO) in the initial conditions of forecasts improve performance. Previous research at the European Centre for Medium-Range Weather Forecasts (ECMWF) has focused on how the incorporation of observations during active phases of the Madden–Julian Oscillation (MJO) in the initial conditions of forecasts influences the ability to predict meteorological variables in the

Northern Hemisphere (Vitart and Molteni, 2016). A similar analysis would be useful for the Amazon to explore whether or not hydrological forecasts of river flow have increased skill during particular phases of the ENSO, the tropical Atlantic or the MJO. If model performance were found to increase for particular climate conditions, humanitarian managers using information from climate models could have more confidence in the forecasts when using such information for decision-making. Moreover, knowing how different models capture large-scale climate features and if, or not, they increase forecast performance can provide a useful input when trying to eliminate unrealistic models and focus on more realistic models for certain variables.

### 2.6.5 Calculating flood probabilities

The ultimate question, particularly with regards to decision-making, would be how much higher are the chances of flooding if a climate mode is in a particular phase. For example, by how much does the likelihood of flooding increase in the Amazon during the cold phase of the ENSO? Similar to the global scale analysis performed by Emerton et al. (2017) for the ENSO, it would be a worthwhile task to undertake a similar analysis specifically for the Amazon Basin and to extend it to include a range of indices such as the TNA, TSA and MJO. Within such a study, it would be worth considering the probabilities of both single and combined phases of different indices (e.g. just La Niña and warm TSA and La Niña combined), in addition to calculating the probabilities for different types of the ENSO events (e.g. east Pacific versus central Pacific). Doing so could provide added predictability over the use of a single index as a predictor (Emerton et al., 2019), and would provide a more complete picture of a range of different climate scenarios. Finally, the analysis could be further broken down to consider the probabilities of exceeding a particular percentile or threshold of river flows for different intensities of climate phases (e.g. for weak, medium or strong La Niña events). Again, although complicated by the limited number of events, this analysis could help one to understand some of the uncertainties surrounding the impacts of climate indices. For instance, Nobre et al. (2019) provide the example of several countries taking preparedness measures during the strong 2015–2016 El Niño event for expected flooding associated with the elevated probability of flooding during the warm phase of the ENSO. In this instance, Peru (northern regions outside of the Amazon) experienced severe floods, while no flooding occurred in Japan, despite the elevated probability during this particular ENSO phase. Extending the analysis to consider the intensity, spatial complexities and combinations of various climate indices could allow further insights into the uncertainties surrounding the influence of climate phases on the

likelihood of floods in certain locations. This work would ideally be supplemented to consider the socioeconomic impacts to different phases of climate (Di Baldassarre et al., 2015), as the recording of floods also depends on a region's ability to mitigate, cope, and recover.

**Acknowledgements.** This work was supported by the Natural Environment Research Council (NERC) as part of the SCENARIO Doctoral Training Partnership (grant agreement number NE/L002566/1). The first author is grateful for additional travel support and funding provided by the Red Cross Red Crescent Climate Centre. A special thanks to the observational and national services, SO-HYBAM, SENAMHI, ANA, INAMHI and IRD, for providing observed river discharge data and advice throughout the writing of the paper. For access to river flow data please contact the Institute of Research for Development (IRD). The authors declare that they have no conflict of interest.

## 2.7 Supplementary material

Supplementary tables associated with Figures 2 to 5 can be found below.

**Table S1.** *Details of results (e.g. analysis type, location, period) from previous studies exploring the relationship between rainfall and the warm phase of ENSO, on an annual timescale.*

| Fig/ Driver | Annual/ season | Author | Location | Analysis/strength of signal | Period | Wet/ dry | Colour on map |
|---|---|---|---|---|---|---|---|
| **Fig. 2a – El Niño** | Annual (Aug-Jul) | Ronchail and Gallaire (2006) | Trinidad station (Bolivian lowlands) | Correlation and composite analysis between annual rainfall and DJF ENSO indices - El Niño/dry signal | 1971-2001 | Wet | Blue |
| **Fig. 2a – El Niño** | Annual (Sep-Aug) | Ronchail et al. (2002) | NEA stations (~ north of $7^0$ S; east of $60^0$ W) | Composite analysis of annual rainfall anomalies during El Niño years<br><br>Mean annual rainfall anomaly = -1.1 S.D (mostly significant; 72% in NEA region) | 1977-1999 | Dry | Red |
| **Fig. 2a – El Niño** | Annual (Sep-Aug) | Ronchail et al. (2002) | Branco basin stations (far north) | Composite analysis of annual rainfall anomalies during El Niño years<br><br>Mean annual rainfall anomaly = -0.5 to -1.1 S.D (mostly insignificant) | 1977-1999 | Dry | Red |
| **Fig. 2a – El Niño** | Annual (Sep-Aug) | Ronchail et al. (2002) Tobar & Wyseure (2018) | Ecuadorian Amazon stations | Composite analysis of annual rainfall anomalies during El Niño years<br><br>Mean annual rainfall anomaly = ~0.5 S.D (all insignificant | 1977-1999 | Wet/ No difference | Black |
| **Fig. 2a – El Niño** | Annual (Sep-Aug) | Ronchail et al. (2002) | Peruvian Amazon – Tamshiyacu station | Composite analysis of rainfall anomalies during El Niño years<br><br>Rainfall anomaly = ~0.3 S.D (insignificant) | 1977-1999 | Wet | Blue |
| **Fig. 2a – El Niño** | Annual (Jan-Dec) | Yoon and Zeng (2010) | Throughout the basin | Correlation analysis - strong and widespread, with highest correlations towards the mouth of the Amazon River (-0.2 to -0.9) | 1979-2006 | Dry | Red hatching and dark red |

**Table S2.** *Details of results (e.g. analysis type, location, period) from previous studies exploring the relationship between rainfall and the warm phase of ENSO, for the Amazon wet season.*

| Fig/ Driver | Annual/ season | Author | Location | Analysis/strength of signal | Period | Wet/ dry | Colour on map |
|---|---|---|---|---|---|---|---|
| **Fig. 2b – El Niño** | Wet (DJF) | Ronchail et al. (2002) | NEA stations (north of $7^0$ S; east of $60^0$ W) | Composite analysis of DJF rainfall anomalies during El Niño years<br><br>Mean annual rainfall anomaly = -0.7 (mostly significant) | 1977-1999 | Dry | Red |
| **Fig. 2b – El Niño** | Wet (DJF) | Ronchail et al. (2002) | Branco basin stations – far north | Composite analysis of DJF rainfall anomalies during El Niño years<br><br>Mean annual rainfall anomaly = -0.5 to -0.8 S.D (mostly significant) | 1977-1999 | Dry | Red |
| **Fig. 2b – El Niño** | Wet (MAM) | Ronchail et al. (2002) | Ecuadorian Amazon stations | Composite analysis of DJF rainfall anomalies during El Niño years<br><br>Mean annual rainfall anomaly = 0.5 to 1 S.D (many stations are deemed significant) | 1977-1999 | Wet | Blue |
| **Fig. 2b – El Niño** | Wet (DJF) | Liebman n and Mareng o (2001) | Eastern equatorial Amazon (East of $60^0$ W to $50^0$ W and south of the equator to $5^0$ S) | Correlation analysis between area averaged station DJF rainfall and 3-monthly DJF Niño 3.4 SSTs<br><br>Large negative correlation up to -0.9 | 1976-1997 | Dry | Dark red |

| | | | | | | | |
|---|---|---|---|---|---|---|---|
| **Fig. 2b – El Niño** | Wet (DJF) | Liebmann and Marengo (2001) | North-north-western Amazon (west of $60^0$ W to around $65^0$ W and centered north of the equator (Branco) | Correlation analysis between area averaged station DJF rainfall and 3-monthly DJF Niño 3.4 SSTs<br><br>Large negative correlation up to -0.7 | 1976-1997 | Dry | Red |
| **Fig. 2b – El Niño** | Annual (Dec-Apr) | Yoon and Zeng (2010) | Throughout the basin | Correlation analysis - strong and widespread, with highest correlations towards the mouth of the Amazon River (-0.2 to -0.9) | 1979-2006 | Dry | Red hatching and dark red |
| **Fig. 2b – El Niño** | Wet (Oct-Mar) | Lagos et al. (2008) | Peruvian Amazon – Tamshiyacu station | Correlation coefficient (Lagos et al., 2008) varies between -0.29 and 0.29 when comparing monthly rainfall | 1950-2002 | Wet and dry | Black |

**Table S3.** *Details of results (e.g. analysis type, location, period) from previous studies exploring the relationship between rainfall and the warm phase of ENSO, for the Amazon dry season.*

| Fig/ Driver | Annual/ season | Author | Location | Analysis/strength of signal | Period | Wet/ dry | Colour on map |
|---|---|---|---|---|---|---|---|
| **Fig. 2c – El Niño** | Dry (Jun-Oct) | Yoon and Zeng (2010) | Towards the north and east of the basin (~east of $65^0$ W and north of ~$5^0$ S) | Correlation analysis - Correlation limited to far north and east of the basin (-0.2 to -0.8) | 1979-2006 | Dry | Red |

**Table S4.** *Details of results (e.g. analysis type, location, period) from previous studies exploring the relationship between rainfall and the cold phase of ENSO, on an annual timescale.*

| Fig/ Driver | Annual/ season | Author | Location | Analysis/strength of signal | Period | Wet/ dry | Colour on map |
|---|---|---|---|---|---|---|---|
| **Fig. 2d – La Niña** | Annual (Aug-Jul) | Ronchail and Gallaire (2006) | Trinidad station (Bolivian lowlands) | Correlation and composite analysis between annual rainfall and DJF ENSO indices - La Niña/dry signal (r = 0.51 for Niño 3.4 region) | 1971-2001 | Dry | Red |
| **Fig. 2d – La Niña** | Annual (Sep-Aug) | Ronchail et al. (2002) | North eastern Amazon stations (~ north of $7^0$ S; east of $60^0$ W) | Composite analysis of annual rainfall anomalies during La Niña years<br><br>Mean annual rainfall anomaly = 1 S.D (mostly significant) | 1977-1999 | Wet | Blue |
| **Fig. 2d – La Niña** | Annual (Sep-Aug) | Ronchail et al. (2002) | Branco basin stations – far north | Composite analysis of annual rainfall anomalies during La Niña years<br><br>Mean annual rainfall anomaly = 1 S.D (mostly significant) | 1977-1999 | Wet | Blue |
| **Fig. 2d – La Niña** | Annual (Sep-Aug) | Ronchail et al. (2002) | Peruvian Amazon – Tamshiyacu station (Iquitos) | Composite analysis of annual rainfall anomalies during La Niña years<br><br>Rainfall anomaly = ~-0.3 S.D (insignificant) | 1977-1999 | Dry | Red |
| **Fig. 2d – La Niña** | Annual (Jan-Dec) | Yoon and Zeng (2010) | Throughout the basin | Correlation analysis - strong and widespread, with highest correlations towards the mouth of the Amazon River (-0.2 to -0.9) | 1979-2006 | Wet | Blue hatching and dark blue |
| **Fig. 2d – La Niña** | Annual | Poveda and Mesa, 1993; Espinoza et al., 2009b) | Colombian Amazon | Correlation analysis – weak correlation | NA | Wet | Light blue |

**Table S5.** *Details of results (e.g. analysis type, location, period) from previous studies exploring the relationship between rainfall and the cold phase of ENSO, for the Amazon wet season.*

| Fig/ Driver | Annual/ season | Author | Location | Analysis/strength of signal | Period | Wet/ dry | Colour on map |
|---|---|---|---|---|---|---|---|
| **Fig. 2e – La Niña** | Wet (Feb) | Ronchail and Gallaire (2006) | Trinidad station (Bolivian lowlands) | Correlation and composite analysis between DJF rainfall and monthly ENSO anomalies - La Niña/dry signal identified | 1971-2001 | Dry | Red |
| **Fig. 2e – La Niña** | Wet (DJF) | Ronchail et al. (2002) | NEA stations (north of $7^0$ S up to the equator; east of $60^0$ W) | Composite analysis of MAM rainfall anomalies during La Niña years<br><br>Mean annual rainfall anomaly = ~0.8 S.D (mostly significant) | 1977-1999 | Wet | Blue |
| **Fig. 2e – La Niña** | Wet (DJF) | Ronchail et al. (2002) | Branco basin stations – far north | Composite analysis of MAM rainfall anomalies during La Niña years<br><br>Mean annual rainfall anomaly = ~0.8 S.D (mostly significant) | 1977-1999 | Wet | Blue |
| **Fig. 2e – La Niña** | Wet | Poveda and Mesa, 1993; Espinoza et al., 2009b) | Colombian Amazon | Correlation analysis – weak correlation | NA | Wet | Light blue |
| **Fig. 2e – La Niña** | Wet (Dec-Apr) | Yoon and Zeng (2010) | Throughout the basin | Correlation analysis - strong and widespread, with highest correlations towards the mouth of the Amazon River (-0.2 to -0.9) | 1979-2006 | Wet | Blue hatching and dark blue |
| **Fig. 2e – La Niña** | Wet (DJF) | Liebmann and Marengo (2001) | Eastern equatorial Amazon (East of $60^0$ W to $50^0$ W and south of the equator to $5^0$ S) | Correlation analysis between area averaged station DJF rainfall and 3-monthly DJF Niño 3.4 SSTs<br><br>Large negative correlation up to -0.9 | 1976-1997 | Wet | Dark blue |

| | | | | | | | |
|---|---|---|---|---|---|---|---|
| **Fig. 2e – La Niña** | Amazon wet (DJF) | Liebmann and Marengo (2001) | North-north-western Amazon (west of $60^0$ W to around $65^0$ W and centered north of the equator (Branco) | Correlation analysis between area averaged station DJF rainfall and 3-monthly DJF Niño 3.4 SSTs<br><br>Large negative correlation up to -0.7 | 1976-1997 | Wet | Blue |

**Table S6.** *Details of results (e.g. analysis type, location, period) from previous studies exploring the relationship between rainfall and the cold phase of ENSO, for the Amazon dry season.*

| Fig/ Driver | Annual/ season | Author | Location | Analysis/strength of signal | Period | Wet/ dry | Colour on map |
|---|---|---|---|---|---|---|---|
| **Fig. 2f – La Niña** | Amazon dry (May and September) | Ronchail and Gallaire (2006) | Trinidad station (Bolivian lowlands) | Correlation analysis - La Niña/dry signal | 1971-2001 | Dry | Red |
| **Fig. 2f – La Niña** | Amazon dry (JJA) | Ronchail et al. (2002) | NEA stations (~ north of $7^0$ S; east of $60^0$ W) | Composite analysis of JJA rainfall anomalies during La Niña years<br><br>Mean annual rainfall anomaly = ~0.1 to 1 S.D (mostly insignificant) | 1977-1999 | Wet | Light blue |
| **Fig. 2f – La Niña** | Amazon dry (JJA) | Ronchail et al. (2002) | Branco basin stations – far north | Composite analysis of JJA rainfall anomalies during La Niña years<br><br>Mean annual rainfall anomaly =~1 S.D (mostly significant) | 1977-1999 | Wet | Blue |
| **Fig. 2f – La Niña** | Amazon dry (JJA) | Ronchail et al. (2002) | Stations in the southern Amazon, particularly in the Bolivian Amazon (East of ~$70^0$ W and below -$10^0$ S) | Composite analysis of JJA rainfall anomalies during La Niña years<br><br>Mean annual rainfall anomaly = -0.5 to -0.75 S.D (mostly significant but stations are widespread) | 1977-1999 | Dry | Red |

| | | | | | | | |
|---|---|---|---|---|---|---|---|
| **Fig. 2f – La Niña** | Amazon dry (JJA) | Ronchail et al. (2002) | Peruvian Amazon – Tamshiyacu station (Iquitos) | Composite analysis of JJA rainfall anomalies during La Niña years<br><br>Rainfall anomaly = ~-0.7 S.D (significant) | 1977-1999 | Dry | Red |

**Table S7.** *Details of results (e.g. analysis type, location, period) from previous studies exploring the relationship between rainfall and warm SSTs in the TNA, on an annual timescale.*

| **Fig/ Driver** | **Annual/ season** | **Author** | **Location** | **Analysis/strength of signal** | **Period** | **Wet /dry** | **Colour on map** |
|---|---|---|---|---|---|---|---|
| **Fig. 3a Warm TNA** | Annual (Jan-Dec) | Yoon and Zeng (2010) | Whole basin | Correlation analysis - strong and widespread, with highest correlations towards the southern Amazon (-0.2 to -0.7) | 1979-2006 | Dry | Red hatching (dark red for southern Amazon) |
| **Fig. 3a Warm TNA** | Annual (Jan-Dec) | Zeng (2008) | Whole basin | Correlation analysis between SST in the TNA and averaged outgoing longwave radiation precipitation index (OPI) satellite rainfall – strong and widespread with highest correlations towards the southern Amazon (-0.4 to -0.8) | 1979-2006 | Dry | Red hatching (dark red for southern Amazon) |

**Table S8.** *Details of results (e.g. analysis type, location, period) from previous studies exploring the relationship between rainfall and warm SSTs in the TNA, for the Amazon wet season.*

| Fig/ Driver | Annual /season | Author | Location | Analysis/strength of signal | Period | Wet /dry | Colour on map |
|---|---|---|---|---|---|---|---|
| **Fig. 3b Warm TNA** | Wet (Dec-Apr) | Yoon and Zeng (2010) | Predominately southern Amazon | Correlation analysis - strong and widespread, with highest correlations towards the southern Amazon (-0.2 to -0.7) | 1979-2006 | Dry | Red |
| **Fig. 3b Warm TNA** | Wet (MAM) | Ronchail et al. (2002) | NEA stations (~ north of $7^0$ S; east of $60^0$ W) | Composite analysis of MAM rainfall anomalies during phases of warm TNA SST anomalies<br><br>MAM rainfall anomalies = ~-0.5 to -0.8 S.D (mostly significant) | 1977-1999 | Dry | Red |
| **Fig. 3b Warm TNA** | Wet (MAM) | Ronchail et al. (2002) | Iquitos station, Peruvian Amazon | Composite analysis of annual rainfall anomalies during cold TSA years (excludes years with ENSO)<br><br>Annual rainfall anomaly = ~0.8 S.D | 1977-1999 | Wet | Blue |

**Table S9.** *Details of results (e.g. analysis type, location, period) from previous studies exploring the relationship between rainfall and warm SSTs in the TNA, for the Amazon dry season.*

| Fig/ Driver | Annual/ season | Author | Location | Analysis/strength of signal | Period | Wet /dry | Colour on map |
|---|---|---|---|---|---|---|---|
| **Fig. 3c Warm TNA** | Dry (June-October) | Yoon and Zeng (2010) | Majority of the eastern basin | Correlation analysis - strong and widespread, with highest correlations towards the south-eastern Amazon (-0.2 to -0.8) | 1979-2006 | Dry | Red |
| **Fig. 3c Warm TNA** | Dry (JJA) | Ronchail et al. (2002) | Ecuadorian Amazon | Composite analysis of JJA rainfall anomalies during phases of warm TNA SST anomalies<br><br>JJA rainfall anomalies = 0.5 to 1 S.D (mostly significant) | 1977-1999 | Dry | Red |
| **Fig. 3c Warm TNA** | Dry (May-Sep) | Yoon (2016) | Southern Amazon Basin ($65^0$ W to $50^0$ W and $-20^0$ S to $-5^0$ S) | Idealised experiments using 5 atmospheric global climate models (AGCMs) to test the response of rainfall to warm/cold TNA SST compared to neutral conditions<br><br>Daily rainfall anomalies ranged between -0.1 and -0.35 mm/day depending on the model | | Dry | Red |

**Table S10.** *Details of results (e.g. analysis type, location, period) from previous studies exploring the relationship between rainfall and cold SSTs in the TNA, on an annual timescale.*

| Fig/ Driver | Annual/ season | Author | Location | Analysis/strength of signal | Period | Wet /dry | Colour on map |
|---|---|---|---|---|---|---|---|
| **Fig. 3d Cold TNA** | Annual (Jan-Dec) | Yoon and Zeng (2010) | Whole basin | Correlation analysis - strong and widespread, with highest correlations towards the southern Amazon (-0.2 to -0.7) | 1979-2006 | Wet | Blue |
| **Fig. 3d Cold TNA** | Annual (Jan-Dec) | Zeng (2008) | Whole basin | Correlation analysis – strong and widespread with highest correlations towards the southern Amazon (-0.4 to -0.8) | 1979-2006 | Wet | Blue |

**Table S11.** *Details of results (e.g. analysis type, location, period) from previous studies exploring the relationship between rainfall and cold SSTs in the TNA, for the Amazon wet season.*

| Fig/ Driver | Annual/ season | Author | Location | Analysis/strength of signal | Period | Wet /dry | Colour on map |
|---|---|---|---|---|---|---|---|
| **Fig. 3e Cold TNA** | Wet (MAM) | Ronchail et al. (2002) | NEA stations (~ north of $7^0$ S; east of $60^0$ W) | Composite analysis of MAM rainfall anomalies during phases of cold TNA SST anomalies<br><br>Mean MAM rainfall anomaly = 0.5 S.D (mostly significant) | 1977-1999 | Wet | Blue |
| **Fig. 3e Cold TNA** | Wet (Dec-Apr) | Yoon and Zeng (2010) | Predominately southern Amazon | Correlation analysis - strong and widespread, with highest correlations towards the southern Amazon (-0.2 to -0.7) | 1979-2006 | Wet | Blue |

| | | | | | | | |
|---|---|---|---|---|---|---|---|
| **Fig. 3e Cold TNA** | Wet (MAM) | Ronchail et al. (2002) | Iquitos station, Peruvian Amazon | Composite analysis of annual rainfall anomalies during cold TSA years (excludes years with ENSO)<br><br>annual rainfall anomaly = ~-0.7 S.D | 1977-1999 | Red | Dry |

**Table S12.** *Details of results (e.g. analysis type, location, period) from previous studies exploring the relationship between rainfall and cold SSTs in the TNA, for the Amazon dry season.*

| Fig/ Driver | Annual /season | Author | Location | Analysis/strength of signal | Period | Wet /dry | Colour on map |
|---|---|---|---|---|---|---|---|
| **Fig. 3f Cold TNA** | Dry (Jun-Oct) | Yoon and Zeng (2010) | Majority of the eastern basin | Correlation analysis - strong and widespread, with highest correlations towards the south-eastern Amazon (-0.2 to -0.8) | 1979-2006 | Wet | Blue |
| **Fig. 3f Cold TNA** | Dry (May-Sep) | Yoon (2016) | Southern Amazon Basin ($65^0$ W to $50^0$ W and -$20^0$ S to -$5^0$ S) | Idealised experiments using 5 atmospheric global climate models (AGCMs) to test the response of rainfall to warm/cold TNA SST compared to neutral conditions<br><br>Daily rainfall anomalies ranged between -0.1 and 0.4 mm/day depending on the model | | Wet | Blue |

**Table S13.** *Details of results (e.g. analysis type, location, period) from previous studies exploring the relationship between rainfall and warm SSTs in the TSA, on an annual timescale.*

| Fig/ Driver | Annual/ season | Author | Location | Analysis/strength of signal | Period | Wet /dry | Colour on map |
|---|---|---|---|---|---|---|---|
| **Fig. 3g Warm TSA** | Annual (Sep-Aug) | Ronchail et al. (2002) | Stations situated near to the mouth of the Amazon River | Composite analysis of MAM rainfall anomalies during phases of cold TSA SST anomalies<br>Rainfall anomalies deemed positively significant | 1977-1999 | Wet | Blue |

**Table S14.** *Details of results (e.g. analysis type, location, period) from previous studies exploring the relationship between rainfall and warm SSTs in the TSA, for the Amazon wet season.*

| Fig/ Driver | Annual/ season | Author | Location | Analysis/strength of signal | Period | Wet /dry | Colour on map |
|---|---|---|---|---|---|---|---|
| **Fig. 3h Warm TSA** | Wet (Dec-Apr) | Yoon and Zeng (2010) | Branco catchment | Correlation analysis – correlations between TSA and wet season rainfall constricted to far north (r = ~-0.2 to -0.6) | 1979-2006 | Wet | Blue |
| **Fig. 3h Warm TSA** | Wet (MAM) | Ronchail et al. (2002) | NEA stations (~ north of $7^0$ S; east of $60^0$ W) | Composite analysis of MAM rainfall anomalies during phases of cold TSA SST anomalies<br>MAM rainfall anomalies = 0.5 to 0.1 S.D (mostly significant) | 1977-1999 | Wet | Blue |

**Table S15.** *Details of results (e.g. analysis type, location, period) from previous studies exploring the relationship between rainfall and warm SSTs in the TSA, for the Amazon dry season.*

| Fig/ Driver | Annual /season | Author | Location | Analysis/strength of signal | Period | Wet /dry | Colour on map |
|---|---|---|---|---|---|---|---|
| **Fig. 3i Warm TSA** | Dry (June-Oct) | Yoon and Zeng (2010) | Southern Amazon (below $12^0$ S and east of $65^0$ W) | Correlation analysis – significant correlation between TSA and wet season rainfall constricted to southern Amazon (r = ~-0.3 to -0.5) | 1979-2006 | Wet | Blue |

**Table S16.** *Details of results (e.g. analysis type, location, period) from previous studies exploring the relationship between rainfall and cold SSTs in the TSA, on an annual timescale.*

| Fig/ Driver | Annual/ season | Author | Location | Analysis/strength of signal | Period | Wet/ dry | Colour on map |
|---|---|---|---|---|---|---|---|
| **Fig. 3j Cold TSA** | Annual (Sep-Aug) | Ronchail et al. (2002) | NEA stations (~ north of $7^0$ S; east of $60^0$ W) | Composite analysis of annual rainfall anomalies during cold TSA years (includes years with ENSO)<br><br>Annual rainfall anomalies = mostly -0.9 S.D (mostly significant) | 1977-1999 | Dry | Red |
| **Fig. 3j Cold TSA** | Annual (Sep-Aug) | Ronchail et al. (2002) | Branco catchment stations – far north | Composite analysis of annual rainfall anomalies during cold TSA years (includes years with ENSO)<br><br>annual rainfall anomalies = ~0.8 S.D (mostly significant) | 1977-1999 | Dry | Red |
| **Fig. 3j Cold TSA** | Annual (Sep-Aug) | Ronchail et al. (2002) | Ecuadorian Amazon | Composite analysis of annual rainfall anomalies during cold TSA years (excludes years with ENSO)<br><br>annual rainfall anomalies = ~-0.5 to -1 S.D (mostly significant) | 1977-1999 | Dry | Red |

| | | | | | | | |
|---|---|---|---|---|---|---|---|
| **Fig. 3j Cold TSA** | Annual (Sep-Aug) | Ronchail et al. (2002) | Selection of stations in the Bolivian Amazon | Composite analysis of annual rainfall anomalies during cold TSA years (excludes years with ENSO)<br><br>annual rainfall anomalies = ~0.5 to 0.75 S.D | 1977-1999 | Wet | Blue |
| **Fig. 3j Cold TSA** | Annual (Sep-Aug) | Ronchail et al. (2002) | Iquitos station, Peruvian Amazon | Composite analysis of annual rainfall anomalies during cold TSA years (includes years with ENSO)<br>Annual rainfall anomaly = ~0.4 S.D | 1977-1999 | Wet | Blue |

**Table S17.** *Details of results (e.g. analysis type, location, period) from previous studies exploring the relationship between rainfall and cold SSTs in the TSA, for the Amazon wet season.*

| Fig/ Driver | Annual /season | Author | Location | Analysis/strength of signal | Period | Wet /dry | Colour on map |
|---|---|---|---|---|---|---|---|
| **Fig. 3k Cold TSA** | Wet (Dec-Apr) | Yoon and Zeng (2010) | Branco catchment | Correlation analysis – significant correlation between TSA and wet season rainfall constricted to far north (r = ~-0.2 to -0.6) | 1979-2006 | Dry | Red |

**Table S18.** *Details of results (e.g. analysis type, location, period) from previous studies exploring the relationship between rainfall and cold SSTs in the TSA, for the Amazon dry season.*

| Fig/ Driver | Annual /season | Author | Location | Analysis/strength of signal | Period | Wet /dry | Colour on map |
|---|---|---|---|---|---|---|---|
| **Fig. 3l Cold TSA** | Dry (June-Oct) | Yoon and Zeng (2010) | Southern Amazon (below $12^0$ S and east of $65^0$ W) | Correlation analysis – significant correlation between TSA and wet season rainfall constricted to southern Amazon (r = ~-0.3 to -0.5) | 1979-2006 | Dry | Red |

**Table S19.** *Details of results (e.g. analysis type, location, period) from previous studies exploring the relationship between river discharge and the warm phase of ENSO, on an annual timescale.*

| Fig/ Driver | Annual/ season | Author | Location | Analysis/strength of signal | Period | Wet/ dry | Colour on map |
|---|---|---|---|---|---|---|---|
| **Fig. 4a El Niño** | Annual | Espinoza et al. (2009a) | Most of the Amazon with the exception of the Madeira basin | Principal Components Analysis (PCA). Bravais–Pearson correlation between the PC1-Qmean time series and SOI<br><br>r = 0.52 | 1974-2004 | Dry | Red hatched markings |
| **Fig. 4a El Niño** | Annual | Ronchail et al. (2005b) | Majority of the basin, particularly NEA rivers and downstrea m in the Xingu river (Altamira station) | Composites and correlation analysis between observed discharge (annual mean, max and min) and SSTs<br><br>Major negative discharge anomalies. Up to 50% reduction in river flow | 1981-2002 | Dry | Red |
| **Fig. 4a El Niño** | Annual | Ronchail et al. (2005b) | Along the Purus River and some right-hand tributaries of the Madeira River (Ji-Parana, Aripuana, and Sucunduri) | Composites and correlation analysis between observed discharge (annual mean, max and min) and SSTs<br><br>Significant negative discharge anomalies. Discharge reduced by 25% | 1981-2002 | Dry | Red |
| **Fig. 4a El Niño** | Annual | Ronchail et al. (2005b) | In the upper Negro River (Tiquie, Uaupes) and in the Japura River, in the north-western most regions | Composites and correlation analysis between observed discharge (annual mean, max and min) and SSTs<br><br>Tendency for higher flows, though insignificant | 1981-2002 | Wet | Light blue |

| | | | | | | | |
|---|---|---|---|---|---|---|---|
| **Fig. 4a El Niño** | Annual | Ward et al. (2010) | Stations located in tropical regions (23.4°N and 23.4°S) | Correlation between river discharge and the atmospheric SOI index | 1921-1950 and 1951-1980 | Dry | Red hatched markings |
| **Fig. 4a El Niño** | Annual | Foley et al. (2002) | Óbidos gauging station | Comparison of average annual river discharge for composites of El Niño and La Niña years<br><br>Changes in discharge for El Niño years are close to zero | 1970-1995 | No change | Black |
| **Fig. 4a El Niño** | Annual | Richey et al. (1989) | Manacapuru gauging station | Cross spectrum analysis of flow anomalies with ENSO indicators<br><br>Low levels of discharge are strongly correlated to warm events | 1903-1985 | Dry | Red |

**Table S20.** *Details of results (e.g. analysis type, location, period) from previous studies exploring the relationship between river discharge and the warm phase of ENSO, for the Amazon wet season.*

| Fig/ Driver | Annual/ season | Author | Location | Analysis/strength of signal | Period | Wet/ dry | Colour on map |
|---|---|---|---|---|---|---|---|
| **Fig. 4b El Niño** | Wet (Apr-Jun) | Emerton et al. (2017) | Much of the Brazilian Amazon, south of the Amazon River, particularly towards eastern catchments | Estimates of historical probabilities of river flows during El Niño and La Niña years<br><br>Probability of 40-60%, during the decaying phase | 1901-2010 | Dry | Red |

| | | | | | | | |
|---|---|---|---|---|---|---|---|
| **Fig. 4b El Niño** | Wet (Feb-Jun) | Emerton et al. (2017) | North of the Amazon River towards the north-eastern Amazon | Estimates of historical probabilities of river flows during El Niño and La Niña years<br><br>Probability of 40-80%, during the decaying phase | 1901-2010 | Dry | Red |
| **Fig. 4b El Niño** | Wet (Feb-Apr) | Emerton et al. (2017) | Edge of the Peruvian Amazon, around the Ucayali catchment and Bolivian Amazon | Estimates of historical probabilities of river flows during El Niño and La Niña years<br><br>Probability of 40-60%, during the decaying phase | 1901-2010 | Dry | Red |
| **Fig. 4b El Niño** | Wet (Feb) | Schöngart and Junk, 2007 | Negro River | Correlations between maximum water levels and SOI and Niño 3.4 SST anomalies<br>T value = -3.97, p < 0.001<br>r = -0.49 (Niño 3.4 SST)<br>During El Niño events water levels are significantly lower | 1950-2000 | Dry | Red |
| **Fig. 4b El Niño** | Wet (Apr-Jun) | Foley et al. (2002) | Whole basin – majority of rivers | Analysis of land surface model coupled with a hydrological routing algorithm (HYDRA) to examine how phases of ENSO affect land surface parameters including discharge<br><br>A decrease in river discharge in found in many rivers which leads to a decrease in flooded area along the main-stem | 1950-1995 | Dry | Red |

**Table S21.** *Details of results (e.g. analysis type, location, period) from previous studies exploring the relationship between river discharge and the warm phase of ENSO, for the Amazon dry season.*

| Fig/ Driver | Annual/ season | Author | Location | Analysis/strength of signal | Period | Wet/ dry | Colour on map |
|---|---|---|---|---|---|---|---|
| **Fig. 4c El Niño** | Dry (Jul-Sep) | Emerton et al. (2017) | South of the Amazon River towards the west of the basin | Estimates of historical probabilities of river flows during El Niño and La Niña years<br><br>Probability of 40-60%, during the evolution phase | 1901-2010 | Wet | Blue |
| **Fig. 4c El Niño** | Dry (Aug-Dec) | Emerton et al. (2017) | North of the Amazon River towards the north-eastern Amazon | Estimates of historical probabilities of river flows during El Niño and La Niña years<br><br>Probability of 40-70%, during the evolution phase | 1901-2010 | Dry | Red |
| **Fig. 4c El Niño** | Dry (Dec) | Emerton et al. (2017) | Brazilian Amazon, south of the Amazon River towards the east | Estimates of historical probabilities of river flows during El Niño and La Niña years<br><br>Probability of 40-50%, during the evolution phase | 1901-2010 | Dry | Red |

**Table S22.** *Details of results (e.g. analysis type, location, period) from previous studies exploring the relationship between river discharge and the cold phase of ENSO, on an annual timescale.*

| Fig/ Driver | Annual/ season | Author | Location | Analysis/strength of signal | Period | Wet/ dry | Colour on map |
|---|---|---|---|---|---|---|---|
| **Fig. 4d La Niña** | Annual | Espinoza et al. (2009a) | Most of the Amazon with the exception of the Madeira basin | Principal Components Analysis (PCA). Bravais–Pearson correlation between the PC1-Qmean time series and SOI<br><br>r = 0.52 | 1974-2004 | Wet | Blue hatched markings |
| **Fig. 4d La Niña** | Annual | Ronchail et al. (2005b) | Mainly observed in the north-eastern rivers and along the Branco River | Composites and correlation analysis between observed discharge (annual mean, max and min) and SSTs<br><br>La Niña high discharge signal. No specific values given. | 1981-2002 | Wet | Blue |
| **Fig. 4d La Niña** | Annual | Ronchail et al. (2005b) | In the majority of the southern Amazon Basins and especially along the Mamoré and Madeira rivers | Composites and correlation analysis between observed discharge (annual mean, max and min) and SSTs<br><br>Inverse signal with low discharge during La Niña | 1981-2002 | Dry | Red |
| **Fig. 4d La Niña** | Annual | Foley et al. (2002) | Óbidos gauging station | Comparison of average annual river discharge for composites of El Niño and La Niña years<br><br>Average increase of 7% in discharge during La Niña events | 1970-1995 | Wet | Blue |

**Table S23.** *Details of results (e.g. analysis type, location, period) from previous studies exploring the relationship between river discharge and the cold phase of ENSO, for the Amazon wet season.*

| Fig/ Driver | Annual/ season | Author | Location | Analysis/strength of signal | Period | Wet/ dry | Colour on map |
|---|---|---|---|---|---|---|---|
| **Fig. 4e La Niña** | Wet (Feb-Apr) | Emerton et al. (2017) | North of the Amazon River towards the north-eastern Amazon | Estimates of historical probabilities of river flows during El Niño and La Niña years<br><br>Probabilities of 40-70%, during the decaying phase | 1901-2010 | Wet | Blue |
| **Fig. 4e La Niña** | Wet (Feb) | Schöngart and Junk, 2007 | Negro River | Correlations between maximum water levels and SOI and Niño 3.4 SST anomalies<br><br>T value = 3.02 $p < 0.01$<br>$r = -0.49$ (Niño 3.4 SST) | 1950-2000 | Wet | Blue |
| **Fig. 4e La Niña** | Wet (Apr-Jun) | Foley et al. (2002) | Whole basin – majority of rivers | Analysis of land surface model coupled with a hydrological routing algorithm (HYDRA) to examine how phases of ENSO affect land surface parameters including discharge<br><br>An increase in river discharge in found in many rivers (mainly from northern and western tributaries which leads to an increase in flooded area along the main-stem | 1950-1995 | Wet | Blue |

**Table S24.** *Details of results (e.g. analysis type, location, period) from previous studies exploring the relationship between river discharge and the cold phase of ENSO, for the Amazon dry season.*

| Fig/ Driver | Annual/ season | Author | Location | Analysis/strength of signal | Period | Wet/ dry | Colour on map |
|---|---|---|---|---|---|---|---|
| **Fig. 4f La Niña** | Dry (Sep & Dec) | Emerton et al. (2017) | Towards the north-western Amazon around the confluence of the Amazon River | Estimates of historical probabilities of river flows during El Niño and La Niña years<br><br>Probabilities of 40-60%, during the evolution phase | 1901-2010 | Dry | Red |
| **Fig. 4f La Niña** | Dry (Aug-Dec) | Emerton et al. (2017) | North of the Amazon River towards the north-eastern Amazon | Estimates of historical probabilities of river flows during El Niño and La Niña years<br><br>Probabilities of 40-70%, during the evolution phase | 1901-2010 | Wet | Blue |
| **Fig. 4f La Niña** | Dry (Dec) | Emerton et al. (2017) | Edge of the southern Amazon | Estimates of historical probabilities of river flows during El Niño and La Niña years<br><br>Probabilities of 40-50%, during the evolution phase | 1901-2010 | Wet | Light blue |

**Table S25.** *Details of results (e.g. analysis type, location, period) from previous studies exploring the relationship between river discharge and warm SSTs in the TNA, on an annual timescale.*

| Fig/ Driver | Annual/ season | Author | Location | Analysis/strength of signal | Period | Wet /dry | Colour on map |
|---|---|---|---|---|---|---|---|
| **Fig. 5a Warm TNA** | Annual | Espinoza et al. (2009a) | Whole basin except the Madeira and Branco Rivers | Principal Components Analysis (PCA). Bravais–Pearson correlation between the PC1-Q mean time series and TNA SSTs<br><br>r = -0.63<br><br>Q max is also lower when the TNA is warm | 1974-2004 | Dry | Red hatched markings |
| **Fig. 5a Warm TNA** | Annual | Ronchail et al. (2005a) | Large portion of the Amazon Basin from the Amazon River to $10^0$ S | Composites and correlation analysis between observed discharge (annual min and mean) and SSTs<br><br>Warm events are characterised by weaker than usual discharges | 1981-2002 | Dry | Red |

**Table S26.** *Details of results (e.g. analysis type, location, period) from previous studies exploring the relationship between river discharge and cold SSTs in the TNA, on an annual timescale.*

| Fig/ Driver | Annual/ season | Author | Location | Analysis/strength of signal | Period | Wet/ dry | Colour on map |
|---|---|---|---|---|---|---|---|
| **Fig. 5b Cold TNA** | Annual | Espinoza et al. (2009a) | Whole basin except the Madeira and Branco Rivers | Principal Components Analysis (PCA). Bravais–Pearson correlation between Q max time series and TNA SSTs<br><br>r = 0.52<br><br>Higher Q max associated with colder SSTs in the TNA | 1974-2004 | Wet | Blue hatched markings |
| **Fig. 5b Cold TNA** | Annual | Ronchail et al. (2005a) | Large portion of the Amazon Basin from the Amazon River to $10^0$ S | Composites and correlation analysis between observed discharge (annual min and mean) and SSTs<br><br>Low flow discharge increases by 20-40% during cold events. Higher than normal mean flows also noted | 1981-2002 | Wet | Blue |
| **Fig. 5b Cold TNA** | Annual | Ronchail et al. (2005a) | Branco River | Composites and correlation analysis between observed discharge (annual min and mean) and SSTs<br><br>Inverse relationship (i.e. decrease in low and mean flows) identified in the Branco River | 1981-2002 | Dry | Red |

| | | | | | | | |
|---|---|---|---|---|---|---|---|
| **Fig. 5b Cold TNA** | Wet (Mar-Apr) | Marengo et al. (1992) | Negro River | Correlation maps between SSTs in the Atlantic Ocean and water levels along the Negro River<br><br>High water levels associated with anonymously cold TNA conditions in contrast to relatively warm TSA SSTs | 1951-1983 | Wet | Blue |

**Table S27.** *Details of results (e.g. analysis type, location, period) from previous studies exploring the relationship between river discharge and warm SSTs in the TSA, on an annual timescale.*

| Fig/ Driver | Annual/ season | Author | Location | Analysis/strength of signal | Period | Wet /dry | Colour on map |
|---|---|---|---|---|---|---|---|
| **Fig. 5c Warm TSA** | Annual | Ronchail et al. (2004; 2005a) | Beni basin | Correlation between discharge in the Southern Amazon and SSTs in the TSA | 1974-1994 | Wet | Blue |
| **Fig. 5c Warm TSA** | Wet (Mar-Apr) | Marengo et al. (1992) | Negro River | Correlation maps between SSTs in the Atlantic Ocean and water levels along the Negro River<br><br>High water levels associated with anonymously cold TNA conditions in contrast to relatively warm TSA SSTs | 1951-1983 | Wet | Blue |

# Chapter 3

# Assessing the performance of global hydrological models for capturing peak river flows in the Amazon Basin

In Chapter 2, one of the main conclusions raised issues in the data length and completeness of daily records at many gauging stations within the Amazon Basin, therefore limiting the strength of any results. One way around this is to use climate reanalysis data (i.e. a combination of observations and model predictions to construct climate variables in the past), produced from large-scale hydrometeorological models (i.e. an integrated meteorological model that is used as input into a hydrological and routing model) which can now extend analysis back to 1950 with a complete record. However, first, such datasets must be thoroughly examined against observed data to assess their suitability for further research, particularly at their ability to capture high-water periods. This analysis provides the steppingstone in which to choose the appropriate datasets for analyses linking flooding in the Amazon to large-scale climate variability.

This paper has been published as a research article in the journal of Hydrology and Earth System Sciences (HESS), with the following reference:

Towner, J., Cloke, H. L., Zsoter, E., Flamig, Z., Hoch, J. M., Bazo, J., Coughlan de Perez, E., and Stephens, E. M.: Assessing the performance of global hydrological models for capturing peak river flows in the Amazon Basin, Hydrol. Earth Syst. Sci., 23, 3057-3080, https://doi.org/10.5194/hess-23-3057-2019, 2019.



The contributions of the authors of this paper are as follows: J.T undertook the research in addition to writing the paper. J.T, E.M.S, and H.L.C designed the analysis. J.T interpreted the results with input from E.M.C and H.L.C. E.Z provided data and information for all simulations incorporating Lisflood and for the ERA-Interim Land H-TESSEL CaMa-Flood set-up. Z.F and J.M provided data and information for the TRMM CREST EF5 and ERA-Interim Land PCR-GLOBWB CaMa-Flood runs respectively. E.M.S, H.L.C, J.B, and E.C supervised the research and provided

important advice. All authors were involved in discussions throughout the development and commented on the paper. Overall, 90% of the research and 85% of the writing was conducted by J.T.

**Abstract.** Extreme flooding impacts millions of people that live within the Amazon floodplain. Global hydrological models (GHMs) are frequently used to assess and inform the management of flood risk, but knowledge on the skill of available models is required to inform their use and development. This paper presents an intercomparison of eight different GHMs freely available from collaborators of the Global Flood Partnership (GFP) for simulating floods in the Amazon Basin. To gain insight into the strengths and shortcomings of each model, we assess their ability to reproduce daily and annual peak river flows against gauged observations at 75 hydrological stations over a 19-year period (1997–2015). As well as highlighting regional variability in the accuracy of simulated streamflow, these results indicate that (a) the meteorological input is the dominant control on the accuracy of both daily and annual maximum river flows, and (b) groundwater and routing calibration of Lisflood based on daily river flows has no impact on the ability to simulate flood peaks for the chosen river basin. These findings have important relevance for applications of large-scale hydrological models, including analysis of the impact of climate variability, assessment of the influence of long-term changes such as land-use and anthropogenic climate change, the assessment of flood likelihood, and for flood forecasting systems.

## 3.1 Introduction

Flooding is notably the most common and damaging natural hazard affecting millions of people worldwide every year, producing economic losses exceeding billions of dollars (Hirabayashi et al., 2013). Flood risk associated with a particular location can be highly variable depending on levels of exposure, resilience, and preparedness (Alfieri et al., 2018), in addition to the increased uncertainty surrounding trends of hydrological extremes in a warming climate (Arnell and Gosling, 2016). For the Amazon Basin, flood risk is considered to have increased, with a greater frequency of extreme flood events (e.g. in 2009, 2012, and 2014; Marengo and Espinoza, 2016) coinciding with a hypothesized intensification of the hydrological cycle since the 1980s (Gloor et al., 2013). Floods in Amazonian communities are known to have large socioeconomic consequences impacting ecosystems, health, and transport links, and are particularly damaging to agricultural and fishery practices (Schöngart and Junk, 2007; Marengo et al., 2012, 2013; Correa et al., 2017). Single flood events (e.g. 2012 in the Amazonian city of

Iquitos, Peru) have impacted the lives of over 73 000 people (IFRC, 2013), with average annual damages estimated at USD 1.4 billion over a 4-year period (2008–2011) in the Brazilian Rio Branco basin alone (Mundial Grupo Banco, 2014).

### 3.1.1 Global hydrological models and applications

In its simplest form, a hydrological model can be considered a representation of a real-world hydrological system used to better understand various water and environmental processes, predict system behaviour, and provide consistent impact assessment (Devia et al., 2015). They work by simulating the hydrological response to meteorological variations incorporating run-off generation and river routing processes (Sutanudjaja et al., 2018). As such, global hydrological models (GHMs) have been used in a wide range of applications, including short- to extended-range flood forecasting (Alfieri et al., 2013; Emerton et al., 2018), climate assessment (Hattermann et al., 2017), hazard and risk-mapping (Ward et al., 2015), drought prediction (van Huijevoort et al., 2014), and water resource assessment (e.g. water availability models; Meigh et al., 1999; Sood and Smakhtin, 2015). Depending on the application and the needs of decision makers, different properties of the hydrograph simulated by hydrological models are important. For example, an accurate representation of peak river flows and their likelihood is key for decision-makers who wish to understand the area at risk of flooding. In contrast, estimates of daily streamflow may be more beneficial for the assessment of water resources such as irrigation requirements.

### 3.1.2 GHM development

The availability of GHMs has grown in recent years thanks to increased efforts in addressing water-related issues in developing countries (De Groeve et al., 2015; Ward et al., 2015; Trigg et al., 2016), the development of flood forecasting systems (Aliferi et al., 2013; Werner et al., 2013; Emerton et al., 2018), improvements within precipitation datasets (Mittermaier et al., 2013; Novak et al., 2014; Forbes et al., 2015), the emergence of new global satellite and remote sensing datasets, and advancements in numerical modelling techniques (Yamazaki et al., 2014a; Sampson et al., 2015; Andreadis et al., 2017; Balsamo et al., 2018). For an overview of available GHMs, see Bierkens et al. (2015), who have provided the details of 22 large-scale hydrological models, with those used for operational flood forecasting being summarized in Emerton et al. (2016).

### 3.1.3 Land surface vs. hydrological models

GHMs have differing spatial and temporal resolutions, parameter estimation approaches, number of parameters, calibration methods, input–output variables, and overall structures (Sood and Smakhtin, 2015). Their set-ups can generally be divided into two categories: land surface models (LSMs) and hydrological models (Gudmundsson et al., 2012). The majority of LSMs and hydrological models share the same conceptualization of the water balance (Haddeland et al., 2011) but differ in their objective. LSMs evolve from coupled land–atmosphere models with the purpose of solving the surface energy balance equations to provide the necessary lower boundary conditions to the atmosphere (Wood et al., 2011). In contrast, hydrological models tend to focus less on the partitioning of radiation and more on hydrological resources and understanding the lateral movement and transport of water along the land surface.

In terms of differences in model performance, the Gudmundsson et al. (2012) intercomparison study of six LSMs and five GHMs (i.e. hydrological models) concluded that the main differences were due to the snow scheme implemented with snow water equivalent values and mean runoff fractions lower in LSMs. No significant differences between LSMs and hydrological models were found for runoff and evapotranspiration globally, but rather the differences between the models themselves created large sources of uncertainty, highlighting the importance of analysing a range of different GHMs rather than a group consisting of a specific model type. For the purposes of this study, we categorize both LSM and hydrological models as GHMs.

### 3.1.4 Motivation

For GHMs to be considered effective, end users need to know their accuracy and reliability (Ward et al., 2015). Thus, the evaluation of these models against observed data is an important procedure in efforts to reduce flood risk. Currently, no intercomparison analysis of GHMs has been conducted specifically for the Amazon Basin, with previous studies focusing solely on the performance of individual models for the Amazon (e.g. Yamazaki et al., 2012; Paiva et al., 2013; Hoch et al., 2017a, b) or as part of a global study (e.g. Gudmundsson et al., 2012; Alfieri et al., 2013; Hirpa et al., 2018), which lack an in-depth focus on skill within the Amazon Basin.

Finally, many of the GHMs (or their components) analysed in this study are used for specific applications, for instance, in water resources management (PCRaster Global Water Balance; PCR-GLOBWB), flash flood forecasting (Ensemble Framework for Flash Flood Forecasting; EF5), and extended-range flood forecasting (Global Flood Awareness System; GloFAS). Investigating the performance of hydrological simulations therefore can provide valuable information to researchers and model developers with which to better understand some of the strengths and weaknesses which exist within the model set-ups and help to distinguish how different parts of the hydrological chain can cause particularly “good” or “bad” model performance, thus having implications for their different applications.

### 3.1.5 Objectives

In this study, the main objective is to assess the ability of different GHMs freely available from collaborators within the Global Flood Partnership (GFP), identifying which approaches are most suitable in different areas of the Amazon Basin for simulating flood peaks. To pursue this objective, the analysis is designed to answer the following research questions.

1. How well do GHMs represent the annual hydrological regime in terms of the Kling–Gupta efficiency (KGE) and its individual components?
2. Which model set-up best represents annual maximum river flows?
3. Which hydrological routing model allows the best representation of daily and peak river flows?
4. Which precipitation dataset allows the best representation of daily and peak river flows?
5. How do results differ when using a LSM as opposed to a hydrological model?
6. By how much does calibration of groundwater and routing model parameters improve performance?

## 3.2 Data and methodology

The experimental design involves comparing the output of daily and annual maximum discharge estimates produced by different GHMs forced using atmospheric reanalysis or satellite precipitation datasets against observations of streamflow. The common validation period is 1997–2015, with results also analysed for the shorter period of 2004–2015 to account for the shorter record length of one simulation.

### 3.2.1 Observations

Observed daily discharge data are used to evaluate each of the model runs. The network of hydrometric gauges is controlled and maintained by the national institutions responsible for hydrological monitoring in countries situated within the Amazon Basin. These include the Agência Nacional de Águas (Water National Office – ANA, Brazil), Servicio Nacional de Meteorología e Hidrología (National Meteorology and Hydrology Service – SENAMHI, Peru and Bolivia), Instituto Nacional Meteorologia e Hidrologia (Institute to Meteorology and Hydrology, INAMHI, Ecuador), and the Instituto de Hidrología, Meteorología y Estudios Ambientales (Institute of Hydrology, Meteorology and Environmental Studies – IDEAM, Colombia).

Daily water level values are collected by the respective institutions and are sourced through the ORE-HYBAM observational service (http://www.ore-hybam.org/, last access: 1 December 2018), in collaboration with the Institute of Research for Development (IRD) or directly from the national services. A time series of daily river flow for each station is obtained using stage and rating curve measurements which were determined using an acoustic Doppler current profiler (ADCP) conducted by the ORE-HYBAM observatory and SENAMHI (Espinoza et al., 2014). In total 75 hydrological stations throughout the Amazon Basin are selected, with an average record length of 17 years within the main validation period (1997–2015). The locations of stations and their characteristics are displayed in Fig. 1a and Table S1 in the Supplement respectively. Stations selected have a minimum of 5 consecutive years' worth of data during the main validation period. The threshold was set to 5 to prevent the elimination of stations in data-scarce areas such as Peru, Bolivia, and Colombia.

### 3.2.2 Routing models and meteorological datasets

Eight GHMs composed of different meteorological datasets, hydrological models/LSMs, and river routing models are used to each simulate river discharge across the Amazon Basin. Four meteorological products (ERA-Interim Land reanalysis, ERA-5 reanalysis, European Centre for Medium-range Weather Forecasts (ECMWF) 20-year control reforecasts (hereafter defined as reforecasts), and the real-time TRMM TMPA 3B42 v.7), three hydrological models/LSMs (PCR-GLOBWB, the Hydrology-Tiled ECMWF Scheme for Surface Exchanges over Land; H-TESSEL, EF5), and three river routing models (Catchment-based Macro-scale Floodplain model, CaMa-Flood; Lisflood; and the Coupled Routing and Excess Storage, CREST) are employed. While the focus of this study is on GHMs made available by the GFP community, other models are available within the Amazon Basin. Some examples include MGB-IPH (Paiva et al., 2013),

LPJmL (Lund–Potsdam–Jena managed Land; Bondeau et al., 2007), WaterGAP (water – global analysis and prognosis; Döll et al., 2003), and MAC-PDM.09 (the Macro-scaleProbability-Distributed Moisture model.09; Gosling and Arnell, 2011).

As a result of using freely available datasets from collaborators within the GFP, simulations are composed of a combination of routing models and meteorological datasets and do not all use the same precipitation input or hydrological set-up. However, the available combinations allow enough insight into the model components to draw conclusions for the objectives stated. For example, to analyse the performance of precipitation inputs, ERA-Interim Land, ERA-5, and the reforecasts are forced through the calibrated version of Lisflood, whereby the routing and LSM remain consistent. To evaluate the differences between using the Lisflood and CaMa-Flood routing models, two simulations which use ERA-Interim Land precipitation and the H-TESSEL LSM are compared. To identify the differences between employing a hydrological model (PCR-GLOBWB) or LSM (HTESSEL), two set-ups which use the ERA-Interim Land precipitation reanalysis and the CaMa-Flood river routing model are directly compared. Finally, to see how much benefit model calibration within Lisflood provides, ERA-Interim Land and ERA-5 are forced through the calibrated and uncalibrated Lisflood model versions. The CREST EF5 run is the sole simulation to have a unique hydrological model and meteorological input, and although it is more challenging to analyse the performance of specific components of the model set-up against other simulations, it was included in the analysis for completeness.

An alternative approach would be to implement a full intercomparison experiment and run a new set of simulations which included all combinations of precipitation input, GHM, and routing scheme. However, this is a very large undertaking, and the time and computational expense to achieve this are prohibitive. Instead, by using freely available datasets with different hydrological set-ups, our method allows a first analysis providing enough evidence of dataset reliability and accuracy in order to determine the utility of the differing approaches for climate studies and to forecast applications. Moreover, by using iterative runs of similar model set-ups (i.e. changing a specific part of the hydrological model chain), it allows us to make conclusive statements regarding the differences in skill. Finally, short descriptions of each model and atmospheric product are outlined below, with a summary of each simulation provided in Table 1.

**Table 1.** *Characteristics of the eight GHMs used to produce estimates of daily river discharge.*

| Model Run | Meteorological forcing[1] | GHM[2] | GHM Spatial Resolution | Routing Model[3] | Routing Spatial Resolution | Temporal Resolution | Start | End | Calibration | Authors |
|---|---|---|---|---|---|---|---|---|---|---|
| ERA-I Land H-TESSEL Lisflood_uc | ERA-I Land | H-TESSEL | ~0.75$^0$ (~80 km) | Lisflood | 0.10$^0$ (~10 km) | Daily | 01 Jan 1997 | 31 Dec 2015 | None | Balsamo et al. (2015)[1]<br>Balsamo et al. (2009)[2]<br>van der Knijff et al. (2010)[3] |
| ERA-I Land H-TESSEL Lisflood_c | ERA-I Land | H-TESSEL | ~0.75$^0$ (~80 km) | Lisflood | 0.10$^0$ (~10 km) | Daily | 01 Jan 1997 | 31 Dec 2015 | See Hirpa et al. (2018) | Balsamo et al. (2015)[1]<br>Balsamo et al. (2009)[2]<br>van der Knijff et al. (2010)[3] |
| ERA-5 H-TESSEL Lisflood_uc | ERA-5 | H-TESSEL | ~0.28$^0$ (~31 km) | Lisflood | 0.10$^0$ (~10 km) | Daily | 01 Jan 1997 | 31 Dec 2015 | None | See ECMWF (2018)[1]<br>Balsamo et al. (2009)[2]<br>van der Knijff et al. (2010)[3] |
| ERA-5 Lisflood H-TESSEL_c | ERA-5 | H-TESSEL | ~0.28$^0$ (~31 km) | Lisflood | 0.10$^0$ (~10 km) | Daily | 01 Jan 1997 | 31 Dec 2015 | See Hirpa et al. (2018) | See ECMWF (2018)[1]<br>Balsamo et al. (2009)[2]<br>van der Knijff et al. (2010)[3] |
| Reforecasts H-TESSEL Lisflood_c | ECMWF 20-year control Reforecasts | H-TESSEL | ~0.28$^0$ (~31 km) | Lisflood | 0.10$^0$ (~10 km) | Daily | 01 Jan 1997 | 31 Dec 2015 | See Hirpa et al. (2018) | See ECMWF (2017)[1]<br>Balsamo et al. (2009)[2]<br>van der Knijff et al. (2010)[3] |
| ERA-I Land H-TESSEL CaMa-Flood | ERA-I Land | H-TESSEL | ~0.75$^0$ (~80 km) | CaMa-Flood | 0.25$^0$ (~25 km) | Daily | 01 Jan 1997 | 31 Dec 2015 | None | Balsamo et al. (2015)[1]<br>Balsamo et al. (2009)[2]<br>Yamazaki et al. (2011)[3] |
| ERA-I Land PCR-GLOBWB CaMa-Flood | ERA-I Land | PCR-GLOBWB | ~0.50$^0$ (~50 km) | CaMa-Flood | 0.25$^0$ (~25 km) | Daily | 01 Jan 1997 | 31 Dec 2015 | None | Balsamo et al. (2015)[1]<br>Sutanudjaja et al. (2018)[2]<br>Yamazaki et al. (2011)[3] |
| TRMM CRESTEF5 | TMPA 3B42 v7. Real-time | EF5/CREST | ~0.25$^0$ (~25 km) | EF5/CREST | 0.05$^0$ (~5 km) | Daily | 01 Jan 2003 | 31 Dec 2015 | None | Huffman et al. (2007)[1]<br>Wang et al. (2011)[2]<br>Clark et al. (2016)[3] |

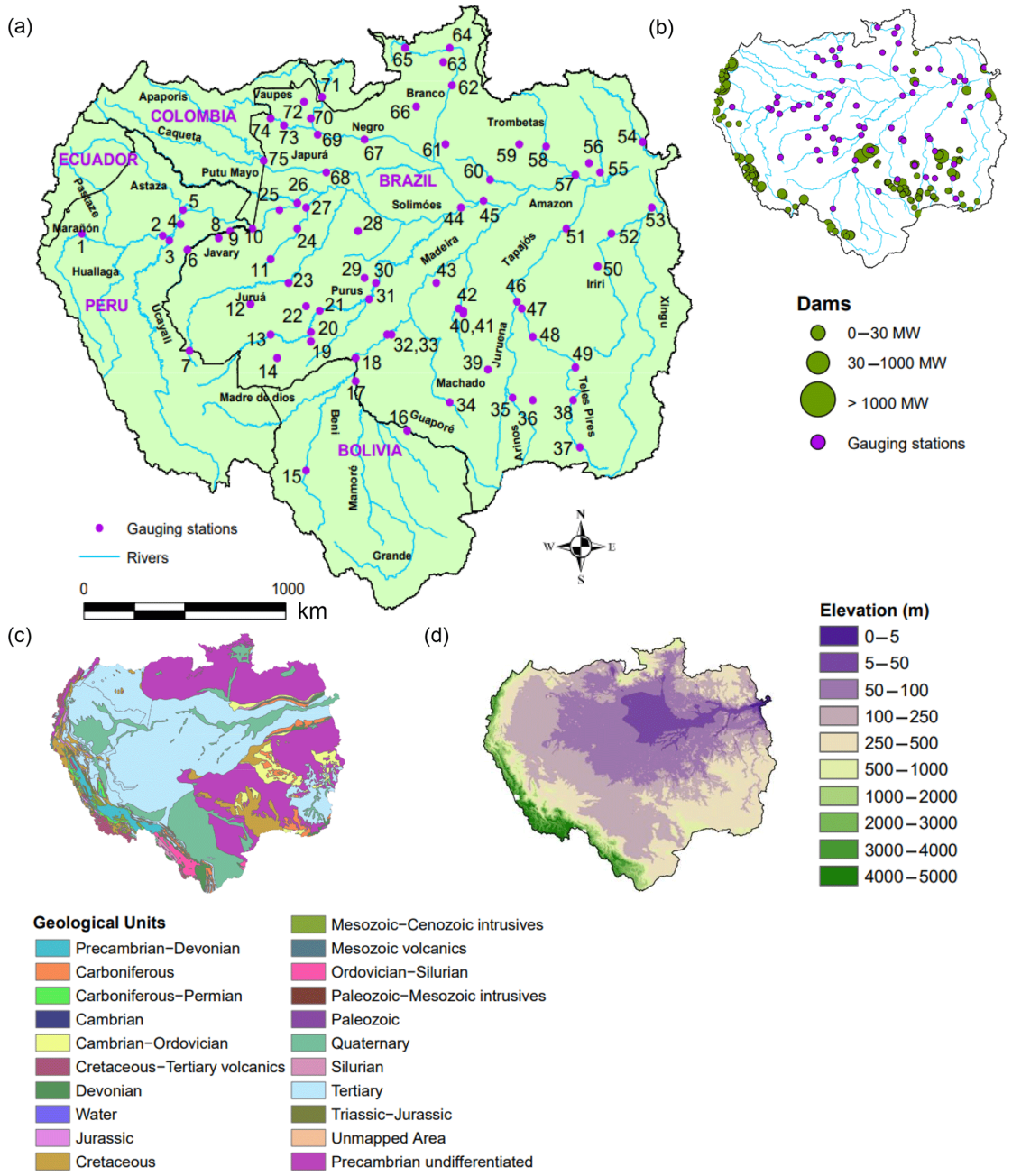


**Figure 1.** *a) Locations of the 75 hydrological gauges and the river network of the Amazon Basin. Numbers represent stations which are referred to throughout the main text in italics. For station information, see Table S1. (b) Locations of existing and under-construction dams as of 2017 (see Latrubesse et al., 2017). (c) Geological map of the Amazon (Schenk et al., 1999). (d) Elevation map of the basin from the digital elevation model (DEM), GTOPO30, at a horizontal resolution of approximately 1 km (US Geological Survey, 1996).*

### 3.2.3 Precipitation datasets

ERA-Interim Land is a global reanalysis of land surface parameters produced by the ECMWF with a T255 spectral resolution (∼80 km or ∼0.75◦; Balsamo et al., 2015). ERA-Interim Land was produced using the latest version of the land surface H-TESSEL model using atmospheric forcing from ERA-Interim (Dee et al., 2011), with precipitation adjustments based on the Global Precipitation Climate Project (GPCP) v2.1. Precipitation improvements were achieved by Balsamo et al. (2010) using a scale-selective rescaling procedure in which ERA-Interim 3-hourly precipitation was corrected to match the monthly accumulation provided by the GPCP at grid point scale (Huffman et al., 2009). All simulations which use ERA-Interim Land are run offline to force the associated rainfall–runoff models (see Table 1). For a detailed description of the ERA-Interim Land and ERA-Interim datasets, see Balsamo et al. (2015) and Dee et al. (2011) respectively. Dataset available at http://apps.ecmwf.int/datasets/data/interim-full-daily/levtype=sfc/ (last access: 1 July 2018).

ERA-5 is the latest reanalysis product of the ECMWF producing consistent estimates of atmospheric, land, and ocean variables at a horizontal resolution of ∼31 km, while the vertical atmosphere is discretized into 137 levels to 0.01 hPa (ECMWF, 2018). ERA-5 is based on the Integrated Forecasting System (IFS) Cycle 41r2 which was used operationally at the ECMWF in 2016. Early analysis has shown that ERA-5 has an improved representation of precipitation (particularly over land in the deep tropics), evaporation, and soil moisture compared to its predecessor ERA-Interim Land (ECMWF, 2017). ERA-5 is currently being produced in three “streams” and will eventually cover the period 1950 to near real time (∼3 d) with its completion due in 2019 (Emerton et al., 2018). Dataset available at https://software.ecmwf.int/wiki/display/CKB/How+to+download+ERA5+data+via+the+ECMWF+Web+API (last access: 1 July 2018).

ECMWF reforecasts are a collection of historical forecasts from start dates at the same day of the year going back for a specific number of years to provide a consistent model climatology from which to compare forecasts (ECMWF, 2016). In this study we use the control member of the reforecasts which are created based on a retrospective run of the most recent version of the ECMWF's IFS to provide surface and subsurface runoff as input to the Lisflood routing model at a resolution of 0.1◦. The reforecast run is computed using a lighter configuration (11 ensemble members, run twice a week on Mondays and Thursdays) to reduce computational time. The purpose of running the ECMWF forecasts through the Lisflood routing model is to generate a long-term (20-year) dataset which is consistent with operational GloFAS forecasts

enabling the suitability of the dataset for use in the calibration of the Lisflood model parameters (Hirpa et al., 2018). These data cover the period June 1995 to June 2015 and due to frequent model updates of the IFS are based on multiple model cycles: Cycle 41r1 (July through to March) and Cycle 41r2 (March through to June). The control reforecasts from Mondays and Thursdays are used subsequently to fill the whole weeks by taking the first 3- and 4-d forecast periods respectively throughout the 20 years.

TRMM TMPA 3B42 RT v7 is a global merged multi-satellite precipitation product generated at the National Aeronautics and Space Administration (NASA). TMPA is computed for two products: a near-real-time version (TMPA 3B42RT v7) and a post-real-time gauged adjusted research version (TMPA 3B42 v7), both of which run at resolution of 3-hourly × 0.25◦ × 0.25◦ (Huffman et al., 2007). The TMPA 3B42 RT gridded dataset used in this study covers the global latitude belt from 60◦ N to 60◦ S. For further information, see Huffman et al. (2007). Dataset available at https://pmm.nasa.gov/data-access/downloads/trmm (last access: 4 March 2018).

### 3.2.4 Hydrological and land surface models

H-TESSEL provides the land surface component of the ECMWF IFS (van den Hurk et al., 2000; van den Hurk and Viterbo, 2003; Balsamo et al., 2009). H-TESSEL simulates the land surface response to atmospheric conditions estimating water and energy fluxes (heat, moisture, and momentum) on the land surface (Zsoter et al., 2019). H-TESSEL is predominately used within the operational set-up of short- to seasonal-range weather forecasts coupled with the atmosphere, but it can also be used in an “offline mode” to calculate the land surface response to atmospheric forcing, whereby input data (e.g. near-surface meteorological conditions) are provided on a 3-hourly time step (Pappenberger et al., 2012). In this study, H-TESSEL receives boundary conditions from the atmospheric input provided by either the ERA-5 reanalysis, ERA-Interim Land reanalysis, or the reforecasts providing total runoff for the CaMa-Flood routing model, and the surface and sub-surface water fluxes for Lisflood. Runs forced using the ERA-Interim Land reanalysis are run in the offline mode. For a detailed description of H-TESSEL, see Balsamo et al. (2009).

PCR-GLOBWB is a global hydrological and water resource model developed at the Department of Physical Geography, Utrecht University, Netherlands (Sutanudjaja et al., 2018). For each grid cell and time step, PCR-GLOBWB simulates moisture storage in two vertically stacked upper soil layers, as well as the water exchange among the soil, the atmosphere, and the underlying groundwater reservoir. Besides, water demands for irrigation, livestock, industry, and

households can be integrated within the model. Run-off is routed along a local drainage direction (LDD) network using the kinematic routing wave equation. PCR-GLOBWB was applied at a resolution of 30 arcmin (~55 km × 55 km at the Equator) with meteorological forcing provided from the ERA-Interim Land reanalysis dataset between 1997 and 2015. For further information on PCR-GLOBWB, see van Beek and Bierkens (2008), van Beek et al. (2011), and Sutanudjaja et al. (2018).

EF5 is an open-source software package developed at the University of Oklahoma (OU) that consists of multiple hydrological model cores producing outputs of streamflow, water depth, and soil moisture (Clark et al., 2016). Since 2016, EF5 has been used operationally for local forecasts across the US National Weather Service (NWS) for flash flooding purposes (Gourely et al., 2017). EF5 incorporates CREST, which is a distributed hydrological model created by OU and NASA (Wang et al., 2011). Within CREST, runoff generation, evapotranspiration, infiltration, and surface and subsurface routing are computed at each grid cell within the model domain, with surface and subsurface water routed using a kinematic wave assumption. Four excess storage reservoirs characterize the vertical profile within a cell representing interception by the vegetation canopy and subsurface water storage in the three soil layers (Meng et al., 2013). In addition, the representation of sub-grid cell routing and soil moisture variability is made through the use of two linear reservoirs for overland and subsurface runoff individually (Wang et al., 2011). Locations of major streams, flow direction maps, and flow accumulation are all derived from the HydroSHEDS (Hydrological Data and Maps Based on Shuttle Elevation Derivatives at Multiple Scales) dataset (Lenhner et al., 2008).

In this study, an un-calibrated version of EF5 was run using CREST version 2.0 (Xue et al., 2013; Zhang et al., 2015) for 13 years (2003–2015), with a 1-year spin-up at a spatial resolution of 0.05∘ × 0.05∘. Parameters are estimated a priori from soil and geomorphological variables, with meteorological forcing provided by the TMPA 3B42 RT product for precipitation and monthly averaged potential evapotranspiration (PET) from the Food and Agriculture Organisation (FAO). For full details on the system set-up, see Clark et al. (2016).

### 3.2.5 Routing models

Lisflood is a global spatially distributed, grid-based hydrological and channel routing model commonly used for the simulation of large-scale river basins (van Der Knijff et al., 2010). It is currently used as an operational rainfall–runoff model within the European Flood Awareness System (EFAS) for streamflow forecasts over Europe (Smith et al., 2016). Unlike EFAS, which

uses the full Lisflood set-up, GloFAS and the simulations included in this study use only the routing component of the Lisflood set-up, with surface and sub-surface input fluxes (e.g. vertical water, water/snow storage) provided by the H-TESSEL module of the IFS at a resolution of 0.1◦. Surface runoff is routed through Lisflood using a four-point implicit finite-difference solution of the kinematic equations. Sub-surface storage and transport are routed to the nearest downstream channel pixel within one time step through two linear reservoirs (Alfieri et al., 2013). The water in each channel pixel is finally routed through the river network taken from the HydroSHEDS project (Lenhner et al., 2008) using the same kinematic wave equations as for the overland flow. Subsurface flow from the upper and lower groundwater zones is routed into the nearest downstream channel as a scaled sum of the total outflow from both the upper and lower groundwater zones.

Lisflood also represents lakes and reservoirs as simulated points on the river network (Zajac et al., 2017). The outflows of lakes and reservoirs are based on (a) upstream inflow, (b) precipitation over the lake or reservoir, (c) evaporation from the lake or reservoir, (d) the lakes' initial level, (e) lake outlet characteristics, and (f) reservoir-specific characteristics. For further details on the parameterization of lakes and reservoirs within Lisflood, see Appendix A within Zajac et al. (2017). In the Amazon, represented lakes are predominately located along the main stem, with very few reservoirs throughout the basin. For exact lake and reservoir locations within the global Lisflood model, see Zajac et al. (2017).

In this study, two set-ups of Lisflood are used (Lisflood_uc and Lisflood_c). Lisflood_c represents the calibrated set-up of the Lisflood routing and groundwater parameters (see Hirpa et al., 2018), while Lisflood_uc represents the uncalibrated model run. Parameters were calibrated with the reforecasts initialized with the ERA-Interim land reanalysis from 1995 to 2015 as forcing against observed discharge data at 1278 gauging stations worldwide. All but one station (40; see Fig. 1a and Table S1) used in this study were included within the calibration. An evolutionary optimization algorithm was used to perform the calibration, with the KGE used as the objective function. The calibration was carried out for parameters controlling the time constants in the upper and lower zones, percolation rate, groundwater loss, channel Manning's coefficient, the lake outflow width, the balance between normal and flood storage of a reservoir, and the multiplier used to adjust the magnitude of the normal outflow from a reservoir. The results were validated by Hirpa et al. (2018) using the KGE (Gupta et al., 2009) over the period 1995–2015. In calibration (validation) KGE skill scores were greater than 0.08 compared to the default Lisflood simulation for 67 % (60 %) of stations globally. For a detailed description of the calibration of the Lisflood parameters and the range

of values used for each parameter, see Hirpa et al. (2018). Further details of the Lisflood model are described in van Der Knijff et al. (2010).

CaMa-Flood is a global distributed river routing model which is forced by runoff input from a LSM or hydrological model to simulate water storage where further hydrological variables (i.e. river flow, water level, and inundated area) can be derived along a prescribed river network. Horizontal water transport along the river network is calculated using the local inertia equations (Yamazaki et al., 2011). The backwater effect (i.e. upstream water levels which affect flow velocity downstream; see Meade et al., 1991) is represented by estimating flow velocity based on water slope (Yamazaki et al., 2011). Moreover, floodplain inundation is represented within CaMa-Flood as a subgrid-scale process by discretizing the river basin into unit catchments which consist of subgrid river and floodplain topography parameters (Yamazaki et al., 2014b). These parameters describe the relationship between the total water storage in each grid point and water stage and are automatically generated using the Flexible Location of Waterways (FLOW) method with the generation of the river map created by upscaling the HydroSHEDS flow direction map (Lehner et al., 2008). For further information about the CaMa-Flood model, see the aforementioned references. In this study, daily river discharge was obtained using CaMa-Flood version 3.6.1 at a spatial resolution of 0.25∘ (∼25 km grid size) for both runs. Manning's river and floodplain roughness coefficients were set at 0.03 and 0.10 s m−1/3 uniformly for both CaMa-Flood simulations.

### 3.2.6 Verification metrics

#### 3.2.6.1 Spearman’s ranked correlation

The non-parametric Spearman ρ is used to measure the strength and direction of the monotonic relationship between the ranks of the observed and simulated annual maximum values. The non-parametric Spearman ρ was preferred to Pearson's statistic as non-parametric measures are less sensitive to outliers in the data and are widely considered a more robust measure of the correlation between observed and predicted values (Legates and McCabe, 1999). Correlation scores for ρ range from − to 1, with 1 being a perfect correlation. We consider scores which have a value of 0.6 or more to be skilful. Similar scores (between 0.5 and 0.7) are considered to represent a good level of agreement between observed and simulated values in similar studies (see Yamazaki et al., 2012; Alfieri et al., 2013).

### 3.2.6.2 KGE

The KGE (Gupta et al., 2009) measures the goodness-of-fit between estimates of simulated discharge and gauged observations and is a modified version of the dimensionless Nash–Sutcliffe efficiency (NSE; Nash and Sutcliffe, 1970). The metric decomposes the NSE into three independent hydrograph components – linear correlation (r), bias ratio (β), and relative variability between the observed and simulated streamflow (α) – by re-weighting the relative importance of each (Revilla-Romero et al., 2015). KGE values range from $-\infty$ to 1, with values closer to 1 indicating better model performance. To provide further context to the computed KGE scores, we use the breakdown of KGE values into four benchmark categories as according to (Kling et al., 2012). These are classified as follows:

- "Good" (KGE $\geqslant$ 0.75),
- "Intermediate" (0.75 > KGE $\geqslant$ 0.5),
- "Poor" (0.5 > KGE > 0),
- "Very poor" (KGE $\leqslant$ 0).

Although originally for the modified version of the KGE, these categories provide an informative benchmark by which to evaluate results. A similar study (Thiemig et al., 2013) assessing the performance of satellite-based precipitation products for hydrological evaluation also adopted the same approach.

When analysing the results, each component of the KGE is also considered independently, enabling model errors to be directly related to either the variability (KGE_α), bias ratio (KGE_β), or correlation (KGE_r; Guse et al., 2017). KGE_α values greater than 1 indicate that variability in the simulated time series is higher than that observed. Values less than 1 show the opposite effect. KGE_β values greater than 1 indicate a positive bias whereby predictions overestimate flows relative to the observed data, while values less than 1 represent an underestimation.

To evaluate the relative improvement of using one model set-up relative to another (e.g. using the calibrated Lisflood routing model as opposed to the uncalibrated model version), metrics are calculated as skill scores:

$$KGE_{SS} = \frac{KGE_a - KGE_{def}}{1 - KGE_{def}}, \quad (1)$$

where KGESS signifies the KGE skill score, KGEa is the KGE score for the improved run or simulation of interest (e.g. Lisflood_c), and KGEdef is the KGE score for the "default" or

comparative run (e.g. Lisflood_uc). Positive KGESS indicates improved skill, whilst a negative score represents a decrease in skill. For each case, KGE scores are calculated against observed river flow data. The correlation skill score is calculated similarly. All metrics are computed in the R environment using the "verification" (Gilleland, 2015) and "hydroGOF" (Zambrano-Bigiarini, 2017) R packages.

## 3.3 Results and discussion

To allow for easier interpretation, the results and discussion are separated into six sections which match the research questions presented in Sect. 3.1.5, in addition to an outline of potential future work. Due to similar results between the two validation periods (1997–2015 and 2004–2015), only results for 1997–2015 are shown. For 2004–2015 results, see Figs. S1 and S2 in the Supplement. Results and discussions for individual stations are commonly referred to by the station numbers in italics and are presented in Fig. 1a and Table S1.

### 3.3.1 How well is the hydrological regime represented?

The annual hydrological regime on average is well represented by all models (Fig. 2), with the rationale for poorer performance at specific gauges dependent on either the temporal correlation, bias ratio, or variability ratio components of the KGE (Figs. 3–5). An average of 50 % of stations note scores above 0.5 for the KGE metric across all eight simulated runs, with a maximum value of 0.92 observed at the Santa Rosa gauging site (48, Fig. 1a) for the ERA-5 Lisflood_c simulation (Fig. 2f). The two CaMa-Flood set-ups using the PCR-GLOBWB hydrological model and the H-TESSEL LSM show the lowest skill, with 19 and 18 stations noting scores greater than 0.5 respectively. By contrast, the best performance is from the calibrated Lisflood set-ups, with median scores across stations of 0.56, 0.63, and 0.64 for runs forced with ERA-Interim Land, the reforecasts, and ERA-5 respectively. Such results are unsurprising given that the KGE was used as the objective function in the calibration algorithm of the Lisflood routing model.

In terms of spatial distribution, the poorest performance is consistent for the majority of simulations at the Arapari (55), Boca Do Inferno (56), and Base Alalau (61) gauging stations located north of Manaus, at the Fazenda Cajupiranga gauge (64) in the northernmost Branco catchment, and at the Fontanilhas (35) and Indeco (49) stations in the south-eastern Brazilian Amazon (Fig. 2). In the south-eastern Amazon, particularly in the Madeira and Tapajos sub-

basins, the number of existing or under-construction dams is at its highest (Fig. 1b). Damming of rivers is known to have impacts on different aspects of the flow regime, with possible alterations in the timing, magnitude, and frequency of low and high flows (Magilligan and Nislow, 2005). Indeed, the frequency and duration of low- and high-flow pulses at stations downstream of dams have been shown to be particularly affected by the construction of cumulative dams (Timpe and Kaplan, 2017). Thus, discrepancies between observed and modelled data shown in Fig. 2 could be due to alterations to key features of the flow regime.

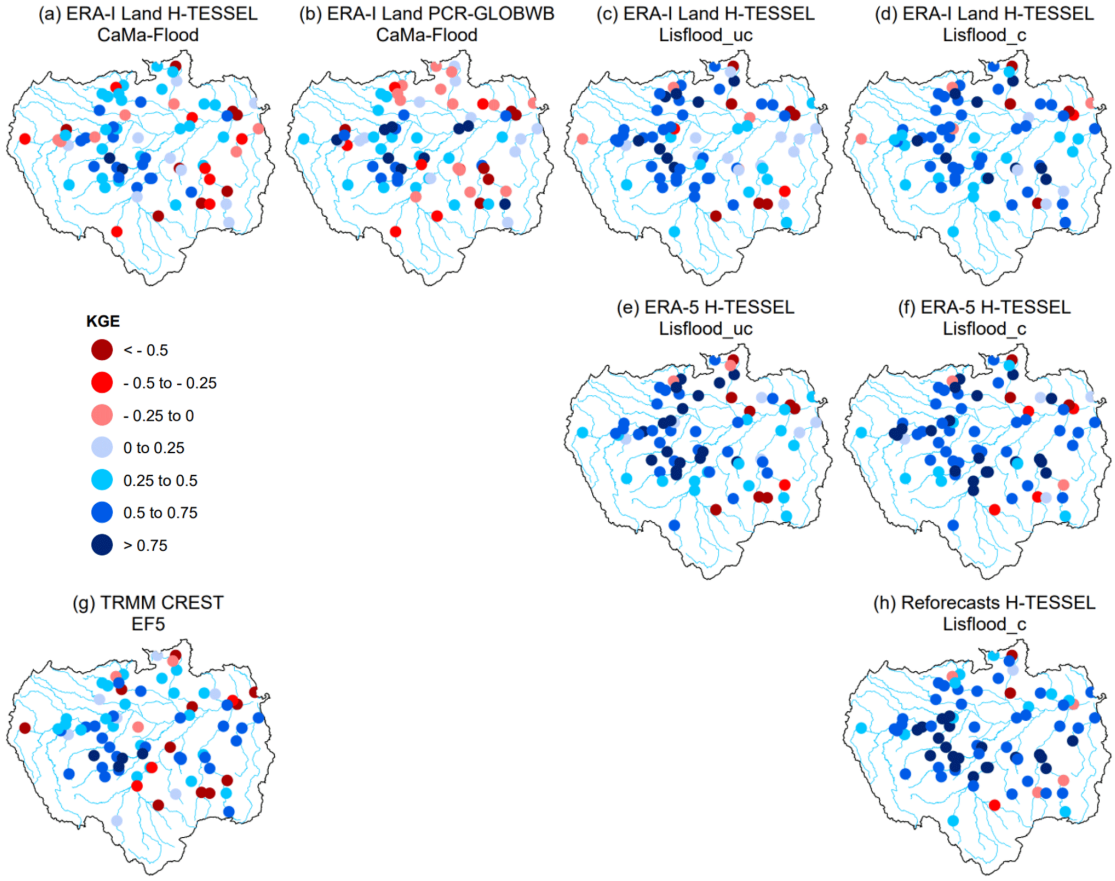


**Figure 2.** *Full Kling–Gupta efficiency (KGE) scores at the 75 hydrological gauging stations for all simulations. For the periods 1997–2015 and 2004–2015 for the Coupled Routing and Excess Storage, Ensemble Framework for Flash Flood Forecasting (CREST EF5) run (g). Values greater than 0.75 are considered to indicate good performance (i.e. dark blue circles). To allow for easier model comparisons, plots are arranged by the different precipitation datasets (rows) and routing models (columns), with the exception of CREST EF5 (g). For example, the final column consists of model runs using the calibrated Lisflood routing model.*

The highest scoring stations (KGE score > 0.75) are predominately found in the south-western Brazilian Amazon where the network of tributaries remains relatively unaffected by damming and where slopes are gentle (Fig. 1b and d). However, high skills at stations (32, 33, and 43)

along the Madeira River for most simulations (Fig. 2) highlight that the impacts of hydroelectric dams need to be considered on an individual basis, with two of the largest dams (>3000 MW) situated along the river (see Fig. 1b).

Figures 3–5 show the breakdown of the KGE scores for each hydrological component to evaluate differences in performance with respect to the correlation (i.e. timing), flow variability (α), and bias ratio (β). An average of 79 % of stations note correlation coefficients exceeding 0.6 across all runs, with those using the Lisflood routing model performing similarly in both spatial distribution and magnitude (Fig. 3).

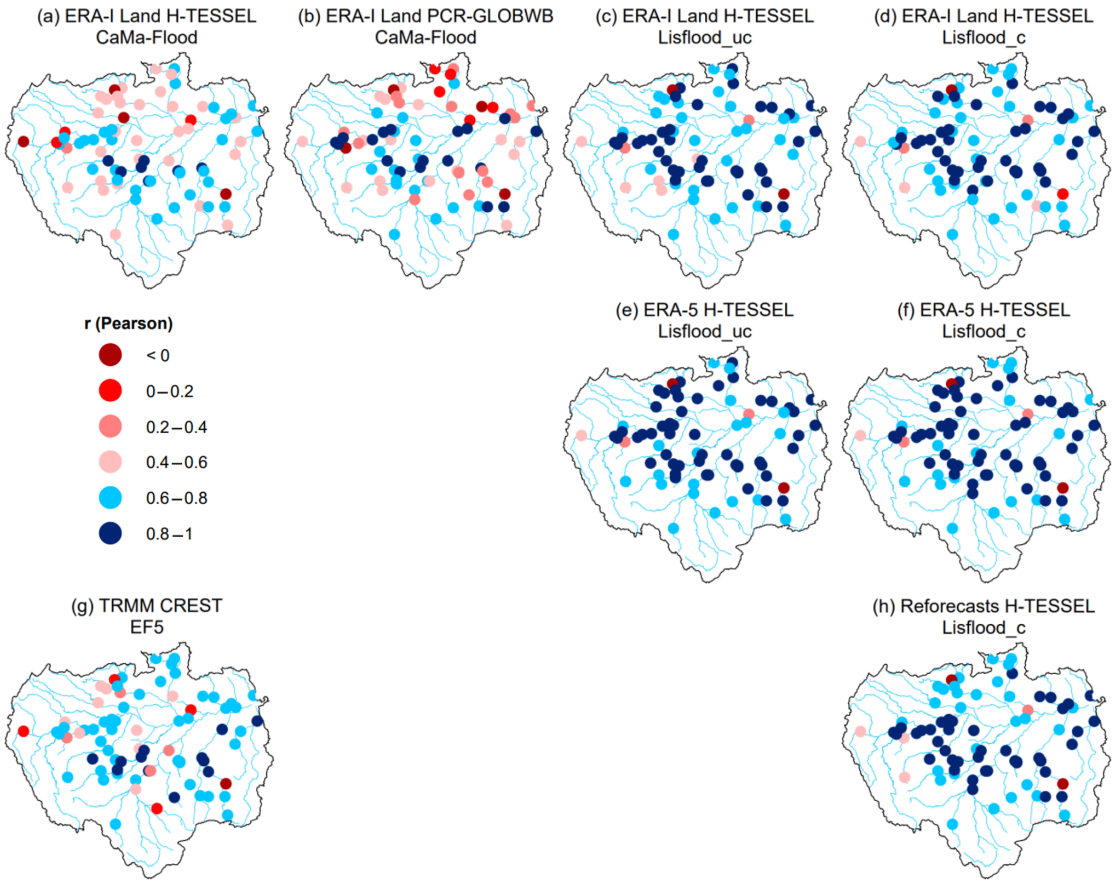


**Figure 3.** *Correlation component (Pearson's) of the KGE at the 75 hydrological gauging stations for all simulations. For the periods 1997–2015 and 2004–2015 for the Coupled Routing and Excess Storage, Ensemble Framework for Flash Flood Forecasting (CREST EF5) run (g). Values greater than 0.6 are considered skilful (i.e. blue circles).*

In contrast, 51 % and 47 % of stations achieve values exceeding 0.6 for CaMa-Flood H-TESSEL and CaMa-Flood PCR-GLOBWB respectively, with the hydrological model, PCR-GLOBWB, noting better performance at stations along the main stem. The increased performances of Lisflood relative to simulations incorporating CaMa-Flood are likely due to the increased

spatial resolution of the routing component (see Table 1). This is supported by results for CREST EF5, with 76 % of stations noting values above 0.6 and the model occupying a finer spatial resolution than that of CaMa-Flood (Fig. 3g).

The variance of modelled river flow is on average higher than the observed time series in all of the simulations, with the exception of the ERA-Interim Land PCR-GLOBWB CaMa-Flood simulation. For this run, 85 % of stations observe values of less than one, with stations situated in the Peruvian Amazon (2–5) the notable exception (Fig. 4b). In contrast, 79 % of stations for the CaMa-Flood set-up using the H-TESSEL LSM note values greater than one (Fig. 4a).

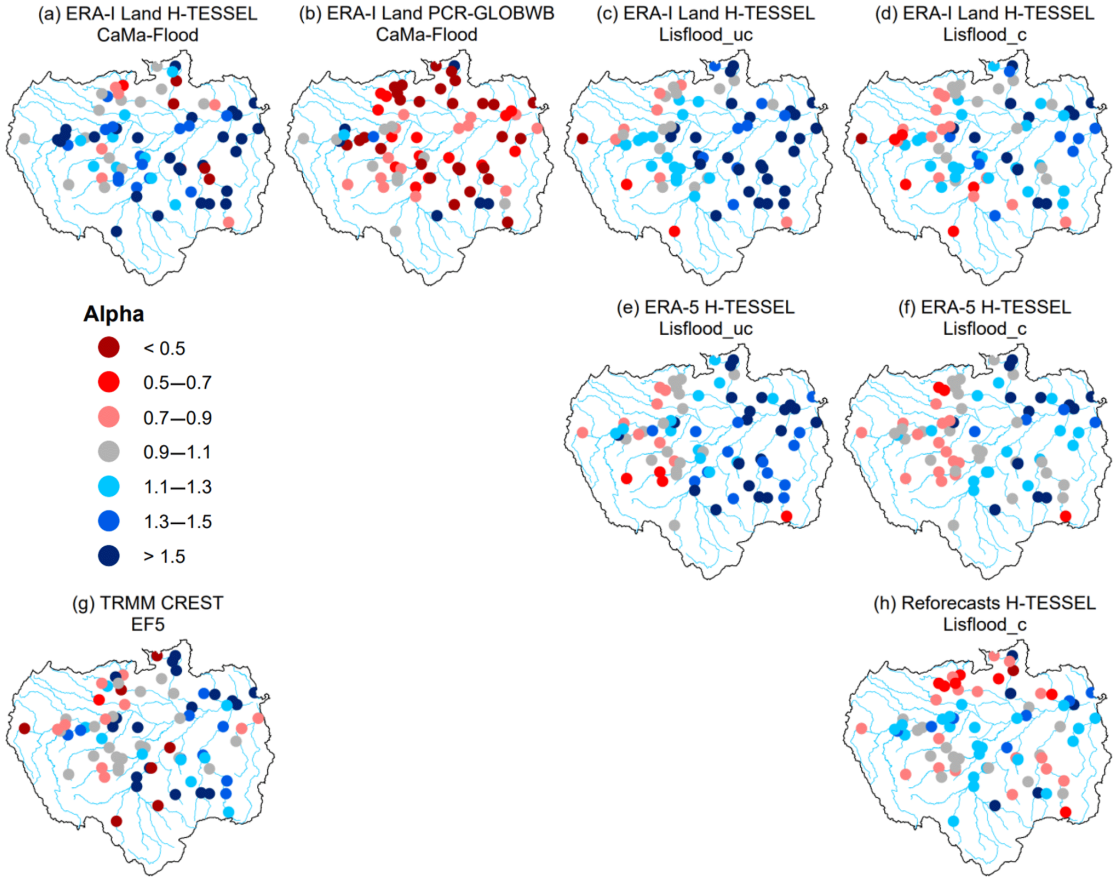


**Figure 4.** *Alpha (i.e. variability ratio) component of the KGE at the 75 hydrological gauging stations for all the simulations. For the periods 1997–2015 and 2004–2015 for the Coupled Routing and Excess Storage, Ensemble Framework for Flash Flood Forecasting (CREST EF5) run (g). Blue circles indicate that the variability in the simulated time series is higher than that of the observed one, while red circles show the opposite effect. Values closer to one indicate better model performance (i.e. grey circles).*

All runs tend to underestimate river flows relative to the observed time series, with the majority of stations observing a beta value of less than one (Fig. 5). In the calibrated Lisflood

simulation forced with the reforecasts, almost half of all the stations observe scores between 0.9 and 1.1 (i.e. grey circles), with a median of 0.99 (Table 2). These results are not replicated in the other two calibrated runs when using either ERA-Interim Land or ERA-5 as the precipitation input (Fig. 5d and f). For both of these runs a decrease is found in the number of stations achieving scores between 0.9 and 1.1 relative to the associated uncalibrated Lisflood set-ups (Fig. 5c and e). This is also highlighted by a decrease in the median scores of the two respective runs (Table 2), meaning that a greater water deficit exists in the calibrated set-ups.

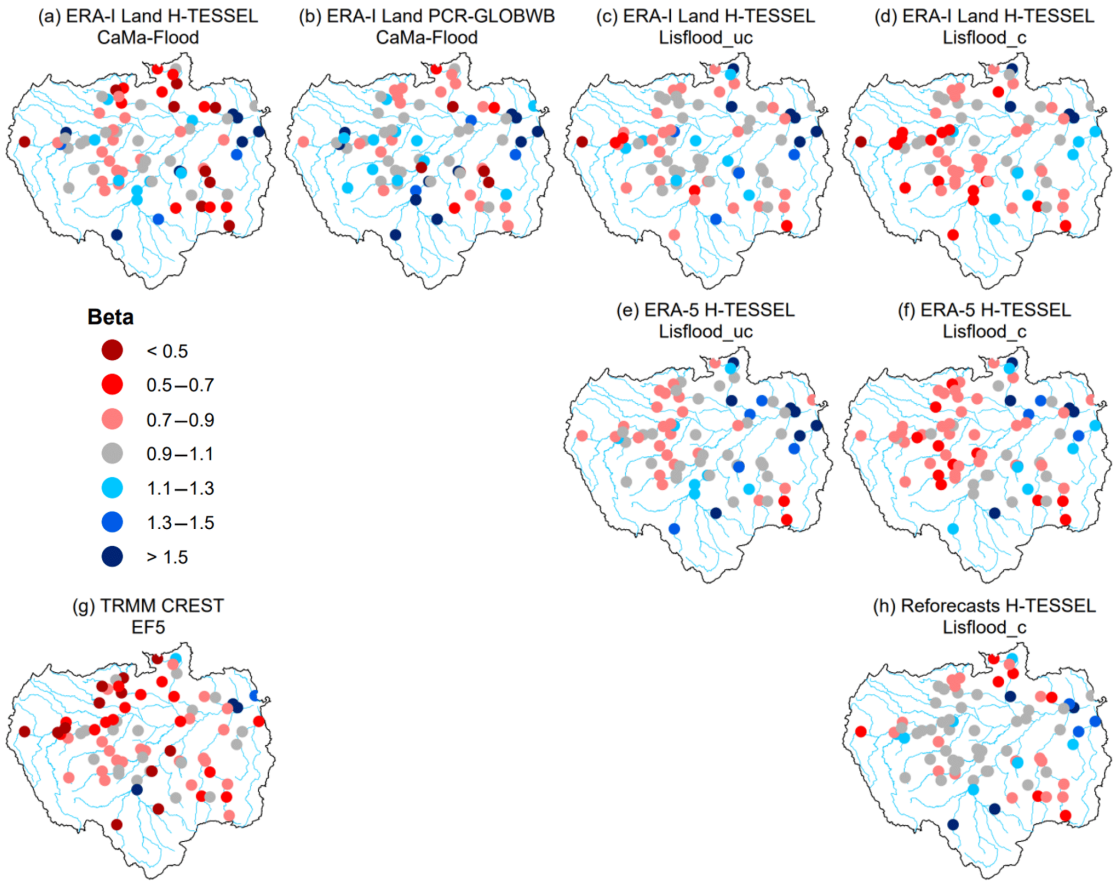


**Figure 5.** *Beta (i.e. bias ratio) component of the KGE at the 75 hydrological gauging stations for all the simulations. For the periods 1997–2015 and 2004–2015 for the Coupled Routing and Excess Storage, Ensemble Framework for Flash Flood Forecasting (CREST EF5) run (g). Blue circles indicate that the bias in the simulated time series is higher than that of the observed one, while red circles show the opposite effect. Values closer to one indicate better model performance (i.e. grey circles).*

The variance of modelled river flow is on average higher than the observed time series in all of the simulations, with the exception of the ERA-Interim Land PCR-GLOBWB CaMa-Flood simulation. For this run, 85 % of stations observe values of less than one, with stations situated

in the Peruvian Amazon (2–5) the notable exception (Fig. 4b). In contrast, 79 % of stations for the CaMa-Flood set-up using the H-TESSEL LSM note values greater than one (Fig. 4a). All runs tend to underestimate river flows relative to the observed time series, with the majority of stations observing a beta value of less than one (Fig. 5). In the calibrated Lisflood simulation forced with the reforecasts, almost half of all the stations observe scores between 0.9 and 1.1 (i.e. grey circles), with a median of 0.99 (Table 2). These results are not replicated in the other two calibrated runs when using either ERA-Interim Land or ERA-5 as the precipitation input (Fig. 5d and f). For both of these runs a decrease is found in the number of stations achieving scores between 0.9 and 1.1 relative to the associated uncalibrated Lisflood set-ups (Fig. 5c and e). This is also highlighted by a decrease in the median scores of the two respective runs (Table 2), meaning that a greater water deficit exists in the calibrated set-ups.

**Table 2.** *Median scores for the 75 hydrological gauging stations for all metrics.*

| Model Runs | Spearman Annual Max Correlations | KGE | r (Pearson's) | Beta | Alpha |
|---|---|---|---|---|---|
| ERA-Interim Land H-TESSEL CaMa-Flood | 0.24 | 0.30 | 0.61 | 0.92 | 1.33 |
| ERA-Interim Land PCR-GLOBWB CaMa-Flood | 0.23 | 0.18 | 0.59 | 0.98 | 0.64 |
| ERA-Interim Land H-TESSEL Lisflood_uc | 0.40 | 0.51 | 0.80 | 0.99 | 1.25 |
| ERA-Interim Land H-TESSEL Lisflood_c | 0.42 | 0.56 | 0.80 | 0.86 | 1.15 |
| ERA-5 H-TESSEL Lisflood_uc | 0.53 | 0.63 | 0.85 | 0.97 | 1.26 |
| ERA-5 H-TESSEL Lisflood_c | 0.54 | 0.64 | 0.86 | 0.87 | 1.06 |
| TRMM CREST EF5 | 0.24 | 0.46 | 0.71 | 0.80 | 1.08 |
| Reforecasts H-TESSEL Lisflood_c | 0.32 | 0.63 | 0.83 | 0.96 | 1.06 |
| Median across models | 0.35 | 0.50 | 0.78 | 0.91 | 1.11 |

Stations in the south-eastern Amazon, particularly in the upper reaches of the Teles Pires River (37, 38, and 49), tend to underestimate river flow for most simulations (Fig. 5). In this region of the basin precipitation is controlled by frontal systems in the South Atlantic Convergence Zone (SACZ), which is prevalent during austral summer (Ronchail et al., 2002; Espinoza et al., 2009b). In addition, rainfall variability in the Amazon is strongest in the south-east, with a distinct dry season (Paiva et al., 2012; Espinoza et al., 2009b). Further analysis could be useful in evaluating seasonal patterns of model performance to establish whether climatological features such as the SACZ are accurately represented within the precipitation datasets. Other factors impacting performance in the south-east could be associated with the geology and topography (Fig. 1c and d). Stations in this area of the basin are located within the Brazilian Shields, composed predominately of Precambrian rock, and are characterized by gentle slopes and low erosion rates (Filizola and Guyot, 2009). Paiva et al. (2012) demonstrated the importance of accurate initial conditions of groundwater state variables in the Tapajos and Xingu river basins, particularly for low flows. In comparison, the majority of the central parts of the basin are characterized by tertiary rocks, flat terrain, large floodplains, and high sediment yields. In these regions (e.g. in the south-western Brazilian Amazon), KGE scores are generally higher (Fig. 2), with surface water variables (e.g. water levels, surface runoff, and floodplain storage) considered more important in hydrological prediction uncertainties (Paiva et al., 2012).

The KGE allows us to make explicit interpretations of the hydrological performance of each model owing to decomposition into correlation, bias, and variability terms (Kling et al., 2012). The results indicate that the required developments to improve the representation of daily river flows are specific to each individual model and to the area of interest. For instance, for the ERA-Interim Land PCR-GLOBWB run, daily correlation scores (Fig. 3b) showed the model suffers in reproducing the temporal dynamics of flow (as measured by *r*) in northern catchments. Calibration of parameters which control the timing of the flood wave (e.g. river flow velocity) may improve performance, whereas model set-ups incorporating the uncalibrated Lisflood routing model generally had lower KGE values in the east of the basin corresponding to an overestimation of river flow variability (Fig. 4c and e). For these runs, performance slightly improved upon the calibration of the groundwater and routing parameters relating to timing, flow variability, and groundwater loss (Fig. 4d and f).

### 3.3.2 Which model set-up best represents annual maximum river flows?

Both the calibrated and uncalibrated versions of Lisflood simulations forced with the ERA-5 reanalysis are the best-performing runs, with median scores of 0.53 and 0.54 for the uncalibrated and calibrated simulations respectively (Fig. 7 and Table 2). However, a large deterioration in skill is evident for all simulations for Spearman's ranked coefficients between observed and predicted annual maximum river flows (Fig. 6), with only 21 % of stations on average observing scores exceeding 0.6 across all simulations. Here, it is important to note that due to the length of some station time series the number of overlapping data points can be small, and therefore the spatial distribution of model performance should be interpreted with caution. To provide a certain level of confidence between results, stations whose time series equals or exceeds 15 years are denoted using a circle, whereas those between 10–14 and 5–9 are represented using a square and triangle respectively.

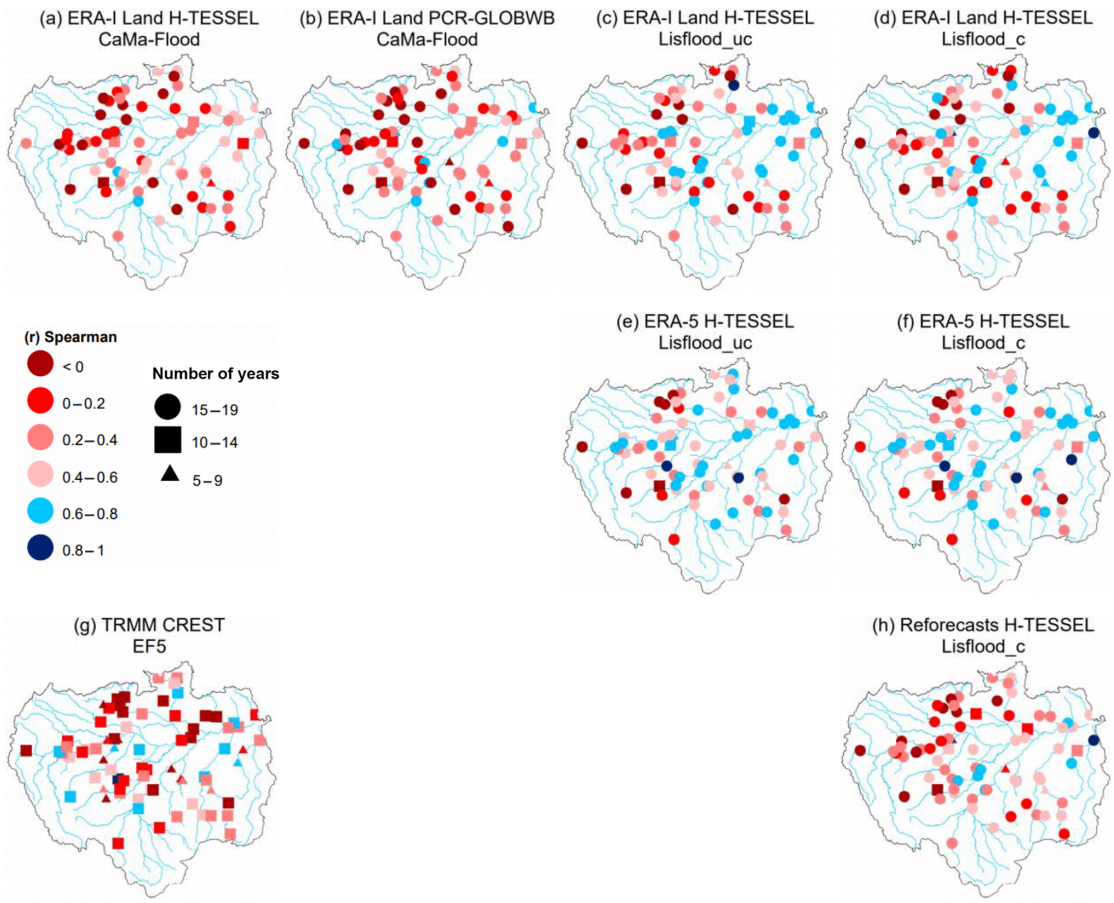


**Figure 6.** *Spearman's ranked correlation coefficients for observed against simulated annual maximum discharge values at the 75 hydrological gauging stations for all simulations. For the periods 1997–2015 and 2004–2015 for the Coupled Routing and Excess Storage, Ensemble*

*Framework for Flash Flood Forecasting (CREST EF5) run (g). Values exceeding 0.6 are considered skilful (i.e. blue shapes). The number of overlapping years of data between observations and simulations are denoted by different shapes. A triangle represents 5–9 years, a square 10–14 years, and a circle 15–19 years of overlapping data.*

The highest scores are generally located towards the eastern side of the basin and along the main Amazon River where the terrain is predominately flat, and rivers drain extensive floodplains. These are constrained to runs using the Lisflood routing model with either ERA-Interim Land or ERA-5 as forcing (Fig. 6c–f). Interestingly, the calibrated Lisflood set-up forced using the reforecasts does not replicate good performance in these regions (Fig. 6h), indicating that the error between simulated and observed peak river flows could be associated with the precipitation input. When observing daily mean precipitation totals over the validation period (1997–2015), the reforecasts observe lower precipitation totals over central to northern areas of the basin relative to both of the climate reanalysis datasets (Fig. 8). However, when comparing the results of the ERA-Interim Land H-TESSEL CaMa-Flood and ERA-Interim Land H-TESSEL Lisflood_uc set-ups, correlations are much lower in the CaMa-Flood simulation, suggesting that both precipitation and routing processes are equally important (Fig. 6a and c).

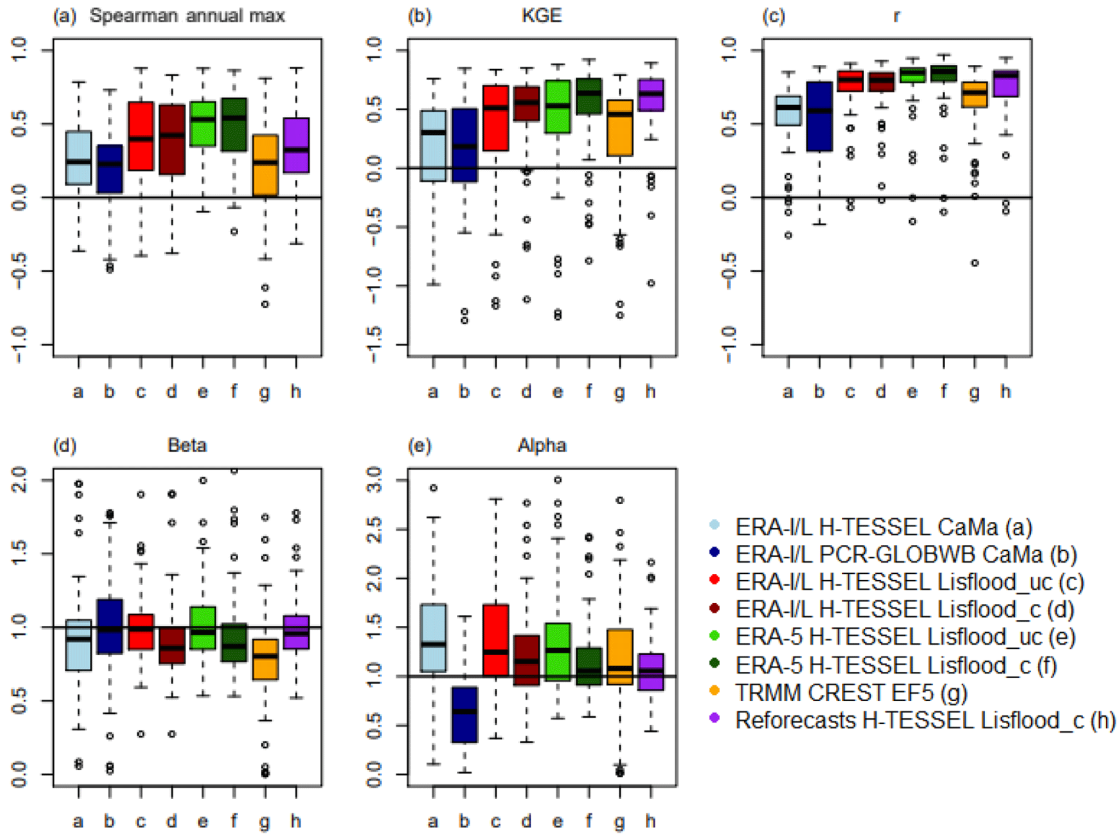


**Figure 7**. *Boxplots showing the distribution of scores for the (a) Spearman annual maximum correlation, (b) KGE, (c) KGE Pearson's coefficient, (d) KGE beta, and (e) KGE alpha, for all simulations. For the period 1997–2015.*

Low agreement between peaks is consistent in the south-east and north-west of the basin across all simulations (Fig. 6). In the south-east, a lack of skill could again be associated with the abundance of hydroelectric dams in the region or with the poor representation of the SACZ rainfall regime. Evaluating the ability to represent the timing and magnitude of the annual flood wave has important implications for models predicting flood hazard and for practices providing early warning information. These results identify that while the representation of daily river flows improves upon model calibration of the Lisflood routing model (Sect. 3.3.1), the influence of routing calibration for simulating flood peaks has no impact.

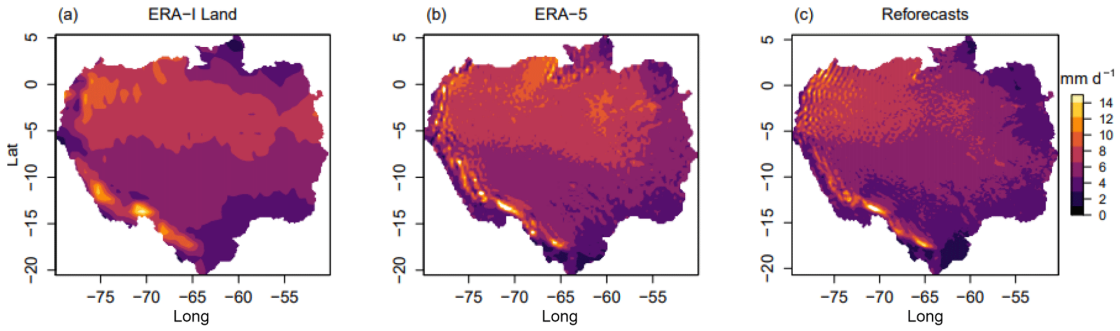


**Figure 8.** *Mean daily precipitation totals throughout the Amazon Basin. For (a) ERA-Interim Land, (b) ERA-5, and (c) the European Centre for Medium-Range Weather Forecasts (ECMWF) 20-year reforecasts. For the period 1997–2015.*

### 3.3.3 Which is the best performing hydrological model?

We assessed the performance of the CaMa-Flood and Lisflood_uc routing models by comparing the two runs which are forced using the ERA-Interim Land reanalysis dataset. On average the uncalibrated Lisflood run outperforms CaMa-Flood for all metrics analysed (Fig. 7 and Table 2). Results from the CREST EF5 model are also discussed but are not directly comparable due to using differing meteorological inputs.

The median score of the correlation component of the KGE (i.e. Pearson's correlation coefficient) is found to increase by 0.19 when using the un-calibrated Lisflood model relative to CaMa-Flood, with 28 more stations achieving a correlation score of 0.6 or higher (Fig. 3a and c). This number increases when considering correlation scores greater than 0.8, with 38 and 7 stations reaching this value for Lisflood and CaMa-Flood respectively. The most notable increase in skill is found in Peru along the Marañón and Napo rivers (2 and 5), which note increases of 0.85 and 0.71 respectively when using the Lisflood model. In comparison, the CREST EF5 simulation fits between the CaMa-Flood and Lisflood runs with a median daily correlation score of 0.71 and notes 12 stations which have scores greater than 0.8 (Fig. 3g).

For the overall KGE metric, 24 % and 3 % of stations have values exceeding 0.5 and 0.75 for CaMa-Flood. These figures rise to 52 % and 11 % respectively in the uncalibrated Lisflood run. Large differences are particularly notable at stations situated in the upper reaches of the Solimões River (2–6) and within a cluster of stations situated towards the Colombian Amazon in the north-west (Fig. 2c). Significant differences are identified for peak flow correlations, with only three stations (27, 17, and 22) achieving scores exceeding 0.6 for the CaMa-Flood simulation compared to 22 using the uncalibrated Lisflood routing scheme (Fig. 6a and c). In

comparison, the CREST EF5 simulation has 11 stations exceeding this threshold, with no distinguishable spatial pattern (Fig. 6g). For this run, the time series of modelled data is shorter (2004–2015), and so peak flow correlations should be interpreted with caution.

Stations located in and around the main Amazon River observe better performance for representing flood peaks in the Lisflood simulation (Fig. 6c), aligning with the locations of lakes included within the Lisflood set-up (see Zajac et al., 2017). This level of skill was not replicated in the CaMa-Flood simulation, where the representation of lakes is not included (Fig. 6a), suggesting the potential importance of lake parameterization for accurate peak flow estimations. However, Zajac et al. (2017) demonstrated that although the inclusion of lakes in Lisflood was found to generally improve the representation of extreme discharge for the 5- and 20-year return periods on the global domain, the change in skill upon the inclusion of lakes and reservoirs in the Amazon was minimal for several metrics. Very few reservoirs are included within Lisflood in the Amazon, and therefore the estimated effects on simulated streamflow are restricted.

Zhao et al. (2017) concluded the importance in the choice of different river routing schemes for simulating peak discharge across the globe, while the Hoch et al. (2017b) comparison of two routing models found results to differ despite having identical boundary conditions. It is therefore of interest to evaluate not only the entire GHM set-up, but also to assess the suitability of each model component of the hydrological chain in order to determine which routing model is most suitable for certain applications within the Amazon Basin. Results suggest that adjustments of certain parameters such as Manning's channel coefficient could potentially improve the performance of the CaMa-Flood model, with the default coefficient higher in the uncalibrated Lisflood set-up (0.10 as opposed to 0.03; see Hirpa et al., 2018, for all default parameter values).

### 3.3.4 Which is the best performing precipitation dataset?

Three precipitation products (ERA-Interim Land, ERA-5, and the reforecasts) are used to force the calibrated Lisflood routing model, with the most recent ERA-5 reanalysis product the best-performing dataset. Figure 8 displays mean daily precipitation totals for each dataset over the main validation period (1997–2015). The main differences can be seen in the far west of the basin towards the Andes mountains, where precipitation is higher in ERA-5 compared to ERA-Interim Land, and in the north-west, where average daily precipitation totals are smaller in the reforecasts. On the other hand, values in the south-eastern corner of the basin are very similar

between the three datasets. When comparing observed and simulated annual peak flows, median correlation scores improve by 0.12 and 0.22 when using ERA-5 compared to when using ERA-Interim Land and the reforecasts respectively (Table 2); 28 stations reach the 0.6 threshold relative to 22 and 9 stations for ERA-Interim Land and the reforecasts respectively, with the range of coefficients smaller for ERA-5 (Fig. 7a).

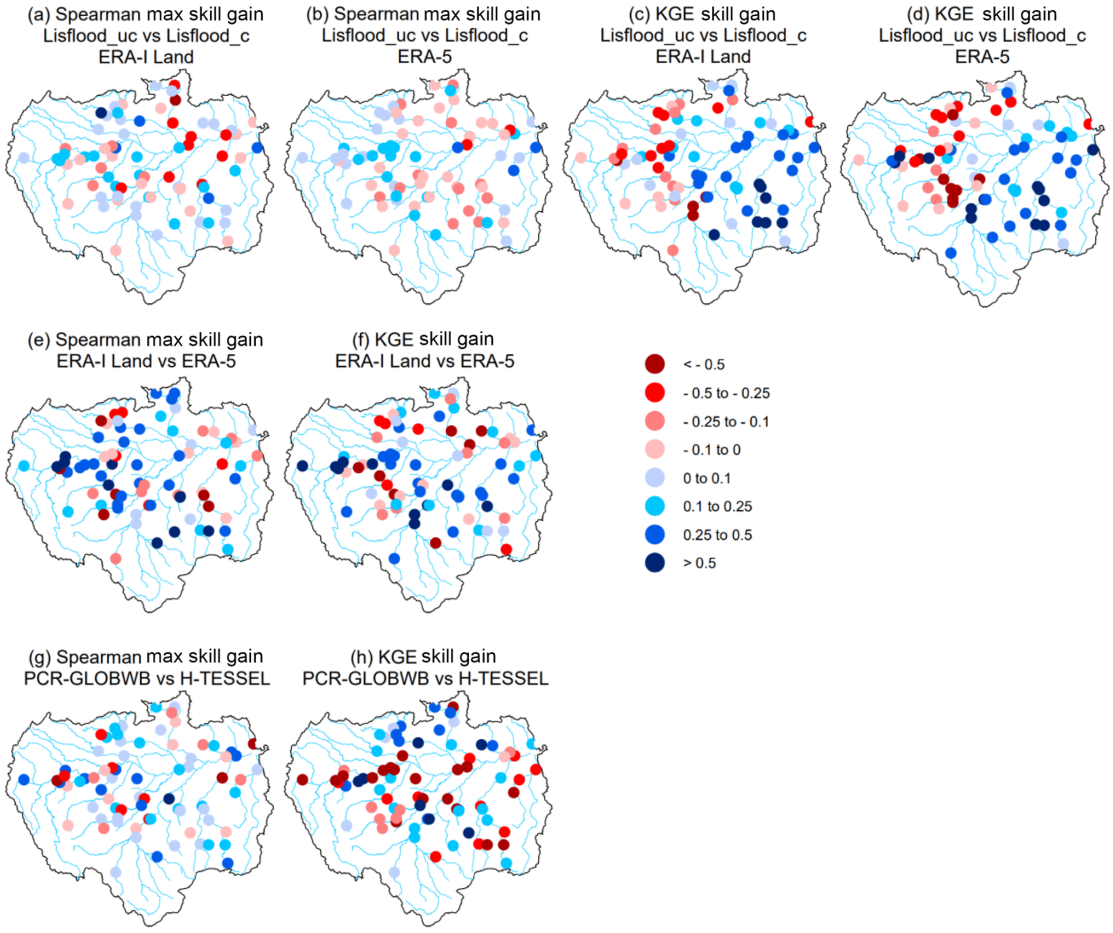


**Figure 9.** *Relative improvement in skill at each gauging station for Spearman annual maximum correlations and KGE values (i.e. skill scores). (a–d) show relative gain or loss in skill when using the calibrated Lisflood run (Lisflood_c) relative to the uncalibrated model run (Lisflood_uc), using precipitation forcing from both ERA-Interim Land and ERA-5. (e) and (f) show the relative gain or loss in skill when using ERA-5 as opposed to ERA-Interim Land. (g) and (h) show the relative gain or loss in skill when using the land surface model (LSM), the Hydrology-Tiled ECMWF Scheme for Surface Exchanges over Land (H-TESSEL), compared to the hydrological model, PCRaster Global Water Balance (PCR-GLOBWB). All scores are calculated using the skill scores in Eq. (1). Red circles indicate a decrease in skill, whereas blue circles represent an increase.*

In the other main tributary to the Solimões River, the Ucayali River, simulated annual peak flows show little agreement with observed data, with a decrease in skill identified when using ERA-5 as opposed to ERA-Interim Land (Fig. 9e). Despite the lack of agreement between observed and modelled data in the Ucayali River, the higher correlation scores identified downstream at Tamshiyacu suggest that better representation of high-water periods at the start of the Solimões River is likely modulated by the larger Marañón River. Therefore, the ability to represent flood hazard in communities near to the city of Iquitos is more dependent on how well we can predict river flow in the Marañón River.

All three runs perform well for the KGE metric, with little difference in results spatially (Fig. 2d, f, h). The reforecast simulation used within the Lisflood calibration is found to be superior, with 75 % of stations achieving scores which exceed 0.5 relative to 71 % and 59 % for ERA-5 and ERA-Interim Land respectively. Increased skill in the Peruvian Amazon is again the most noteworthy (Fig. 9f), with KGE skill scores of 0.67 for the Requena (3) (Ucayali River) and San Regis (2) (Marañón River) stations and 0.71 for Tamshiyacu (4) (Solimões River) when using ERA-5 relative to ERA-Interim Land. This increase in KGE skill can be attributed to an improvement in the variability and bias ratios found between the simulated and observed time series. Daily correlation scores for the three stations (2–4) are near identical to the variance and bias ratios underestimated for ERA-Interim Land while being much closer to the observed data for ERA-5 (Figs. 4d, f and 5d, f).

The Tamshiyacu gauging station (4) is used to measure flood hazard in the city of Iquitos at the start of the Solimões River (Espinoza et al., 2013) and is therefore of particular interest. At this important location, scatterplots of observed against simulated river discharge (Fig. 10) show that the negative bias observed when using ERA-Interim Land is corrected for when using ERA-5, with the magnitude of the 90th percentile of river flows almost identical to that of the observed dataset. Improvement is likely associated with the increased resolution of the ERA-5 reanalysis, which observes higher daily mean precipitation totals in regions towards the Andes in the far north-west of the basin (Fig. 8b). Waters found at Tamshiyacu are of Andean origin, meaning that the representation of rainfall in the Andes Mountains is fundamental to accurately predicting streamflow. ERA-5 runs at a horizontal resolution of ∼31 km and includes an additional 73 vertical levels to 0.01 hPa compared to ERA-Interim Land, meaning the representation of the troposphere is enhanced (ECMWF, 2017).

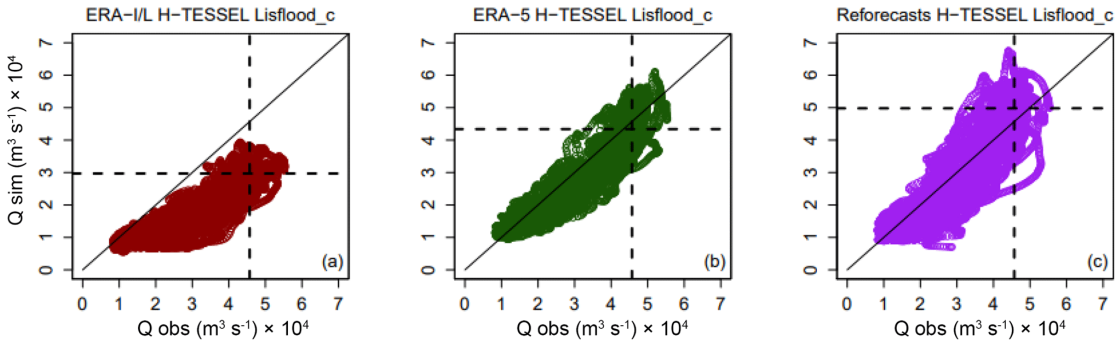


**Figure 10.** *Scatterplots of observed against simulated river flow at the Tamshiyacu gauging site, Peru (4). For (a) ERA-Interim Land, (b) ERA-5, and (c) the European Centre for Medium-Range Weather Forecasts (ECMWF), 20-year reforecasts forced through the calibrated Lisflood routing model. Dashed black lines indicate the observed and simulated 90th percentile of river flow. For the period 1997–2015.*

The success of GHMs in producing adequate estimates of river flow is underpinned by uncertainties within the meteorological input (Butts et al., 2004; Beven, 2012; Sood and Smakhtin, 2015). These results have particular importance for flood forecasting applications and research concerning extreme floods, with the higher-resolution ERA-5 dataset providing closer agreement between observed and simulated annual maximum river flows, particularly for the Peruvian Amazon. With the time series of observed data often beginning in the 1980s in the Amazon, ERA-5 could provide a useful tool for analysing historical flows and establishing links to climate variability. Upon completion, ERA-5 will date back to 1950 (Zsoter et al., 2019), meaning locations in which model skill is considered high could benefit from up to 30 years' worth of additional data for use in climate studies, thus allowing for more robust analysis. In future work, it could be of interest to compare the performance of ERA-5 against a wider range of precipitation datasets, such as the Multi-Source Weighted-Ensemble Precipitation (MSWEP) product that carefully integrates gauge, satellite, and reanalysis-based estimates. The Beck et al. (2017b) evaluation of 22 precipitation datasets previously demonstrated the advantages of using merged products for hydrological modelling purposes.

### 3.3.5 How do results differ between using a LSM and a hydrological model?

The H-TESSEL LSM and the PCR-GLOBWB hydrological model are directly compared whereby the precipitation forcing (ERA-Interim Land) and river routing scheme (CaMa-Flood) are consistent. Overall, it appears that the choice between using a LSM or a hydrological model in the Amazon Basin is dependent not only on the specific region of interest, but also on the

application and needs of the user. Previous studies (Zhang et al., 2016; Beck et al., 2017a) have found that LSMs, on average, perform better in rainfall-dominant regions, whereas hydrological models tend to achieve better results in snow-dominated regions owing to the use of complex energy balance equations introducing additional uncertainties. For the Amazon Basin, Spearman's rank correlation coefficients between simulated and observed peak river flow are closely matched, with medians of 0.24 and 0.23 for H-TESSEL and PCR-GLOBWB respectively (Table 2). However, the number of stations with Spearman's maximum correlation scores exceeding 0.6 is slightly higher in PCR-GLOBWB at seven compared to three with H-TESSEL (Fig. 6a and b).

To illustrate the gain or loss in skill when using H-TESSEL relative to PCR-GLOBWB, Spearman's annual maximum correlation and KGE skill scores were calculated for each station (Fig. 9g and h). Overall, 68 % of the stations show improved skill for peak river flow correlations when using the LSM, though the gain in skill is minimal (median correlation skill score = 0.06). This percentage drops to 37 % and 22 % for improvements in skill which exceed 0.1 and 0.2 respectively (Fig. 9g). By contrast, over half of the stations see improvements in the KGE skill score for the hydrological model, PCR-GLOBWB, and 23 % of the stations observe KGE skill score increases which exceed 0.25 (Fig. 9h).

A large loss in performance for the KGE is observed when using H-TESSEL for stations in the Peruvian Amazon at the confluence point to the Solimões River (Fig. 9h). Model performance in this region can largely be attributed to the failure of the H-TESSEL CaMa-Flood run to accurately represent the variance of flow and the temporal correlation component of the KGE, with the variability of modelled flow far higher than in the observed data (Fig. 4a). Northern regions in the Branco basin and stations situated towards the Colombian Amazon show the opposite effect with higher KGE coefficients found for the H-TESSEL CaMa-Flood run (Fig. 2a), indicating that model suitability is regionally specific.

### 3.3.6 By how much does calibration of groundwater and routing parameters improve performance?

Calibration of hydrological models is known to be a useful tool in providing more accurate estimates of river flow (Beck et al., 2017a). However, due to a lack of data and the computational expense required in the calibration of GHMs, many remain uncalibrated (Bierkens, 2015; Sood and Smakhtin, 2015). Both Gupta et al. (2009) and Mizukami et al. (2019) demonstrate that square error-type metrics are unsuitable for model calibration when

the model in question requires robust performance for high river flows. Improvement of flow variability estimates was documented in both studies when switching the calibration metric from the NSE to the KGE for both a simple rainfall–runoff model (similar to the HBV model; Bergström, 1995) and for two more complex hydrological models (Variable Infiltration Capacity and mesoscale Hydrologic Model), suggesting similar results are likely to be achieved for other hydrological models. To investigate the potential benefits of routing model calibration, whereby the KGE was used as the objective function, the time series of river discharge for the calibrated Lisflood runs forced using the ERA-Interim Land and ERA-5 reanalysis datasets were compared against the associated default set-ups without routing calibration.

Overall, hydrological performance improves upon model parameter calibration, with positive KGE skill scores (i.e. an increase in skill) at 61 % (59 %) of gauging stations for simulations forced with ERA-Interim Land (ERA-5) (Fig. 9c and d). The influence of calibration is stronger for the simulation forced with ERA-5, with the number of stations achieving "intermediate" KGE scores (i.e. $0.75 > \mathrm{KGE} \geqslant 0.5$) totalling 53 compared to 43 for ERA-Interim Land, an increase of 9 and 12 stations relative to the associated uncalibrated runs. When observing the spatial distribution of relative improvements, an east–west divide can be seen (Fig. 9c and d). Generally, decreases in skill are concentrated to stations on the western side of the basin, whereas stations located to the east display improved hydrological representation.

Three stations (2–4) in the Peruvian Amazon show increased KGE skill scores when using the calibrated ERA-5 run relative to the similar uncalibrated set-up (Fig. 9d). Conversely, a loss in skill is observed at each station for the calibrated run forced using ERA-Interim Land (Fig. 9c). These results are likely associated with a larger negative runoff bias within the ERA-Interim Land Lisflood_uc run relative to the ERA-5 Lisflood_uc simulation for the three stations (Fig. 5c and e). This is supported by Hirpa et al. (2018), who concluded that stations which have a negative streamflow bias in the default run (i.e. Lisflood_uc) also have a negative KGE skill score in the calibrated simulation owing to the challenge of correcting for a water deficit within the routing component. Thus, for GHMs which tend to underestimate runoff, adjustments of parameters within the LSM or hydrological model (e.g. those responsible for the portioning of precipitation into runoff) or through bias-correction measures within the precipitation dataset may be advantageous in efforts to accurately represent floods.

No significant differences between calibrated and uncalibrated Lisflood annual maximum correlation scores are identified (Fig. 7a and Table 2). In total, the number of stations

exceeding the 0.6 threshold for peak flow correlations remains the same for runs involving ERA-5 and decreases by one for ERA-Interim Land, meaning that the routing model calibration has very little impact on the ability to capture annual peaks. This suggests that calibrated parameters controlling flow timing (e.g. Manning's channel coefficient) are not as important for simulating the magnitude of higher flows in the Amazon Basin and that bias correction of the precipitation or calibration of parameters associated with runoff and evapotranspiration might be more useful. As previously highlighted by Hirpa et al. (2018), the inclusion of an objective function that is explicitly based on flood peaks could improve the ability of Lisflood to simulate floods. This is supported by previous studies (Greuell et al., 2015; Beck et al., 2017a; Mizukami et al., 2019) which have also identified that improved performance in calibrated models is predominately specific to metrics which are incorporated into the objective function used within the calibration. For instance, in Mizukami et al. (2019), they find that when using an application-specific metric (annual peak flow bias; APFB) for the calibration of two hydrological models, it produced the best peak flow annual estimates compared to using the NSE, KGE, and its components. However, despite this improvement, flood magnitudes were still underestimated for all metrics used in calibration, and the use of the APFB as the calibration metric resulted in poorer performance across the individual KGE components upon evaluation.

### 3.3.7 Limitations and future work

While estimating the magnitude of peak river flows is fundamental, more evaluation is required in assessing the ability to represent the timing of flood peaks. Modelled flood peaks have been known to occur too early in large Amazonian rivers (Alfieri et al., 2013; Hoch et al., 2017b), with accurate flow timing of significant importance in the Amazon Basin. For example, the time displacements between peak flows in coinciding tributaries are known to play a major role in the dampening of the Amazon flood wave (Tomasella et al., 2010) and in the synchronization of flood peaks, commonly associated with exceptional flood events (e.g. Marengo et al., 2012; Espinoza et al., 2013; Ovando et al., 2016). Additional evaluation using metrics which focus specifically on the timing aspect, such as the delay index (Paiva et al., 2013), would enable a more complete assessment of the hydrological modelling regime.

A limitation of this type of study is due to the intercomparison being restricted to the macroscale (i.e. only a subset of potential modelling configurations is considered). In future work it would be useful to increase the granularity of the modelling decision matrix to allow conclusions to be more generalized across the modelling community. For instance, when

comparing the performance of the Lisflood and CaMa-Flood routing models, the results are specific to the simulations forced using the ERA-Interim Land reanalysis dataset. Although useful in providing a general indication of routing performance for each model when using a climate reanalysis dataset, the conclusions are specific to that particular comparison, with differing results possible when using another precipitation input. Future work could investigate one of the research questions stated in the objectives (Sect. 3.1.5) at a finer resolution, for example by comparing several different runs which use the Lisflood and CaMa-Flood routing models, whereby a greater variety of precipitation inputs are considered (e.g. MSWEP, CHIRP V2.0, ERA-5, TRMM v.7). Such analysis would allow more general conclusions and recommendations to be made to the modelling community, who are interested in those particular routing schemes. A similar approach could be adopted for the assessment of other components of the hydrological modelling chain.

## 3.4 Conclusions

In this paper, eight different GHMs were employed in an intercomparison analysis using two verification metrics to assess model performance against gauged river discharge observations. The motivation for this work stemmed from the need to evaluate the ability of GHMs to reproduce historical floods in the Amazon Basin for use in climate analysis and to identify the strengths and weaknesses which exist along the hydrological modelling chain in order to provide insight to model developers. The implications of these results suggest that the choice of precipitation dataset is the most influential component of the GHM set-up in terms of our ability to recreate annual maximum river flows in the Amazon Basin. This is evident with average station correlations between observed and simulated annual maximum river flows increasing when using the new ERA-5 reanalysis dataset, with significant improvements in locations of the Peruvian Amazon. In this region, waters are sourced from Andean origins where rainfall can often be poorly represented due to topographically complex terrains (Paiva et al., 2013). Thus, those wishing to simulate higher flows in the upper reaches of the Amazon may benefit from choosing a precipitation dataset which has a high spatial resolution, whereby the upper atmosphere is discretized at finer scales. Although an exact recommended spatial resolution cannot be provided based on the results of this study alone, previous works (e.g. Beck et al., 2017b) support the need for a comparatively high-resolution dataset in addition to other advantageous factors such as a long temporal record and the inclusion of daily gauge corrections.

Although parameter calibration of the Lisflood routing model improved the representation of the whole hydrological regime across the basin, the agreement between observed and simulated peak discharge values saw no change upon calibration. This indicates that the benefit of calibration is confined to the objective function used, in this case the KGE, and highlights that further model calibration using an objective function that fits the purpose of the application (e.g. RMSE of flood peaks or APFB for flood forecasting systems) could be worth considering. It is important to reiterate however that thoughtful consideration is required if choosing application-specific metrics, with the potential to degrade performance in other aspects of the hydrological regime (e.g. bias and flow variability ratios) a concern (Mizukami et al., 2019). The relative importance of good performance in the specific target metric compared to better performance for a range of metrics should be assessed on a model-by-model and circumstantial basis, taking into account the needs of potential users.

**Data availability.** All of the data and models used in this study were obtained from collaborators of the Global Flood Partnership (GFP) and are freely available. Access to these sources is mentioned in Sect. 3.2.

**Acknowledgements.** Jamie Towner is grateful for financial support from the Natural Environment Research Council (NERC) as part of the SCENARIO Doctoral Training Partnership (grant agreement NE/L002566/1). The first author is grateful for travel support and funding provided by the Red Cross Red Crescent Climate Centre, to the research and national services, SO-HYBAM, IRD, SENAMHI, ANA, and INAMHI, for providing observed river discharge data, and to the ECMWF for computer access and technical support. Finally, specific thanks go to Christel Prudhomme and the Environmental Forecasts team in the Evaluation Section at the ECMWF for their advice and support throughout the analysis and writing of the manuscript.

## 3.5 Supplementary material

Gauging station information can be found in Table S1 below, with results of the analysis between 2004 and 2015 displayed in Figs. S1 and S2.

**Table S1**. Characteristics of the 75 hydrological gauging stations used in the analysis. Station numbers correspond to those in Fig. 1a. Mean observed discharge is taken from observed values.

| Station name (number) | Country | River | Drainage area ($Km^2$) | Lat | Lon | Start | End | Mean Q ($m^3s^{-1}$) |
|---|---|---|---|---|---|---|---|---|
| Borja (1) | Peru | Marañón | 114232 | -4.45 | -77.55 | 01/01/1997 | 10/01/2015 | 5122.614 |
| San Regis (2) | Peru | Marañón | 356274 | -4.45 | -73.95 | 01/01/1997 | 29/09/2015 | 17418.04 |
| Requena (3) | Peru | Ucayali | 346049 | -4.75 | -73.65 | 01/07/1996 | 29/09/2015 | 11895.5 |
| Tamshiyacu (4) | Peru | Solimões | 721521 | -4.05 | -73.15 | 01/01/1997 | 31/12/2015 | 30205.58 |
| Bellavista (5) | Peru | Napo | 100136 | -3.45 | -73.05 | 01/01/1997 | 29/09/2015 | 6734.2 |
| Palmeiras Do Javari (6) | Brazil | Javari | 16256 | -5.15 | -72.85 | 01/01/1997 | 31/12/2015 | 611.3425 |
| Foz Do Breu (7) | Brazil | Jurua | 10446 | -9.45 | -72.75 | 01/01/1997 | 31/12/2015 | 178.0443 |
| Santa Maria (8) | Brazil | Curuca | 24351 | -4.65 | -71.45 | 02/04/1999 | 22/12/2015 | 1009.045 |
| Estirao Do Repouso (9) | Brazil | Javari | 62105 | -4.35 | -70.95 | 02/11/1980 | 31/12/2015 | 2563.211 |
| Tabatinga (10) | Brazil | Peru | 874000 | -4.25 | -69.95 | 01/01/1997 | 31/12/2015 | 36514.11 |
| Colocacao Caxias (11) | Brazil | Jutai | 10257 | -5.55 | -69.15 | 01/01/1997 | 14/07/2011 | 476.0549 |
| Envira (12) | Brazil | Tarauaca | 48317 | -7.45 | -70.05 | 01/01/1997 | 16/09/2015 | 1261.317 |
| Manouel Urbano (13) | Brazil | Purus | 33693 | -8.75 | -69.15 | 01/01/1997 | 30/12/2009 | 788.6026 |
| Seringal Sao Jose (14) | Brazil | Iaco | 10471 | -9.75 | -68.85 | 01/01/1997 | 06/12/2012 | 232.0125 |
| Rurrenabaque (15) | Bolivia | Beni | 70000 | -14.55 | -67.55 | 01/01/1997 | 31/12/2015 | 2189.476 |

| Station name (number) | Country | River | Drainage area ($Km^2$) | Lat | Lon | Start | End | Mean Q ($m^3s^{-1}$) |
|---|---|---|---|---|---|---|---|---|
| Pedras Negras (16) | Bolivia | Guapore | 110000 | -12.85 | -62.95 | 01/01/1997 | 31/07/2014 | 852.545 |
| Guajara-Mirim (17) | Brazil | Mamore | 609000 | -10.75 | -65.35 | 01/01/1997 | 29/06/2014 | 7810.131 |
| Abuna (18) | Brazil | Madeira | 921000 | -9.75 | -65.35 | 01/01/1997 | 29/06/2014 | 18152.22 |
| Floriano Peixoto (19) | Brazil | Acre | 33469 | -9.05 | -67.35 | 01/01/1997 | 31/12/2015 | 692.1766 |
| Valparaiso (20) | Brazil | Purus | 103285 | -8.65 | -67.35 | 01/01/1997 | 31/12/2015 | 13832.18 |
| Seringal Fortaleza (21) | Brazil | Purus | 153016 | -7.75 | -66.95 | 01/01/1997 | 31/12/2015 | 4003.07 |
| Fazenda Borangaba (22) | Brazil | Pauini | 23365 | -7.55 | -67.55 | 04/01/1997 | 31/12/2015 | 799.6944 |
| Santos Dumont (23) | Brazil | Jurua | 142646 | -6.55 | -68.35 | 01/01/1997 | 31/12/2015 | 4304.748 |
| Barreira Alta (24) | Brazil | Jutai | 35880 | -4.25 | -67.95 | 01/01/1997 | 14/04/2009 | 1641.192 |
| Sao Paulo De Olivenca (25) | Brazil | Amazon | 990781 | -3.45 | -68.75 | 01/01/1997 | 30/12/2011 | 47554.85 |
| Santo Antonio Do Ica (26) | Brazil | Amazon | 1134540 | -3.15 | -67.95 | 01/01/1997 | 26/02/2014 | 56355.19 |
| Porto Seguro (27) | Brazil | Jutai | 64400 | -3.35 | -67.55 | 01/01/2008 | 31/12/2015 | 2548.144 |
| Estirao Da Santa Cruz (28) | Brazil | Tefe | 13708 | -4.35 | -65.25 | 01/01/1997 | 31/12/2015 | 571.2913 |
| Bacaba (29) | Brazil | Tapaua | 38270 | -6.35 | -64.95 | 01/01/1997 | 31/12/2015 | 1668.033 |
| Canutama (30) | Brazil | Purus | 230012 | -6.55 | -64.45 | 01/01/1997 | 31/12/2015 | 6478.216 |
| Labrea (31) | Brazil | Purus | 226351 | -7.25 | -64.75 | 01/01/1997 | 31/12/2015 | 5639.943 |
| Porto Velho (32) | Brazil | Madeira | 976000 | -8.75 | -63.95 | 01/01/1997 | 31/12/2015 | 18485.47 |

| Station name (number) | Country | River | Drainage area ($Km^2$) | Lat | Lon | Start | End | Mean Q ($m^3s^{-1}$) |
|---|---|---|---|---|---|---|---|---|
| Santa Isabel (33) | Brazil | Candeias | 12600 | -8.75 | -63.75 | 01/01/1997 | 29/06/2014 | 330.8341 |
| Sitio Bela Vista (34) | Brazil | Ji-Parana | 16100 | -11.65 | -61.15 | 01/01/1997 | 30/07/2014 | 381.4905 |
| Fontanilhas (35) | Brazil | Juruena | 55900 | -11.45 | -58.35 | 01/01/1997 | 29/06/2014 | 1359.172 |
| Porto Dos Gauchos (36) | Brazil | Arinos | 37100 | -11.55 | -57.45 | 01/01/1997 | 30/05/2014 | 688.1856 |
| Porto Roncador (37) | Brazil | Teles Pires | 10800 | -13.55 | -55.35 | 01/01/1997 | 30/05/2014 | 249.8181 |
| Cachoeirao (38) | Brazil | Teles Pires/Sao Manuel | 34600 | -11.55 | -55.65 | 01/01/1997 | 30/07/2014 | 858.4991 |
| Humboldt (39) | Brazil | Aripuana | 15200 | -10.25 | -59.45 | 01/01/1997 | 29/06/2014 | 319.7378 |
| Leontino (40) | Brazil | Guariba | 16300 | -7.85 | -60.55 | 01/01/1997 | 30/12/2011 | 375.8513 |
| Boca Do Guariba (41) | Brazil | Aripuana | 70100 | -7.75 | -60.55 | 01/01/1997 | 30/12/2011 | 1403.749 |
| Fazenda Boa Lembranca (42) | Brazil | Roosevelt | 59400 | -7.65 | -60.75 | 01/01/1997 | 30/08/2011 | 1527.78 |
| Nova Esperanca (43) | Brazil | Marmelos | 26200 | -6.55 | -61.75 | 01/01/2009 | 27/02/2014 | 973.4268 |
| Manacapuru (44) | Brazil | Amazon | 2147736 | -3.35 | -60.65 | 01/01/1997 | 31/12/2015 | 105720 |
| Jatuarana (45) | Brazil | Amazon | 2854286 | -3.05 | -59.65 | 01/01/1997 | 30/01/2015 | 126994.8 |
| Barra Do Sao Manuel (46) | Brazil | Tapajos | 333000 | -7.35 | -58.15 | 01/01/1997 | 30/03/2014 | 7736.416 |
| Tres Marias (47) | Brazil | Teles Pires | 138000 | -7.65 | -57.95 | 01/01/1997 | 30/03/2014 | 3663.747 |
| Santa Rosa (48) | Brazil | Teles Pires | 131000 | -8.85 | -57.45 | 03/06/2005 | 30/03/2013 | 3646.457 |
| Indeco (49) | Brazil | Teles Pires | 52200 | -10.15 | -55.55 | 01/01/1997 | 09/12/2013 | 1193.669 |

| Station name (number) | Country | River | Drainage area ($Km^2$) | Lat | Lon | Start | End | Mean Q ($m^3s^{-1}$) |
|---|---|---|---|---|---|---|---|---|
| Cajueiro (50) | Brazil | Curua | 35213 | -5.85 | -54.55 | 01/01/1997 | 08/05/2011 | 784.37 |
| Itaituba (51) | Brazil | Tapajos | 458000 | -4.25 | -55.95 | 01/01/1997 | 31/12/2015 | 11376.96 |
| Pedra Do O (52) | Brazil | Iriri | 123827 | -4.45 | -53.95 | 01/01/1997 | 30/07/2012 | 2413.806 |
| Altamira (53) | Brazil | Xingu | 446203 | -3.35 | -52.15 | 01/01/1997 | 29/04/2014 | 7736.717 |
| Sao Francisco (54) | Brazil | Jari | 51343 | -0.55 | -52.55 | 01/01/1997 | 21/03/2014 | 1218.271 |
| Arapari (55) | Brazil | Maicuru | 17072 | -1.85 | -54.45 | 01/01/1997 | 27/02/2014 | 127.2518 |
| Boca Do Inferno (56) | Brazil | Curua | 20803 | -1.45 | -54.95 | 01/01/1997 | 29/09/2013 | 192.2409 |
| Óbidos (57) | Brazil | Amazon | 4680000 | -1.95 | -55.55 | 01/01/1997 | 31/12/2015 | 178193.9 |
| Garganta (58) | Brazil | Trombetas | 37910 | -0.75 | -56.85 | 01/01/1997 | 29/04/2014 | 1493.961 |
| Aldeia Wai-Wai (59) | Brazil | Mapuera/Urucurina | 21400 | -0.65 | -58.05 | 01/01/1997 | 27/02/2013 | 664.3051 |
| Cachoeira Morena (60) | Brazil | Uatuma | 20394 | -2.15 | -59.35 | 02/01/2005 | 30/05/2014 | 673.3568 |
| Base Alalau (61) | Brazil | Alalau | 7080 | -0.65 | -61.35 | 01/01/1997 | 30/05/2014 | 245.8977 |
| Caracarai (62) | Brazil | Branco | 124980 | 1.85 | -61.05 | 01/01/1997 | 31/12/2015 | 3170.343 |
| Fe E Esperanca (63) | Brazil | Mucajai | 13658 | 2.85 | -61.45 | 01/01/1997 | 29/04/2014 | 348.695 |
| Fazenda Cajupiranga (64) | Brazil | Uraricoera | 35727 | 3.45 | -61.15 | 01/01/1997 | 30/03/2014 | 635.5902 |
| Uaicas (65) | Brazil | Uraricoera | 16065 | 3.45 | -63.15 | 01/01/1997 | 27/02/2014 | 602.7468 |

| **Station name (number)** | Country | River | Drainage area ($Km^2$) | Lat | Lon | Start | End | Mean Q ($m^3s^{-1}$) |
|---|---|---|---|---|---|---|---|---|
| Posto Ajuricaba (66) | Brazil | Demeni | 14756 | 0.95 | -62.65 | 01/01/1997 | 29/04/2014 | 550.2058 |
| Serrinha (67) | Brazil | Negro | 279945 | -0.45 | -64.95 | 01/01/1997 | 31/12/2015 | 16845.52 |
| Acanaui (68) | Brazil | Caqueta/Japura | 242259 | -1.85 | -66.65 | 01/01/1997 | 31/12/2015 | 14399.93 |
| Jusante Da Cachoeira Do Caju (69) | Brazil | Curicuriari | 10228 | -0.25 | -67.05 | 01/01/1997 | 30/03/2014 | 937.4047 |
| Sao Felipe (70) | Brazil | Negro | 110862 | 0.45 | -67.35 | 01/01/1997 | 29/04/2014 | 8314.548 |
| Cucui (71) | Brazil | Negro | 61781 | 1.35 | -66.85 | 01/01/1997 | 29/04/2014 | 5113.101 |
| Missao Icana (72) | Brazil | Icana | 22282 | 1.15 | -67.65 | 01/01/1997 | 30/03/2014 | 1902.729 |
| Taraqua (73) | Brazil | Vaupes | 44732 | 0.15 | -68.55 | 01/01/1997 | 29/04/2014 | 2665.905 |
| Uaracu (74) | Brazil | Vaupes | 40506 | 0.45 | -69.15 | 01/01/1997 | 29/11/2011 | 2415.104 |
| Vila Bittencourt (75) | Colombia | Caqueta/Japura | 197136 | -1.35 | -69.45 | 01/01/1997 | 31/12/2015 | 2188.119 |

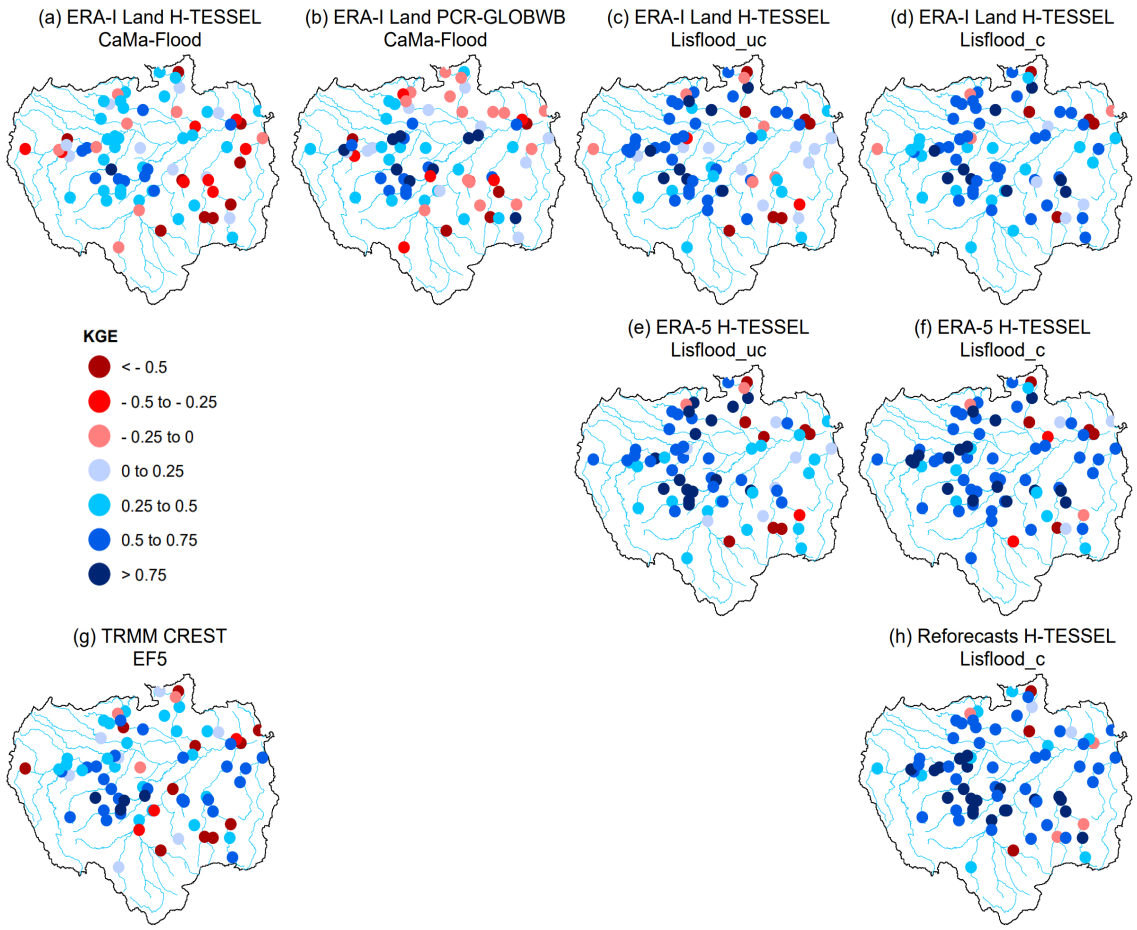


**Figure S1.** *Full KGE scores at 75 hydrological gauging stations for all simulations (2004-2015). Values greater than 0.75 are considered to indicate good performance (i.e. dark blue circles).*

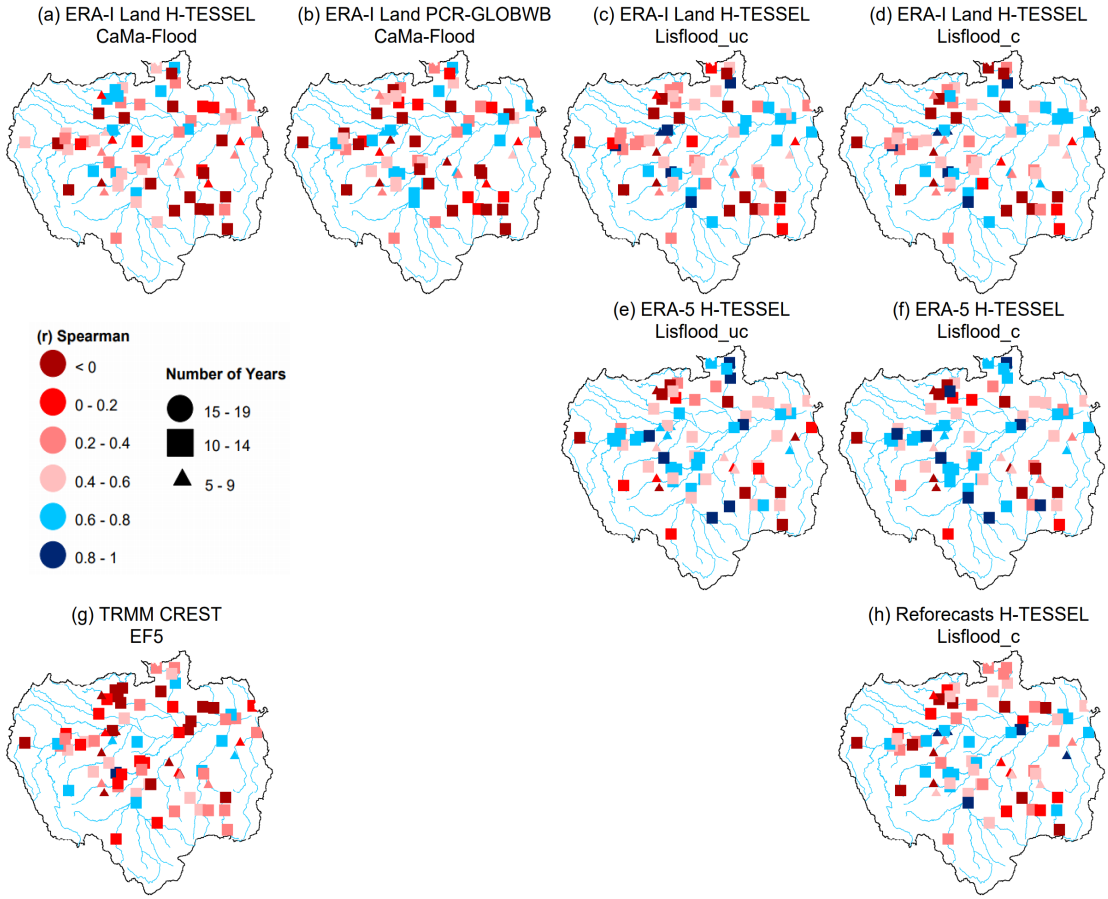


**Figure S2.** *Spearman ranked correlation coefficients for observed against simulated annual maximum discharge at 75 hydrological gauging stations for all simulations (2004-2015). Values exceeding 0.6 are considered skilful (i.e. blue shapes). Number of overlapping years of data between observations and simulations are denoted by different shapes. A triangle represents 5-9 years, a square 10-14 years, and a circle 15-19 years of overlapping data.*

# Chapter 4

# Influence of ENSO and tropical Atlantic climate variability on flood characteristics in the Amazon Basin

In Chapter 2, one of the main conclusions called for an extended climate variability analysis of flood characteristics which included, a) a basin wide approach, b) the use of several climate indices, including the ability to distinguish between central and eastern Pacific ENSO events, and c) a study that focuses on the timing, and duration of high flows in addition to flood magnitude. While results from Chapter 3 highlighted the improved performance of GloFAS at detecting peak river flows when ERA5 was used as the precipitation input. Thus, to assess how phases of large-scale climate variability impacts flood characteristics (i.e. magnitude, timing, and duration of flows) in the Amazon, a basin wide analysis is undertaken for both observed and simulated data.

This paper has been published as a research article in the journal of Hydrology and Earth System Sciences (HESS), with the following reference:

Towner, J., Ficchí, A., Cloke, H. L., Bazo, J., Coughlan de Perez, E., and Stephens, E. M.: Influence of ENSO and tropical Atlantic climate variability on flood characteristics in the Amazon basin, Hydrol. Earth Syst. Sci., 25, 3875–3895, https://doi.org/10.5194/hess-25-3875-2021, 2021.



The contributions of the authors of this paper are as follows: J.T, A.F, E.M.S, and H.L.C designed the analysis, with A.F providing the original methodology and R scripts for the flood timing section of the analysis. J.T undertook all of the analysis, produced all figures, in addition to writing the research paper. A.F, E.M.S, H.L.C, J.B, and E.C supervised the research, provided important advice, and commented on the manuscript. Overall, 90% of the research and 85% of the writing of the manuscript was undertaken by J.T.

**Abstract.** Flooding in the Amazon Basin is frequently attributed to modes of large-scale climate variability, but little attention is paid to how these modes influence the timing and

duration of floods despite their importance to early warning systems and the significant impacts that these flood characteristics can have on communities. In this study, river discharge data from the Global Flood Awareness System (GloFAS 2.1) and observed data at 58 gauging stations are used to examine whether positive/negative phases of several Pacific and Atlantic indices significantly alter the characteristics of river flows throughout the Amazon Basin (1979–2015). Results show significant changes in both flood magnitude and duration, particularly in the north-eastern Amazon for negative ENSO years when the SST anomaly is positioned in the central tropical Pacific. This response is not identified for the eastern Pacific index, highlighting how the response can differ between ENSO types. Although flood magnitude and duration were found to be highly correlated, the impacts of large-scale climate variability on these characteristics are non-linear; some increases in annual flood maxima coincide with decreases in flood duration. The impact of flood timing however does not follow any notable pattern for all indices analysed. Finally, observed and simulated changes are found to be much more highly correlated for negative ENSO years compared to the positive phase, meaning that GloFAS struggles to accurately simulate the differences in flood characteristics between El Niño and neutral years. These results have important implications for both the social and physical sectors working towards the improvement of early warning action systems for floods.

## 4.1 Introduction

Flooding in the Amazon basin is frequently attributed to positive and negative phases of large-scale climate variability, such as the El Niño–Southern Oscillation (ENSO), and to anomalous sea surface temperatures (SSTs) in the tropical Atlantic Ocean (Richey et al., 1989; Ronchail et al., 2005a; Marengo et al., 2012, 2013; Satyamurty et al., 2013; Espinoza et al., 2013, 2014, 2019; Marengo and Espinoza, 2016; Barichivich et al., 2018). Such phases are considered to promote atmospheric anomalies (e.g. zonal winds, 850 hPa geopotential height and moisture transport flux), which enhance or weaken moisture and humidity fluxes over the Amazon basin affecting rainfall and river discharge regimes and, therefore, influencing flood likelihood (Espinoza et al., 2013, 2014). For instance, flooding is consistently linked to La Niña conditions and to a configuration of cold (warm) SST anomalies in the tropical north (south) Atlantic Ocean (Marengo and Espinoza, 2016). Conversely, droughts are commonly attributed to El Niño events and to warm SST anomalies in the tropical North Atlantic (TNA) and associated with a sustained northward position of the inter-tropical convergence zone (ITCZ; Zeng et al., 2008; Tomasella et al., 2011).

The impact of different climatic phases tends to cause a similar response for both rainfall and river discharge (Towner et al., 2020), though the relationship between flooding and rainfall can be non-linear (Stephens et al., 2015; Coughlan de Perez et al., 2017) with significant differences identified between the mean state of the two variables in response to the same climate phase (Dettinger and Diaz, 2000). An example of this for the Amazon is detailed by Marengo et al. (2012) in a comparison study of the 1989, 1999 and 2009 floods, whereby the worst flood event did not correspond with the largest rainfall anomaly ($mm^{-1}$ $d^{-1}$). It is therefore important to consider the effect of climate phases for river discharge specifically.

To date, the scientific community has mainly focused on how anomalous SST conditions affect the magnitude of rainfall or river discharge (Ronchail et al., 2002, 2005b; Espinoza et al., 2009; Yoon and Zeng, 2010; Yoon, 2016), despite the importance of other characteristics such as flood timing and duration. In early 2018, the Red Cross Climate Centre (RCCC) led an inter-agency assessment mission to establish how communities living within the Peruvian Amazon floodplain are affected by exceptional flood events. Impacts of flooding (e.g. lack of food, fresh water and medical supplies) have been associated with the duration of inundation as opposed to simply the magnitude of flood extent by community members. For example, a study by Langill and Abizaid (2019) provided direct feedback from community members within the Peruvian Amazon when classifying types of flood events and presented both positive and negative feedback for high, long, early and late flood events. These interviews provided real-life examples of the significance of each flood type. For instance, long floods were found to have a significant toll on agricultural and food security (e.g. manioc and plantains can only survive short flood periods), while also providing more food and income due to a longer fishing season. These works follow from previous studies demonstrating that the interannual variability of the Amazon wet season (e.g. precipitation onset date and timing of peak river flows) has important consequences for fisheries, hydroelectricity production and transport, with irregular inundation periods known to influence the length and productivity of the growing season (Marengo et al., 2001; Schöngart and Junk, 2007; Coomes et al., 2016; Ronchail et al., 2017; Langill and Abizaid, 2019). Finally, the timing of peak river flows in coinciding tributaries is known to control the magnitude of the travelling flood wave (Tomasella et al., 2010; Ronchail et al., 2006) and is commonly associated with exceptional flood events (e.g. 2012 in Peru; Tomasella et al., 2011; Marengo et al., 2012; Espinoza et al., 2013). Therefore, understanding how variations in large-scale climate features impact flood timing and duration is also of significant importance in the Amazon basin and for early warning system (EWS) protocols, such as forecast-based financing (FbF; Coughlan de Perez et al., 2017).

An EWS is a procedure that utilises climate forecasts and observations to predict and provide early warning information of natural hazards before they materialise, allowing the implementation of humanitarian actions (e.g. earlier evacuation of people likely to be flooded) before rather than after an event has occurred (Coughlan de Perez et al., 2017).

Previous studies examining the seasonality of the Amazon wet season have found a link between the onset and end dates of rainfall and SST anomalies (e.g. Fu et al., 2001; Liebmann and Marengo, 2001; Marengo et al., 2001; Yin et al., 2014), though the period of analysis is often restricted to before the millennium, focuses only on rainfall and is predominately for the Brazilian Amazon. Using rainfall pentads, Marengo et al. (2001) found that when SSTs in the Pacific (south tropical Atlantic) are anomalously warm (cold) there is a delayed onset and early withdrawal of the Amazon wet season. This configuration of SSTs acts to delay the seasonal migration of convection from the Northern to the Southern hemisphere (i.e. the ITCZ migration). The relationship was found to be the strongest in the northern Amazon and towards the mouth of the Amazon River, with little association in the southern Amazon. This is supported by Fu et al. (1999) who found that land surface heating has a stronger influence on wet season length in southern catchments relative to SSTs. Finally, Liebmann and Marengo (2001) find that the association with SSTs is stronger during the transitional period between the wet and dry seasons and that for areas that exhibit strong correlations, SSTs influence the timing of rainfall in a similar fashion to the correlation with seasonal rainfall totals. Thus, the prediction of seasonal rainfall totals could potentially be used where SSTs are known to influence the onset of the wet season in global climate models (GCMs).

### 4.1.1 Objective and research questions

The objective of this work is two-fold. The first and main objective is to establish whether positive or negative phases of several climate indices significantly alters the magnitude, timing, and duration of floods throughout the Amazon Basin. To achieve this objective, we consider the following research questions.

Do positive/negative phases of different climate indices significantly alter:

a) the magnitude of annual maximum river flows,
b) the timing of annual maximum river flows,
c) flood duration (i.e. days spent above the 95$^{th}$ percentile of the climatology),

relative to years in which the SSTs are considered neutral? The second objective is to examine and discuss in greater detail the results for particular areas of the basin to better understand the response of flood characteristics to climate variability and how the results from the two datasets compare (i.e. observations and GloFAS 2.1).

## 4.2 Data and methods

We first define the climatological baseline for the Amazon basin flow regime, calculating the average magnitude and timing of peak river flows in addition to the mean flood duration (i.e. the number of days that river flows exceed the 95th percentile of the climatology) over the entire 36-year period (Fig. 1). For the calculation of the average flood timing, circular statistics are used. We use both a hydrological reanalysis and observed gauged dataset to enable the comparison and evaluation of the ERA5 reanalysis dataset, which allows for complete coverage over the full period of analysis without gaps and focuses on the natural variability of river flow whereby human interventions (e.g. rapid land changes such as deforestation from forest to cropland and damming) that impact the observations are not modelled.

### 4.2.1 Observed streamflow

Fifty-eight station time series of observed river discharge throughout the Amazon basin are obtained from the national institutions responsible for the hydrological monitoring in countries situated within the Amazon basin. These data are sourced through the ORE-HYBAM observation service (see https://hybam.obs-mip.fr/; last access: 27 July 2020) in association with the Institute of Research and Development (IRD) or directly from the national services. Daily water levels are converted to river discharge using stage and rating curve measurements, determined using an acoustic Doppler current profiler (ADCP). The locations and details of each gauging station can be found in Fig. S1 and Table S1 in the Supplement, respectively. Stations are selected based on the following criteria:

- At least 18 years' worth of data over the 36-year analysis period (1979-2015),
- No more than 5 % of missing data in each hydrological year (i.e. Oct-Sep),
- Have at least five hydrological years per climate phase of ENSO and tropical Atlantic variability.

### 4.2.2 GloFAS 2.1 streamflow

A global daily reanalysis of river discharge is provided at a resolution of 0.1° (~32 km) for the 36-year analysis period (1979–2015). The data are derived from the operational Global Flood Awareness System, version 2.1 (GloFAS; Alfieri et al., 2013; Harrigan et al., 2020), where runoff output from the H-TESSEL module of the European Centre for Medium-Range Weather Forecasts (ECMWF), integrated forecast system (IFS; cycle 41r2), is coupled to the calibrated LISFLOOD routing model (van Der Knijff et al. (2010); see Hirpa et al. (2018) for details on calibration) to produce deterministic estimates of historic river flows. All of the 58 stations were used within the calibration of Lisflood. Calibration was carried out on parameters controlling the time constants in the upper and lower zones, percolation rate, groundwater loss, channel Manning's coefficient, the lake outflow width, the balance between normal and flood storage of a reservoir, and the multiplier used to adjust the magnitude of the normal outflow from a reservoir (Towner et al., 2019). Meteorological input is provided by ERA5, the fifth generation of climate reanalysis at the ECMWF, succeeding ERA-Interim. ERA5 runs at a high spatial resolution (~31 km) and covers the period from 1950 to present, providing a long and consistent record of discharge and meteorological variables at each grid cell (Hersbach et al., 2018; Zsoter et al., 2019). Towner et al. (2019) showed the potential benefits of using ERA5 to force global hydrological models (GHMs) to produce river discharge time series that accurately represent annual maximum river flows in the Amazon basin. Reanalysis data are extracted at the locations of the observed gauging stations for direct comparisons. For access to GloFAS datasets, see http://www.globalfloods.eu/ (last access: 17 July 2019).

### 4.2.3 Land and atmospheric data

Oceanic and atmospheric features are analysed using the ERA5 climate reanalysis product of the ECMWF, produced on latitude–longitude grids at 0.25°×0.25° resolution and is available from 1950 to present for the entire globe (Hersbach et al., 2020). To describe the average conditions during particular climate phases (e.g. negative ENSO), averaged monthly data on single levels are obtained for SST anomalies and total rainfall from 1979 to 2015 for the October–November–December (OND) season. These data were obtained from the Copernicus climate data store (see https://cds.climate.copernicus.eu/; last access: 12 October 2020).

### 4.2.4 Hydroclimatic drivers and modes of climate variability

Numerous hydroclimatic drivers have been identified to cause anomalous rainfall and river discharge conditions in the Amazon basin (Towner et al., 2020), with ENSO and tropical Atlantic SST variability considered to be the most influential (Marengo, 1992; Ronchail et al., 2005b; Yoon and Zeng, 2010; Espinoza et al., 2019; Jimenez et al., 2019). Several indices of ENSO are available, differing in spatial location, variable type and on the number of variables used. Wolter and Timlin (1998, 2011) express favour towards the use of indices that incorporate a range of atmospheric and oceanic variables over the tropical Pacific, such as the multi-variate ENSO index (MEI), which is described to provide a more complete and flexible description of ENSO. More recently, Takahashi et al. (2011) provided two new tropical Pacific SST indices, the central and eastern Pacific indices (hereafter CP and EP), estimated as the first two empirical orthogonal functions (EOFs) of monthly SST anomalies of the tropical Pacific. The CP and EP indices have the advantage of having a poor linear relationship amongst themselves and have been found to have different impacts on South American rainfall (Sulca et al., 2018). In this study, we investigate the influence of four different ENSO indices in addition to two tropical Atlantic SST modes (i.e. TNA and TSA; Enfield et al., 1999) on the magnitude, timing and duration of high river flows in the Amazon basin. The ENSO indices used include: the conventional ENSO index in the Niño 3.4 region (hereafter EN3.4), the CP and EP indices (Takahashi et al., 2011) and the MEI v.2 (Wolter and Timlin, 2011), which is based on the original MEI index (Wolter and Timlin, 1993). Correlations between most ENSO indices are strong, particularly for boreal winter (Wolter and Timlin, 2011), with the exception of the CP and EP indices (Sulca et al., 2018), but multiple options have been included to provide a more comprehensive evaluation. Other indices such as the Madden–Julian Oscillation (MJO), Pacific decadal oscillation (PDO), and Atlantic multidecadal oscillation (AMO) have been linked to wetter or drier conditions across South America (Shimizu et al., 2017; Towner et al., 2020), but have not been included in this study owing to the frequencies at which these indices operate (i.e. intraseasonal, decadal or multi-decadal for the MJO, PDO and AMO, respectively). The Pacific meridional mode (PMM), which has been linked to increased rainfall in June–July–August, has not been included due to its impact being significant only during the dry season (Zhang et al., 2017).

We use a quantile-based (tercile) approach as adopted by Ficchí and Stephens (2019) for Africa to categorise negative, neutral and positive modes of each climate index. Tercile categories are divided into positive (upper 33 %), neutral (middle 33 %) and negative (bottom 33 %)

values and thus each tercile is represented by 12 years' worth of data. Conventional ENSO events (i.e. El Niño or La Niña) are classified using the Oceanic Niño Index (ONI) from the NOAA Climate Prediction Center (CPC). The dataset consists of monthly mean SST anomalies obtained from the NOAA ERSST.v5 dataset for the EN3.4 region (170 to 120◦ W, 5◦ N to 5◦ S; Huang et al., 2017). In this study an El Niño (La Niña) event is defined when the average August to February monthly SST anomaly is in the top (bottom) 12-year averages of the entire 36-year dataset. The classification of years for each phase for each index can be found in Tables S2–S7 in the Supplement. The period from August to February was chosen as ENSO events tend to span across 2 years, developing around boreal spring and typically peak in boreal winter (Emerton et al., 2017), thus aligning with the Amazon wet season and preceding peak river flows (Fig. 1b). Events for the CP and EP indices are categorised using monthly anomalies from the ERSST v3b dataset (see http://www.met.igp.gob.pe/datos/ EC.txt; last access: 6 August 2020) using the same methodology. The MEI index is classified using a bi-monthly time series of the leading combined empirical orthogonal function (EOF) of five variables (sea level pressure, SST, zonal and meridional components of the surface wind and outgoing longwave radiation (OLR)) over the tropical equatorial Pacific basin (30◦ S–30◦ N and 100◦ E–70◦ W), with events defined similarly to the EN3.4, CP and EP indices but using bi-monthly values (i.e. August/September to January/February).

Tropical Atlantic positive and negative phases are classified using the TNA and TSA indices (Enfield et al., 1999), which are based on monthly SST data from the HadISST and NOAA 1×1 datasets. SST data are averaged for the region from 5.5 to 23.5◦ N and 15 to 57.5◦ W (0◦ to 20◦ S and 10◦ E to 30◦ W) for the TNA (TSA). Positive and negative phases are defined as in the ENSO indices (i.e. top and bottom 12 August–February averages for the upper and lower terciles). TNA SST variability is known to be modulated by conditions in the tropical Pacific and lags by 4 to 6 months, usually peaking in boreal spring (Enfield, 1996; García-Serrano et al., 2017). Amazon rainfall and discharge peaks can appear to “lead” North Atlantic SSTs but were found to be “in phase” with the Amazon wet season when removing the influence of ENSO (Yoon and Zeng, 2010). Builes-Jaramillo et al. (2018) postulate that the relationship between streamflow and SSTs in TNA may be a two-way feedback system whereby hydrological conditions in the Amazon can influence future states of SSTs in the Atlantic Ocean, and thus the TNA-streamflow teleconnection is still of interest despite flood peaks preceding the development phase of a positive or negative event.

### 4.2.5 Flood peak magnitude

Owing to the Amazon spanning across both the Northern and Southern hemispheres, the seasonality of rainfall varies across the basin (Espinoza et al., 2009). Throughout the majority of the Amazon, the wet season typically spans between December and April (Yoon and Zeng, 2010), with flood peak occurrences generally taking place between February and July (Fig. 1b). Thus, for each gauging station or grid point we extract annual maximum river flows over a hydrological year starting from October to the following September. The difference between the mean of positive and negative phases (e.g. positive years of ENSO) relative to neutral conditions are calculated and expressed as a percentage to allow comparisons to be drawn between gauging stations.

### 4.2.6 Flood peak timing

From the set of extracted values of annual maximum river flows from each river point, we calculate the average seasonality of peak flows (i.e. the timing of peak river flow occurrence) and their variability using the Burn's vector (Burn, 1997), which is an index based on circular statistics (Mardia, 1972). The vector components represent the average timing of peak river flows (i.e. date of occurrence) and its variability ($r$) as polar coordinates on a unit circle (Burn, 1997). The date of occurrence is defined by converting the Julian date (where 1 January is day 1 and 31 December is day 365) of each flood peak $i$ to an angular value in radians to then calculate the circular mean of all annual peaks. The variability of flood timing ($r$) ranges from 0 to 1, where $r$=0 represents a highly variable regime, with flood peaks occurring evenly throughout the year, while $r$=1 indicates a regime where flood peaks occur consistently at the same time of the year. Therefore, higher values of $r$ represent lower variability, which is expected in larger rivers in the Amazon, as the delay between peaks in rainfall and river discharge is large. By contrast, lower values of $r$ represent higher variability, which could be associated with rivers where climate phases are found to influence the timing between individual years (Ficchí and Stephens, 2019). We calculate the difference between the average timing of flood peaks for positive and negative phases against neutral conditions using circular statistics.

### 4.2.7 Flood duration

For each gauging station or grid point, we consider the duration of flooding as the number of days (not consecutive) spent above the 95th percentile of the climatology. Although the 95th percentile does not necessarily represent flooding, this threshold has been chosen to better understand how anomalous oceanic conditions can influence the length of high-water periods throughout the basin, which have been found to have both positive and adverse effects on community member livelihoods (Langill and Abizaid, 2019). Like for flood magnitude and timing, the average number of days spent above the 95th percentile each year for positive and negative phases are compared against neutral conditions.

### 4.2.8 Significance testing

To test for significance, we apply a non-parametric bootstrapping technique (10 000 replicates) to provide a distribution for the average magnitude, timing and duration of flood peaks in each climate phase. Here, each 12-year time series for each climate phase is resampled 10 000 times with replacement to provide a bootstrap distribution in which the mean is taken. The difference in the means of the distributions of each climate phase is then calculated, with significance determined using the 95 % confidence interval (i.e. if the confidence interval includes 0, then we can conclude that there is no significant change between the climate phases and we fail to reject the null hypothesis).

## 4.3 Results and discussion

There is widespread agreement between the gauged and reanalysis climatology (i.e. 36 years) of annual maximum river flows, flood peak timings and its variability (Fig. 1). Annual means of peak river flows are similar between the two datasets ($\rho$=0.9), with the largest flows constrained to the main Amazon River and towards the junctions of its major tributaries, such as the Madeira River stemming from the south (Fig. 1a and d). A strong regional pattern in the timing of annual flood peaks is evident between the northern and southern halves of the basin owing to the differing precipitation regimes in association with the alternative warming between the Northern and Southern hemispheres (Espinoza et al., 2009). Stations situated in the southern Amazon typically experience peak river flows between February and April, while stations in the northern half generally peak between May and July (Fig. 1b and e).

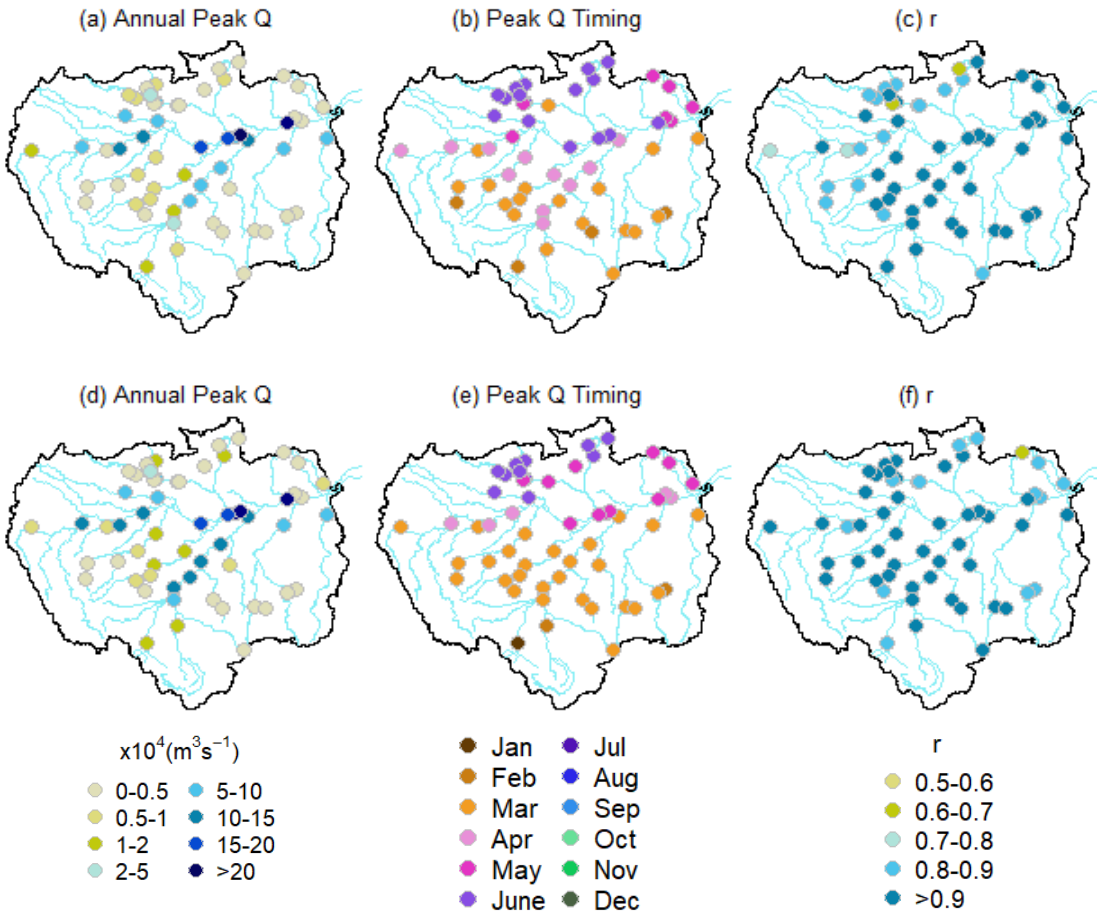


**Figure 1.** *36-year climatology of observed (top row) and GloFAS 2.1 streamflow reanalysis (bottom row) datasets (1979- 2015). For (a, d) mean annual maximum river flows, (b, e), average timing of peak flow occurrences, (c, f) interannual variability of peak flow timing.*

Yearly annual maximums from the GloFAS 2.1 dataset tend to peak slightly earlier (9 d on circular average), particularly in southern tributaries where a large quantity of dams exist (Towner et al., 2019) and along parts of the main Amazon River (Fig. 1e). Not all dams and reservoirs across the globe have been included within GloFAS (see Fig. 2 in Zajac et al., 2017), meaning that the flood timing may differ from the observations in the simulated dataset (Ficchí and Stephens, 2019). In addition, GloFAS does not model floodplain–river interactions and instead mimics them by using a simple loss function. As such, floodplain storage and interactions are known to be one of the main sources of uncertainty in the model and is particularly prominent in large river basins like the Amazon causing flood peaks to occur too early (Alfieri et al., 2013). The timing of peak river flows is highly predictable at most stations, with a median Burn's vector variability component (*r*) of 0.92 and 0.93 across all stations for the observed and reanalysis dataset, respectively (Fig. 1c and f). However, flood timing variability is greater at two gauging stations (45 and 51) situated towards the north of the basin, with *r* values as low as 0.62 within the observed dataset.

Hereafter, the results are broken down to match the research questions outlined in Sect. 4.1.1, with reference to individual gauging stations denoted by the station numbers in italics as indicated in Fig. S1 and Table S1 in the Supplement.

### 4.3.1 Flood magnitude

#### 4.3.1.1 ENSO

Out of the 58 gauging stations, 48 (51) observe a decrease in annual maximum river flows during El Niño years relative to neutral conditions, with a median deficit of 7 % (13 %) across stations that acknowledged a reduction in peak river flows for the observed (GloFAS 2.1) dataset (Fig. 2a and e). Of these, 11 (17) are statistically significant for the observed (GloFAS 2.1) dataset, with GloFAS 2.1 observing more significant results in the north-west of the basin. Decreases in peak river flows are consistent with what has been previously identified in the literature, with drier conditions and droughts more common when SSTs in the equatorial Pacific are anomalously warm (Marengo, 1992; Foley et al., 2002; Ronchail et al., 2005b; Espinoza et al., 2009; Marengo et al., 2018; Jimenez et al., 2019). SST anomalies are created via the slowdown of the trade winds inducing anomalies in the east–west Walker circulation, whereby convection is more prominent over the central equatorial Pacific and subsidence that inhibits rainfall is found over most of central and eastern locations of the Amazon basin (Panisset et al., 2018). The largest decreases are acknowledged in central to south-western regions (Fig. 2a and e), particularly along the Purus River (13–15), where Ronchail et al. (2005b) previously noted decreases of river discharge up to 25 % during El Niño phases (based on the period 1981–2002). A similar pattern is observed for the MEI index (Fig. 2c and g), with the exception of several stations (2, 4, 5, 9, 11, 32 and 34) situated along and near to the main stem of the Solimões-Amazon River. Here, the percentage change is relatively small for MEI-based positive years (mainly between −5 % and 5 %; grey circles), with no significant findings despite the EN3.4 and MEI indices differing by just 2 years for their positive phases (see Tables S2 and S3 in the Supplement). The reasoning for this is due to peak river flows being higher for the neutral years of the EN3.4 index in comparison to neutral years of the MEI index. When taking the difference between MEI positive and EN3.4 neutral years,

the median across the aforementioned stations goes from −1 % to −5 %, with slightly higher peak river flows found for the MEI positive index relative to the EN3.4 positive index.

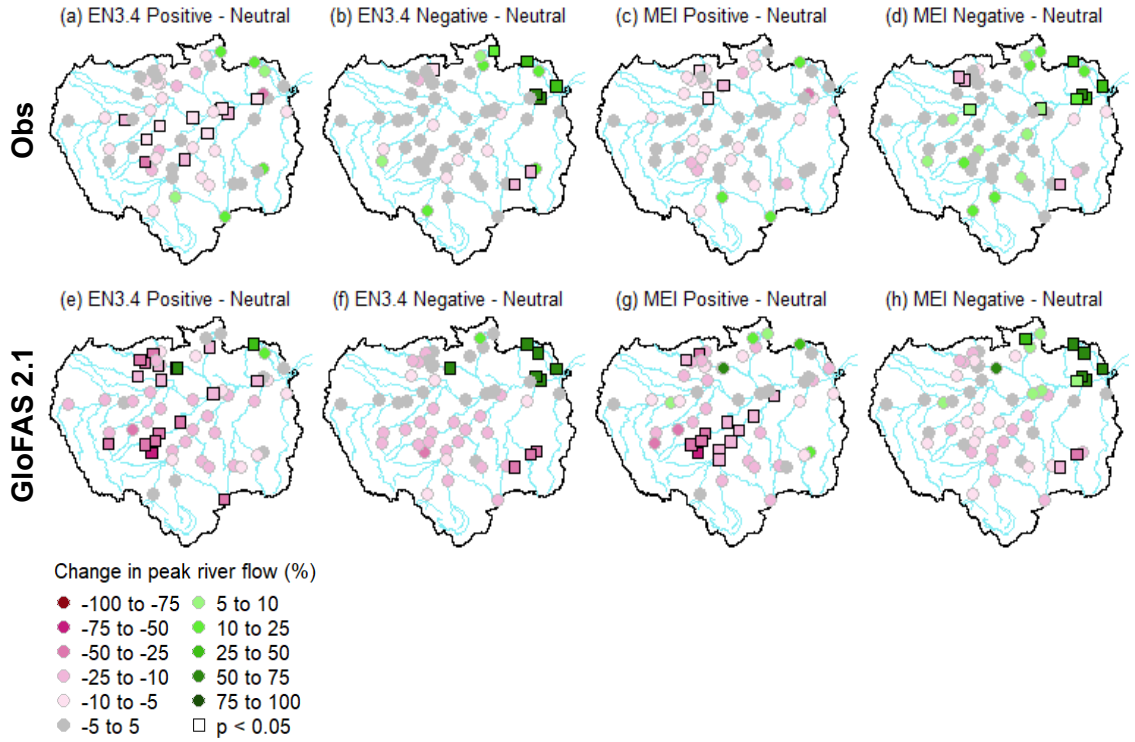


**Figure 2**. *Percentage change of observed and simulated mean annual peak river flows between different phases of the EN3.4 and MEI indices, for (a, c, e, g) positive with respect to neutral years and (b, d, f, h) negative with respect to neutral years. Top row represents changes for observations, bottom row shows changes for GloFAS 2.1 streamflow reanalysis data. Pink (green) points represent where the average annual peak flow decreases (increases). Significant results at the 95 % confidence level are denoted using a square (i.e. p<0.05).*

The impact of La Niña on flood peaks is not symmetric, nor as strong as El Niño at most gauging stations for all of the ENSO indices, including the CP and EP, particularly in central locations of the basin (Figs. 2b, d and 3b, d). Typically, above normal river flows and flooding in parts of the north-western Amazon are associated with cooler than usual SSTs in the equatorial Pacific Ocean (Marengo et al., 2012; Espinoza et al., 2013; Espinoza et al., 2014). These conditions favour a configuration of positive 850-hPa geopotential heights anomalies which maintain a strong humidity flux convergence over the Amazon (see Espinoza et al., 2013), and a westward displacement of the Walker Circulation, whereby its ascending limb is situated over the Amazon Basin, as opposed to the Pacific Ocean, increasing rainfall totals (Satyamurty et al., 2013). However, a median deficit of 2 % (8 %) are observed for peak river flows during the cold phase of ENSO for observed (GloFAS 2.1), with the majority of the basin witnessing a decrease relative to neutral years for GloFAS 2.1 (Figs. 2b, f). Tributaries in the

north-eastern Amazon stand out for negative ENSO years, with significant increases in annual flood peaks for three out of four of the ENSO indices (EN3.4, MEI, and CP), for both datasets (Figs. 2 and 3). The most notable increases are observed at the Arapari (*39*) and Boca Do Inferno (*40*) gauging stations, with an average increase of > 60 % at both stations for EN3.4 (Fig. 2b). These findings in the northeast have been previously identified for both rainfall (Ronchail et al., 2002) and river discharge (Ronchail et al., 2005b), who also found lower discharge levels during La Niña throughout the southern Amazon.

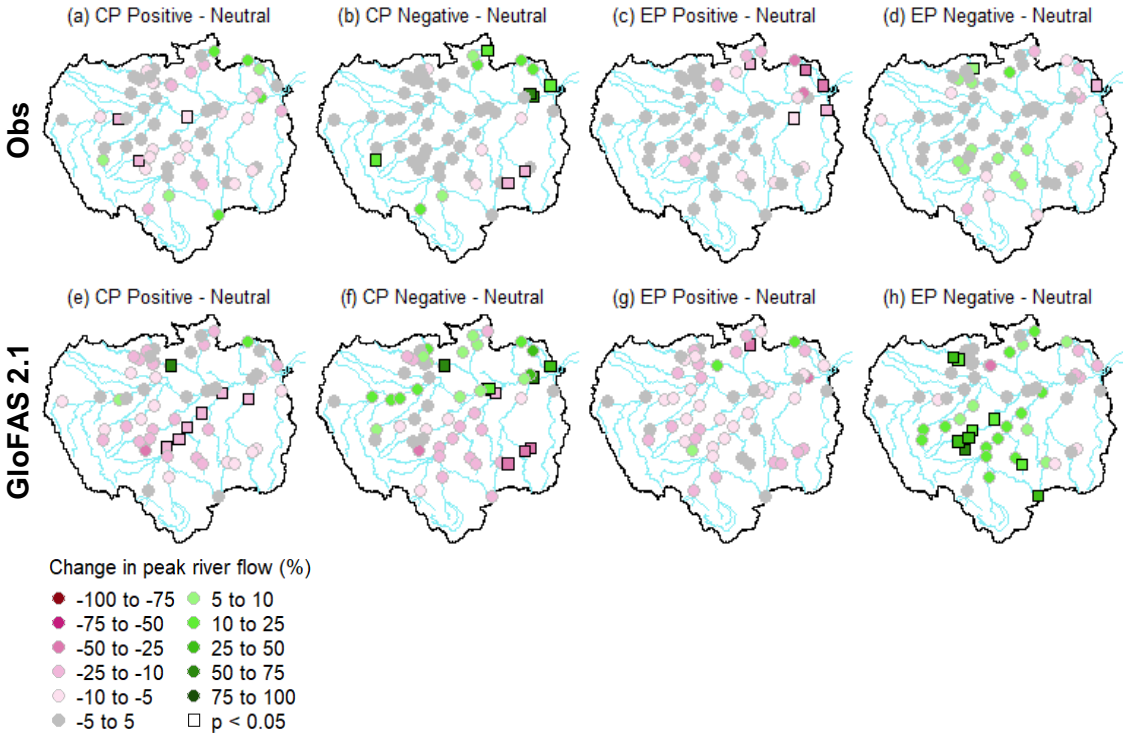


**Figure 3.** *Percentage change of observed and simulated mean annual peak river flows between different phases of the CP and EP indices, for (a, c, e, g) positive with respect to neutral years and (b, d, f, h) negative with respect to neutral years. Top row represents changes for observations, bottom row shows changes for GloFAS 2.1 streamflow reanalysis data. Pink (green) points represent where the average annual peak flow decreases (increases). Significant results at the 95 % confidence level are denoted using a square (i.e. p <0.05).*

No wet signal is found in the north-eastern Amazon basin for observed negative EP phases (Fig. 3d), in contrast to what was identified for the negative phases of the other ENSO indices (i.e. EN3.4, MEI and CP). This response was also identified for rainfall (Fig. 12), indicating that the wet response in the north-east is restricted to years when the cooling of tropical Pacific SSTs is constrained to the central equatorial Pacific. Observing Fig. 3c (i.e. positive EP), the typical drying trend associated with warm SST anomalies in the tropical Pacific is shifted

further towards the north-eastern Amazon showing the opposite pattern to the negative EN3.4 phase in this region. This could potentially be associated with the descending limb of the Walker circulation being displaced further east in response to the eastward shift of anomalously warm SSTs in EP El Niño years (Alizadeh-Choobari, 2017). The positive CP phase (Fig. 3a) shows a similar pattern to EN3.4 (Fig. 2a), as expected owing to them occupying similar spatial locations across the equatorial Pacific and differing by just one year for their warm phases (see Tables S2 and S4 in the Supplement). However, the number of significant values is notably less (3 compared to 11), with largest differences found along and near the Amazon River in Brazil. The negative CP phase (Fig. 3b) is almost identical to the negative EN3.4 index (Fig. 2b) with a handful of stations showing increased (decreased) peak flows in the north-eastern (south-eastern) basin, which is also shown for GloFAS 2.1 (Figs. 2f and 3f).

#### 4.3.1.2 Tropical Atlantic

For positive TNA years, 57 % of the stations experience a decrease relative to neutral conditions, with a minimal percentage change (median = −4 % for stations that observe a decrease and +5 % for stations observing an increase) (Fig. 4a). Of these decreases, both datasets have seven statistically significant results concentrated to the western and south-western Amazon. The decrease is stronger for GloFAS 2.1 (Fig. 4e) relative to the observed data, which is found to be true for several other climate indices (e.g. negative EP and TSA phases; Figs. 3h and 4h). The reasoning for these results could be associated with the lack of accurate representation of floodplain interactions and smaller-scale processes that occur in the observed data that could dampen or increase the magnitude of change in river flow (e.g. a lack of floodplain storage could result in increased river flow in the model). Therefore, the magnitude of the response to climate phases in GloFAS is more likely a direct reflection of the increase or decrease in rainfall witnessed during that particular climate phase. The contrast between positive and negative phases for both tropical Atlantic indices is far less apparent than for the Pacific indices, with a prevalence of grey circles for the observed dataset results (Fig. 4a–d), highlighting that the signal is weak for all phases (i.e. positive, neutral and negative). Decreases in river flow were to be expected for positive TNA years based on previous results for both rainfall and river discharge. For instance, Yoon and Zeng (2010) identified that warmer TNA SSTs were found to induce subsidence (i.e. downward motion) over the Amazon basin, resulting in reduced moisture convergence over the basin and thus less rainfall. The same was identified for abnormally low river discharge in the upper Solimões River, the headwaters to the Amazon River, where low-discharge years (i.e. 1995, 2005

and 2010) were associated with higher than usual SSTs in the North Atlantic Ocean (Espinoza et al., 2011).

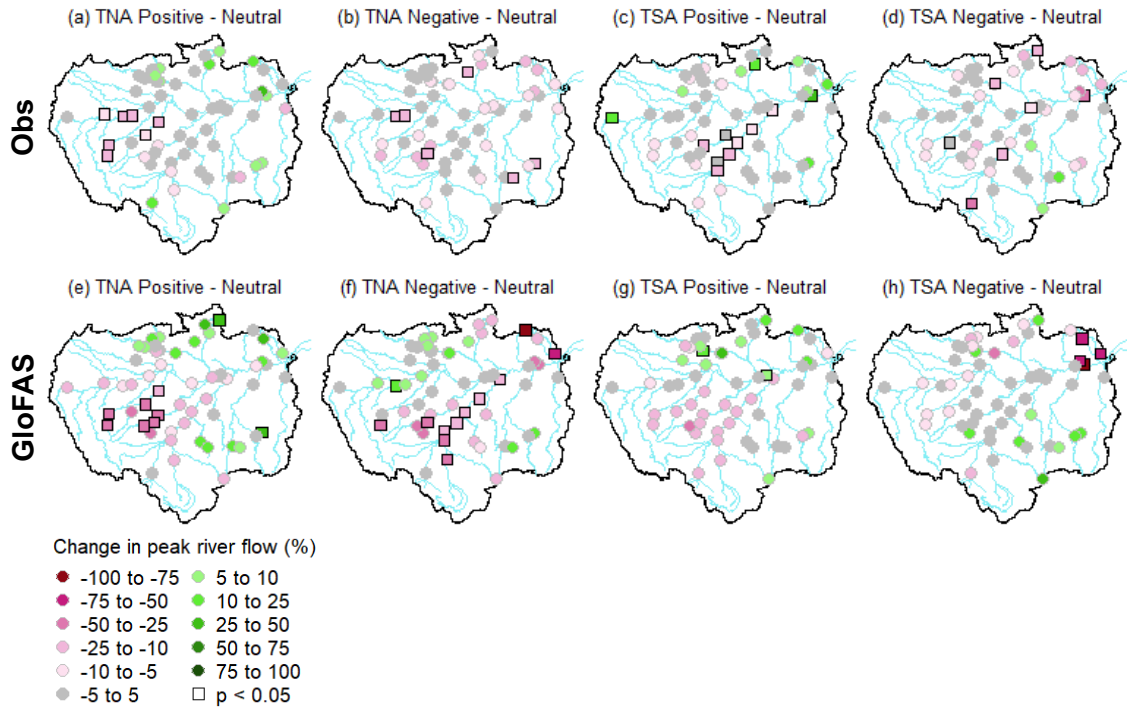


**Figure 4.** *Percentage change of observed and simulated mean annual peak river flows between different phases of tropical Atlantic indices. For (a, c, e, g) positive with respect to neutral years. (b, d, f, h) Negative with respect to neutral years. Top row represents changes for observations, bottom row shows changes for GloFAS 2.1 streamflow reanalysis data. Pink (green) points represent where the average annual peak flow decreases (increases). Significant results at the 95 % confidence level are denoted using a square (i.e. p <0.05).*

The decrease observed in peak river flows from our results is not as strong as those found previously for rainfall and river discharge (e.g. Yoon and Zeng, 2010; Espinoza et al., 2011) due to the signal being stronger for the Amazon dry season (July–October), particularly for the southern Amazon when the influence of ENSO is more limited. A similar case was identified in the study by Ronchail et al. (2005b) where negative TNA years were found to cause higher than usual low flows in a large portion of the Amazon basin along the main stem during the dry season but not for the wet season. As we focus on floods, the period of analysis precedes and aligns with the Amazon wet season (i.e. August–February), where the influence is found to be less substantial, concluding that tropical Atlantic SSTs are less important at most locations with regards to peak river flow variability. Focusing on Fig. 4, notable results are prevalent in the western Amazon for positive TNA years (Fig. 4a) and along the Madeira River, the largest

southern tributary, during positive TSA years (Fig. 4c). These results are replicated for modelled data (Fig. 4d and g).

### 4.3.2 Flood timing

#### 4.3.2.1 ENSO

Results in changes to peak flow timing are less obvious with no clear spatial coherence (Figs. 5–7) and fewer stations reaching statistical significance relative to flood magnitude and duration. For instance, only four stations for the observed dataset reach statistical significance during the positive EN3.4 phase, compared to 11 and 15 stations for flood magnitude and duration, respectively. Of the total stations, 52 % and 48 % observe earlier (later) flood peaks for the positive EN3.4 phase for observed data, with a median change of −6 (8) d for stations that observe earlier (later) peaks.

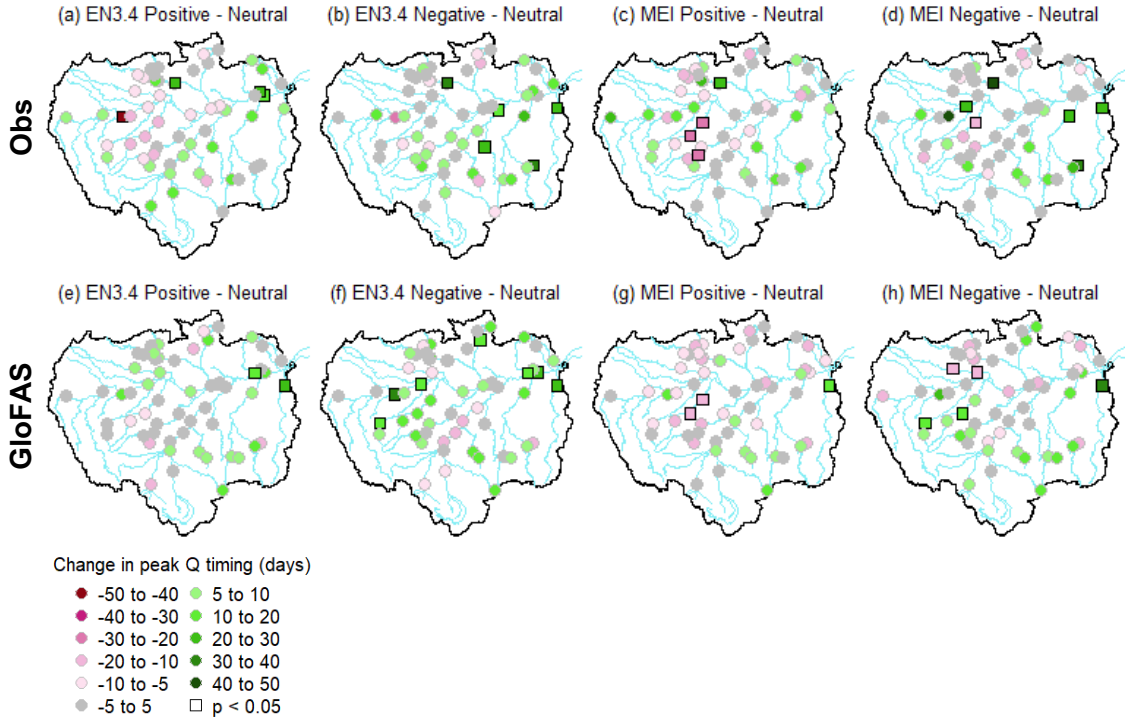


**Figure 5.** *Average change in the timing of observed and simulated annual peak river flows between different phases of the EN3.4 and MEI indices. For (a, c, e, g) positive with respect to neutral years. (b, d, f, h) Negative with respect to neutral years. Top row represents changes for observations, bottom row shows changes for GloFAS 2.1 streamflow reanalysis data. Pink (green) points represent where flood peaks occur earlier (later) compared to neutral conditions. Significant results at the 95 % confidence level are denoted using a square (i.e. p<0.05).*

Only Estirao Do Repouso gauging station (3) shows changes in peak flow timing between positive and neutral phases (EN3.4) greater than 1 month (48 d earlier), while three stations (4, 31, 48) show changes greater than 1 month between the negative and neutral phase (EN3.4 and MEI). Sucunduri station (*48*), in the central north of the Amazon (Negro River) is of interest as the flood timing becomes significantly later relative to neutral years (between 21 and 42 days) for both positive and negative phases for all ENSO indices with the exception of negative EP years (Figs. 5a-d and 6a-d), and both tropical Atlantic indices (Fig. 7a-d). As was the case for changes to peak river flows (Figs. 2a, b and 3a, b), peak flow timing results are comparable between the two central equatorial Pacific indices (i.e. EN3.4 and CP) (Figs. 5a, b and 6a, b).

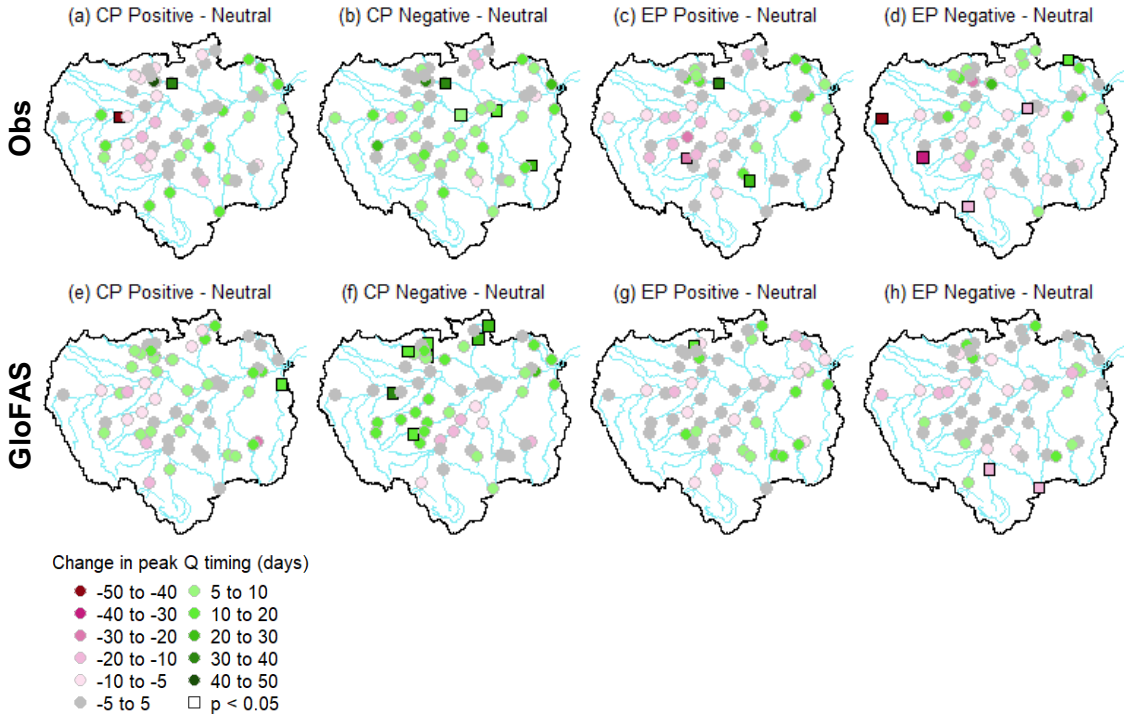


**Figure 6.** *Average change in the timing of observed and simulated annual peak river flows between different phases of the CP and EP indices. For (a, c, e, g) positive with respect to neutral years. (b, d, f, h) Negative with respect to neutral years. Top row represents changes for observations, bottom row shows changes for GloFAS 2.1 streamflow reanalysis data. Pink (green) points represent where flood peaks occur earlier (later) compared to neutral conditions. Significant results at the 95 % confidence level are denoted using a square (i.e. p<0.05)*

### 4.3.2.2 Tropical Atlantic

The largest and most consistent differences in flood timing are found for negative TSA years relative to neutral conditions (Fig. 7d and h), where 70 % of observed stations witness earlier flood peaks (median = 9 d early across stations observing earlier peaks). For GloFAS 2.1 modelled data, a consistent earlier peak is observed in northern sub-basins (Fig. 7h), while the observed data shows earlier flood peaks are more common along the main Amazon River and towards south-western tributaries in the Acre state (Fig. 7d). Here, flood peak timings are observed much earlier in the upper headwater of the Marañón River (34 d; 1), the main western Amazon River tributary, with significant results found along the Brazilian stretch of the Amazon River (11, 32 and 34). These significant results are likely due to earlier peaks found in and around the Negro, Madeira, Purus and Juruá rivers (6, 7, 8 and 10), where annual peaks are 20 d earlier on average.

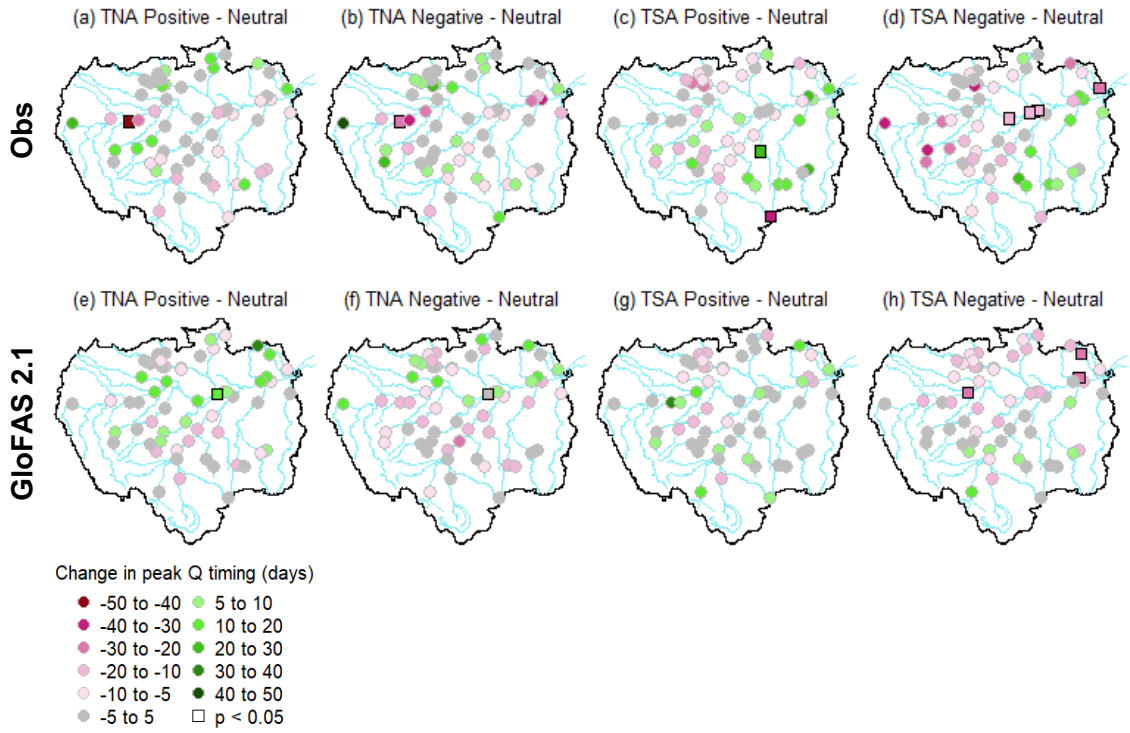


**Figure 7.** *Average change in the timing of observed and simulated annual peak river flows between different phases of tropical Atlantic indices. For (a, c, e, g) positive with respect to neutral years. (b, d, f, h) Negative with respect to neutral years. Top row represents changes for observations, bottom row shows changes for GloFAS 2.1 streamflow reanalysis data. Pink (green) points represent where flood peaks occur earlier (later) compared to neutral conditions. Significant results at the 95 % confidence level are denoted using a square (i.e. p <0.05).*

### 4.3.3 Flood duration

#### 4.3.3.1 ENSO

Decreases in flood duration (i.e. the number of days spent above the 95th percentile) are common throughout the basin during the EN3.4 phase relative to neutral conditions (Fig. 8a and e), consistent with reduced peak river flows during this phase (Fig. 2a and e) though with a higher number of significant stations (15 compared to 11). Out of 58 gauging stations, 47 (46) observe decreases in days over threshold (DOT), with a median decrease of 12 (8) d across stations that observed a decrease for EN3.4 (MEI). The largest and most significant decreases are concentrated within the central Amazon, where a decrease of 31 d is identified at the Fazenda Vista Alegre gauging station (35), situated near to the mouth of the southern Madeira River for EN3.4.

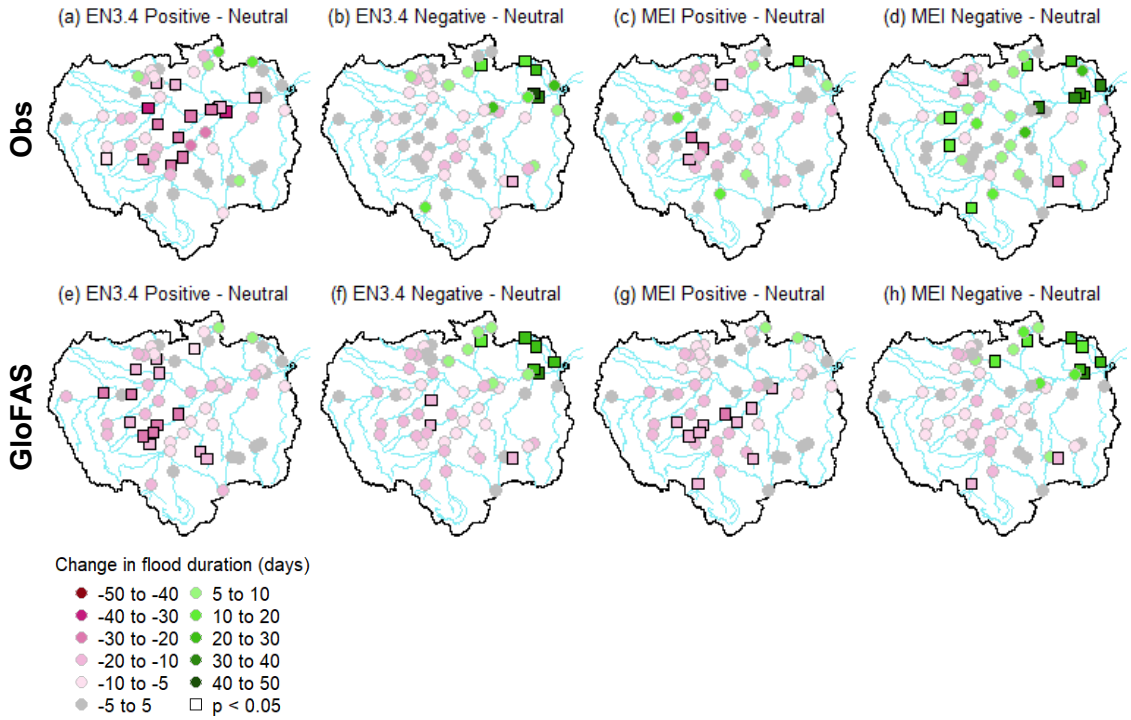


**Figure 8.** *Changes in flood duration (i.e. mean number of days river flows exceed the 95th percentile of each stations/grid point climatology) for different phases of the EN3.4 and MEI indices. For (a, c, e, g) positive with respect to neutral years. (b, d, f, h) Negative with respect to neutral years. Top row represents changes for observations, bottom row shows changes for GloFAS 2.1 streamflow reanalysis data. Pink (green) points represent decreases (increases) in the number of days spent above the 95th percentile compared to neutral conditions. Significant results at the 95 % confidence level are denoted using a square (i.e. p <0.05).*

The increase in peak river flows observed in the north-eastern Amazon for the negative ENSO phase (Fig. 2b, d, f and h) is replicated for flood duration for both EN3.4 and MEI indices (Fig. 8b, d, f and h).

The influence of La Niña is stronger in downstream tributaries of the Amazon River compared to tributaries upstream (Fig. 8b). At Óbidos (38), an average of 19 extra days are spent above the 95th percentile of the climatology relative to neutral years, while a decrease in DOT is observed at the start of the Solimões River in the Peruvian Amazon at Tamshiyacu (2). The additional flood days at Óbidos (38) could be explained by increased flood duration in northern rivers of the basin (i.e. Negro and Branco; Fig. 8b) and highlights how the hydrological regime between the upper and lower Amazon can respond differently to particular climate phases (e.g. La Niña). This has been previously highlighted for the extreme flooding in 2009, which affected central and eastern parts of the basin but not the upstream Peruvian Amazon (Espinoza et al., 2013). Similar results have previously been found in the southern Amazon basin for rainfall and river discharge (Ronchail et al., 2005b; Ronchail and Gallaire, 2006), where the effect of climate variability was found to be regionally specific and time dependent. Land use changes could also be a factor in the differences identified between different parts of the basin as regions of deforestation have previously been found to reduce latent heat and evapotranspiration, leading to a reduction in rainfall in the south-eastern Amazon (Silvério et al., 2015; Gutierrez-Cori et al., 2021).

A reduction in flood duration is common for both the positive and negative phases for the CP index, with a median reduction of seven days for each (Fig. 9a and b). Significant results are common at stations situated within or around the Amazon River for the CP index, similar to the positive EN3.4 phase, with 13 stations reaching the statistical threshold. The increase in peak river flow for the negative CP phase (Fig. 3b) in the north-east is not associated with flood duration (Fig. 9b) as it was for the EN3.4 and MEI indices, meaning that although the magnitude is more likely to increase when SSTs in the CP are colder than usual, the duration of higher flows does not increase. This could suggest that the increase in peak flow may be short-lived (i.e. higher peak flow but lower high flows over the wet season). For the EP, the most notable finding can be observed along the Madeira and Purus rivers, where several stations show a significant increase in flood duration for GloFAS 2.1 (Fig. 9h). This increase is also identified at a number of the stations for the observed dataset, although the results are not significant (Fig. 9d).

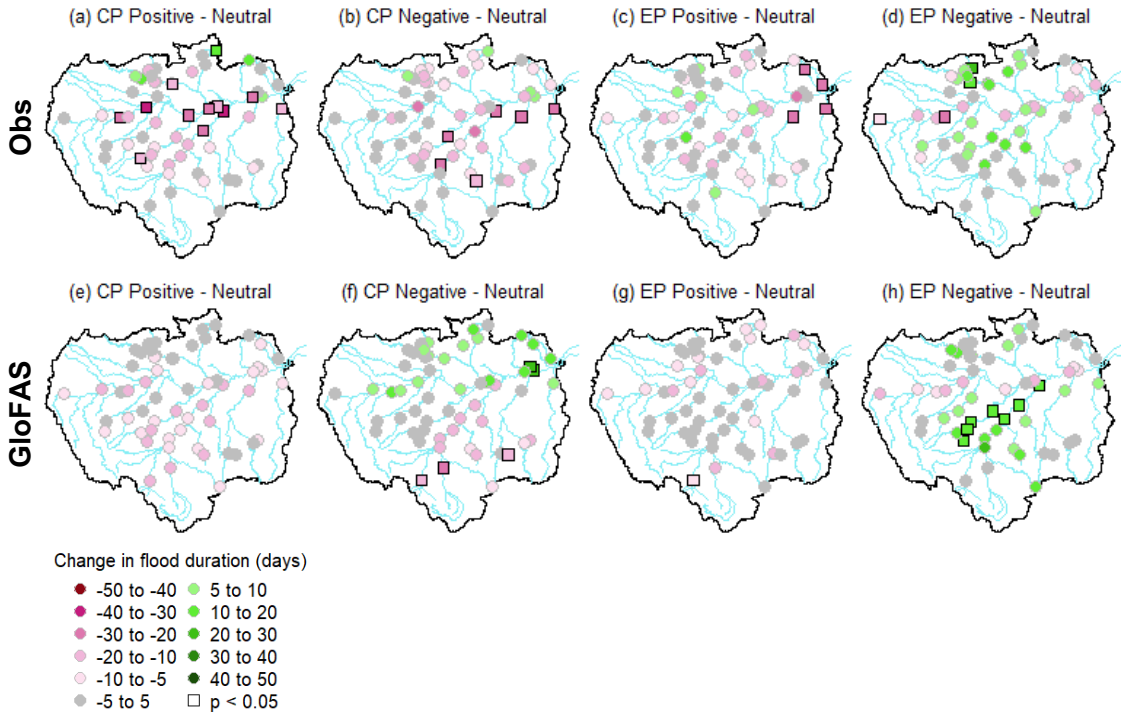


**Figure 9.** *Changes in flood duration (i.e. mean number of days river flows exceed the 95th percentile of each stations/grid point climatology) for different phases of the CP and EP indices. For (a, c, e, g) positive with respect to neutral years. (b, d, f, h) Negative with respect to neutral years. Top row represents changes for observations, bottom row shows changes for GloFAS 2.1 streamflow reanalysis data. Pink (green) points represent decreases (increases) in the number of days spent above the 95th percentile compared to neutral conditions. Significant results at the 95 % confidence level are denoted using a square (i.e. p<0.05).*

#### 4.3.3.2 Tropical Atlantic

The most significant finding can be observed at stations situated along the Madeira River for positive TSA years for both datasets (Fig. 10c and g), where statistically significant decreases in flood duration are found, matching the results of significant decreases in annual flood peaks (Fig. 4c). Four out of the five gauging stations (23, 24, 25 and 35) along the Madeira River reach statistical significance and note at least a 21 d reduction in days over threshold, with the Humaita gauging station (25) seeing a reduction of over 1 month. Overall, decreases in flood duration are more common for both Atlantic indices regardless of whether the climate phase is positive or negative for the observed dataset (Fig. 10a–d).

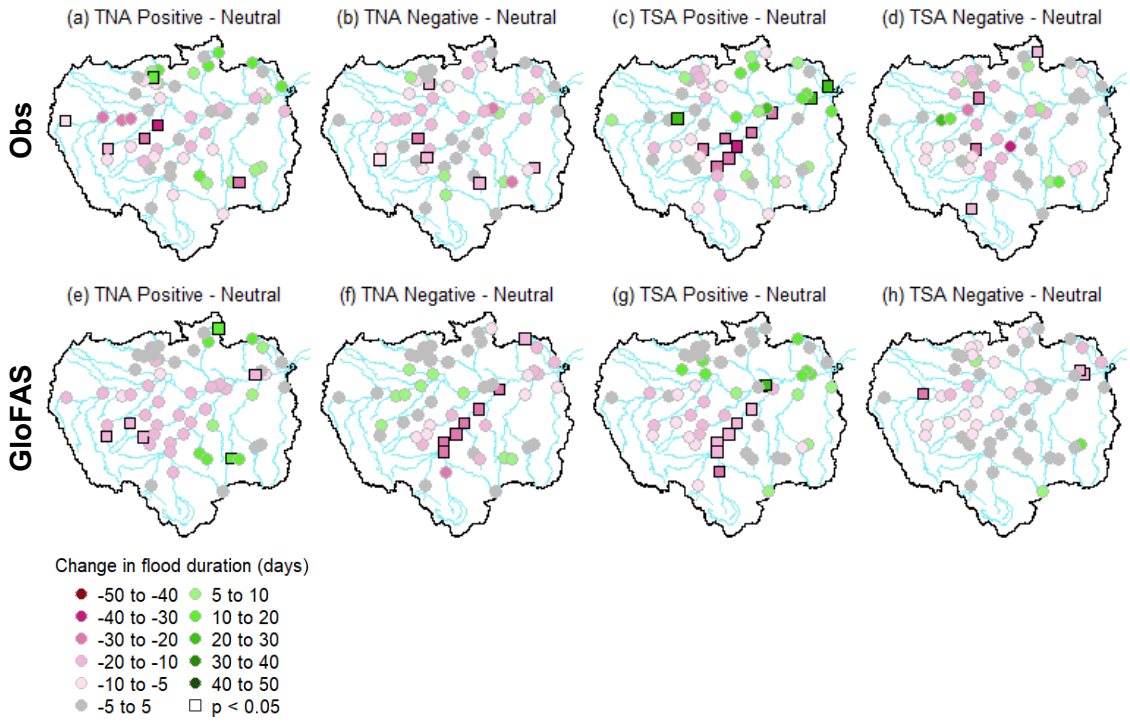


**Figure 10.** *Changes in flood duration (i.e. mean number of days river flows exceed the 95th percentile of each stations/grid point climatology) for different phases of tropical Atlantic indices. For (a, c, e, g) positive with respect to neutral years. (b, d, f, h) Negative with respect to neutral years. Top row represents changes for observations, bottom row shows changes for GloFAS 2.1 streamflow reanalysis data. Pink (green) points represent decreases (increases) in the number of days spent above the 95th percentile compared to neutral conditions. Significant results at the 95 % confidence levels are denoted using a square (i.e. p<0.05).*

### 4.3.4 Notable results

A few regions show distinctive changes to flood characteristics or discrepancies to what is expected relative to previous studies during certain climate phases. Three particular findings stand out; (a) the absence of significant change at the Tamshiyacu gauging station (*2*) in the Peruvian Amazon, where previous floods have been attributed to La Niña events (Espinoza et al., 2013), (b) the response to negative ENSO years in the north-eastern Amazon, where increases in peak flow magnitude and high flow duration are identified for EN3.4, MEI and CP but not for the EP index, and (c) the regional similarities and differences found between simulated GloFAS 2.1 flows and the observed data. To better understand these results, each are explored in further detail.

#### 4.3.4.1 Response to SST anomalies in the Peruvian Amazon

Tamshiyacu (2) is one of the key gauging stations for monitoring flooding in the Peruvian Amazon due to its location upstream from the city of Iquitos. Extreme floods in this region have been previously associated with La Niña SSTs in the equatorial Pacific (e.g. in 1999 and 2012, Espinoza et al., 2013). However, when using a tercile approach for the period 1979–2015, this station observes a small decrease (2–5 d) in the number of days above the 95th percentile of river flow for all ENSO indices during the cold phase (Fig. 8b and d), whilst the increase in peak river flow is minimal (+1 %; Fig. 2b and d). All 12 EN3.4 negative years in this study are classified as La Niña years when comparing the years identified to the classic NOAA ONI index classification of positive and negative ENSO phases (see Table S2 in the Supplement). These results suggest that although La Niña conditions have been shown to produce atmospheric anomalies responsible for extreme flooding (e.g. as in Espinoza et al., 2013), weak cold events (e.g. five consecutive 3-month running mean SSTs just below or at about −0.5 ◦C based on the ONI classification) may not be enough to produce high flood characteristics (e.g. increased high flow durations) in the Peruvian Amazon. It is therefore of interest to understand if a particular threshold of anomalous cooling in the central Pacific is needed to reproduce the atmospheric response witnessed in the buildup to the 2012 event.

In an attempt to better understand the response to tropical Pacific SSTs, we compare annual peak flow magnitude, timing and the duration of high flows for all years at Tamshiyacu (2) against the preceding OND averaged SSTs in the tropical Pacific EN3.4 region before the Peruvian Amazon flood season takes place (Fig. 11). Results show a modest but significant increase (Pearson's $p$<0.05) in annual peak river flows as SSTs become more negative, although high river flows exceeding 50 000 $m^3 s^{-1}$ are recorded regardless of whether SSTs are in a positive, neutral or negative phase (Fig. 11a). Regression analysis shows that only 17 % of the variance in peak flow magnitude can be explained by OND EN3.4 SSTs. Moreover, though a negative SST anomaly of −1.08 ◦C in OND 2011 (sixth largest SST anomaly) relates to the largest peak in 2012, a further five cases with larger negative SST anomalies note lower magnitude river flows indicating that the relationship is non-linear and multi-variate. Three years (1998, 1999 and 2007) with similar SST anomalies (∼−1.5 ◦C) are found to have differences in peak river flows of up to 7750 $m^3 s^{-1}$, meaning that other factors (e.g. SST temporal evolution, spatial complexities, local factors including topography, land cover changes, other land surface anomalies, response upstream and SSTs in the Atlantic) beyond the Pacific SSTs magnitude are likely responsible for the variability seen in annual flood maximums.

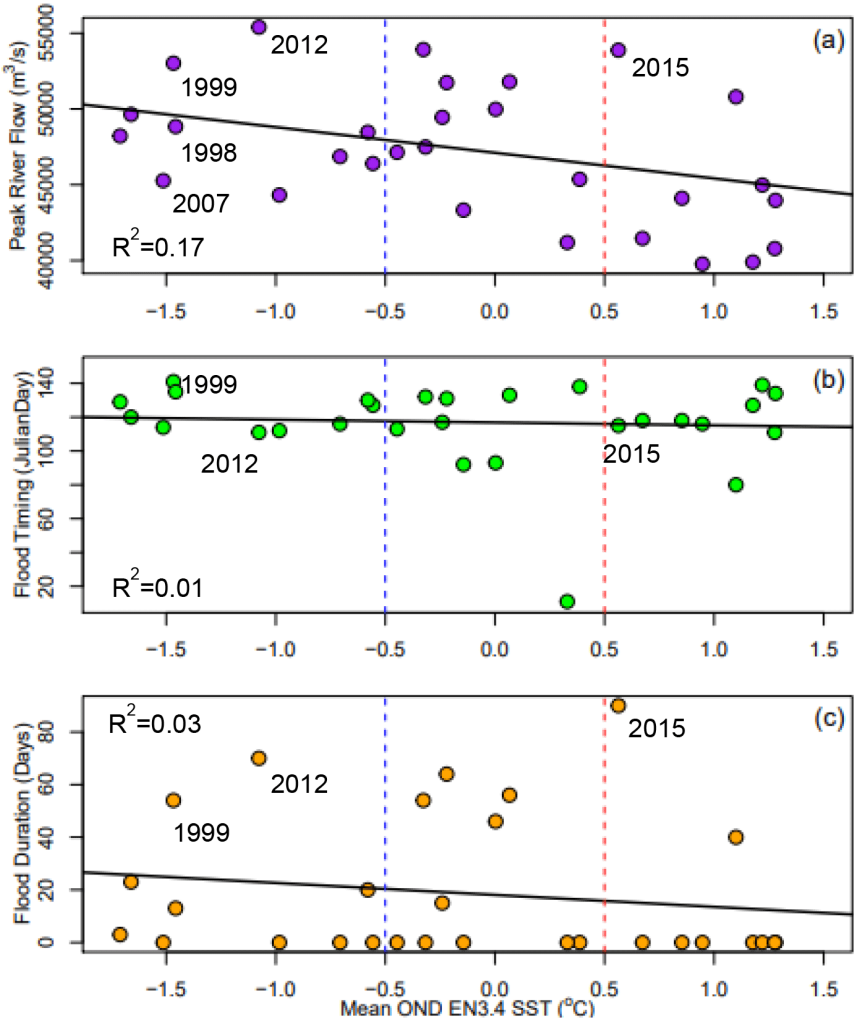


**Figure 11.** *Scatterplot of the mean OND SST anomaly in the EN3.4 region vs. (a) the annual river flow magnitude, (b) peak flow timing and (c) flood duration (i.e. days over the 95th percentile of flow) for the Tamshiyacu (2) gauging station for the period 1986–2015. Straight black lines represent the regression line, with the R2 value provided for each. Major flood events are highlighted by the respective year.*

The regression line for flood timing (Fig. 11b) is flat, with no significant differences in peak flow timing with SST variability. In 2004 the peak river flow occurred significantly earlier than usual, taking place in January as opposed to late April (Fig. 1b), with neutral SST conditions present in the preceding months in the EN3.4 region. The reasoning behind this deserves further attention by investigating the antecedent and upstream conditions prior to the flood peak and considering variables including soil moisture, total rainfall and river levels. Finally, no notable relationship is acknowledged at the Tamshiyacu gauging (2) between DOT and SST anomalies, with the longest flood duration occurring during a weak El Niño event in 2014–2015 (Fig. 11c). Comparing the flood magnitude and duration, it shows that although they are closely linked

(i.e. as the magnitude increases, the flood duration generally goes up), they do not have a linear relationship. For instance, in 2012, Tamshiyacu (2) recorded a flow of 55 400 $m^3 s^{-1}$, whilst in 2015 the value was slightly under at 53 880 $m^3 s^{-1}$. Despite the higher river flow, Tamshiyacu (2) records show that river flows were above the 95th percentile of the station's climatology for 70 d in 2012, with the 2015 event totalling 91 d. Examining results further downstream in Brazil at Óbidos (38), no DOT are observed in 2015. This suggests that the flooding was specific to upstream locations and that major tributaries joining the Amazon River after Peru could have been experiencing decreases in river flow. This agrees with the suggestion by Espinoza et al. (2013) that the mechanisms responsible for flooding can differ between upstream and downstream sub-basins of the Amazon River, with a previous flood in 2009 found to only affect central and eastern regions of the Amazon Basin.

Owing to extreme flooding at Tamshiyacu (2) in the Peruvian Amazon commonly coinciding with negative SSTs in the tropical Pacific (Espinoza et al., 2013) and due to El Niño events on average producing a slight decrease in flood duration relative to neutral years at this station (Fig. 8a), an analysis that determines all possible drivers of the 2015 event where a weak El Niño features would be of interest. Such an analysis could help us understand the atmospheric response for this specific event and how it differs from previous floods already analysed in the literature (e.g. 2012; Espinoza et al., 2013). Ideally, such an analysis would incorporate stations both upstream and downstream to identify any regional differences and consider SSTs in all adjacent Oceans. Finally, though the results of this study do not replicate the wet signal associated with La Niña found previously (e.g. Espinoza et al., 2013), it could be worth investigating how the timing of La Niña events (i.e. timing of onset and peak) impacts river flows. This arises from the results of Espinoza et al. (2013) who identified that the intensity of the 2012 floods were likely related to an early La Niña event that caused earlier than usual rainfall resulting in simultaneous peak flows in combining tributaries of the Amazon River. Therefore, it raises the question as to whether the magnitude, timing, or location of ENSO events are more important for predicting flood events in the Amazon basin.

### 4.3.4.2 Response to SST anomalies in the North-eastern Amazon

Wetter conditions (i.e. increased annual peak magnitude and flood duration) was a common response in the north-eastern Amazon to negative SST years in the tropical Pacific for multiple ENSO indices and for both datasets. This response is likely owed to cooler than usual SSTs favouring an intensification of northern humidity fluxes in the Caribbean Sea, which are directed towards the north-western Amazon and then across to the northern-eastern Amazon (see Fig. 3c in Espinoza et al., 2013). The exception to this response, however, was identified for the negative EP phase where slight decreases in peak river flows and flood duration were identified (Figs. 3d and 9d).

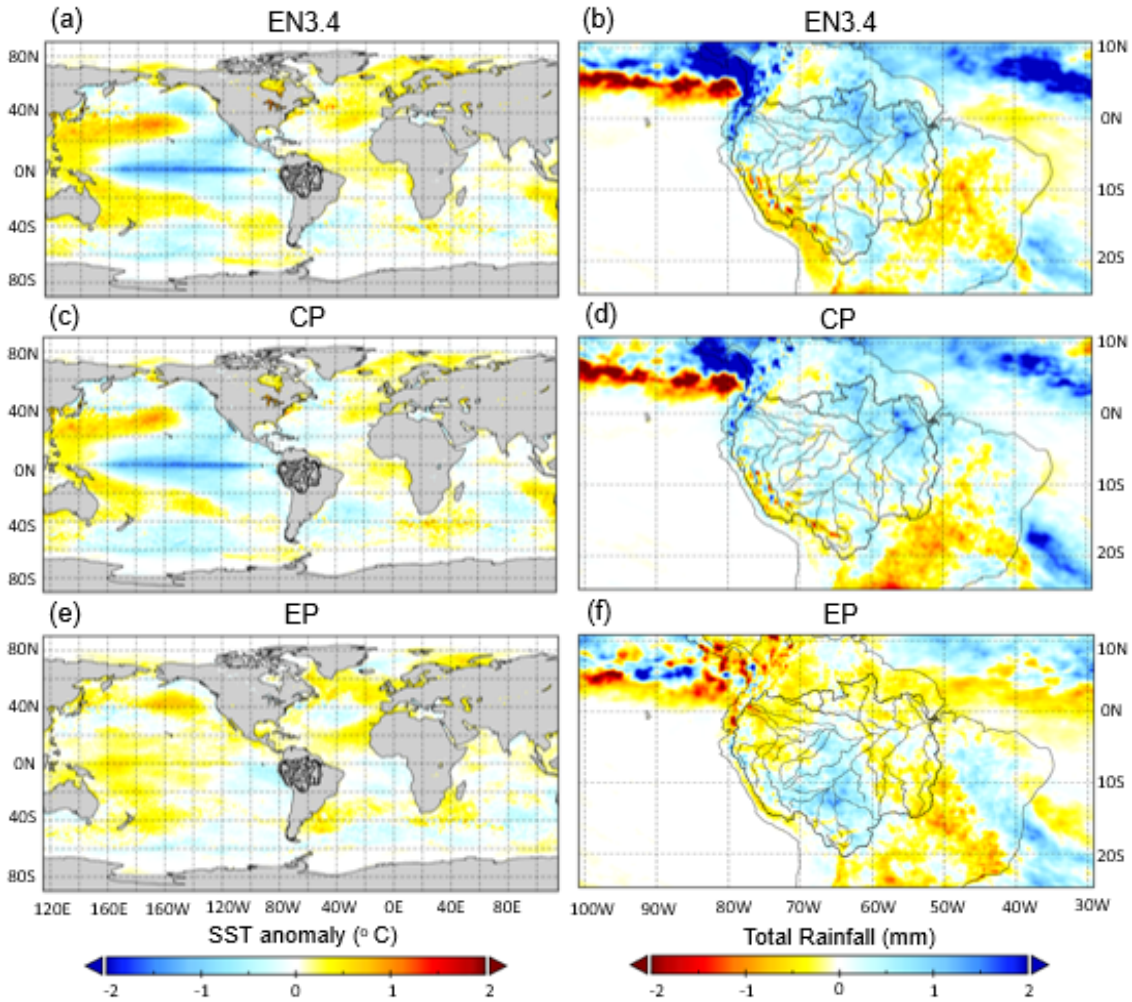


**Figure 12.** *Composite analysis of the difference between the preceding OND average SST (°C) (left) and total rainfall (mm) (right) for the average of the 12 negative years and the average of the 12 neutral years. For the (a, b) EN3.4, (c, d) CP, and (e, f) EP indices. A list of the negative and neutral years for each index can be found in Tables S2, S4, and S5.*

To better understand the similarities and differences between ENSO indices, Fig. 12 plots the average preceding OND SST anomalies and total precipitation over the Amazon basin for the negative years of the EN3.4, CP and EP indices relative to their associated neutral years (e.g. EN3.4 negative minus EN3.4 neutral). SST anomalies for negative EN3.4 and CP phases are found to be similar, with a concentration of negative SSTs (∼−1.5 ◦C) situated in a long stretch of the central equatorial Pacific and warmer SSTs common in coastal areas of Indonesia to the west of the Pacific (Fig. 12a and c). In contrast, preceding OND SST anomalies for the negative EP phase are in general weaker, with slightly negative (∼−0.5 ◦C) SSTs located off the coast of Peru in the eastern Pacific with warmer waters spreading further east into the central Pacific Ocean (Fig. 12e). Other notable differences between the two centrally focused indices (EN3.4 and CP) and the EP can be found in the sub-tropical to south Atlantic Ocean (20–50◦ S), where cooler (warmer) SSTs are situated for the central ENSO indices (EP index). For EN3.4 and CP negative years, rainfall totals from the ERA5 reanalysis (inputs to GloFAS 2.1) are greater relative to neutral conditions in the north-eastern Amazon (Fig. 12b and d), whereas a deficit in rainfall is acknowledged for the negative EP phase (Fig. 12f), explaining why flood magnitude and duration did not increase for this climate index.

#### 4.3.4.3 Observed vs GloFAS 2.1

Significant changes to flood characteristics are present in both datasets for the results presented in Sect. 4.3. For instance, the increased flood magnitude and duration witnessed during the negative ENSO phase are identified at locations in the north-eastern Amazon for both the observed and reanalysis data, as is the case for the decrease in flood duration witnessed during positive TSA years (Figs. 2b, f and 10c, g). River flow data produced from global hydrological models form an important role in the ability to forecast and mitigate floods (Alfieri et al., 2019). This is because observed data are often limited in time, with a downward trend in global data availability since the 1980s, and has a restricted coverage in many parts of the world (including sparse areas of the Ecuadorian and Colombian Amazon) (Lavers et al., 2020). Though simulated data can extend the period of analysis back in time and have a wide spatial coverage, the data needs to be sufficient and validated against observations regularly. Table 1 shows Pearson's correlation coefficients between the results for observation and GloFAS 2.1 in Sect. 4.3. It is important to note that both datasets will incur errors that need to be considered. For instance, many gauges in the Amazon Basin are produced based on water levels that are converted to river flow based on the use of the stage–discharge relation, which

has large uncertainties due to systematic errors such as sensor drift and calibration errors and does not take into account non-stationarities (Horner et al., 2018). Non-stationarities can include anthropogenic change, land use change (e.g. inclusion of a reservoir) and low frequency climate variability (e.g. PDO and AMO) and can therefore can cause gradual or sudden changes in river flow influencing the accuracy of the stage-to-discharge relation and produce uncertainties within the discharge time series. Extreme flows or flooding can result in changes to the morphology, which in turn could affect the accuracy of these measurements and thus conversion and affect both the archived observed time series and the forecasted product (Lavers et al., 2020).

**Table 1.** *Pearson's correlation coefficients between observed and GloFAS 2.1 results of the differences between climate phases for all indices (e.g. EN3.4 positive minus EN3.4 neutral) for flood magnitude, timing and duration. Values in bold are significant at the 95 % confidence level.*

| Index and Phase | Magnitude | Timing | Duration |
|---|---|---|---|
| EN3.4 Pos | 0.14 | -0.10 | **0.50** |
| EN3.4 Neg | **0.72** | **-0.27** | **0.79** |
| MEI Pos | 0.13 | 0.19 | **0.30** |
| MEI Neg | **0.72** | 0.16 | **0.64** |
| CP Pos | -0.03 | 0.09 | **0.32** |
| CP Neg | **0.59** | -0.25 | 0.21 |
| EP Pos | -0.05 | 0.21 | 0.03 |
| EP Neg | **0.47** | 0.11 | **0.59** |
| TNA Pos | **0.56** | -0.02 | **0.56** |
| TNA Neg | 0.04 | **0.28** | **-0.37** |
| TSA Pos | **0.39** | 0.04 | **0.67** |
| TSA Neg | **0.65** | 0.10 | -0.08 |
| Median | 0.43 | 0.10 | 0.41 |

Flood magnitude and duration have the highest correlation between observed and simulated results, where median values of 0.43 and 0.41 (across all climate indices) are noted, respectively. In contrast, correlation for changes in flood timing are particularly weak (median = 0.10), with correlations for only two climate indices found to be significant (Table 1). As GloFAS struggles to capture changes to flood timing for most climate indices and phases, it indicates that the model suffers at capturing peak flow timing in general rather than in one specific climate phase. Though restricted to just 12 years for each climate phase, the correlation for flood magnitude and duration are much higher for the negative phases of the

ENSO indices, particularly when compared to the positive phases of these indices. For instance, comparing the correlation values for the percentage changes of flood magnitude, a significant correlation value of 0.72 is identified for the EN3.4 negative, dropping to 0.14 for the warm phase. The reasoning for the poorer performance during the warm ENSO phase is not yet known but deserves further investigation. It is unlikely due to the number of missing years for the observed data, with a median of 2 missing years and 1 missing year across all stations for the positive and negative EN3.4 phases, respectively. When removing the stations in the north-east (39, 40, 41 and 43) that produce strong changes for both datasets during negative ENSO phases, the correlation is much lower but still remains higher than during the positive phase ($r$=0.41, $p$<0.05), indicating that GloFAS 2.1 can overall better simulate the response to negative ENSO phases relative to neutral conditions.

## 4.4 Physical Mechanisms

In this study the question of whether particular climatic drivers (e.g. ENSO) impact flood characteristics in the Amazon Basin was addressed. The next step required would be to investigate how the climatic drivers found in this study increase the likelihood of flooding in particular areas and understanding the physical mechanisms behind a flood event. This is because floods are generated through a combination of climatic, meteorological, hydrological, and anthropogenic processes (Wyżga et al., 2016), which represent a cascading chain of events. For instance, flooding that is related to La Niña conditions stem from changes in temperature, altering pressure gradients and thus large-scale atmospheric circulation (e.g. zonal winds). In turn, this can move the location of moisture convection and divergence, and consequently rainfall patterns. Though a simplistic example, understanding these processes and how they link can allow us to determine how and why floods occur in certain areas and can provide a better understanding of past, present and future flood risk (Berghuijs et al., 2019).

A first step could follow studies such as Zhang et al. (2017) where they use moisture flux convergence and divergence to diagnose precipitation changes during phases of the PMM before describing the impact on other dynamical variables (e.g. 850 hPa velocity potential and divergent wind) for different phases of PMM. By analysing intermediate variables between the overall climatic driver (i.e. PMM) and the dependent variable (i.e. rainfall), a more robust picture of the relationship between a climatic driver and rainfall or river discharge can be built. Moreover, by investigating the underlying connections between the SST anomalies and floods

for specific events, it allows a picture to be built of what the dominant processes (e.g. evaporation or convection) are and how the circulation may differ from neutral conditions or other types of events (e.g. how an EP event differs from a CP event). Knowing these dominant processes would give model developers insight on where to focus efforts to improve seasonal forecasting systems. For example, if evaporation is found to be particularly important, calibration of the land surface or hydrological component of a flood model could be a more important aspect to focus on.

## 4.5 Conclusions

This paper has investigated whether the differences between positive, negative and neutral phases of various climate indices in the tropical Pacific and Atlantic Oceans significantly impact flood characteristics (i.e. flood magnitude, timing and duration) in the Amazon Basin for the period 1979–2015. Previous research and fieldwork had highlighted the need to consider flood timing and duration as opposed to simply the magnitude of river flows, with longer floods known to cause significant impacts to communities situated along rivers within the basin (Langill and Abizaid, 2019), and that the flood timing in coinciding tributaries is known to impact the magnitude of flow in the main travelling flood wave along the Amazon River (Tomasella et al., 2011; Marengo et al., 2012). While the results presented show regional differences and varying levels of significance among climate indices, we can draw the following conclusions to answer the research objectives outlined in Sect. 4.1.1.

1. Flood magnitude increases at stations situated in the north-eastern Amazon for climate indices where the cooling of SST anomalies is stronger in the central equatorial Pacific (i.e. EN3.4, CP, and MEI) as identified for both the observed and reanalysis dataset. This response is not reproduced for years in which the SST cooling is more concentrated to the eastern Pacific.
2. Positive ENSO years (EN3.4, MEI) result in a reduction of peak river flows and flood duration throughout the majority of the basin, while the influence of negative ENSO years (i.e. La Niña conditions) is found to be weak across much of the Amazon Basin, with the exception of areas in north-east.
3. No significant increases are found in peak river flows in the Peruvian Amazon when comparing negative ENSO years to neutral conditions, with decreases observed in DOT despite previous extreme floods being attributed to La Niña events.

4. Flood timing is the least impacted flood characteristic, with limited significant and notable changes across the basin for most climate indices.
5. Despite strong links between flood characteristics (e.g. flood magnitude and duration), the same climate phase can impact these characteristics differently. This is evident from the CP index, where flood magnitude increased in the north-eastern Amazon, with flood duration decreasing during negative years.
6. There is greater agreement between the observed and simulated GloFAS 2.1 changes to flood magnitude and duration in negative than positive ENSO years; suggesting the reanalysis is better at representing La Niña teleconnections.

Insights into the understanding of how large-scale climate variability influences flood characteristics has the potential to help predict and prepare for different flood types (e.g. high, long, early and late; Langill and Abizaid, 2019). These findings are important for highlighting locations such as the north-eastern Amazon that are sensitive to particular oceanic anomalies and has the potential to help community members and local businesses (e.g. fisheries and agriculture) with decision making within the Amazon Basin. For example, the results found for the Sao Francisco gauging station (41), located along the Jari River, showed that flood magnitude and duration significantly increase during negative ENSO phases. This gives humanitarian organisations and local authorities acting within areas such as Laranjal do Jari, located just downstream of this gauging station, the potential to use these results to better prepare and make decisions based on an increased probability of a longer high-water period. The next steps should consider specific case studies in locations such as the north-eastern Amazon that evaluate how certain sectors or livelihoods could be affected by certain climate phases and suggest adaptation measures such as examining the possible shifts in cropping patterns (i.e. sowing, growing and harvesting) during particular climate phases as in Ficchí and Stephens (2019) for rivers in Africa. Further exploratory analysis could consider breaking this study down further to consider the intensity of climate anomalies, for example, by comparing differences between weak, medium and strong El Niño events to neutral years. Such work could be extended to investigate the impact of co-occurring climatic phases (e.g. La Niña and a warm TSA) to understand if the probability of wetter or drier conditions changes. This is owed to previous flood events having been linked to more than one index. For instance, in 2014, floods in the Madeira basin were related to both warm conditions in the West Pacific–Indian Ocean and exceptionally warm SST conditions in the sub-tropical South Atlantic (Espinoza et al., 2014). Yoon and Zeng (2010) demonstrate a method to separate

indices via linear regression, which can remove the issue of one climate index influencing another to determine if each index has a direct influence on the hydrology. Finally, a similar analysis would ideally be performed for observed precipitation, which could help confirm or further explain the results found in this work.

**Data availability.** All of the datasets, with the exception of certain gauged data used in this study are freely available and their sources can be found in Sect. 4.2. For gauges whose data is restricted please contact the Institute of Research and Development (IRD) for further information on potential access.

**Author contributions.** AF, ES, HC, and JT designed the analysis, with AF and ES providing the original methodology and R scripts for the flood timing section of the analysis. JT produced all figures and undertook the research, in addition to writing the research paper. AF, ES, HC, JB and EC supervised the research and provided important advice. All of the authors were involved in discussions throughout the development and commented on the manuscript.

## 4.6 Supplementary material

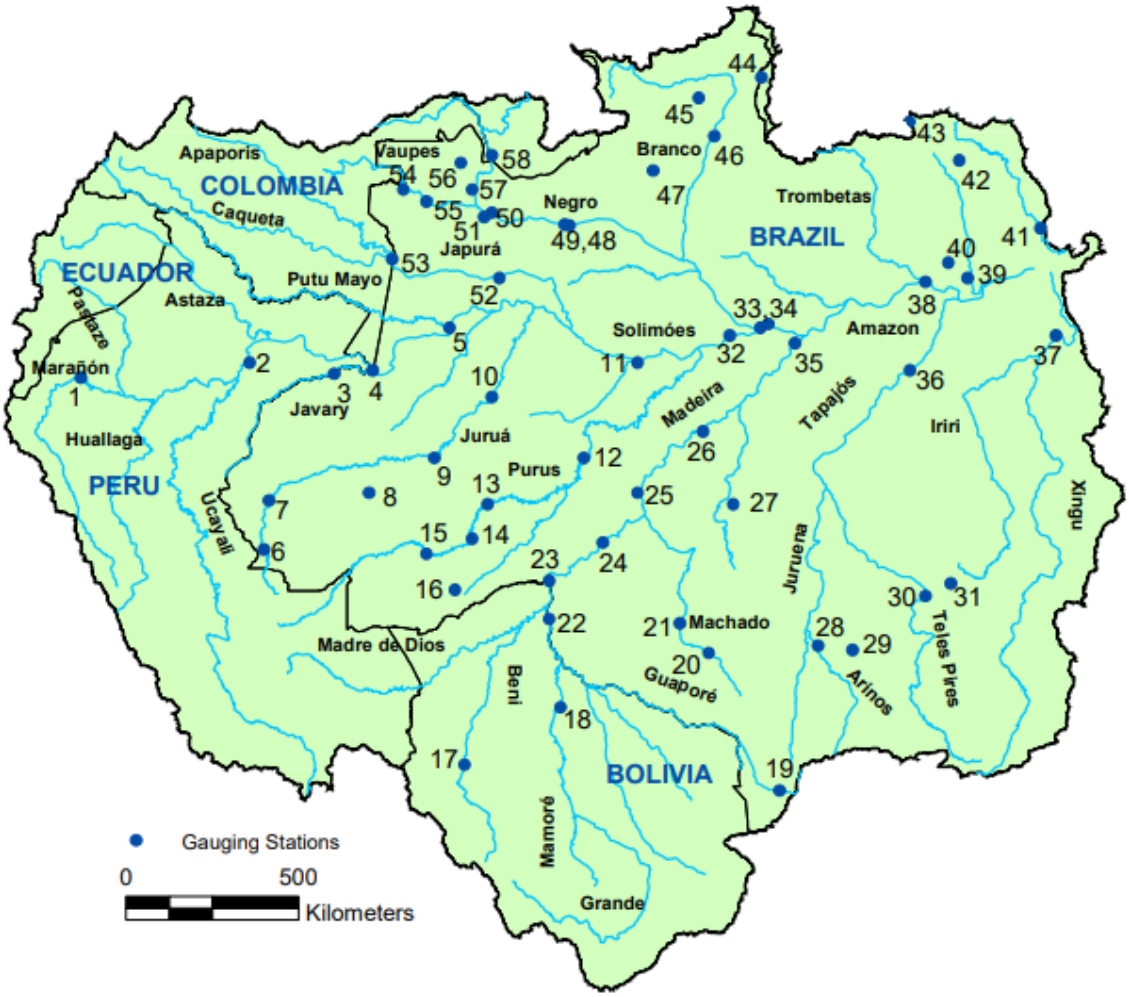


**Figure S1.** Map of the gauging stations and their locations used within this study. Number are referred to within the main text in italics to help direct the reader to the locations highlighted. The basin shapefile and river network are provided by HydroSHEDS (https://www.hydrosheds.org/; last access: 07 December 2020).

**Table S1.** Characteristics of the hydrological gauging stations throughout the Amazon Basin

| Station Name (number) | River | Drainage Basin Area ($Km^2$) | Lat | Lon | Start | End | Mean Q ($m^3s^{-1}$) |
|---|---|---|---|---|---|---|---|
| Abuna (23) | Madeira | 921000 | -9.75 | -65.35 | 01/10/1979 | 30/09/2015 | 6430.839 |
| Acanaui (52) | Caqueta/Japura | 242259 | -1.85 | -66.65 | 01/10/1979 | 30/09/2015 | 14304.51 |
| Altamira (37) | Xingu | 446203 | -3.35 | -52.15 | 01/10/1979 | 29/09/2014 | 7856.263 |
| Apalai (42) | Paru De Este | NA | 1.22 | -54.66 | 01/10/1980 | 29/09/2012 | 142.8763 |
| Arapari (39) | Maicuru | 17072 | -1.85 | -54.45 | 01/10/1979 | 30/09/2013 | 123.8534 |
| Boca Do Guariba (27) | Aripuana | 70100 | -7.75 | -60.55 | 01/10/1979 | 30/09/2010 | 1428.181 |
| Boca Do Inferno (40) | Curua | 20803 | -1.45 | -54.95 | 01/10/1979 | 29/09/2009 | 154.9359 |
| Bom Fim (44) | Tacutu | NA | 3.38 | -59.82 | 01/10/1984 | 30/09/2013 | 214.241 |
| Borja (1) | Maranon | 114232 | -4.45 | -77.55 | 01/10/1986 | 30/09/2015 | 4993.966 |
| Cachimbo (31) | Branco Sul | NA | -9.82 | -54.89 | 01/10/1979 | 30/09/2013 | 39.08 |
| Canutama (12) | Purus | 230012 | -6.55 | -64.45 | 01/10/1979 | 30/09/2015 | 6430.839 |
| Caracarai (46) | Branco | 124980 | 1.85 | -61.05 | 01/10/1979 | 30/09/2015 | 2947.296 |
| Careiro (33) | Parana Do Careiro | 2583079 | -3.15 | -59.85 | 01/10/1979 | 30/09/2014 | 12507.61 |
| Cruzeiro Do Sul (7) | Jurua | 38537 | -7.65 | -72.65 | 01/10/1979 | 30/09/2010 | 925.4951 |
| Cucui (58) | Negro | 61781 | 1.35 | -66.85 | 01/10/1980 | 30/09/2013 | 4984.06 |
| Curicuriari (50) | Negro | 194462 | -0.15 | -66.85 | 01/10/1979 | 30/09/2013 | 12067.93 |
| Envira (8) | Tarauaca | 48317 | -7.45 | -70.05 | 01/10/1979 | 30/09/2011 | 1234.752 |
| Estirao Do Repouso (3) | Javari | 62105 | -4.35 | -70.95 | 01/10/1981 | 30/09/2012 | 2486.017 |
| Fazenda Vista Alegre (35) | Madeira | 1310000 | -3.55 | -58.95 | 01/10/1979 | 30/09/2015 | 28015.34 |
| Fe E Esperanca (45) | Mucajai | 13658 | 2.85 | -61.45 | 01/10/1979 | 30/09/2012 | 306.2561 |
| Fontanilhas (28) | Juruena | 55900 | -11.45 | -58.35 | 01/10/1980 | 30/09/2013 | 1433.657 |
| Gaviao (10) | Jurua | 162000 | -4.95 | -66.85 | 01/10/1979 | 30/09/2010 | 4619.165 |
| Gujara-Mirim (22) | Mamore | 609000 | -10.75 | -65.35 | 01/10/1979 | 30/09/2013 | 8062.95 |
| Humaita (25) | Madeira | 1090000 | -7.45 | -63.05 | 01/10/1979 | 30/09/2013 | 20334.79 |
| Indeco (30) | Teles Pires | 52200 | -10.15 | -55.55 | 01/10/1980 | 30/09/2013 | 1166.612 |
| Itaituba (36) | Tapajos | 458000 | -4.25 | -55.95 | 01/10/1979 | 30/09/2014 | 11745.5 |
| Itapeua (11) | Solimoes | 1769000 | -4.05 | -63.05 | 01/10/1979 | 30/09/2014 | 82396.76 |

| Station Name (number) | River | Drainage Basin Area ($Km^2$) | Lat | Lon | Start | End | Mean Q ($m^3s^{-1}$) |
|---|---|---|---|---|---|---|---|
| Jatuarana (34) | Amazonas | 2854286 | -3.05 | -59.65 | 01/10/1979 | 30/09/2012 | 124924.5 |
| Ji-Parana (21) | Jiparana | 32800 | -10.85 | -61.95 | 01/10/1979 | 30/09/2012 | 692.7674 |
| Jusante Da Cachoeira Do Caju (51) | Jusante | 10228 | -0.25 | -67.05 | 01/10/1982 | 30/09/2013 | 942.8736 |
| Manacapuru (32) | Solimoes | 2147736 | -3.35 | -60.65 | 01/10/1979 | 30/09/2015 | 103025.6 |
| Manicore (26) | Madeira | 1150000 | -5.85 | -61.35 | 01/10/1979 | 30/09/2013 | 27077.35 |
| Missao Icana (56) | Icana | 22282 | 1.15 | -67.65 | 01/10/1980 | 30/09/2013 | 1877.793 |
| Obidos (38) | Amazon | 4680000 | -1.95 | -55.55 | 01/10/1979 | 30/09/2015 | 174057.4 |
| Pimenta Bueno (20) | Apedia | NA | -11.63 | -61.19 | 01/10/1980 | 29/09/2013 | 203.5903 |
| Pontes E Lacerda (19) | Guapore | NA | -15.22 | -59.35 | 01/10/1979 | 30/09/2013 | 54.46617 |
| Porto Dos Gauchos (29) | Arinos | 37100 | -11.55 | -57.45 | 01/10/1979 | 30/09/2011 | 712.8329 |
| Porto Velho (24) | Madeira | 976000 | -8.75 | -63.95 | 01/10/1979 | 30/09/2015 | 19137.55 |
| Posto Ajuricaba (47) | Demeni | 14756 | 0.95 | -62.65 | 01/10/1982 | 30/09/2013 | 508.2344 |
| Puerto Siles (18) | Mamore | 227000 | -13.05 | -65.05 | 01/10/1983 | 30/09/2012 | 4710.79 |
| Rio Branco (16) | Acre | NA | -9.98 | -67.80 | 01/10/1979 | 30/09/2015 | 316.8874 |
| Rurrenabaque (17) | Beni | 70000 | -14.55 | -67.55 | 01/10/1979 | 30/09/2015 | 2066.844 |
| Santo Antonio Do Ica (5) | Solimoes | 1134540 | -3.15 | -67.95 | 01/10/1979 | 30/09/2013 | 54591.62 |
| Santos Dumont (9) | Solimoes | 142234 | -6.55 | -68.35 | 01/10/1981 | 30/09/2015 | 4301.033 |
| Sao Felipe (57) | Jurua | 110862 | 0.45 | -67.35 | 01/10/1979 | 30/09/2013 | 8065.875 |
| Sao Francisco (41) | Jari | 51343 | -0.55 | -52.55 | 01/10/1979 | 30/09/2013 | 1057.156 |
| Seringal Da Caridade (15) | Purus | 63166 | -9.05 | -68.55 | 01/10/1979 | 30/09/2012 | 1320.563 |
| Seringal Fortaleza (13) | Purus | 153016 | -7.75 | -66.95 | 01/10/1979 | 30/09/2015 | 3829.863 |
| Serrinha (49) | Negro | 279945 | -0.45 | -64.95 | 01/10/1979 | 30/09/2015 | 16541.23 |
| Sucunduri (48) | Negro | NA | -0.48 | -64.83 | 01/10/1979 | 29/09/2013 | 376.7507 |
| Tabatinga (4) | Solimoes | 874000 | -4.25 | -69.95 | 01/10/1982 | 21/09/2015 | 36225.36 |
| Tamshiyacu (2) | Solimoes | 721521 | -4.05 | -73.15 | 02/10/1985 | 30/09/2015 | 30419.4 |
| Taraqua (55) | Vaupes _ Uaupes | 44732 | 0.15 | -68.55 | 01/10/1979 | 30/09/2012 | 2718.3 |
| Thaumaturgo (6) | Jurua | 16581 | -8.93 | -72.79 | 01/10/1981 | 30/09/2011 | 393.6696 |
| Tirios (43) | Cumina | NA | 2.22 | -55.96 | 01/10/1979 | 30/09/2012 | 19.51056 |
| Uaracu (54) | Uaupes | 40506 | 0.45 | -69.15 | 01/10/1979 | 30/09/2011 | 2409.46 |

| Station Name (number) | River | Drainage Basin Area ($Km^2$) | Lat | Lon | Start | End | Mean Q ($m^3s^{-1}$) |
|---|---|---|---|---|---|---|---|
| Valparaiso – Montante (14) | Purus | 103285 | -8.65 | -67.35 | 01/10/1981 | 30/09/2015 | 2158.127 |
| Vila Bittencourt (53) | Caqueta/Japura | 197136 | -1.35 | -69.45 | 01/10/1980 | 30/09/2015 | 13749.5 |

**Table S2.** EN3.4 positive, neutral, and negative years. Calculated based on the average SST anomaly between August to February preceding flood peaks in the Amazon Basin.

| Positive | Neutral | Negative |
|---|---|---|
| 1979-1980 | 1980-1981 | 1983-1984 |
| 1982-1983 | 1981-1982 | 1984-1985 |
| 1986-1987 | 1985-1986 | 1988-1989 |
| 1987-1988 | 1989-1990 | 1995-1996 |
| 1991-1992 | 1990-1991 | 1998-1999 |
| 1994-1995 | 1992-1993 | 1999-2000 |
| 1997-1998 | 1993-1994 | 2000-2001 |
| 2002-2003 | 1996-1997 | 2005-2006 |
| 2004-2005 | 2001-2002 | 2007-2008 |
| 2006-2007 | 2003-2004 | 2008-2009 |
| 2009-2010 | 2012-2013 | 2010-2011 |
| 2014-2015 | 2013-2014 | 2011-2012 |

**Table S3.** MEI positive, neutral, and negative years. Calculated based on the average SST anomaly between August to February preceding flood peaks in the Amazon Basin.

| Positive | Neutral | Negative |
|---|---|---|
| 1982-1983 | 1979-1980 | 1983-1984 |
| 1986-1987 | 1980-1981 | 1988-1989 |
| 1987-1988 | 1981-1982 | 1995-1996 |
| 1991-1992 | 1984-1985 | 1996-1997 |
| 1992-1993 | 1985-1986 | 1998-1999 |
| 1993-1994 | 1989-1990 | 1999-2000 |
| 1994-1995 | 1990-1991 | 2000-2001 |
| 1997-1998 | 2001-2002 | 2005-2006 |
| 2002-2003 | 2003-2004 | 2007-2008 |
| 2004-2005 | 2012-2013 | 2008-2009 |
| 2006-2007 | 2013-2014 | 2010-2011 |
| 2009-2010 | 2014-2015 | 2011-2012 |

**Table S4.** CP positive, neutral, and negative years. Calculated based on the average SST anomaly between August to February preceding flood peaks in the Amazon Basin.

| Positive | Neutral | Negative |
|---|---|---|
| 1982-1983 | 1979-1980 | 1983-1984 |
| 1986-1987 | 1980-1981 | 1984-1985 |
| 1987-1988 | 1981-1982 | 1985-1986 |
| 1990-1991 | 1989-1990 | 1988-1989 |
| 1991-1992 | 1992-1993 | 1995-1996 |
| 1994-1995 | 1993-1994 | 1998-1999 |
| 1997-1998 | 1996-1997 | 1999-2000 |
| 2002-2003 | 2001-2002 | 2000-2001 |
| 2004-2005 | 2003-2004 | 2007-2008 |
| 2006-2007 | 2005-2006 | 2008-2009 |
| 2009-2010 | 2012-2013 | 2010-2011 |
| 2014-2015 | 2013-2014 | 2011-2012 |

**Table S5.** EP positive, neutral, and negative years. Calculated based on the average SST anomaly between August to February preceding flood peaks in the Amazon Basin.

| Positive | Neutral | Negative |
|---|---|---|
| 1982-1983 | 1979-1980 | 1980-1981 |
| 1983-1984 | 1981-1982 | 1985-1986 |
| 1986-1987 | 1984-1985 | 1989-1990 |
| 1987-1988 | 1988-1989 | 1990-1991 |
| 1991-1992 | 1992-1993 | 1995-1996 |
| 1997-1998 | 1993-1994 | 1996-1997 |
| 1998-1999 | 1994-1995 | 2001-2002 |
| 2002-2003 | 1999-2000 | 2004-2005 |
| 2003-2004 | 2000-2001 | 2005-2006 |
| 2006-2007 | 2009-2010 | 2007-2008 |
| 2008-2009 | 2010-2011 | 2012-2013 |
| 2014-2015 | 2011-2012 | 2013-2014 |

**Table S6.** TNA positive, neutral, and negative years. Calculated based on the average SST anomaly between August to February preceding flood peaks in the Amazon Basin.

| Positive | Neutral | Negative |
|---|---|---|
| 1987-1988 | 1979-1980 | 1982-1983 |
| 1995-1996 | 1980-1981 | 1983-1984 |
| 1997-1998 | 1981-1982 | 1984-1985 |
| 2001-2002 | 1990-1991 | 1985-1986 |
| 2003-2004 | 1996-1997 | 1986-1987 |
| 2004-2005 | 1998-1999 | 1988-1989 |
| 2005-2006 | 1999-2000 | 1989-1990 |
| 2006-2007 | 2002-2003 | 1991-1992 |
| 2009-2010 | 2007-2008 | 1992-1993 |
| 2010-2011 | 2008-2009 | 1993-1994 |
| 2012-2013 | 2011-2012 | 1994-1995 |
| 2013-2014 | 2014-2015 | 2000-2001 |

**Table S7.** TSA positive, neutral, and negative years. Calculated based on the average SST anomaly between August to February preceding flood peaks in the Amazon Basin.

| Positive | Neutral | Negative |
|---|---|---|
| 1984-1985 | 1981-1982 | 1979-1980 |
| 1987-1988 | 1983-1984 | 1980-1981 |
| 1988-1989 | 1985-1986 | 1982-1983 |
| 1993-1994 | 1994-1995 | 1986-1987 |
| 1997-1998 | 2000-2001 | 1989-1990 |
| 1998-1999 | 2001-2002 | 1990-1991 |
| 1999-2000 | 2002-2003 | 1991-1992 |
| 2003-2004 | 2006-2007 | 1992-1993 |
| 2004-2005 | 2007-2008 | 1995-1996 |
| 2008-2009 | 2012-2013 | 1996-1997 |
| 2009-2010 | 2013-2014 | 2005-2006 |
| 2010-2011 | 2014-2015 | 2011-2012 |

# Chapter 5

# Comparison of flood prediction methodologies

## 5.1 Motivation

Originally, this chapter was going to form a further analysis linking heavy rain events in the Amazon Basin to large-scale climate variability extending upon the analysis on the magnitude, timing, and duration of river flows. However, after the submission of Chapter 4 to HESS, the dialogue between reviewer 2 and the authors provoked the idea of a discussion article between the use of statistical methods versus those that investigate the physical mechanisms that lead to teleconnections.

Below are snippets of the exchanges between anonymous reviewer 2 and the authors from our paper titled "Influence of ENSO and tropical Atlantic climate variability on flood characteristics in the Amazon Basin" (i.e. Chapter 4). For the full set of reviewer and author comments, see the Appendices.

Reviewer comments are in bold font, with our responses shown in normal font.

**"The study examines the influence of ENSO on the flood characteristics in the Amazon Basin. While the article is packed with the statistical analyses, it fails to explore the large-scale physical mechanism associated with ENSO and flood characteristics, which plays a important role in the prediction and projections. Therefore, the article in the present form is not in the publication level of HESS and requires major modifications".**

"We disagree with the reviewer that this article in present form is not in the publication level of HESS due to the following reasons:

- The major criticism does not reflect on the research objective of this paper.
- Statistical analyses play a huge role in meteorological and hydrological research and are consistently published in many established journals including HESS.
- A multitude of highly cited papers use statistical analysis to identify relationships between hydrometeorological variables and climatic drivers without exploring the physical mechanisms directly. Examples include Ward et al. (2014) global analysis of discharge sensitivities to ENSO, Emerton et al. (2017) description on the complexities

of ENSO driving flood hazard, and Nobre et al. (2017) analysis into how climate variability affects flood damage in Europe.

- The findings of this research can inform further studies that wish to characterise the largescale physical mechanisms behind the conclusions".

**"My comments/suggestion are: 1. Authors should explore more towards explaining the physical mechanism associated with the relation they found in the present article".**

"While we understand the importance of research that tackles the physical mechanisms that lead to teleconnections, there is a wide body of literature that addresses the statistical link between climate variability and natural hazards that underpins both operational forecasting products (e.g., IRI forecasts; see https://iri.columbia.edu/our-expertise/climate/forecasts/irireal-time-seasonal-climate-forecasts-and-models/) and decision-making on the ground (e.g. IASC, 2018). We believe that our research article falls within this bracket and provides important information on how climate variability impacts poorly researched flood characteristics (i.e. flood timing, and duration) in the Amazon Basin".

Whilst we disagree with the reviewer's comments for our paper as we believe that it extends beyond the scope of the objective and research questions (i.e. we examined if rather than how particular climate indices altered flood characteristics), we do believe it provides a valuable topic of discussion that could provide useful insights for future work. The objective of this chapter is to compare the value of different approaches for hydrometeorological research and flood prediction.

## 5.2 A statistical methods approach

Examples on the use and importance of statistical methods spans across all scientific disciplines, with its value showcased during some of the most important events in modern history (e.g. Bayes' theorem during World War Two and regression statistics for epidemics such as COVID19). When thinking about statistical methods we should first consider what they are. On a basic level, statistical tests can be described as a way to examine data to understand whether apparent relationships are meaningful and that they do not happen simply by chance. The second point to consider is what is the purpose of the statistics? Is it to establish a relationship which can form the building blocks for further work or is it to provide information to inform decision making?

For hydrometeorology, statistical methods have widely been used to identify the links between particular climate indices (e.g. ENSO) and the magnitude of river levels/discharge across the world (e.g. Ward et al., 2010; 2014; 2016), while others have gone onto use information from statistical tests to produce forecasts based on probabilities for upcoming natural hazards (e.g. droughts and floods; Schöngart and Junk, 2007; Emerton et al., 2017; 2019).

In Chapter 4 we used a tercile based framework in which we compared the influence of positive/negative phases of several climate indices against neutral conditions. This method to our knowledge has not been widely used in field of hydrology and had not been applied specifically to the Amazon Basin. This approach was already applied by Ficchí and Stephens (2019) for Africa, observing the differences in peak flow timings across Africa between the warm and cold phases of different climatic indices. The authors demonstrated the potential usefulness of the results in identifying the most suitable times for farming practices based on how the flood seasonality changes during the positive or negative phases of ENSO.

Information from statistical methods can also be used to provide information on the need to consider further research or advice on the uncertainties that may be involved in flood prediction. For instance, Emerton et al. (2017) calculated historical probabilities of increased or decrease flood hazard in any given month during El Niño/La Niña events. This was based on the thought that historical evidence of the typical impacts of ENSO could be used to provide useful information on what we can expect at different locations in the future (i.e. wetter or drier conditions). The results showed that though large areas of the globe could be circled as being wetter or drier during a particular climate phase, when compared to the observations during specific ENSO events, some countries observed the expected flooding while others did not. These results could be used as a reason not to use forecasts based on climate variability, with the authors stressing the need for further works such as to consider how specific regions may respond to different types of climate events (e.g. central vs eastern ENSO events).

Other common statistical methods used in the literature include examining the impact of climate indices on the frequency of flooding (e.g. Villarini et al., 2013; Mallakpour and Villarini, 2016; Mallakpour et al., 2017). This methodology uses regression models to evaluate whether large-scale climate features such as ENSO significantly influences the frequency of events over a particular period of time (e.g. per rainy season or year). For example, Mallakpour et al. (2017) uses the Cox regression model to compare seasonal count data (i.e. the occurrence/non-occurrence of events) against the daily time series of SSTs. Both rainfall and

discharge data were used over the central United States, with events determined as daily rainfall that exceeded the 95$^{th}$ percentile of the distribution and a peaks over threshold approach for river flow, where the threshold was set to have an average of two flood events per year at each gauging station. The application of this methodology allows the user to identify if extreme hydrometeorological events tend to occur independently of each other or in clusters. The answer to this question can have profound implications. For instance, if we imagine a scenario in which the number of heavy rainfall events is the same between two seasons, but in the first season events are independent and are evenly spaced in time and in the other events are clustered in time, the resulting socioeconomic implications could be totally different. The clustering of flooding for instance, can impact flood estimates, design, and risk management, whilst causing issues with the pricing of insurance contracts (Merz et al., 2016), as the cost to an insurance company after re-insurance from a cluster of floods can be higher than from a single event (Mallakpour et al., 2017).

The above studies do not all mention how the links between climate indices and flood events manifest or explain the underlying mechanisms that cause floods. Rather they produce a statistical framework that serves a purpose. The purpose of a study is the key factor in understanding the value of using a particular method. For instance, the way you want to assess the frequency of flooding can change how appropriate a particular modelling framework is (Mallakpour et al., 2017). If the goal is to examine the frequency of flood events in a season against climate indices, then the Poisson regression model would be the appropriate choice. However, if the objective were to model whether the frequency of events within a season are clustered then the Cox regression model would be a better candidate.

The region of interest and the behaviour of variables (e.g. precipitation vs river discharge) can also influence the suitability and value of using a particular statistical approach. For example, for larger rivers in the Amazon Basin, the hydrographs tend to have one defined peak of river discharge. This can be problematic if trying to apply the Cox regression model to these rivers as the number of events will be small and where a river discharge series is volatile (i.e. goes under and back over a set threshold), it would violate the requirement of events being independent of one another. However, if we changed the variable of interest to rainfall and we were to examine the temporal frequency of heavy rain events against climate indices, the study can be become much more valuable. For instance, this type of analysis could provide insights into the clustering of rain events over a certain tributary during a particular climate phase which in turn could have impacts on the timing of flood peaks in coinciding tributaries.

## 5.3 A physical mechanism approach

Floods can be described as a destructive abundance of water, that is generated through a combination of climatic, meteorological, hydrological, and anthropogenic processes (Wyżga et al., 2016). For example, factors can include abnormal SSTs that stem from changes in temperature (natural or anthropogenic), altering pressure gradients and thus the atmospheric circulation (i.e. zonal winds). In turn this can move the location of the convection of moisture into the atmosphere and the locations of moisture convergence and divergence (i.e. large-scale atmospheric circulation), and consequently rainfall patterns. Though a simplistic example, understanding these processes and how they link can allow us to determine how and why floods occur in certain areas and can provide understanding of past, present, and future flood risk (Berghuijs et al., 2019).

Most studies that investigate the mechanisms between climatic drivers (e.g. TNA, ENSO) and flooding typically examine several variables such as moisture fluxes, the divergence and convergence of moisture, precipitation, geo-potential height, and vorticity during the growth, peak, and decay of a climatic event (e.g. El Niño). This can either be performed for a single climate event or for a composite of the same type of event (i.e. the mean of moisture fluxes during several El Niño events). Plots are then typically analysed to identify certain patterns that can explain the links between anomalous SST conditions and flooding and how it occurs. This is performed either by studying the absolute values for a specific period or observing how different each variable of choice is compared to the climatology or another climate phase (e.g. positive against neutral years).

A detailed example of this type of analysis can be found in Zhang et al. (2017) study where they investigate the influence of the Pacific Meridional Mode (PMM), a coupled mode of SSTs and surface winds that are linked to increased rainfall during June-July-August in the Amazon Basin. Here, they use moisture flux convergence/divergence to diagnose precipitation changes using both observed and simulated data. First, they carry out a correlation and regression analysis between PMM and moisture flux convergence over the Amazon basin, finding a positive relationship that suggests increased moisture convergence over most of the Amazon Basin (excluding the north-west) is associated with the positive phase of PMM. Next, they examined the 850 hPa velocity potential and divergent wind which resembled the pattern found for the moisture flux highlighting the key role of low-level convergence/divergence. Further diagnosis explored the moisture stream function and low- and high-level stream function and rotational winds related to PMM. Moisture stream function was found to have a

clear spatial pattern, with negative (positive) stream function anomalies over South America (North Atlantic), respectively. From this the authors identified cyclonic (anticyclonic) moisture flux centres west (east) of the PMM related forcing resembling a baroclinic Gill response (Gill 1980). They hypothesise that this baroclinic Gill response may contribute to anomalous moisture convergence (divergence) over the Amazon region, related to increase (decreased) precipitation during the positive (negative) PMM phase. Similar style analyses for floods in the Amazon can be found in Espinoza et al. (2013; 2014) and Satyamurty et al. (2013) whereby they examine a variety of variables to build up a picture of how each responds to anomalous SSTs.

The clear benefit of using this type of approach is that many more variables are assessed which can then be linked to the prediction of wetter or drier conditions. For instance, most statistical analyses simply investigate the relationship between the climatic index (e.g. SST anomalies) and rainfall/river discharge. However, when analysing the physical mechanisms, as in the example above, a positive phase of PMM is associated with increased rainfall as is moisture flux convergence and the baroclinic Gill responses. When the PMM begins a positive phase, these additional variables and the patterns of cyclonic/anti-cyclonic activity can be used to monitor the situation and build up a more confident picture on the likelihood of wetter conditions.

Returning to the results produced by Emerton et al. (2017) which called for further work investigating how different types of ENSO may affect specific locations. This type of analysis may benefit from a physical mechanisms perspective as opposed to a statistical framework owing to the limited number of specific types of events (e.g. eastern Pacific El Niño events) preventing strong conclusions to be made from typical correlation or regression based statistics. However, by investigating the underlying connections between the SST anomaly and flooding for specific climate events, it allows a picture to be built of what the dominant processes (e.g. evaporation, convection) are and how the circulation may differ to neutral conditions or other types of events (e.g. how does an EP event differ from a CP event). Knowing these dominant processes would allow model developers information on where to focus efforts to improve seasonal forecasting systems.

An often-overlooked element and indeed a limitation of this thesis is a lack of focus to the land surface component of the modelling chain and the physical processes within. Though the focus of this thesis is on whether climatic drivers such as ENSO impact flood variables in the Amazon Basin, better understanding the physical processes at the land surface could help to explain

how ENSO is driving wetter or drier conditions throughout the basin. Indeed, this is true for both understanding the results from a statistical model or through the development of a physical based flood model such as GloFAS. For instance, in the results of Chapter 4, it was found that GloFAS is able to better predict the changes to flood magnitude and duration during the cold ENSO phase relative to neutral conditions compared to the warm ENSO phase relative to neutral conditions. Though an interesting result, it is still unclear why GloFAS performs better during the negative phase. By incorporating experiments into the land surface processes further evidence may be able to provide an explanation for these results. For instance, it is well known that large-scale climate variability such as ENSO has implications for temperature and rainfall across the globe. However, digging deeper, questions could be asked about how the changes in temperature and rainfall impacts additional variables such as soil moisture, snowpack conditions, vegetation cover amongst many more. For instance, during El Niño, changes in temperature could lead to a change in the mass of frozen water in the snow layer and/or the timing of snowpack melting and thus a change in the albedo and vegetation cover. In models such as GloFAS 2.1 where the soil and snowpack are parameterised (Bousetta et al., 2021), the model may not provide an accurate reflection of these processes during these particular climatic periods which may cause a deterioration in the skill of the model.

By understanding how climate variability impacts not just the model output, but additional variables throughout the modelling chain, it can help explain why a particular climate feature increases the likelihood of flooding, but also helps to pinpoint why a particular model is or is not able to accurately simulate the hydrological response to climate variability. This is true when evaluating model performance in general as previous works have shown that errors in river flow were not reflected by precipitation biases and that other errors within the modelling chain (e.g. errors in soil moisture storage/timing, missing processes such as dams or within the river routing model parameters; Follen et al., 2011). Indeed, this was found to be the case at Sao Paulo di Olivenca in the Amazon, where the HadGEM1 model was found to underpredict (boreal) summer rainfall in contrast to the overprediction in river flow, meaning that the error in flow must have been due to another physical variable.

## 5.4 Machine learning

More traditional methods of flood forecasting involve a chain of hydrologic and hydraulic models that describes the physical processes (e.g. evaporation, infiltration, water routing etc.). Although such models provide an understanding of the hydrological system, they often have

high computational and data requirements, particularly at the global scale which can become particularly problematic in data scarce parts of the world and often rely on in-depth knowledge and expertise on model parameters. In addition, physically based models need to be calibrated to a particular geographical area to optimise performance but consequently their outputs are not always generalisable across most river basins owing to the individual characteristics to each basin (Sidrane et al., 2019). Such issues have encouraged the use of data driven models to mimic the complex mathematical expressions of physical processes (Mosavi et al., 2018) and provide the flexibility and power to map flood prone areas even with limited data (Pham et al., 2021). This is achieved by linking GIS and remote sensing techniques to better interpret and visualise the terrain which is being modelled.

Numerous types of machine learning algorithms exist (e.g. artificial neural networks (ANNs), neuro-fuzzy, support vector machine (SVM), and support vector regression (SVR)) and work by learning the relationship between flooding occurrence and explanatory factors from historical flood records. Such models have been found to be effective for both short- and long-term flood predictions (Mosavi et al., 2018). Indeed, Abbot and Marohasy (2014) comparison of physical and machine learning models for rainfall forecasting in Queensland, Australia showed the potential of data driven models with a higher accuracy found for machine learning models.

Like many physical based models, the output of machine learning techniques can also provide estimates of additional hydrological variables such as flood depth. Hosseiny et al. (2020) developed two different machine learning models using a random forest and ANN approach to simulate flood depth in the Green River, Utah. The random forest model identifies wet and dry nodes to represent areas of flooding, whilst the ANN model incorporates coordinates so the user can identify the flood depth anywhere in the model domain. The results showed that the machine learning models could accurately simulate flood extent and flood depth, whilst reducing the computational time 60-fold. As this was for case study for a catchment in Utah, the computational time saved is expected to be much larger for large-scale modelling.

Despite the success of machine learning to date, it is important to consider that the models can only be considered as good as their training, whereby the system learns the model objective based on past data and patterns. Despite being in the ‘earlier’ stages of discovery when it comes to its application to hydrology and flood prediction, there is a sense of fear and apprehension when it comes to machine learning and artificial intelligence from some members of the hydrological community. This is because, these models take away the sense of

understanding the physical processes and requirements for hydrological expertise due to their automated approach. However, Nearing et al. (2020) caution that if hydrologists do not take investment into these new technologies then someone else will. This has already been seen with the likes of Google investing heavily in creating a global flood prediction system using a machine learning and big data approach.

## 5.5 Combining the if and the how

It can sometimes be useful to consider both if there is a relationship between climate and flood events and if so, how it causes it. An example of this is provided by Mallakpour and Villarini (2017) where they first identify if climatic drivers are responsible for observed changes in flood frequency over central United States using a regression analysis. They find that the Arctic Oscillation and Pacific-North American pattern (PNA) are important predictors in 78% of 774 stream gauges. After establishing these relationships, the authors relate their results from statistical analysis to the physical processes by calculating the integrated vapor transport (IVT) over the study area, which describes the total amount of transported water vapor to a region. To do this they observe IVT anomalies on days where heavy rain events occurred and seven days beforehand. At locations where the PNA was identified to be the dominant mode of climate variability, the IVT was found to be anomalously high, showing a higher-than-average transport of moisture to that area (Fig. 1d). This matched with previous studies that found an association between the negative phase of the PNA and increased water vapour transport over the central United State (Harding and Snyder, 2015).

In terms of forecasting floods, the idea of combining models which use different methodologies has become increasingly popular. Commonly termed hybrid models, the idea behind this is to take the advantages of individual model types in order to improve forecast performance. For instance, Phan and Hguyen (2020) concluded that a hybrid model can yield superior and more reliable results when combining a traditional linear statistical model with a machine learning model relative to individual model performance. The authors explain that a hydrological time series often consists of both linear and non-linear correlation types, meaning that a combination of models could be better suited for the problem at hand. The same could be argued for combing machine learning methods with traditional physically based models. This approach could be well suited for those who wish to allow the conceptual components to capture the hydrologic modelling while the machine learning could be utilised for calibration, bias corrections and modelled processes in which data is lacking (Nevo et al., 2019).

Yang et al. (2019) experimented with improving five GHMs flood simulations by using a hybrid physics-guided machine learning approach (LSTM). This hybrid approach was found to drastically improve the performance of simulated flood peak amplitude on the global scale. Despite this improvement, the LSTM was not able to significantly improve the timing of peak flow discharge, likely associated with the model's sensitivity to extreme precipitation, snowmelt and soil moisture. This implies that further development may be required within the GHM, river routing model or input data itself as opposed to the LSTM and emphasises the need to continue the development of models that use a physically based approach.

# Chapter 6

# Conclusions

The aim of this thesis was to provide evidence for the potential use of variations in large-scale climate features (i.e. atmospheric and oceanic anomalies) to extend the lead time of skilful flood forecasts in the Amazon for early warning and early action. While the magnitude of river flows/water levels are often linked with climate anomalies (Ronchail et al., 2005b; Espinoza et al., 2009a), studies examining the relationship with the timing and duration of river discharge are less common. This is despite the length of the wet season and timing of peak river flows in coinciding tributaries playing a major role in the dampening or super positioning of the travelling Amazon flood wave (Tomasella et al., 2010), and having been previously associated with extreme flood events (e.g. 2009 in the Brazilian Amazon; Marengo et al., 2012).

Additionally, although previous extreme flood events have been attributed to particular climate patterns, the usefulness of this information within a flood prediction capacity is still limited and the mechanisms in the build up to these events are not fully understood. For instance, cooler than usual SSTs in the equatorial Pacific Ocean have been identified to provide the atmospheric conditions that maintains a strong humidity flux over the basin and consequently produces increased rainfall and flooding (Espinoza et al., 2013). However, it is not understood, if a particular magnitude of SST anomaly is required or how the spatial extent of SST anomalies would impact the atmospheric response.

To tackle the aforementioned aim, this thesis has made progress in the understanding of how variations in large-scale climate variability affect flood characteristics in the Amazon Basin through the following three research objectives:

1. To provide an up-to-date depiction on what we currently know and do not know about how large-scale variability influences precipitation and river discharge regimes in the Amazon Basin, and thus flooding.
2. To determine whether river flow data produced from global or large-scale hydrological models are sufficient for use in climate analysis, linking large-scale climate patterns and teleconnections to anonymously high river flows.
3. A statistical investigation of whether warm or cold phases of different hydroclimatic drivers significantly alter the characteristics of river flows throughout the Amazon Basin (e.g. the magnitude, timing and duration of river flows) relative to neutral conditions.

4. To discuss whether statistical methods provide sufficient information to support extended-range forecasting in the Amazon Basin, and what could potentially be offered by methods that address the physical mechanisms.

This thesis has been structured around three research papers. These include a comprehensive review of how climate variability influences flooding in the Amazon Basin (Chapter 2; Towner et al., 2020a), and two research articles (Chapters 3-4; Towner et al., 2019, 2020b) addressing objectives two and three. The following sections summarise the key lessons learnt from each objective stated above, addresses the scientific advancements made and proposes avenues for future research.

## 6.1 Key conclusions

### 6.1.1 Objective 1: What do we know and not know

The first objective of this thesis was addressed in Chapter 2 (paper 1) and was to provide a comprehensive picture on the state of knowledge on the influence of large-scale climate variability in the Amazon Basin. To achieve this, maps were created showing the influence of several climate indices over the entire basin for both rainfall and river discharge independently, aggregating results from previous studies. Results predominately identified consistent patterns for both rainfall and river discharge (e.g. widespread drier conditions during El Niño or a warm TNA and wetter conditions in the north-eastern Amazon during La Niña), though the understanding of these results for a flood forecasting capacity was weak.

The review was extended to document and evaluate flood events attributed to particular climate indices since 1950 based on previous work. Here, an assessment of each study was undertaken to assess the confidence in the results linking certain floods to certain phase of climate variability. **Most disagreements took place in the Peruvian Amazon, with discrepancies identified for certain flood events** (e.g. 1986 and 1993; Espinoza et al., 2013). These floods had been found to be associated with La Niña conditions despite not reaching the typical ONI SST threshold. Though certain extreme floods are examined in detail (e.g. 2014 in the Madeira basin; Espinoza et al., 2014), certain events are only evaluated as part of a composite analysis where results are smoothed. Moving forwards, it could be useful to analyse individual events linked to the same climate phase (e.g. La Niña) to better understand the mechanisms behind each event.

**A key message from this paper was the need to divert attention to how climate variability influences flood timing and duration.** Most studies have identified the relationship for how the magnitude of streamflow is affected, but few were able to provide relevant information on whether climate indices such as ENSO increased/decreased the period of flooding or altered the timing of the flood peak. These characteristics play a huge role in determining the type of flood event, with early or long flood periods know to have a range of effects to those living within the floodplain (Langill and Abizaid, 2019).

### 6.1.2 Objective 2: Assessing the capabilities of GHMs for capturing annual peak river flows

Consistent links have previously been identified between SST anomalies in the Atlantic and Pacific Oceans and observed streamflow in the Amazon. However, Chapter 2 identified that the time series of individual gauging stations commonly have large gaps without data and are limited in time, with the period of investigation in many studies restricted to between 10-20 years, meaning that it is only able to capture a few strong climate events (e.g. strong El Niño). Datasets produced from GHMs can extend the period of analysis, but the suitability of such data requires robust evaluation, exploring the strengths and shortcomings of individual components across the modelling chain. The objective of this paper was to assess the performance of several different GHMs for capturing both daily and annual peak river flows in the Amazon Basin. This was achieved by comparing the output of river discharge from eight large-scale hydrometeorological models, with varying model components (e.g. precipitation input, hydrological model, and routing model) to discharge observations (1997-2015). **The results of this paper provided a first indication of the suitability of river flow reanalysis data for the Amazon Basin which are produced through a GHM, with ERA5 as the meteorological input,** compared to its predecessor ERA-Interim Land and satellite data. As expected, the results suggests that the meteorological input was deemed the most important component within the hydrometeorological modelling chain. Model runs which incorporated the latest climate reanalysis dataset, ERA5, showed the most accurate reflection of previously observed annual maximum river flows, particularly at gauging stations situated within the Peruvian Amazon.

In addition to providing an evaluation of a range of GHMs for capturing peak river flows, this paper explored the potential benefits of routing scheme calibration through two specific model run comparisons. **When comparing the calibrated ERA5 Lisflood simulation to the associated uncalibrated model run (i.e. ERA5 Lisflood_uc) no improvement was found in the**

**ability to predict annual maximum river flows.** Improvement was found however for the calibrated simulation for metrics related to the evaluation of the whole hydrological regime (e.g. timing, variability and, bias of the hydrograph), **meaning that the improvement may be restricted to the objective function used, in this case the KGE.** This suggests, models that seek to capture flooding, may be better off using an objective function that fits the model's purpose and users interests (e.g. APFB for flood forecasting).

The implications of these results suggest that when using river flow data produced through GHMs, **the meteorological input is the dominant factor and causes the largest measure of uncertainty.** Therefore, future work should focus on the improvement of precipitation products.

### 6.1.3 Objective 3: Do SST anomalies alter flood characteristics?

In Chapter 2 it was identified that whilst many studies concluded the relationship between various climate indices and the magnitude of streamflow, very few had examined the links to flood timing, and duration in the Amazon Basin. While the results of Chapter 3 provided evidence of the usefulness of using data from GloFAS forced from ERA5 reanalysis precipitation data to help bridge data gaps in the respective time series. The third objective of this thesis was to examine whether positive or negative phases of several climate indices in the tropical Pacific and Atlantic altered flood characteristics (i.e. flood magnitude, timing, and duration), in the Amazon Basin. This objective was addressed in paper 3 (Chapter 4) and assessed seven climate indices, with streamflow data provided from GloFAS reanalysis and observed data at 58 gauging station throughout the analysis period (i.e. 1979 to 2015).

**The results of this paper identified significant changes in both flood magnitude and duration, particularly for rivers located in the north-east of the basin for both datasets when ENSO is in its cold phase.** The result identified in the north-east differs when the centre of the SST anomaly moves from the central to the eastern Pacific (i.e. CP vs EP). When the centre of cooling is further east towards South America, the increase in flood magnitude and duration dissipates. This is due to a shift in the rainfall patterns over the Amazon during the cold EP phase, whereby a deficit in rainfall is observed over the north-eastern Amazon. **These results highlight how the type of ENSO event in terms of their spatial complexities can alter the response in hydro meteorological conditions.**

**No evidence is found to suggest that climate phases significantly impact flood timing across the Amazon, with no notable pattern identified for all indices examined.** Correlations

between the results of the observed and simulated datasets showed that GloFAS can more accurately simulate the negative phase of ENSO relative to neutral conditions for multiple indices. In contrast, the correlation reduces significantly for the positive phase, meaning that GloFAS struggles to accurately simulate the differences in flood characteristics for El Niño and neutral phases.

**The conclusions from this work suggest the need to consider other intricacies within typically analysed climate indices such as EN3.4.** For instance, there is a need to consider how the intensity and/or timing of an event impacts the hydrological response in the Amazon. Espinoza et al. (2013) highlighted how an early La Niña event led to the 2012 floods in the Peruvian Amazon, suggesting the possibility that the timing could be an essential component in understanding the response to specific climate events. In addition, the combination of climate events (e.g. La Niña and a warm TSA) deserves further attention based on evidence of previous flood events (e.g. 2014 in the Madeira basin; Espinoza et al., 2014).

### 6.1.4 Objective 4: Understanding the value of statistical vs physical based methods

The methods from Chapter 4 led to an interesting discussion between a reviewer and the authors leading to the idea of a discussion paper. The fourth objective of this thesis was to discuss the value statistical methods for supporting extended-flood forecasting in the Amazon Basin, while determining the potential value of methods addressing the physical mechanisms of climate events.

**Though both types of methods have been found to provide value in terms of supporting extended-flood forecasting, statistical methods alone can be sufficient providing that it can provide the answers to the question at hand.** For instance, if the objective is to determine if La Niña increases the likelihood of flooding, or by how much does La Niña increase the likelihood of flooding, then statistical approaches are a better suited approach. This is because statistical methods can provide quantitative information on the significance of the relationship whilst providing statistical uncertainty (e.g. use of ensembles to provide probabilities). Though statistical uncertainty has been criticised in its usefulness for decision making as many decisions are binary by nature, this is not a criticism of statistics directly but more of a case of how it is communicated and understood (Pappenberger and Beven, 2006).

If the question however is more related to how La Niña results in flooding and the teleconnections involved, then the physical mechanisms would need to be analysed. From this

a greater picture can be built of the key processes linking climate anomalies and flooding and provide the information on the most important physical processes that need to be simulated more accurately to improve flood predictions. **The key conclusion therefore is the need to focus on the purpose of a study when applying and reviewing the methods.**

## 6.2 Scientific advances

This thesis has determined what we currently know and do not know about the influence of large-scale climate features on Amazon floods, enabling the enhancement in the understanding of different hydroclimatic anomalies for early flood warning. The specific scientific advances of this work are summarised below:

1. This thesis builds upon previous work (e.g. Ronchail et al., 2002; 2005a; Espinoza et al., 2009a) providing a comprehensive up to date review of how large-scale hydroclimatic drivers (e.g. ENSO and tropical Atlantic SSTs) impact both rainfall and river discharge which can be visualised in the form of composite maps.
2. Several recommendations are given to better understand the usefulness of climate research linking SST anomalies to river flow for early flood warnings.
3. Evaluation and usability of simulated river flow data produced from several state-of-the-art GHMs and their components (e.g. river routing model) in the Amazon Basin, providing the strengths and shortcomings for various model components and highlighting regions in the Amazon Basin where simulated data is skilful (not skilful).
4. Recommendations are given for the objective function choice for routing model calibration where the purpose of the model is to capture flooding. Comparisons between uncalibrated and calibrated models runs of Lisflood forced with both ERA-Interim and ERA5 reanalysis showed that the ability to simulate flood peaks in the Amazon does not increase upon routing calibration, whereby the objective function is the KGE.
5. The importance of considering peak flow timing and flood duration in addition to flood magnitude within climate analysis is consistently highlighted throughout this thesis. Differences between positive/negative and neutral phases of several climate indices were assessed for both flood characteristics; the impact on flood timing was found to be limited with no clear signal.

## 6.3 Recommendations for further study

The work in this thesis has raised several questions and motivation for future research. Though avenues of future work have been touched upon in each chapter, this section provides specific examples of ways in which this research could be extended.

- **Full hydrometeorological model comparison study.** One of the next steps raised in Chapter 3 was to carry out the analysis at a more granular scale. For example, due to time restraints associated with this thesis, data was used that was already freely accessible through the GFP. However, ideally a similar analysis would be undertaken whereby the number of models used is larger and incorporates all possible combinations of meteorological input, hydrological/LSM, and river routing component. This would allow a better evaluation of what is the best data input and model selection for the metric and region of choice (e.g. peak river flows for the Amazon).
- **Impact of hydrological data and processes.** One of the main limitations of this thesis was a lack of attention to hydrological and land surface processes that modulate the hydrological cycle and form a key part of the hydrometeorological modelling chain. When undertaking model comparisons, it would be important to consider the impact of soil hydraulics (e.g. infiltration, rate of retention, rate of water flow) and vegetation properties (e.g. leaf area index; LAI, canopy height) on model performance. For instance, many land surface/hydrological models represent LAI, a measure of vegetation thickness, using look up tables based on vegetation type and seasonality. However, when using global LAI datasets derived from remote sensing observations to provide monthly values of LAI, forecasts of near surface variables such as air temperature and relative humidity were improved (Boussetta et al., 2013). An analysis investigating the impact of different soil and vegetation maps would provide a good first indication on the importance of soil type relative to meteorological forcing. This analysis would use the same hydrometeorological model set-up (i.e. same meteorological input, hydrological and routing model) changing only the soil fields.
- **Performance of GloFAS during particular climate phases.** Results of Chapter 4 identified that GloFAS better simulated the differences between the negative and neutral phases of ENSO compared to the differences between the positive and neutral phases. It would be useful to understand why these results emerge. It could

be due one or two El Niño events not being simulated correctly, or it could be that the model fails to represent conditions during the positive phase. It would be useful to carry out further evaluation of GloFAS similar to analyses performed by Alfieri et al. (2013) and Bischiniotis et al. (2019) for the globe and Peru, respectively, but evaluating the performance of GloFAS for different phases of climate variability.

- **Analysis of ENSO variations.** Several times within this thesis the conclusions have called for further analysis into how variations of ENSO events can result in different responses to hydrometeorological variables in the Amazon. Results from Chapter 4 have already shown differences in the magnitude and duration of river flows between the cold phase of central or eastern Pacific events, where the wet signal dissipates when the centre of cooling is shifted east towards South America. Further work should consider the magnitude (i.e. weak vs medium vs strong ENSO events), timing (i.e. when an event begins and decays), and spatial location (e.g. central vs eastern) of events. The timing is an interesting component for the Amazon as work by Espinoza et al. (2013) suggests an earlier La Niña signal could be related to flooding in the Peruvian Amazon. This work could be applied to other locations or even globally.
- **Frequency of heavy rainfall events.** Chapter 4 investigated how large-scale climate variability impacts the flood magnitude, timing, and duration of river flow in the Amazon Basin. The next step should examine how these indices impact the frequency of flooding. Similar works have already been performed in the central United States (e.g. Villairni et al., 2013; Mallakpour and Villiarini, 2016) examining how climate indices have affected the frequency of flooding using both river flow and precipitation data using a peak over threshold approach for event determination. Due to the type of flood regimes of large rivers in the Amazon Basin (i.e. one singular flood peak), it would be more useful to analyse heavy precipitation events in the form of a set of Cox regression models to identify whether or not there is a clustering of events at the sub-seasonal level (e.g. Villarini et al., 2013; Mallakpour and Villarini, 2017). Different event determination approaches could also be used for floods, for instance, from the exceedance of return periods (Coughlan de Perez et al., 2017), or from floodiness (Stephens et al., 2015).
- **Calibration of H-TESSEL.** Hirpa et al. (2018) performed a calibration of the Lisflood routing component of GloFAS altering parameters related to flood timing, variability, and groundwater loss (e.g. channel Manning's coefficient, outflow for reservoirs).

Though skill improved in many basins compared to the non-calibrated model run, some basins observed a decrease in performance. The authors acknowledge that this may be due to basins where the forcing bias is the main source of streamflow uncertainty and thus model performance could be improved by calibrating parameters related to evaporation and infiltration. The potential of such work is already highlighted by Baugh et al. (2020) where performance at capturing the peak flow at stations in the United States increased after the assimilation of SMOS soil moisture. It is thought where soil moisture values are larger from the data assimilation of SMOS it could lead to increased surface runoff and thus increased streamflow. Calibrating parameters relating to the soil moisture balance could therefore have the same impact.

- **Incorporation of Amazon dams in GloFAS.** Damming is becoming increasingly more common in the Amazon Basin, particularly in the south-eastern Amazon Basin (Latrubesse et al., 2017). When comparing the average timing of flood peaks from GloFAS to observed data, the flood peaks tend to occur too early along rivers in this region. While GloFAS does contain major dams and reservoirs within the modelled river network, simplified reservoirs operating parameters are used based on Zajac et al. (2017) resulting in expecting differences between river discharge reanalysis and observations (Harrigan et al., 2020). Currently, most of the dams/reservoirs in the Amazon are not represented in GloFAS (see Fig. 2 in Zajac et al., 2017). However, reservoirs were found to affect model performance substantially in other areas of the world when reservoirs were incorporated into GloFAS. This gives hope that the inclusion of existing dams in the Amazon could help increase the skill of flood forecasts in the basin.

## 6.4 Closing remarks

Overall, the work in this thesis has enhanced the understanding of the relationship between large-scale climate variability and flooding in the Amazon Basin. The results have provided a clearer overall picture of how climate variability affects both rainfall and river discharge over the entire basin and has importantly provided evidence of how different climate indices impact flood timing and duration of which evidence has been previously lacking. More work needs to be done in understanding the influence in the diversity of climate indices, in addition to the combination of simultaneous climate phases (e.g. El Niño and warm phase of the TNA). One of the biggest obstacles is the need to have a long and consistent dataset of streamflow

that accurately reflects flood peaks in the observed datasets. This is due to the limiting number of specific climate events (e.g. the number of strong La Niña episodes) that take place. Thus, the next steps heavily rely on the improvement of reanalysis data to extend the period of analysis and provide stronger conclusions. With the precipitation input found to be the most dominant component of the hydrometeorological modelling chain, it is logical to focus efforts on improving the precipitation products.

# References

Aalto, R., Maurice-Bourgoin, L., Dunne, T., Montgomery, D. R., Nittrouer, C. A., and Guyot, J. L.: Episodic sediment accumulation on Amazonian flood plains influenced by El Nino/Southern Oscillation. Nature, 425, 493– 497, https://doi.org/10.1038/nature02002, 2003.

Abbot, J., and Marohasy, J.: Input selection and optimisation for monthly rainfall forecasting in Queensland, Australia, using artificial neural networks, Atmos. Res., 138, 166-178, https://doi.org/10.1016/j.atmosres.2013.11.002, 2014.

Adreadis, K. M., Schumann, G. J. P., Stampoulis, D., Bates, P. D., Brakenridge, G. R., and Kettner, A. J.: Can atmospheric reanalysis datasets be used to reproduce flooding over large scales?, Geophys. Res. Lett., 44, 10369–10377, https://doi.org/10.1002/2017GL075502, 2017.

Alfieri, L., Burek, P., Dutra, E., Krzeminski, B., Muraro, D., Thielen, J., and Pappenberger, F.: GloFAS–global ensemble streamflow forecasting and flood early warning, Hydrol. Earth Syst. Sci., 17, 1161-1175, https://doi.org/10.5194/hess-17-1161-2013, 2013.

Alfieri, L., Bisselink, B., Dottori, F., Naumann, G., de Roo, A., Salamon, P., Wyser, K. and Feyen, L.: Global projections of river flood risk in a warmer world. Earth's Future, 5, 171– 182, https://doi.org/10.1002/2016EF000485, 2017.

Alfieri, L., Cohen, S., Galantowicz, J., Schumann, G. J., Trigg, M. A., Zsoter, E., Prudhomme, C., Kruczkiewicz, A., Coughlan de Perez, E., Flamig, Z., Rudari, R., Wu, H., Adler, F. A., Brakenridge, R. G., Kettner, A., Weerts, A., Matgen, P., Islam, S. A. K. M., and Salamon, P.: A global network for operational flood risk reduction, Environ. Sci. Policy., 84, 149-158, https://doi.org/10.1016/j.envsci.2018.03.014, 2018.

Alfieri, L., Zsoter, E., Harrigan, S., Hirpa, F. A., Lavaysse, C., Prudhomme, C., and Salamon, P.: Range-dependent thresholds for global flood early warning, J. Hydrol. X., 4, 100034, https://doi.org/10.1016/j.hydroa.2019.100034, 2019.

Alizadeh-Choobari, O.: Contrasting global teleconnection features of the eastern Pacific and central Pacific El Niño events. Dyn. Atmos. Oceans, 80, 139-154, https://doi.org/10.1016/j.dynatmoce.2017.10.004, 2017.

Andreadis, K. M., Schumann, G. J. P., Stampoulis, D., Bates, P. D., Brakenridge, G. R., and Kettner, A. J.: Can Atmospheric Reanalysis Data Sets Be Used to Reproduce Flooding Over

Large Scales?, Geophys. Res. Lett., 44, 10369–10377, https://doi.org/10.1002/2017GL075502, 2017.

Andreoli, R. V., de Souza, R. A. F., Kayano, M. T., and Candido, L. A.: Seasonal anomalous rainfall in the central and eastern Amazon and associated anomalous oceanic and atmospheric patterns, Int. J. Climatol., 32, 1193-1205, https://doi.org/10.1002/joc.2345, 2012.

Aragão, L. E., Anderson, L. O., Fonseca, M. G., Rosan, T. M., Vedovato, L. B., Wagner, F. H., Silva, C. V. J., Silva Junior, C. H. L., Arai, E., Aguiar, A. P., Barlow, J., Berenguer, E., Deeter, M. N., Domingues, L. G., Gloor, M., Malhi, Y., Marengo, J. A., Miller, J. B., Phillips, O. L., and Saatchi, S.: 21st century drought-related fires counteract the decline of Amazon deforestation carbon emissions, Nat. Commun., 9, 1-12, https://doi.org/10.1038/s41467-017-02771-y, 2018.

Arnell, N. W., and Gosling, S. N.: The impacts of climate change on river flood risk at the global scale, Climatic Change, 134, 387–401, https://doi.org/10.1007/s10584-014-1084-5, 2016.

Balsamo, G., Beljaars, A., Scipal, K., Viterbo, P., van den Hurk, B., Hirschi, M., and Betts, A. K.: A revised hydrology for the ECMWF model: Verification from field site to terrestrial water storage and impact in the Integrated Forecast System, J. Hydrometeorol., 10, 623–643, https://doi.org/10.1175/2008JHM1068.1, 2009.

Balsamo, G., Pappenberger, F., Dutra, E., Viterbo, P., and Van den Hurk, B. J. J. M.: A revised land hydrology in the ECMWF model: a step towards daily water flux prediction in a fully-closed water cycle, Hydrol. Process., 25, 1046–1054, https://doi.org/10.1002/hyp.7808, 2010.

Balsamo, G., Albergel, C., Beljaars, A., Boussetta, S., Brun, E., Cloke, H., Dee, H., Dutra, D., Muñoz-Sabater, J., Pappenberger, F., de Rosnay, P., Stockdale. T., and Vitart, F.: ERA-Interim/Land: a global land surface reanalysis data set, Hydrol. Earth Syst. Sci., 19, 389–407, https://doi.org/10.5194/hess-19-389-2015, 2015.

Balsamo, G., Agusti-Panareda, A., Albergel, C., Arduini, G., Beljaars, A., Bidlot, J., Bousserez, N., Boussetta, S., Brown, A., Buizza, R., Buontempo, C., Chevallier, F., Choulga, M., Cloke, H., Cronin, M. F., Dahoui, M., De Rosnay, P., Dirmeyer, P. A., Drusch, M., Dutra, E., Ek, M. B., Gentine, P., Hewitt, H., Keeley, S. P. E., Kerr, Y., Kumar, S., Lupu, C., Mahfouf, J. F., McNorton, J., Mecklenburg, S., Mogensen, K., Muñoz-Sabater, J., Orth, R., Rabier, F., Reichle, R., Ruston, B, Pappenberger, F., Sandu, I., Seneviratne, S. I., Tietsche, S., Trigo, I. F., Uijlenhoet, R., Wedi, N., Woolway, R. L., and Zeng, X.: Satellite and In Situ Observations for Advancing Global Earth Surface Modelling: A Review, Remote Sens., 10, 2038, https://doi.org/10.3390/rs10122038, 2018.

Barichivich, J., Gloor, E., Peylin, P., Brienen, R. J., Schöngart, J., Espinoza, J. C., and Pattnayak, K. C.: Recent intensification of Amazon flooding extremes driven by strengthened Walker circulation. Sci. Adv., 4, eaat8785, https://doi.org/10.1126/sciadv.aat8785, 2018.

Barnston, A. G., Van den Dool, H. M., Zebiak, S. E., Barnett, T. P., Ji, M., Rodenhuis, D. R., Cane, M. A., Leetmaa, A., Graham, N. E., Ropelewski, C. R., Kousky, V. E., O'Lenic, E. A., and Livezey, R. E.: Long-lead seasonal forecasts—where do we stand?. Bull. AM. Meteorol. Soc., 75, 2097-2114, https://doi.org/10.1175/1520-0477(1994)075<2097:LLSFDW>2.0.CO;2, 1994.

Bauer, P., Thorpe, A., and Brunet, G.: The quiet revolution of numerical weather prediction. Nature, 525, 47-55, https://doi.org/10.1038/nature14956, 2015.

Baugh, C., de Rosnay, P., Lawrence, H., Jurlina, T., Drusch, M., Zsoter, E., and Prudhomme, C.: The impact of SMOS soil moisture data assimilation within the operational Global Flood Awareness System (GloFAS). Remote Sens., 12, 1490, https://doi.org/10.3390/rs12091490, 2020.

Bazo, J. : Assessing Flood Preparedness in the Peruvian Amazon. Available: https://www.climatecentre.org/news/965/assessing-flood-preparedness-in-the-peruvian-amazon-basin. Last accessed 14/06/2018, 2018.

Beck, H. E., van Dijk, A. I., de Roo, A., Dutra, E., Fink, G., Orth, R., and Schellekens, J.: Global evaluation of runoff from ten state-of-the-art hydrological models, Hydrol. Earth Syst. Sci., 21, 2881–2903, https://doi.org/10.5194/hess-21-2881-2017, 2017a.

Beck, H. E., Vergopolan, N., Pan, M., Levizzani, V., van Dijk, A. I., Weedon, G. P., Brocca, L., Pappenberger, F., Huffman, G. J., and Wood, E. F.: Global-scale evaluation of 22 precipitation datasets using gauge observations and hydrological modeling, Hydrol. Earth Syst. Sci., 21, 6201–6217, https://doi.org/10.5194/hess-21-6201-2017, 2017b.

Berghuijs, W. R., Harrigan, S., Molnar, P., Slater, L. J., and Kirchner, J. W.: The relative importance of different flood-generating mechanisms across Europe. Water Resour. Res., 55, 4582-4593, https://doi.org/10.1029/2019WR024841, 2019.

Bergström, S.: The HBV model, in: Comput. Model. Watershed Hydrol., chap. The HBV mo, edited by: Singh, V., Water Resouces Publications, Highlands Ranch Co., Colorado, USA, 1995.

Beven, K. J.: Rainfall-Runoff Modelling: The Primer, 2nd Edn., Wiley-Blackwell, Chichester, UK, 2012.

Bierkens, M. F.: Global hydrology 2015: State, trends, and directions, Water Resour. Res., 51, 4923–4947, https://doi.org/10.1002/2015WR017173, 2015.

Bierkens, M. F., Bell, V. A., Burek, P., Chaney, N., Condon, L. E., David, C. H., de Roo, A., Döll, P., Drost, N., Famigiletti, J. S., Flörke, M., Gochis, D. J., Houser, P., Hut, R., Keune, J., Kollet, S., Maxwell, R. M., Reager, J. T., Samaniego, L., Sudicky, E., Sutanudiaia, E. H., van de Giesen, N., Winsemius, H., and Wood, E. F.: Hyper-resolution global hydrological modelling: what is next? "Everywhere and locally relevant", Hydrol. Process., 29, 310–320, https://doi.org/10.1002/hyp.10391, 2015.

Bjerknes, J.: Atmospheric teleconnections from the Equatorial Pacific. Mon, Weather Rev., 97, 163– 172, https://doi.org/10.1175/1520-0493(1969)097<0163:ATFTP>2.3.CO;2, 1969.

Bischiniotis, K., van den Hurk, B., Zsoter, E., Coughlan de Perez, E., Grillakis, M., and Aerts, J. C.: Evaluation of a global ensemble flood prediction system in Peru. Hydrol. Sci. J., 64, 1171-1189, https://doi.org/10.1080/02626667.2019.1617868, 2019.

Bondeau, A., Smith, P. C., Zaehle, S., Schaphoff, S., Lucht, W., Cramer, W., Gerten, D., Lotze-Campen, H., Muller, C., Reichstein, M., and Smith, B.: Modelling the role of agriculture for the 20th century global terrestrial carbon balance, Global Change Biol., 13, 679–706, https://doi.org/10.1111/j.1365-2486.2006.01305.x, 2007.

Booth, B. B., Dunstone, N. J., Halloran, P. R., Andrews, T., and Bellouin, N.: Aerosols implicated as a prime driver of twentieth-century North Atlantic climate variability, Nature, 484, 228-232, https://doi.org/10.1038/nature10946, 2012.

Bourrel, L., Phillips, L. and Moreau, S.: The dynamics of floods in the Bolivian Amazon Basin. Hydrol. Processes, 23, 3161– 3167. https://doi.org/10.1002/hyp.7384, 2009.

Boussetta, S., Balsamo, G., Beljaars, A., Kral, T., and Jarlan, L.: Impact of a satellite-derived leaf area index monthly climatology in a global numerical weather prediction model, Int. J. Remote Sens., 34, 3520-3542, https://doi.org/10.1080/01431161.2012.716543, 2013.

Boussetta, S., Balsamo, G., Arduini, G., Dutra, E., McNorton, J., Choulga, M., and Zsoter, E. (2021). ECLand: The ECMWF Land Surface Modelling System, Atmosphere, 12, 723, https://doi.org/10.3390/atmos12060723, 2021.

Builes-Jaramillo, A., Marwan, N., Poveda, G., and Kurths, J.: Nonlinear interactions between the Amazon River basin and the Tropical North Atlantic at interannual timescales, Clim. Dyn., 50, 2951-2969, https://doi.org/10.1007/s00382- 017-3785-8, 2018.

Bunge, L., and Clarke, A. J.: A verified estimation of the El Niño index Niño-3.4 since 1877, J. Clim., 22, 3979-3992, https://doi.org/10.1175/2009JCLI2724.1, 2009.

Burn, D. H.:Catchment similarity for regional flood frequency analysis using seasonality measures, J. Hydrol., 202, 212-230, https://doi.org/10.1016/S0022-1694(97)00068-1, 1997.

Butts, M. B., Payne, J. T., Kristensen, M., and Madsen, H.: An evaluation of the impact of model structure on hydrological modelling uncertainty for streamflow simulation, J. Hydrol., 298, 242-266, https://doi.org/10.1016/j.jhydrol.2004.03.042, 2004.

Cai, W., Santoso, A., Wang, G., Yeh, S. W., An, S. I., Cobb, K. M., Collins, M., Guilyardi, E., Jin, F. F., Kug, J. S., Lengaigne, M., McPhaden, M. J., Takahashi, K., Timmermann, A., Vecchi, G., Watanabe, M., and Wu, L.: ENSO and greenhouse warming, Nat. Clim. Change, 5, 849-859, https://doi.org/10.1038/nclimate2743, 2015.

Cai, W., McPhaden, M. J., Grimm, A. M., Rodrigues, R. R., Taschetto, A. S., Garreaud, R. D., Dewitte, B., Poveda, G., Ham, Y. G., Santoso, A., Ng, B., Anderson, W., Wang, G., Geng, T., Marengo, J. A., Alves, L. M., Osman, S. L., Wu, L., Karamperidou, C., Takahashi, K., and Vera, C.: Climate impacts of the El Niño–Southern Oscillation on South America, Nat. Rev. Earth Environ., 1, 215-231, https://doi.org/10.1038/s43017-020-0040-3, 2020.

Callède, J., Guyot, J. L., Ronchail, J., L'Hôte, Y., Niel, H., and de Oliveira, E.: Evolution du débit de l'Amazone à Óbidos de 1903 à 1999/Evolution of the River Amazon's discharge at Óbidos from 1903 to 1999, Hydrol. Sci. J., 49, 85-97, https://doi.org/10.1623/hysj.49.1.85.53992, 2004.

Callède, J., Cochonneau, G., Alves, F. V., Guyot, J. L., Guimarães, V. S., and De Oliveira, E.: Les apports en eau de l'Amazone à l'Océan Atlantique, Revue des sciences de l'eau/Journal of Water Science, 23, 247-273, https://doi.org/10.7202/044688ar, 2010.

Carvalho, L. M., Jones, C., and Liebmann, B.: The South Atlantic convergence zone: intensity, form, persistence, and relationships with intraseasonal to interannual activity and extreme rainfall, J Clim., 17, 88-108, https://doi.org/10.1175/1520-0442(2004)017<0088:TSACZI>2.0.CO;2, 2004.

CEPAL.: Evaluacion del Impacto Acumulado y Adicional Ocacionado por la Niña 2008 en Bolivia, Ministerio de Planificación del Desarrollo (MPD) de Bolivia. La Paz-Bolivia: Secretaría Ejecutiva de la Comisión Económica para América Latina y el Caribe (CEPAL), 2008.

Chikamoto, Y., Timmermann, A., Luo, J. J., Mochizuki, T., Kimoto, M., Watanabe, M., Ishii, M., Xie, S. P., and Jin, F. F.: Skilful multi-year predictions of tropical trans-basin climate variability, Nat. Commun., 6, 6869, https://doi.org/10.1038/ncomms7869, 2015.

Chiodi, A. M., and Harrison, D. E.: El Niño impacts on seasonal US atmospheric circulation, temperature, and precipitation anomalies: the OLR-event perspective, J. Clim., 26, 822-837, https://doi.org/10.1175/JCLI-D-12-00097.1, 2013.

Chiodi, A. M., and Harrison, D. E.: Global seasonal precipitation anomalies robustly associated with El Niño and La Niña events—an OLR perspective, J. Clim., 28, 6133– 6159, https://doi.org/10.1175/JCLI-D-14-00387.1, 2015.

Clark III, R. A., Flamig, Z. L., Vergara, H., Hong, Y., Gourley, J. J., Mandl, D. J., Frye, S., Handy, M., and Patterson, M.: Hydrological modeling and capacity building in the Republic of Namibia, B. Am. Meteorol. Soc., 98, 1697–1715, https://doi.org/10.1175/BAMS-D-15-00130.1, 2016.

Cloke, H. L., and Pappenberger, F.: Ensemble flood forecasting: A review, J. Hydro., 375, 613-626, https://doi.org/10.1016/j.jhydrol.2009.06.005, 2009.

Cools, J., Innocenti, D., and O'Brien, S.: Lessons from flood early warning systems, Environ. Sci. Policy, 58, 117– 122, https://doi.org/10.1016/j.envsci.2016.01.006, 2016.

Coomes, O. T., Lapointe, M., Templeton, M., and List, G.: Amazon river flow regime and flood recessional agriculture: Flood stage reversals and risk of annual crop loss, J. Hydrol., 539, 214-222., https://doi.org/10.1016/j.jhydrol.2016.05.027, 2016.

Correa, S. W., de Paiva, R. C. D., Espinoza, J. C., and Collischonn, W.: Multi-decadal Hydrological Retrospective: Case study of Amazon floods and droughts, J. Hydrol., 549, 667–684, https://doi.org/10.1016/j.jhydrol.2017.04.019, 2017.

Costa, S. M., and Brondízio, E. S.: Cities along the floodplain of the Brazilian Amazon: characteristics and trends. In The Amazon Várzea (pp. 83-97). Springer, Dordrecht., https://doi.org/10.1007/978-94-007-0146-5_6, 2011.

Coughlan de Perez, E., Monasso, F., Van Aalst, M., and Suarez, P.: Science to prevent disasters. Nat. Geosci., 7, 78-79, https://doi.org/10.1038/ngeo2081, 2014.

Coughlan de Perez, E., van den Hurk, B. J. J. M., Van Aalst, M. K., Jongman, B., Klose, T., and Suarez, P.: Forecast-based financing: an approach for catalyzing humanitarian action based on extreme weather and climate forecasts. Nat. Hazards and Earth Sys. Sci., 15, 895-904, https://doi.org/10.5194/nhess-15-895-2015, 2015.

Coughlan de Perez, E., Stephens, E., Bischiniotis, K., Aalst, M. V., Hurk, B. V. D., Mason, S., Nissan, H., and Pappenberger, F.: Should seasonal rainfall forecasts be used for flood preparedness?. Hydrol. Earth Syst. Sci., 21, 4517-4524, https://doi.org/10.5194/hess-21-4517-2017, 2017.

Coumou, D., and Rahmstorf, S.: A decade of weather extremes, Nat. Clim. Change, 2, 491-496, https://doi.org/10.1038/NCLIMATE1452, 2012.

Cox, P. M., Harris, P. P., Huntingford, C., Betts, R. A., Collins, M., Jones, C. D., Jupp, T. E., Marengo, J. A., and Nobre, C. A.: Increasing risk of Amazonian drought due to decreasing aerosol pollution, Nature, 453, 212-215, https://doi.org/10.1038/nature06960, 2008.

Dartmouth Flood Observatory.: Global Active Archive of Large Flood Events, available at: http://www.dartmouovth.edu/~floods/Archives/index.html. (Accessed 14th June 2018), 2018.

Davidson, E. A., de Araújo, A. C., Artaxo, P., Balch, J. K., Brown, I. F., Bustamante, M. M., Coe, M. T, De Fries, R. S., Keller, M., Longo, M., Munger, J. W., Schroeder, W., Soares-Filho, B. S., Souza, C. M., and Wofsy, S. C.: The Amazon Basin in transition. Nature, 481, 321, https://doi.org/10.1038/nature10717, 2012.

Dee, D. P., Uppala, S. M., Simmons, A. J., Berrisford, P., Poli, P., Kobayashi, S., Andrae, U., Balmaseda, M. A., Balsamo, G., Bauer, P., Bechtold, P., Belijaars, A. C. M., van de Berg, L., Bidlot, J., Bormann, N., Delsol, C., Dragani, R., Fuentes, M., Geer, A. J., Haimberger, L., Healy, S. B., Hersbach, S., Hólm, E .V., Isaksen, L., Kallberg, P., Köhler, M., Matricardi, M., McNally, A. P., Mong-Sanz, B. M., Morcrette, J. J., Park, B. K., Peubey, C., de Rosnay, P., Tavolato, C., Thèpaut, J. N., and Vitart, F.: The ERA-Interim reanalysis: Configuration and performance of the data assimilation system, Q. J. Roy. Meteorol. Soc., 137, 553–597, https://doi.org/10.1002/qj.828, 2011.

De Groeve, T., Thielen-del Pozo, J., Brakenridge, R., Adler, R., Alfieri, L., Kull, D., Lindsay, F., Imperiali, O., Pappenberger, F., Rudari, R., Salamon, P., Villars, N., and Wyjad, K.: Joining forces in a global flood partnership. Bull. AM. Meteorol. Soc., 96, ES97-ES100, https://doi.org/10.1175/BAMS-D-14-00147.1, 2015.

De Linage, C., Famiglietti, J.S., and Randerson, J. T.: Statistical prediction of terrestrial water storage changes in the Amazon Basin using tropical Pacific and North Atlantic Sea surface temperature anomalies, Hydrol. Earth Syst. Sci., 18, 2089-2102, https://doi.org/10.5194/hess-18-2089-2014, 2014.

De Souza, E. B., and Ambrizzi, T.: Modulation of the intraseasonal rainfall over tropical Brazil by the Madden–Julian oscillation, Int. J. Climatol., 26, 1759-1776 10.1002/joc.1331, 2006.

Deser, C., Alexander, M. A., Xie, S. P. and Phillips, A. S.: Sea surface temperature variability: patterns and mechanisms, Annu. Rev. Mar. Science, 2, 115-143, https://doi.org/10.1146/annurev-marine-120408-151453, 2010.

Dettinger, M. D., and Diaz, H. F.: Global characteristics of stream flow seasonality and variability, J. Hydrometeorol., 1, 289-310, https://doi.org/10.1175/1525-7541(2000)0012.0.CO;2, 2000.

Devia, G. K., Ganasri, B. P., and Dwarakish, G. S.: A review on hydrological models, Aquat. Proced., 4, 1001-1007, https://doi.org/10.1016/j.aqpro.2015.02.126, 2015.

Di Baldassarre, G., Viglione, A., Carr, G., Kuil, L., Yan, K., Brandimarte, L., and Blöschl, G.: Debates—perspectives on socio-hydrology: capturing feedbacks between physical and social processes, Water Resour. Res., 51, 4770-4781, https://doi.org/10.1002/2014WR016416, 2015.

Döll, P., Kaspar, F., and Lehner, B.: A global hydrological model for deriving water availability indicators: model tuning and validation, J. Hydrol., 270, 105–134, https://doi.org/10.1016/S0022-1694(02)00283-4, 2003.

ECMWF: A brief description of reforecasts, available at: https://confluence.ecmwf.int/display/S2S/A+brief+description+of+reforecasts (last access: 25 September 2018), 2016.

ECMWF: What are the changes from ERA-Interim to ERA5?, available at: https://confluence.ecmwf.int//pages/viewpage.action?pageId=74764925, (last access: 31 August 2018), 2017.

ECMWF: What is ERA-5?, available at: https://confluence.ecmwf.int/display/CKB/What+is+ERA5, last access: 8 October 2018.

ECMWF: ERA-5 Land, available at: https://www.ecmwf.int/en/era5-land, last access: 2 March 2020, 2020.

Emerton, R., Stephens, E. M., Pappenberger, F., Pagano, T. C., Weerts, A. H., Wood, A. W., Salamon, P., Brown, J. D., Hjerdt, N., Donnelly, C., Baugh, C. A., and Cloke, H. L.: Continental and global scale flood forecasting systems, Wiley Interdisciplinary Reviews: Water, 3, 391–418, https://doi.org/10.1002/wat2.1137, 2016.

Emerton, R., Cloke, H. L., Stephens, E. M., Zsoter, E., Woolnough, S. J., and Pappenberger, F.: Complex picture for likelihood of ENSO-driven flood hazard. Nat. Commun., 8, 1-9, https://doi.org/10.1038/ncomms14796, 2017.

Emerton, R., Zsoter, E., Arnal, L., Cloke, H. L., Muraro, D., Prudhomme, C., Stephens, E. M., Salamon, P., and Pappenberger, F.: Developing a global operational seasonal hydro-meteorological forecasting system: GloFAS v2.2 Seasonal v1.0, Geosci. Model Dev., 11, 3327–3346, https://doi.org/10.5194/gmd-11-3327-2018, 2018.

Emerton, R. E., Stephens, E. M., and Cloke, H. L.: What is the most useful approach for forecasting hydrological extremes during El Niño?. Environ. Res. Commun., 1, 031002, https://doi.org/10.1088/2515-7620/ab114e, 2019.

Enfield, D. B.: Relationships of inter-American rainfall to tropical Atlantic and Pacific SST variability, Geophys. Res. Lett., 23, 3305-3308, https://doi.org/10.1029/96GL03231, 1996.

Enfield, D. B., and Mayer, D. A.: Tropical Atlantic Sea surface temperature variability and its relation to El Niño-southern oscillation, J. Geophys. Res. C: Oceans, 102, 929-945, https://doi.org/10.1029/96JC03296, 1997.

Enfield, D. B., Mestas-Nuñez, A. M., Mayer, D. A., and Cid-Serrano, L.: How ubiquitous is the dipole relationship in tropical Atlantic sea surface temperatures? J. Geophys. Res. Oceans., 104, 7841-7848, https://doi.org/10.1029/1998JC900109, 1999.

Enfield, D. B., Mestas-Nuñez, A. M., and Trimble, P. J.: The Atlantic multidecadal oscillation and its relation to rainfall and river flows in the continental US, Geophy. Res. Lett., 28, 2077-2080, https://doi.org/10.1029/2000GL012745, 2001.

English, S., McNally, T., Bormann, N., Salonen, K., Matricardi, M., Moranyi, A., and Di Tomaso, E. (2013). Impact of satellite data. Technical Memorandum 711. Berkshire, England: ECMWF, https://doi.org/10.21957/b6596ot1s, 2013.

Espinoza, J. C., Guyot, J. L., Ronchail, J., Cochonneau, G., Filizola, N., Fraizy, P, Labat, D., de Oliveira, E., Ordoñez, J. J., and Vauchel, P.: Contrasting regional discharge evolutions in the

Amazon basin (1974–2004), J. Hydrol., 375, 297-311, https://doi.org/10.1016/j.jhydrol.2009.03.004, 2009a.

Espinoza, J. C. E., Ronchail, J., Guyot, J. L., Cochonneau, G., Naziano, F., Lavado, W., Oliveira, D. E., Pombosa, R., and Vauchel, P.: Spatio-temporal rainfall variability in the Amazon basin countries (Brazil, Peru, Bolivia, Colombia, and Ecuador), Int. J. Climatol., 29, 1574-1594, https://doi.org/10.1002/joc.1791, 2009b.

Espinoza, J. C., Ronchail, J., Guyot, J. L., Junquas, C., Vauchel, P., Lavado, W., Drapeau, G., and Pombosa, R.: Climate variability and extreme drought in the upper Solimões River (western Amazon Basin): Understanding the exceptional 2010 drought. Geophys. Res. Lett., 38, https://doi.org/10.1029/2011GL047862, 2011.

Espinoza, J. C. E., Ronchail, J., Guyot, J. L., Junquas, C., Drapeau, G., Martinez, J. M., Santini, W., Vauchel, P., Lavado, W., Ordoñez, J., and Espinoza, R.: From drought to flooding: understanding the abrupt 2010–11 hydrological annual cycle in the Amazonas River and tributaries, Environ. Res. Lett., 7, 024008, https://doi.org/10.1088/1748-9326/7/2/024008, 2012.

Espinoza, J. C., Ronchail, J., Frappart, F., Lavado, W., Santini, W., and Guyot, J. L.: The major floods in the Amazonas River and tributaries (western Amazon basin) during the 1970–2012 period: A focus on the 2012 flood, J. Hydrometeorol., 14, 1000-1008, https://doi.org/10.1175/JHM-D-12-0100.1, 2013.

Espinoza, J. C., Marengo, J. A., Ronchail, J., Carpio, J. M., Flores, L. N., and Guyot, J. L.: The extreme 2014 flood in south-western Amazon basin: the role of tropical-subtropical South Atlantic SST gradient. Environ. Res. Lett., 9, 124007, https://doi.org/10.1088/1748-9326/9/12/124007, 2014.

Espinoza, J. C., Segura, H., Ronchail, J., Drapeau, G., and Gutierrez-Cori, O.: Evolution of wet-day and dry-day frequency in the western Amazon basin: relationship with atmospheric circulation and impacts on vegetation, Water Resour. Res., 52, 8546-8560. https://doi.org/10.1002/2016WR019305, 2016.

Espinoza, J. C., Ronchail, J., Marengo, J. A., and Segura, H.: Contrasting North–South changes in Amazon wet-day and dryday frequency and related atmospheric features (1981–2017), Clim. Dyn., 52, 5413-5430, https://doi.org/10.1007/s00382-018-4462-2, 2019.

Falloon, P., Betts, R., Wiltshire, A., Dankers, R., Mathison, C., McNeall, D., Bates, P., and Trigg, M.: Validation of river flows in HadGEM1 and HadCM3 with the TRIP river flow model, J. Hydrometeorol., 12, 1157-1180, https://doi.org/10.1175/2011JHM1388.1, 2011.

Ficchì, A., and Stephens, L.: Climate variability alters flood timing across Africa. Geophysical Research Letters, 46, 8809-8819, https://doi.org/10.1029/2019GL081988, 2019.

Figueroa, S. N., and Nobre, C. A.: Precipitation distribution over central and western tropical South America. Climanalise, 5, 36-45, 1990.

Filizola, N., and Guyot, J. L.: Suspended sediment yields in the Amazon basin: an assessment using the Brazilian national data set, Hydrol. Process., 23, 3207-3215, https://doi.org/10.1002/hyp.7394, 2009.

Filizola, N., Latrubesse, E. M., Fraizy, P., Souza, R., Guimarães, V., and Guyot, J. L.: Was the 2009 flood the most hazardous or the largest ever recorded in the Amazon?. Geomorphology, 215, 99-105, https://doi.org/10.1016/j.geomorph.2013.05.028, 2014.

Foley, J. A., Botta, A., Coe, M. T., and Costa, M. H.: El Niño–Southern oscillation and the climate, ecosystems and rivers of Amazonia, Global Biogeochem. Cycles, 16, 79-1, https://doi.org/10.1029/2002GB001872, 2002.

Forbes, R., Haiden, T., and Magnusson, L.: Improvements in IFS forecasts of heavy precipitation, Meteorology section of ECMWF newsletter No. 144, ECMWF, Reading, UK, 21–26, https://doi.org/10.21957/jxtonky0, 2015.

Forecast-based-Financing.: Forecast based Financing, available at: https://www.forecast-based-financing.org/wp-content/uploads/2019/01/Brochure-Tecnico-Iquitos-english.pdf (last accessed: 20 February 2020), 2019.

Frauen, C., Dommenget, D., Tyrrell, N., Rezny, M., and Wales, S.: Analysis of the nonlinearity of El Niño–southern oscillation teleconnections, J. Clim., 27, 6225-6244, https://doi.org/10.1175/JCLI-D-13-00757.1, 2014.

Fu, R., Zhu, B., and Dickinson, R. E.: How do atmosphere and land surface influence seasonal changes of convection in the tropical Amazon? J. Clim., 12, 1306-1321, https://doi.org/10.1175/1520- 0442(1999)0122.0.CO;2, 1999.

Fu, R., Dickinson, R. E., Chen, M., and Wang, H.: How do tropical sea surface temperatures influence the seasonal distribution of precipitation in the equatorial Amazon? J. Clim., 14, 4003-4026, https://doi.org/10.1175/1520- 0442(2001)0142.0.CO;2, 2001.

García-García, D., and Ummenhofer, C.C.: Multidecadal variability of the continental precipitation annual amplitude driven by AMO and ENSO, Geophys. Res. Lett., 42, 526-535, https://doi.org/10.1002/2014GL062451, 2015.

García-Serrano, J., Cassou, C., Douville, H., Giannini, A., and Doblas-Reyes, F. J.: Revisiting the ENSO teleconnection to the tropical North Atlantic, J. Clim., 30, 6945-6957, https://doi.org/10.1175/JCLI-D-16-0641.1, 2017.

Gautier, E., Brunstein, D., Vauchel, P., Roulet, M., Fuertes, O., Guyot, J. L., Darrozzes, J., and Bourrel, L.: Temporal relations between meander deformation, water discharge and sediment fluxes in the floodplain of the Rio Beni (Bolivian Amazonia), Earth Surf. Processes Landforms, 32, 230-248, https://doi.org/10.1002/esp.1394, 2006.

Geng, T., Yang, Y., and Wu, L.: On the mechanisms of Pacific decadal oscillation modulation in a warming climate, J. Clim., 32, 1443-1459, https://doi.org/10.1175/JCLI-D-18-0337.1, 2019.

Gill, A. E.: Some simple solutions for heat-induced tropical circulation, Q. J. R. Meteorolg. Soc., 106, 447–462, https://doi.org/10.1002/qj.49710644905, 1980.

Gilleland, M. E.: Package `verification', available at: http://cran.utstat.utoronto.ca/web/packages/verification/verification.pdf (last access: 25 September 2018), 2015.

Gloor, M. R. J. W., Brienen, R. J., Galbraith, D., Feldpausch, T. R., Schöngart, J., Guyot, J. L., Espinoza, J. C., Llyod, J., and Phillips, O. L.: Intensification of the Amazon hydrological cycle over the last two decades, Geophys. Res. Lett., 40, 1729–1733, https://doi.org/10.1002/grl.50377, 2013.

Gosling, S. N. and Arnell, N. W.: Simulating current global river runoff with a global hydrological model: model revisions, validation, and sensitivity analysis, Hydrol. Process., 25, 1129–1145, https://doi.org/10.1002/hyp.7727, 2011.

Gourley, J. J., Flamig, Z. L., Vergara, H., Kirstetter, P. E., Clark III, R. A., Argyle, E., Arthur, A., Martinaitis, S., Terti, G., Erlingis, J. M., Hong, Y., and Howard, K. W.: The FLASH Project: Improving the tools for flash flood monitoring and prediction across the United States, B. Am. Meteorol. Soc., 98, 361–372, https://doi.org/10.1175/BAMS-D-15-00247.1, 2017.

Greuell, J. W., Andersson, J., Donnelly, C., Feyen, L., Gerten, D., Ludwig, F., Pisacane, G., Roudier, P., and Schaphoff, S.: Evaluation of five hydrological models across Europe and their suitability for making projections under climate change Hydrol. Earth Syst. Sci. Discuss., 12, 10289–10330, https://doi.org/10.5194/hessd-12-10289-2015, 2015.

Grimm, A. M., and Tedeschi, R. G.: ENSO and extreme rainfall events in South America, J. Clim., 22, 1589-1609, https://doi.org/10.1175/2008JCLI2429.1, 2009.

Gudmundsson, L., Wagener, T., Tallaksen, L. M., and Engeland, K.: Evaluation of nine large-scale hydrological models with respect to the seasonal runoff climatology in Europe, Water Resour. Res., 48, W11504, https://doi.org/10.1029/2011WR010911, 2012.

Gupta, H. V., Kling, H., Yilmaz, K. K., and Martinez, G. F.: Decomposition of the mean squared error and NSE performance criteria: Implications for improving hydrological modelling, J. Hydrol., 377, 80–91, https://doi.org/10.1016/j.jhydrol.2009.08.003, 2009.

Guse, B., Pfannerstill, M., Gafurov, A., Kiesel, J., Lehr, C., and Fohrer, N.: Identifying the connective strength between model parameters and performance criteria, Hydrol. Earth Syst. Sci., 21, 5663–5679, https://doi.org/10.5194/hess-21-5663-2017, 2017.

Haddeland, I., Clark, D. B., Franssen, W., Ludwig, F., VOß, F., Arnell, N. W., Bertrand, N., Best, M., Folwell, S., Gerten, D., Gomes, S., Gosling, S. N., Hagemann, S., Hanasaki, N., Harding, R., Heinke, J., Kabat, P., Koirala, S., Oki, T., Polcher, J., Stacke, T., Viterbo, P., Weedon, G. P., and Yeh, P.: Multimodel estimate of the global terrestrial water balance: Setup and first results, J. Hydrometeorol., 12, 869–884, https://doi.org/10.1175/2011JHM1324.1, 2011.

Ham, Y. G., Kug, J. S., Park, J. Y., and Jin, F.F.: Sea surface temperature in the north tropical Atlantic as a trigger for El Niño/southern oscillation events, Nat. Geosci., 6, 112-116, https://doi.org/10.1038/ngeo1686, 2013.

Harding, K. J., and Snyder, P. K.: The relationship between the Pacific–North American teleconnection pattern, the Great Plains low-level jet, and North Central US heavy rainfall events. J. Clim., 28, 6729-6742, https://doi.org/10.1175/JCLI-D-14-00657.1, 2015.

Harrigan, S., Zsoter, E., Alfieri, L., Prudhomme, C., Salamon, P., Wetterhall, F., Barnard, C., Cloke, H., and Pappenberger, F.: GloFAS-ERA5 operational global river discharge reanalysis 1979–present. Earth Syst. Sci Data, 12, 2043-2060, https://doi.org/10.5194/essd-12-2043-2020, 2020.

Hattermann, F. F., Krysanova, V., Gosling, S. N., Dankers, R., Daggupati, P., Donnelly, C., Flörke, M., Huang, S., Motovilov, Y., Buda, S., Yang, T., Müller, C., Leng, G., Tang, Q., Portmann, F. T., Hagemann, S., Gerten, D., Wada, Y., Masaki, Y., Alemayehu, T., Satoh, Y., and Samaniego, L.: Cross-scale intercomparison of climate change impacts simulated by regional and global hydrological models in eleven large river basins, J. Clim. Change, 141, 561–576, https://doi.org/10.1007/s10584-016-1829-4, 2017.

Hersbach, H., de Rosnay, P., Bell, B., Schepers, D., Simmons, A., Soci, C., Abdalla, S., Alonso-Balmaseda, M., Balsamo, G., Bechtold, P., Berrisford, P., Bidlot, J.-R., de Boisséson, E., Bonavita, M., Browne, P., Buizza, R., Dahlgren, P., Dee, D., Dragani, R., Diamantakis, M., Flemming, J., Forbes, R., Geer, A. J., Haiden, T., Hólm, E., Haimberger, L., Hogan, R., Horányi, A., Janiskova, M., Laloyaux, P., Lopez, P., Muñoz-Sabater, J., Peubey, C., Radu, R., Richardson, D., Thépaut, J.-N., Vitart, F., Yang, X., Zsótér, E., and Zuo, H.: Operational global reanalysis: progress, future directions and synergies with NWP, ERA Report Series 27, ECMWF, Reading, UK, 2018.

Hersbach, H., Bell, B., Berrisford, P., Hirahara, S., Horányi, A., Muñoz-Sabater, J., Nicolas, J., Peubey, C., Radu, R., Schepers, D., Simmons, A., Soci, C., Abdalla, S., Abellan, X., Balsamo, G., Bechtold, P., Biavati, G., Bidlot, J., Bonavita, 10 M., De Chiara, G., Dahlgren, P., Dee, D., Diamantakis, M., Dragani, R., Flemming, J., Forbes, R., Fuentes, M., Geer, A., Haimberger, L., Healy, S., Hogan, R.J., Hólm, E., Janisková, M., Keeley, S., Laloyaux, P., Lopez, P., Lupu, C., Radnoti, G., de Rosnay, P., Rozum, I., Vamborg, F., Villaume, S. and Thépaut, J.-N.: The ERA5 Global Reanalysis, Q. J. R. Meteorol. Soc., 146, 1999-2049, https://doi.org/10.1002/qj.3803, 2020.

Hill, K. J., Taschetto, A. S., and England, M.H.: South American rainfall impacts associated with inter-El Niño variations, Geophys. Res. Lett., 36, L19702, https://doi.org/10.1029/2009GL040164, 2009.

Hill, K. J., Taschetto, A. S., and England, M.H.: Sensitivity of South American summer rainfall to tropical Pacific Ocean SST anomalies, Geophys. Res. Lett., 38, https://doi.org/10.1029/2010GL045571, 2011.

Hirabayashi, Y., Mahendran, R., Koirala, S., Konoshima, L., Yamazaki, D., Watanabe, S., Kim, H., and Kanae, S.: Global flood risk under climate change, Nat. Clim. Change, 3, 816, https://doi.org/10.1038/nclimate1911, 2013.

Hirpa, F. A., Salamon, P., Beck, H. E., Lorini, V., Alfieri, L., Zsoter, E., and Dadson, S. J.: Calibration of the Global Flood Awareness System (GloFAS) using daily streamflow data. J. Hydrol., 566, 595-606, https://doi.org/10.1016/j.jhydrol.2018.09.052, 2018.

Hoch, J. M., Haag, A. V., Dam, A. V., Winsemius, H. C., van Beek, L. P., and Bierkens, M. F.: Assessing the impact of hydrodynamics on large-scale flood wave propagation–a case study for the Amazon Basin, Hydrol. Earth Syst. Sci., 21, 117–132, https://doi.org/10.5194/hess-21-117-2017, 2017a.

Hoch, J. M., Neal, J., Baart, F., van Beek, L. P. H., Winsemius, H., Bates, P., and Bierkens, M. F.: GLOFRIM v1.0 – A globally applicable computational framework for integrated hydrological–hydrodynamic modelling, Geosci. Model Dev., 10, 3913–3929, https://doi.org/10.5194/gmd-10-3913-2017, 2017b.

Horner, I., Renard, B., Le Coz, J., Branger, F., McMillan, H. K., and Pierrefeu, G.: Impact of stage measurement errors on streamflow uncertainty. Water Resour. Res., 54, 1952-1976, https://doi.org/10.1002/2017WR022039, 2018.

Hosseiny, H., Nazari, F., Smith, V., and Nataraj, C.: A framework for modeling flood depth using a hybrid of hydraulics and machine learning, Sci. Rep, 10, 1-14, https://doi.org/10.1038/s41598-020-65232-5, 2020.

Huang, B., Thorne, P. W., Banzon, V. F., Boyer, T., Chepurin, G., Lawrimore, J. H., Menne, M. J., Smith, T. M., Vose, R. S., and Zhang, H. M.: Extended reconstructed sea surface temperature, version 5 (ERSSTv5): upgrades, validations, and intercomparisons, J. Clim., 30, 8179-8205, https://doi.org/10.1175/JCLI-D-16-0836.1, 2017.

Huffman, G. J., Bolvin, D. T., Nelkin, E. J., Wolff, D. B., Adler, R. F., Gu, G., Hong, Y., Bowman, K. P., and Stocker, E. F.: The TRMM multisatellite precipitation analysis (TMPA): Quasi-global, multiyear, combined-sensor precipitation estimates at fine scales, J. Hydrometeorol., 8, 38–55, https://doi.org/10.1175/JHM560.1, 2007.

Huffman, G. J., Adler, R. F., Bolvin, D. T., and Gu, G.: Improving the global precipitation record: GPCP version 2.1, Geophys. Res. Lett., 36, L17808, https://doi.org/10.1029/2009GL040000, 2009.

IASC.: Inter-Agency SOPs for Early Action to El Niño / La Niña Episodes, Inter-Agency Standing Committee, available at: https://interagencystandingcommittee.org/iasc-reference-group-

riskearly-warning-and-preparedness/iasc-inter-agency-standard-operating, (last access: 18 January 2021), 2018.

IFRC: Disaster Relief Fund (DREF) Peru: Floods, available at: https://reliefweb.int/sites/reliefweb.int/files/resources/MDRPE005du1.pdf (last access: 25 September 2018), 2013.

Jimenez, J. C., Marengo, J. A., Alves, L. M., Sulca, J. C., Takahashi, K., Ferrett, S., and Collins, M.: The role of ENSO flavours and TNA on recent droughts over Amazon forests and the Northeast Brazil region, Int. J. Climatol., 1-20, https://doi.org/10.1002/joc.6453. 2019.

Jones, C., and Carvalho, L. M.: The influence of the Atlantic multidecadal oscillation on the eastern Andes low-level jet and precipitation in South America, npj Clim. Atmos. Sci., 1, 40, https://doi.org/10.1038/s41612-018-0050-8, 2018.

Jones, C., Waliser, D. E., Lau, K. M., and Stern, W.: Global occurrences of extreme precipitation and the Madden–Julian oscillation: observations and predictability, J. Clim., 17, 4575– 4589, https://doi.org/10.1175/3238.1, 2004.

Kayano, M. T., and Andreoli, R. V.: Relations of south American summer rainfall interannual variations with the Pacific decadal oscillation, Int. J. Climatol., 27, 531-540, https://doi.org/10.1002/joc.1417, 2007.

Kayano, M. T., and Capistrano, V. B.: How the Atlantic multidecadal oscillation (AMO) modifies the ENSO influence on the South American rainfall, Int. J. Climatol., 34, 162-178, https://doi.org/10.1002/joc.3674, 2013.

Kayano, M. T., Andreoli, R. V., and Souza, R. A. F. D.: El Niño–southern oscillation related teleconnections over South America under distinct Atlantic multidecadal oscillation and Pacific Interdecadal oscillation backgrounds: La Niña, Int. J. Climatol., 39, 1359-1372, https://doi.org/10.1002/joc.5886, 2019.

Kerr, R. A.: A North Atlantic climate pacemaker for the centuries, Science, 288, 1984-1985, https://doi.org/10.1126/science.288.5473.1984, 2000.

Kling, H., Fuchs, M., and Paulin, M.: Runoff conditions in the upper Danube basin under an ensemble of climate change scenarios, J. Hydrol., 424, 264–277, https://doi.org/10.1016/j.jhydrol.2012.01.011, 2012.

Kobayashi, S., Ota, Y., Harada, Y., Ebita, A., Moriya, M., Onoda, H., Onogi, K., Kamahori, H., Kobayashi, C., Endo, H., Miyaoka, K., and Takahashi, K.: The JRA-55 reanalysis: general

specifications and basic characteristics, Journal of the Meteorological Society of Japan. Ser. II, 93, 5-48, https://doi.org/10.2151/jmsj.2015-001, 2015.

Lagos, P., Silva, Y., Nickl, E., and Mosquera, K.: El Niño? Related precipitation variability in Perú, Adv. Geosci., 14, 231– 237, https://doi.org/10.5194/adgeo-14-231-2008, 2008.

Langerwisch, F., Rost, S., Gerten, D., Poulter, B., Rammig, A., and Cramer, W.: Potential effects of climate change on inundation patterns in the Amazon Basin, Hydrol. Earth Syst. Sci., 17, 2247-2262, https://doi.org/10.5194/hess-17-2247-2013, 2013.

Langill, J. C., and Abizaid, C.: What is a bad flood? Local perspectives of extreme floods in the Peruvian Amazon. Ambio, 1-14, https://doi.org/10.1007/s13280-019-01278-8, 2019.

Laraque, A., Ronchail, J., Cochonneau, G., Pombosa, R., and Guyot, J.L.: Heterogeneous distribution of rainfall and discharge regimes in the Ecuadorian Amazon basin, J. Hydrometeorol., 8, 1364– 1381, https://doi.org/10.1175/2007JHM784.1, 2007.

Laraque, A., Bernal, C., Bourrel, L., Darrozes, J., Christophoul, F., Armijos, E., Fraizy, P., Pombosa, R., and Guyot, J.L.:Sediment budget of the Napo river, Amazon basin, Ecuador and Peru, Hydrol. Processes: An International Journal, 23, 3509-3524, https://doi.org/10.1002/hyp.7463, 2009.

Latrubesse, E. M., Arima, E. Y., Dunne, T., Park, E., Baker, V. R., d'Horta, F. M., Wight, C., Wittmann, F., Zuanon, J., Baker, P. A., Ribas, C. C., Norgaard, R. B., Filizola, N., Ansar, A., Flyvbjerg, B., and Stevaux, J. C.: Damming the rivers of the Amazon basin, Nature, 546, 363–369, https://doi.org/10.1038/nature22333, 2017.

Lavado, W. S., Ronchail, J., Labat, D., Espinoza, J. C., and Guyot, J. L.: Basin-scale analysis of rainfall and runoff in Peru (1969–2004): Pacific, Titicaca and Amazonas drainages, Hydrol. Sci. J., 57, 625-642, https://doi.org/10.1080/02626667.2012.672985, 2012.

Lavado, W. S., Labat, D., Ronchail, J., Espinoza, J. C., and Guyot, J. L.: Trends in rainfall and temperature in the Peruvian Amazon–Andes basin over the last 40 years (1965–2007), Hydrol. Processes, 27, 2944-2957, https://doi.org/10.1002/hyp.9418, 2013.

Lavers, D. A., Ramos, M. H., Magnusson, L., Pechlivanidis, I., Klein, B., Prudhomme, C., Arnal, L., Crochemore, L., Van den Hurk, B., Weerts, A. H., Harrigan, S., Cloke, H. L., Richardson, D. S., and Pappenberger, F.: A vision for hydrological prediction. Atmosphere, 11, 237, https://doi.org/10.3390/atmos11030237, 2020.

Le Cointe, P.: Les crues annuelles de l'Amazone et les récentes modifications de leur regime, Annales de Géogr., 44, 614-619, 1935.

Lee, D., Ward, P., and Block, P.: Attribution of large-scale climate patterns to seasonal peak-flow and prospects for prediction globally, Water Resour. Res., 54, 916-938, https://doi.org/10.1002/2017WR021205, 2018.

Legates, D. R. and McCabe, G. J.: Evaluating the use of "goodness-of-fit" measures in hydrologic and hydroclimatic model validation, Water Resour. Res., 35, 233–241, https://doi.org/10.1029/1998WR900018, 1999.

Lehner, B., Verdin, K., and Jarvis, A.: New global hydrography derived from spaceborne elevation data, Eos Trans. Am. Geophys. Union, 89, 93–94, https://doi.org/10.1029/2008EO100001, 2008.

Liebmann, B., and Marengo, J.: Interannual variability of the rainy season and rainfall in the Brazilian Amazon Basin, J. Clim., 14, 4308-4318, https://doi.org/10.1175/15200442(2001)0142.0.CO;2, 2001.

Liebmann, B., Kiladis, G. N., Vera, C. S., Saulo, A. C., and Carvalho, L. M.: Subseasonal variations of rainfall in South America in the vicinity of the low-level jet east of the Andes and comparison to those in the South Atlantic convergence zone, J. Clim., 17, 3829-3842, https://doi.org/10.1175/1520-0442(2004)017<3829:SVORIS>2.0.CO;2, 2004.

Lopez, M. G., Di Baldassarre, G., and Seibert, J.: Impact of social preparedness on flood early warning systems, Water Resour. Res., 53, 522-534, https://doi.org/10.1002/2016WR019387, 2017.

Madden, R. A., and Julian, P. R.: Detection of a 40–50 day oscillation in the zonal wind in the tropical Pacific, J. Atmos. Sci., 28, 702-708, https://doi.org/10.1175/1520-0469(1971)028<0702:DOADOI>2.0.CO;2, 1971.

Madden, R. A., and Julian, P. R.: Description of global-scale circulation cells in the tropics with a 40–50 day period, J. Atmos. Sci., 29, 1109-1123, https://doi.org/10.1175/1520-0469(1972)029<1109:DOGSCC>2.0.CO;2, 1972.

Madden, R. A., and Julian, P. R.: Observations of the 40–50-day tropical oscillation—a review, Mon, Weather Rev., 122, 814-837, https://doi.org/10.1175/1520-0493(1994)122<0814:OOTDTO>2.0.CO;2, 1994.

Magilligan, F. J., and Nislow, K. H.: Changes in hydrologic regime by dams, Geomorphology, 71, 61–78, https://doi.org/10.1016/j.geomorph.2004.08.017, 2005.

Mallakpour, I., and Villarini, G.: Investigating the relationship between the frequency of flooding over the central United States and large-scale climate. Adv. Water Resour., 92, 159-171, https://doi.org/10.1016/j.advwatres.2016.04.008, 2016.

Mallakpour, I., Villarini, G., Jones, M. P., and Smith, J. A.: On the use of Cox regression to examine the temporal clustering of flooding and heavy precipitation across the central United States. Global Planet. Change, 155, 98-108, https://doi.org/10.1016/j.gloplacha.2017.07.001, 2017.

Makarieva, A. M., and Gorshkov, V. G.: Biotic pump of atmospheric moisture as driver of the hydrological cycle on land, Hydrol. Earth Syst. Sci., 11, 1013-1033, https://doi.org/10.5194/hess-11-1013-2007, 2007.

Mansur, A. V., Brondizio, E. S., Roy, S., Soares, P. P. D. M. A., and Newton, A.: Adapting to urban challenges in the Amazon: flood risk and infrastructure deficiencies in Belém, Brazil. Reg. Environ. Change, 18, 1411-1426., https://doi.org/10.1007/s10113-017-1269-3, 2018.

Mantua, N. J., and Hare, S. R.: The Pacific decadal oscillation, J. Oceanogr., 58, 35-44, https://doi.org/10.1023/A:1015820616384, 2002.

Mantua, N. J., Hare, S. R., Zhang, Y., Wallace, J. M., and Francis, R. C.: A Pacific interdecadal climate oscillation with impacts on salmon production, Bull. Am. Meteorol. Soc., 78, 1069-1080, 1997.

Mardia, K. V.: In E. Birnbaum (Ed.), Statistics of directional data. New York, NY: Academic Press, 1972.

Marengo, J. A.: Interannual variability of surface climate in the Amazon basin, Int. J. Climatol., 12, 853-863, https://doi.org/10.1002/joc.3370120808, 1992.

Marengo, J. A., and Nobre, C.A.: General characteristics and variability of climate in the Amazon Basin and its links to the global climate system. In: M.E. McClain, R.L. Victoria and J.E. Richey (Eds.) The Biogeochemistry of the Amazon Basin. Oxford: Oxford Univ. Press, 2001.

Marengo, J. A., and Espinoza, J. C.: Extreme seasonal droughts and floods in Amazonia: causes, trends and impacts, Int. J. Climatol., 36, 1033–1050, https://doi.org/10.1002/joc.4420, 2016.

Marengo, J. A., Druyan, L. M., and Hastenrath, S.: Observational and modelling studies of Amazonia interannual climate variability, Clim. Change, 23, 267-286, https://doi.org/10.1007/BF01091619, 1993.

Marengo, J. A., Tomasella, J., and Uvo, C.R.: Trends in streamflow and rainfall in tropical South America: Amazonia, eastern Brazil, and northwestern Peru, J. Geophys. Res. D: Atmos., 103, 1775-1783, https://doi.org/10.1029/97JD02551, 1998.

Marengo, J. A., Liebmann, B., Kousky, V. E., Filizola, N. P., and Wainer, I. C.: Onset and end of the rainy season in the Brazilian Amazon Basin, J. Clim., 14, 833-852, www.jstor.org/stable/26247338, 2001.

Marengo, J. A., Nobre, C. A., Tomasella, J., Cardoso, M. F., and Oyama, M. D.: Hydro-climatic and ecological behaviour of the drought of Amazonia in 2005, Philos. Trans. R Soc. London, Ser. B, 363, 1773-1778, https://doi.org/10.1098/rstb.2007.0015, 2008.

Marengo, J. A., Tomasella, J., Alves, L. M., Soares, W. R., and Rodriguez, D. A.: The drought of 2010 in the context of historical droughts in the Amazon region, Geophys. Res. Lett, 38, 1-5, https://doi.org/10.1029/2011GL047436, 2011.

Marengo, J. A., Tomasella, J., Soares, W. R., Alves, L. M., and Nobre, C. A.: Extreme climatic events in the Amazon basin, Theor. Appl. Climatol., 107, 73–85, https://doi.org/10.1007/s00704- 011-0465-1, 2012.

Marengo, J. A., Alves, L. M., Soares, W. R., Rodriguez, D. A., Camargo, H., Riveros, M. P., and Pabló, A. D.: Two contrasting severe seasonal extremes in tropical South America in 2012: flood in Amazonia and drought in northeast Brazil, J. Climate, 26, 9137–9154, https://doi.org/10.1175/JCLI-D-12-00642.1, 2013a.

Marengo, J. A., Borma, L. S., Rodríguez, D.A., Pinho, P., Soares, W. R., and Alves, L. M.: Recent extremes of drought and flooding in Amazonia: vulnerabilities and human adaptation, American Journal of Climate Change, 2, 87-96, https://doi.org/10.4236/ajcc.2013.22009, 2013b.

Marengo, J. A., Williams, E. R., Alves, L. M., Soares, W. R., and Rodriguez, D. A.: Extreme seasonal climate variations in the Amazon basin: droughts and floods. In: Interactions between Biosphere, Atmosphere and Human Land Use in the Amazon Basin, Vol. 36. Berlin, Heidelberg: Springer, pp. 55– 76. https://doi.org/10.1002/joc.4420, 2016.

Marengo, J. A., Souza, C. M., Jr., Thonicke, K., Burton, C., Halladay, K., Betts, R., Alves, L. M., and Soares, W. R.: Changes in climate and land use over the amazon region: current and future variability and trends, Front. Earth Sci., 6, https://doi.org/10.3389/feart.2018.00228, 2018.

Martín-Rey, M., Polo, I., Rodríguez-Fonseca, B., Losada, T., and Lazar, A.: Is there evidence of changes in tropical Atlantic variability modes under AMO phases in the observational record? J. Clim., 31, 515- 536. https://doi.org/10.1175/JCLI-D-16-0459.1, 2018.

Matthews, A. J., Hoskins, B. J., and Masutani, M.: The global response to tropical heating in the Madden–Julian oscillation during the northern winter, Q. J. R. Meteorolog. Soc., 130, 1991-2011, https://doi.org/10.1256/qj.02.123, 2004.

McGregor, S., Timmermann, A., Stuecker, M. F., England, M. H., Merrifield, M., Jin, F. F., and Chikamoto, Y.: Recent Walker circulation strengthening and Pacific cooling amplified by Atlantic warming, Nat. Clim. Change, 4, 888-892, https://doi.org/10.1038/nclimate2330, 2014.

Meade, R. H., Rayol, J. M., Da Conceicão, S. C., and Natividade, J. R.: Backwater effects in the Amazon River basin of Brazil, Environ. Geol. Water Sci., 18, 105–114, https://doi.org/10.1007/BF01704664, 1991.

Meigh, J. R., McKenzie, A. A., and Sene, K. J.: A grid-based approach to water scarcity estimates for eastern and southern Africa, Water Resour. Mange., 13, 85-115, https://doi.org/10.1023/A:1008025703712, 1999.

Meng, J., Li, L., Hao, Z., Wang, J., and Shao, Q.: Suitability of TRMM satellite rainfall in driving a distributed hydrological model in the source region of Yellow River, J. Hydrol., 509, 320-332, https://doi.org/10.1016/j.jhydrol.2013.11.049, 2013.

Merz, B., Nguyen, V. D., and Vorogushyn, S.: Temporal clustering of floods in Germany: Do flood-rich and flood-poor periods exist?. J. Hydrol., 541, 824-838, https://doi.org/10.1016/j.jhydrol.2016.07.041, 2016.

Mittermaier, M., Roberts, N., and Thompson, S. A.: A long-term assessment of precipitation forecast skill using the Fractions Skill Score, Meterol. Appl., 20, 176-186, https://doi.org/10.1002/met.296, 2013.

Mizukami, N., Rakovec, O., Newman, A. J., Clark, M. P., Wood, A. W., Gupta, H. V., and Kumar, R.: On the choice of calibration metrics for “high-flow” estimation using hydrologic models, Hydrol. Earth Syst. Sci., 23, 2601–2614, https://doi.org/10.5194/hess-23-2601-2019, 2019.

Molinier M, Guyot J. L., Oliveira E, Guimaraes V.: Les régimes ' hydrologiques de l'Amazone et de ses affluents. L'hydrologie Tropicale: G'eoscience et outil pour le D'eveloppement 238: 209–222, Paris, Mai 1995. IAHS Publ, 1996.

Montini, T. L., Jones, C., and Carvalho, L. M.: The south American low-level jet: A new climatology, variability, and changes, J Geophys. Res: Atmos., 124, 1200-1218, https://doi.org/10.1029/2018JD029634, 2019.

Moura, A. D., and Shukla, J.: On the dynamics of droughts in Northeast Brazil: observations, theory and numerical experiments with a general circulation model, J Atmos. Sci., 38, 2653-2675, https://doi.org/10.1175/1520-0469(1981)038<2653:OTDODI>2.0.CO;2, 1981.

Mundial Grupo Banco: Lidando com Perdas: opções de Proteção Financeira contra Desastres no Brasil (Dealing with losses: options of financial protection against disasters in Brazil), available at: http://bibliotecadigital.planejamento.gov.br/xmlui/bitstream/handle/iditem/658/Banco Mundial_opcoes_de prote\%C3\%A7\%C3\%A3o financeira contra desastres no Brasil.pdf?sequence=1 (last access: 25 September 2018), 2014.

Nash, J. E., and Sutcliffe, J. V.: River flow forecasting through conceptual models part I – A discussion of principles, J. Hydrol., 10, 282–290, https://doi.org/10.1016/0022-1694(70)90255-6, 1970.

Nearing, G. S., Kratzert, F., Sampson, A. K., Pelissier, C. S., Klotz, D., Frame, J. M., and Gupta, H. V.: What role does hydrological science play in the age of machine learning?, Water Resour. Res., 57, e2020WR028091, https://doi.org/10.1029/2020WR028091, 2021.

Nevo, S., Anisimov, V., Elidan, G., El-Yaniv, R., Giencke, P., Gigi, Y., Hassidim, A., Moshe, Z., Schlesinger, M., Shalev, G., Tirumali, A., Wiesel, A., Zlydenko, O., and Matias, Y.: ML for flood forecasting at scale. *arXiv preprint arXiv:1901.09583*, 2019.

Newman, M., Alexander, M. A., Ault, T. R., Cobb, K. M., Deser, C., Di Lorenzo, E., Mantua, N. J., Miller, A. J., Minobe, S., Nakamura, H., Schneider, N., Vimont, D. J., Phillips, J. S., Scott, J. D., and Smith, C. A.: The Pacific decadal oscillation, revisited, J. Clim., 29, 4399-4442, https://doi.org/10.1175/JCLI-D-15-0508.1, 2016.

Nobre, C. A., Sampaio, G., Borma, L. S., Castilla-Rubio, J. C., Silva, J. S., and Cardoso, M.: Land-use and climate change risks in the Amazon and the need of a novel sustainable development paradigm, PNAS, 113, 10759– 10768, https://doi.org/10.1073/pnas.1605516113, 2016.

Nobre, G. G., Jongman, B., Aerts, J. C. J. H., and Ward, P. J.: The role of climate variability in extreme floods in Europe. Environ. Res. Lett., 12, 084012, https://doi.org/10.1088/1748-9326/aa7c22, 2017.

Nobre, G. G., Muis, S., Veldkamp, T. I., and Ward, P. J.: Achieving the reduction of disaster risk by better predicting impacts of El Niño and La Niña, Prog. Disaster Sci., 2, 100022, https://doi.org/10.1016/j.pdisas.2019.100022, 2019.

Nobre, P., and Shukla, J.: Variations of sea surface temperature, wind stress, and rainfall over the tropical Atlantic and South America, J. Clim., 9, 2464– 2479, https://doi.org/10.1175/1520-0442(1996)009<2464:VOSSTW>2.0.CO;2, 1996.

Novak, D. R., Bailey, C., Brill, K. F., Burke, P., Hogsett, W. A., Rausch, R., and Schichtel, M.: Precipitation and temperature forecast performance at the Weather Prediction Center. Weather and Forecasting, 29, 489-504, https://doi.org/10.1175/WAF-D-13-00066.1, 2013.

O'Connor, J. E., and Costa, J. E.: The world's largest floods, past and present—their causes and magnitude, U.S. Geological Survey Circular 1254.

O'Reilly, C. H., Huber, M., Woollings, T., and Zanna, L.: The signature of low-frequency oceanic forcing in the Atlantic multidecadal oscillation, Geophys. Res. Lett, 43, 2810-2818, https://doi.org/10.1002/2016GL067925, 2016.

Ovando, A., Tomasella, J., Rodriguez, D. A., Martinez, J. M., Siqueira-Junior, J. L., Pinto, G. L. N., Passy, P., Vauchel, P., Noriega, L., and von Randow, C.: Extreme flood events in the Bolivian Amazon wetlands, J. Hydrol.: Reg. Stud., 5, 293–308, https://doi.org/10.1016/j.ejrh.2015.11.004, 2016.

Paccini, L., Espinoza, J. C., Ronchail, J., and Segura, H.: Intra-seasonal rainfall variability in the Amazon basin related to large-scale circulation patterns: a focus on western Amazon–Andes transition region, Int. J. Climatol., 38, 2386-2399, https://doi.org/10.1002/joc.5341, 2018.

Paiva, R. C. D., Collischonn, W., Bonnet, M. P., and De Gonçalves, L. G. G.: On the sources of hydrological prediction uncertainty in the Amazon, Hydrol. Earth Syst. Sci., 16, 3127–3137, https://doi.org/10.5194/hess-16-3127-2012, 2012.

Paiva, R. C. D., Buarque, D. C., Collischonn, W., Bonnet, M. P., Frappart, F., Calmant, S., and Mendes, C. A. B.: Large-scale hydrologic and hydrodynamic modeling of the Amazon River basin, Water Resour. Res., 49, 1226–1243, https://doi.org/10.1002/wrcr.20067, 2013.

Palmer, T. N.: Extended-range atmospheric prediction and the Lorenz model, Bull. AM. Meteorol. Soc., 74, 49-66, 1993.

Palmer, T. N.: Predictability of the atmosphere and oceans: from days to decades. In: Decadal climate variability. Berlin, Heidelberg: Springer, pp. 83– 155, 1996.

Panisset, J. S., Libonati, R., Gouveia, C. M. P., Machado-Silva, F., França, D. A., França, J. R. A., and Peres, L. F.: Contrasting patterns of the extreme drought episodes of 2005, 2010 and 2015 in the Amazon Basin, Int. J. Climatol., 38, 1096-1104, https://doi.org/10.1002/joc.5224, 2018.

Pappenberger, F., and Beven, K. J.: Ignorance is bliss: Or seven reasons not to use uncertainty analysis. Water Resour. Res, 42, https://doi.org/10.1029/2005WR004820, 2006.

Pappenberger, F., Dutra, E., Wetterhall, F., and Cloke, H. L.: Deriving global flood hazard maps of fluvial floods through a physical model cascade, Hydrol. Earth Syst. Sci., 16, 4143–4156, https://doi.org/10.5194/hess-16-4143-2012, 2012.

Pham, B. T., Luu, C., Van Phong, T., Trinh, P. T., Shirzadi, A., Renoud, S., and Clague, J. J.: Can deep learning algorithms outperform benchmark machine learning algorithms in flood susceptibility modeling?, J. Hydrol., 592, 125615, https://doi.org/10.1016/j.jhydrol.2020.125615, 2021.

Phan, T. T. H., and Nguyen, X. H.: Combining statistical machine learning models with ARIMA for water level forecasting: The case of the Red river, Adv. Water Resour., 142, 103656, https://doi.org/10.1016/j.advwatres.2020.103656, 2020.

Pohl, B., and Matthews, A. J.: Observed changes in the lifetime and amplitude of the Madden–Julian oscillation associated with interannual ENSO sea surface temperature anomalies, J. Clim., 20, 2659-2674, https://doi.org/10.1175/JCLI4230.1, 2007.

Poveda G., and Mesa O. J.: Metodologias de prediccion de la hidrologia colombiana considerando el evento de El Nino Oscilaciton del Sur (ENOS), Atmosfera. Sociedad Colombiana de Meteorolog'ıa, 17, 1993.

Poveda, G., Alvarez, D. M., and Rueda, O. A.: Hydro-climatic variability over the Andes of Colombia associated with ENSO: a review of climatic processes and their impact on one of the Earth's most important biodiversity hotspots, Clim. Dyn., 36, 2233-2249, https://doi.org/10.1007/s00382-010-0931-y, 2011.

Revilla-Romero, B., Beck, H. E., Burek, P., Salamon, P., de Roo, A., and Thielen, J.: Filling the gaps: Calibrating a rainfall-runoff model using satellite-derived surface water extent, Remote Sens. Environ., 171, 118–131, https://doi.org/10.1016/j.rse.2015.10.022, 2015.

Richey, J. E., Nobre, C., and Deser, C.: Amazon River discharge and climate variability: 1903 to 1985. Science, 246, 101- 103, https://doi.org/10.1126/science.246.4926.101, 1989.

Robock, A.: Volcanic eruptions and climate, Rev. Geophys., 38, 191– 219. https://doi.org/10.1029/1998RG000054, 2000.

Rodier, J. A., and Roche, M.: World catalogue of maximum observed floods. IAHS Publication, 143, 1984.

Rodrigues, R. R., and McPhaden, M. J.: Why did the 2011–2012 La Niña cause a severe drought in the Brazilian northeast? Geophys. Res. Lett., 41, 1012-1018. https://doi.org/10.1002/2013GL058703, 2014.

Ronchail, J., and Gallaire, R.: ENSO and rainfall along the Zongo valley (Bolivia) from the Altiplano to the Amazon basin. International Journal of Climatology: A Journal of the Royal Meteorological Society, 26, 1223-1236, https://doi.org/10.1002/joc.1296, 2006.

Ronchail, J., Cochonneau, G., Molinier, M., Guyot, J. L., De Miranda Chaves, A. G., Guimarães, V., and De Oliveira, E.: Interannual rainfall variability in the Amazon basin and sea-surface temperatures in the equatorial Pacific and the tropical Atlantic Oceans. Int. J. Climatol., 22, 1663-1686, https://doi.org/10.1002/joc.815, 2002.

Ronchail, J., Bourrel, L., Cochonneau, G., Vauchel, P., Phillips, L., Castro, A., Guyot, J. L., and De Oliveira, E.: Inundations in the Mamore basin (south-western Amazon—Bolivia) and sea-surface temperature in the Pacific and Atlantic Oceans, J. Hydrol., 302, 223-238, https://doi.org/10.1016/j.jhydrol.2004.07.005, 2005a.

Ronchail, J., Labat, D., Callede, J., Cochonneau, G., Guyot, J. L., Filizola, N., and De Oliveira, E.: Discharge variability within the Amazon basin. Climate variability and Change Hydrological Impacts. IAHS Publ, 296, 21-29, 2005b.

Rossel, F.: Influence du Niño sur les régimes pluviométriques de l'equateur. PhD Thesis, Montpellier University, 289 pp, 1997.

Salati, E., Dall'Olio, A., Matsui, E., and Gat, J. R.: Recycling of water in the Amazon basin: an isotopic study, Water Resour. Res., 15, 1250-1258, https://doi.org/10.1029/WR015i005p01250, 1979.

Salati, E., and Vose, P. B.: Amazon basin: a system in equilibrium, Science, 225, 129-138, https://doi.org/10.1126/science.225.4658.129, 1984.

Sampson, C. C., Smith, A. M., Bates, P. D., Neal, J. C., Alfieri, L., and Freer, J. E.: A high-resolution global flood hazard model, Water Resour. Res., 51, 7358–7381, https://doi.org/10.1002/2015WR016954, 2015.

Satyamurty, P., Da Costa, C. P. W., Manzi, A. O., and Candido, L. A.: A quick look at the 2012 record flood in the Amazon Basin. Geophys. Res. Lett., 40, 1396-1401, https://doi.org/10.1002/grl.50245, 2013.

Schenk, C. J., Roland, J., Viger, R. J., and Anderson, C. P.: Maps showing geology, oil and gas fields, and geologic provinces of the South America Region, USGS open-file report 97-470D, US Department of the Interior, Denver, USA, https://doi.org/10.3133/ofr97470D, 1999.

Schöngart, J. and Junk, W. J.: Forecasting the flood-pulse in Central Amazonia by ENSO-indices, J. Hydrol., 335, 124–132, https://doi.org/10.1016/j.jhydrol.2006.11.005, 2007.

Sena, J. A., De Deus, L. A. B., Freitas, M. A. V., and Costa, L.: Extreme events of droughts and floods in Amazonia: 2005 and 2009, Water Resour. Manage., 26, 1665-1676, https://doi.org/10.1007/s11269-012-9978-3, 2012.

Shimizu, M. H., Ambrizzi, T., and Liebmann, B.: Extreme precipitation events and their relationship with ENSO and MJO phases over northern South America, Int. J. Climatol., 37, 2977-2989, https://doi.org/10.1002/joc.4893, 2017.

Sidrane, C., Fitzpatrick, D. J., Annex, A., O'Donoghue, D., Gal, Y., and Biliński, P.: Machine learning for generalizable prediction of flood susceptibility, 2019.

Sigmond, M., Scinocca, J. F., Kharin, V. V., and Shepherd, T. G.: Enhanced seasonal forecast skill following stratospheric sudden warmings, Nat. Geosci., 6, 98-102, https://doi.org/10.1038/NGEO1698, 2013.

Slater, L. J., and Villarini, G.: Evaluating the drivers of seasonal streamflow in the US Midwest. Water, 9, 695, https://doi.org/10.3390/w9090695, 2017.

Smith, P., Pappenberger, F., Wetterhall, F., Thielen, J., Krzeminski, B., Salamon, P., Muraro, D., Kalas, M., and Baugh, C.: On the operational implementation of the European Flood

Awareness System (EFAS), ECMWF Tech. Memorandum 778, ECMWF, Reading, UK., 1–34, 2016.

SO-HYBAM.: Crues 2015 en Amazonie: Les hydrologues du Service d'Observation HYBAM* en état d'alerte, available at: https://hybam.obs-mip.fr/note-on-the-flood-of-the-amazon-in-peru-in-2015-2/#more-4690 (last accessed: 3rd March 2020), 2015.

Sood, A. and Smakhtin, V.: Global hydrological models: a review, Hydrolog. Sci. J., 60, 549–565, https://doi.org/10.1080/02626667.2014.950580, 2015.

Sorribas, M. V., Paiva, R. C., Melack, J. M., Bravo, J. M., Jones, C., Carvalho, L., Beighley, E., Forsberg, B., and Costa, M. H.: Projections of climate change effects on discharge and inundation in the Amazon basin, Clim. Change, 136, 555-570, https://doi.org/10.1007/s10584-016-1640-2, 2016.

Stephens, E., Day, J. J., Pappenberger, F., and Cloke, H.: Precipitation and floodiness. Geophys. Res. Lett., 42, 10-316, https://doi.org/10.1002/2015GL066779, 2015.

Sulca, J., Takahashi, K., Espinoza, J. C., Vuille, M., and Lavado-Casimiro, W.: Impacts of different ENSO flavors and tropical Pacific convection variability (ITCZ, SPCZ) on austral summer rainfall in South America, with a focus on Peru, Int. J Clim., 38, 420-435. https://doi.org/10.1002/joc.5185, 2018.

Sutanudjaja, E. H., Beek, R. V., Wanders, N., Wada, Y., Bosmans, J. H., Drost, N., van der Ent, R. J., de Graaf, I. E. M., Hoch, J. M., de Jong, K., Karssenberg, D., López López, P., Peßenteiner, S., Schmitz, O., Straatsma, M. W., Vannametee, E., Wisser, D., and Bierkens, M. F. P. N.: PCR-GLOBWB 2: a 5 arcmin global hydrological and water resources model, Geosci. Model Dev., 11, 2429–2453, https://doi.org/10.5194/gmd-11-2429-2018, 2018.

Sutcliffe, J. V.: The use of historical records in flood frequency analysis, J Hydrol., 96, 159-171, https://doi.org/10.1016/0022-1694(87)90150-8.

Tedeschi, R. G., Grimm, A. M., and Cavalcanti, I. F.: Influence of central and east ENSO on precipitation and its extreme events in South America during austral autumn and winter, Int. J. Climatol., 36, 4797-4814, https://doi.org/10.1002/joc.4670.

Thiemig, V., Rojas, R., Zambrano-Bigiarini, M., and De Roo, A.: Hydrological evaluation of satellite-based rainfall estimates over the Volta and Baro-Akobo Basin, J. Hydrol., 499, 324–338, https://doi.org/10.1016/j.jhydrol.2013.07.012, 2013.

Timmermann, A., Okumura, Y., An, S. I., Clement, A., Dong, B., Guilyardi, E., Hu, A., Jungclaus, J. H., Renold, M., Stocker, T. F., Stouffer, R. J., Sutton, R., Xie, S. P., and Yin, J.: The influence of a weakening of the Atlantic meridional overturning circulation on ENSO, J. Clim, 20, 4899-4919. https://doi.org/10.1175/JCLI4283.1, 2007.

Timpe, K. and Kaplan, D.: The changing hydrology of a dammed Amazon, Sci. Adv., 3, e1700611, https://doi.org/10.1126/sciadv.1700611, 2017.

Tobar, V., and Wyseure, G.: Seasonal rainfall patterns classification, relationship to ENSO and rainfall trends in Ecuador, Int. J. Climatol., 38, 1808-1819. https://doi.org/10.1002/joc.5297, 2018.

Tomasella, J., Borma, L. S., Marengo, J. A., Rodriguez, D. A., Cuartas, L. A., A. Nobre, C., and Prado, M. C.: The droughts of 1996–1997 and 2004–2005 in Amazonia: hydrological response in the river main-stem. Hydrol. Processes, 25, 1228-1242, https://doi.org/10.1002/hyp.7889, 2010.

Torres, R. R., and Marengo, J. A.: Uncertainty assessments of climate change projections over South America, Theor. Appl. Climatol., 112, 253-272, https://doi.org/10.1007/s00704-012-0718-7, 2013.

Towner, J., Cloke, H. L., Zsoter, E., Flamig, Z., Hoch, J. M., Bazo, J., Coughlan de Perez, E., and Stephens, E. M.: Assessing the performance of global hydrological models for capturing peak river flows in the Amazon basin. Hydrol. Earth Syst. Sci., 23, 3057-3080, https://doi.org/10.5194/hess-23-3057-2019, 2019.

Towner, J., Cloke, H. L., Lavado, W., Santini, W., Bazo, J., Coughlan de Perez, E., and Stephens, E. M.: Attribution of Amazon floods to modes of climate variability: A review. Meteorol. Appl., 27, e1949, https://doi.org/10.1002/met.1949, 2020a.

Towner, J., Ficchí, A., Cloke, H. L., Bazo, J., Coughlan de Perez, E., and Stephens, E. M.: Influence of ENSO and tropical Atlantic climate variability on flood characteristics in the Amazon basin. Hydrol. Earth Syst. Sci. Discuss., 1-35., https://doi.org/10.5194/hess-2020-580, 2020b.

Trenberth, K. E.: The definition of el nino, Bull. Am. Meteorol. Soc., 78, 2771-2777. https://doi.org/10.1175/1520-0477(1997)078<2771:TDOENO>2.0.CO;2, 1997.

Trenberth, K. E., and Stepaniak, D. P.: Indices of el Niño evolution, J. Clim., 14, 1697-1701. https://doi.org/10.1175/1520-0442(2001)014<1697:LIOENO>2.0.CO;2, 2001.

Trenberth, K. E., Fasullo, J. T., and Shepherd, T. G.: Attribution of climate extreme events, Nat. Clim. Change, 5, 725-730. https://doi.org/10.1038/NCLIMATE2657, 2015.

Trigg, M. A.: Amazon River and floodplain hydrodynamics. Doctoral thesis, University of Bristol, Bristol, 2010.

Trigg, M. A., Wilson, M. D., Bates, P. D., Horritt, M. S., Alsdorf, D. E., Forsberg, B. R., and Vega, M.C.: Amazon flood wave hydraulics, J. Hydrol., 374, 92-105, https://doi.org/10.1016/j.jhydrol.2009.06.004, 2009.

Trigg, M. A., Birch, C. E., Neal, J. C., Bates, P. D., Smith, A., Sampson, C. C., Yamazaki, D., Hirabayashi, Y., Pappenberger, F., Dutra, E., Ward, P. J., Winsemius, H. C., Salamon, P., Dottorri, F., Rudari, R., Kappes, M. S., Simpson, A. L., Hadzilacos, G., and Fewtrell, T. J.: The credibility challenge for global fluvial flood risk analysis, Environ. Res. Lett., 11, 094014, https://doi.org/10.1088/1748-9326/11/9/094014, 2016.

US Geological Survey.: Global 30 Arc-Second Elevation (GTOPO30), US Geological Survey, Center for Earth Resources Observation and Science (EROS), available at: https://www.usgs.gov/centers/eros/science/usgs-eros-archive-digital-elevation-global-30-arc-second (last access: 6 June 2019), 1996.

Utida, G., Cruz, F. W., Etourneau, J., Bouloubassi, I., Schefuß, E., Vuille, M., Novello, V. F., Prado, L. F., Sifeddine, A., Klein, V., Zular, A., Viana, J. C. C., and Turcq, B.: Tropical South Atlantic influence on northeastern Brazil precipitation and ITCZ displacement during the past 2300 years, Sci. Rep., 9, 1698, https://doi.org/10.1038/s41598-018-38003-6, 2019.

Uvo, C. B., and Graham, N. E.: Seasonal runoff forecast for northern South America: A statistical model, Water Resour. Res., 34, 3515-3524, https://doi.org/10.1029/98WR02854, 1998.

Uvo, C. B., Tolle, U., and Berndtsson, R.: Forecasting discharge in Amazonia using artificial neural networks, Int. J. Climatol., 20, 1495-1507, https://doi.org/10.1002/1097-0088(200010)20:12<1495::AID-JOC549>3.0.CO;2-F, 2000.

van Beek, L. P. H. and Bierkens, M. F. P.: The Global Hydrological Model PCR-GLOBWB: Conceptualization, Parameterization and Verification, available at: http://vanbeek.geo.uu.nl/suppinfo/vanbeekbierkens2009.pdf (last access: 3 September 2018), 2008.

van Beek, L. P. H., Wada, Y., and Bierkens, M. F. P.: Global monthly water stress: 1. Water balance and water availability, Water Resour. Res., 47, W07517, https://doi.org/10.1029/2010WR009791, 2011.

van den Hurk, B. J. J. M., Viterbo, P., Beljaars, A. C. M., and Betts, A. K.: Offline validation of the ERA40 surface scheme, ECMWF TechMemo 295, ECMWF, Reading, UK, 2000.

van den Hurk, B. J. J. M., and Viterbo, P.: The Torne-Kalix PILPS 2 (e) experiment as a test bed for modifications to the ECMWF land surface scheme, Global Planet. Change, 38, 165–173, https://doi.org/10.1016/S0921-8181(03)00027-4, 2003.

van Der Knijff, J. M., Younis, J., and De Roo, A. P. J.: LISFLOOD: a GIS-based distributed model for river basin scale water balance and flood simulation, Int. J. Geogr. Inf. Sci., 24, 189–212, https://doi.org/10.1080/13658810802549154, 2010.

van Huijgevoort, M. H. J., Van Lanen, H. A. J., Teuling, A. J., and Uijlenhoet, R.: Identification of changes in hydrological drought characteristics from a multi-GCM driven ensemble constrained by observed discharge, J. Hydrol., 512, 421–434, https://doi.org/10.1016/j.jhydrol.2014.02.060, 2014.

Vauchel, P., Santini, W., Guyot, J. L., Moquet, J. S., Martinez, J. M., Espinoza, J. C., Baby, P., Fuertes, O., Noreiga, L., Puita, O., Sondag, F., Fraizy, P., Armijos, E., Cochonneau, C., Timouk, F., de Oliveira, E., Filizola, N., Molina, J., and Ronchail, J.: A reassessment of the suspended sediment load in the Madeira River basin from the Andes of Peru and Bolivia to the Amazon River in Brazil, based on 10 years of data from the HYBAM monitoring programme, J. Hydrol., 553, 35-48, https://doi.org/10.1016/j.jhydrol.2017.07.018, 2017.

Villarini, G., Smith, J. A., Vitolo, R., and Stephenson, D. B.: On the temporal clustering of US floods and its relationship to climate teleconnection patterns. Int. J. Climatol., 33, 629-640, https://doi.org/10.1002/joc.3458, 2013.

Vitart, F., and Molteni, F.: Simulation of the Madden–Julian oscillation and its impact over Europe in ECMWF's monthly forecasts. ECMWF Newsletter, No. 126, ECMWF, Reading, 12-17, 2016.

Vuille, M., Bradley, R. S., and Keimig, F.: Climate variability in the Andes of Ecuador and its relation to tropical Pacific and Atlantic sea surface temperature anomalies, J. Clim., 13, 2520-2535, https://doi.org/10.1175/1520-0442(2000)013<2520:CVITAO>2.0.CO;2, 2000.

Wang, J., Hong, Y., Li, L., Gourley, J. J., Khan, S. I., Yilmaz, K. K., Adler, R. F., Policelli, F. S., Habib, S., Irwn, D., Limaye, A. S., Korme, T., and Okello, L.: The coupled routing and excess storage (CREST) distributed hydrological model, Hydrolog. Sci. J., 56, 84–98, https://doi.org/10.1080/02626667.2010.543087, 2011.

Wang, S., Huang, J., He, Y., and Guan, Y.: Combined effects of the Pacific decadal oscillation and El Nino-southern oscillation on global land dry–wet changes, Sci. Rep., 4, srep06651, https://doi.org/10.1038/srep06651, 2014.

Ward, P. J., Beets, W., Bouwer, L. M., Aerts, J. C., and Renssen, H.: Sensitivity of river discharge to ENSO. Geophys. Res. Lett., 37, https://doi.org/10.1029/2010GL043215, 2010.

Ward, P. J., Eisner, S., Flörke, M., Dettinger, M. D., and Kummu, M.: Annual flood sensitivities to El Niño–Southern Oscillation at the global scale. Hydrol. Earth Syst. Sci., 18, 47-66, https://doi.org/10.5194/hess-18-47-2014, 2014.

Ward, P. J., Kummu, M., and Lall, U.: Flood frequencies and durations and their response to El Niño Southern Oscillation: Global analysis. J. Hydrol., 539, 358-378, https://doi.org/10.1016/j.jhydrol.2016.05.045, 2016.

Webber, B. G., Matthews, A. J., and Heywood, K. J.: A dynamical ocean feedback mechanism for the Madden–Julian Oscillation, Q. J. R. Meteorolog. Soc., 136, 740-754. https://doi.org/10.1002/qj.604, 2010.

Werner, M., Schellekens, J., Gijsbers, P., van Dijk, M., van den Akker, O., and Heynert, K.: The Delft-FEWS flow forecasting system, Environ. Model. Softw., 40, 65–77, https://doi.org/10.1016/j.envsoft.2012.07.010, 2013.

Wills, R. C., Armour, K. C., Battisti, D. S., and Hartmann, D. L.: Ocean–atmosphere dynamical coupling fundamental to the Atlantic multidecadal oscillation, J. Clim, 32, 251-272, https://doi.org/10.1175/JCLI-D-18-0269.1, 2019.

Wolter, K. and Timlin, M.: Monitoring ENSO in COADS with a seasonally adjusted principal component index, in: Proc. of the 17th Climate Diagnostics Workshop, Norman, OK, NOAA/N MC/CAC, NSSL, Oklahoma Clim. Survey, CIMMS and the School of Meteor., Univ. of Oklahoma, 52–57, 1993.

Wolter, K., and Timlin, M. S.: Measuring the strength of ENSO events: How does 1997/98 rank?, Weather, 53, 315-324, https://doi.org/10.1002/j.1477-8696.1998.tb06408.x, 1998.

Wolter, K., and Timlin, M. S.: El Niño/Southern Oscillation behaviour since 1871 as diagnosed in an extended multivariate ENSO index (MEI. ext), Int. J. Climatol., 31, 1074-1087, https://doi.org/10.1002/joc.2336, 2011.

Wood, E. F., Roundy, J. K., Troy, T. J., Van Beek, L. P. H., Bierkens, M. F., Blyth, E., Roo, D. A., Döll, P., Ek, M., Famigiletti, J., Gochish, D., van de Giesen, N., Houser, P., Jaffé, P. R., Kollet, S., Lehner, B., Lettenmaier, D. P., Peters-Lidard, C., Sivapalan, M., Sheffield, J., Wade, A., and Whitehead, P.: Hyperresolution global land surface modeling: Meeting a grand challenge for monitoring Earth's terrestrial water, Water Resour. Res., 47, W05301, https://doi.org/10.1029/2010WR010090, 2011.

Wyżga, B., Kundzewicz, Z. W., Ruiz-Villanueva, V., and Zawiejska, J.: Flood generation mechanisms and changes in principal drivers. In Flood Risk in the Upper Vistula Basin (pp. 55-75). Springer, Cham, 2016.

Xue, X., Hong, Y., Limaye, A., Gourley, J., Huffman, G., Khan, S., Dorji, C., and Chen, S.: Statistical and hydrological evaluation of TRMM-based Multi-Satellite Precipitation Analysis over the Wangchu Basin of Bhutan: Are the latest satellite precipitation products 3B42V7 ready for use in ungauged basins?, J. Hydrol., 499, 91–99, https://doi.org/10.1016/j.jhydrol.2013.06.042, 2013.

Yamazaki, D., Kanae, S., Kim, H., and Oki, T.: A physically based description of floodplain inundation dynamics in a global river routing model, Water Resour. Res., 47, W04501, https://doi.org/10.1029/2010WR009726, 2011.

Yamazaki, D., Lee, H., Alsdorf, D. E., Dutra, E., Kim, H., Kanae, S., and Oki, T.: Analysis of the water level dynamics simulated by a global river model: A case study in the Amazon River, Water Resour. Res., 48, W09508, https://doi.org/10.1029/2012WR011869, 2012.

Yamazaki, D., O'Loughlin, F., Trigg, M. A., Miller, Z. F., Pavelsky, T. M., and Bates, P. D.: Development of the global width database for large rivers, Water Resour. Res., 50, 3467–3480, https://doi.org/10.1002/2013WR014664, 2014a.

Yamazaki, D., Sato, T., Kanae, S., Hirabayashi, Y., and Bates, P. D.: Regional flood dynamics in a bifurcating mega delta simulated in a global river model, Geophys. Res. Lett., 41, 3127–3135, https://doi.org/10.1002/2014GL059744, 2014b.

Yang, T., Sun, F., Gentine, P., Liu, W., Wang, H., Yin, J., Du, M., and Liu, C.: Evaluation and machine learning improvement of global hydrological model-based flood simulations, Environ. Res. Let., 14, 114027, https://doi.org/10.1088/1748-9326/ab4d5e, 2019.

Yeh, S. W., Cai, W., Min, S. K., McPhaden, M. J., Dommenget, D., Dewitte, B., Collins, M., Ashok, K., An, S. I., Yim, B. Y., and Kug, J. S.: ENSO atmospheric teleconnections and their response to greenhouse gas forcing, Rev. Geophys, 56, 185-206, https://doi.org/10.1002/2017RG000568, 2018.

Yin, L., Fu, R., Zhang, Y. F., Arias, P. A., Fernando, D. N., Li, W., Fernandes, K., and Bowerman, A. R. What controls the interannual variation of the wet season onsets over the Amazon?. J. Geophys. Res. D: Atmos., 119, 2314-2328, https://doi.org/10.1002/2013JD021349, 2014.

Yoon, J. H., and Zeng, N.: An Atlantic influence on Amazon rainfall, Clim. Dyn., 34, 249-264, https://doi.org/10.1007/s00382-009-0551-6, 2010.

Yoon, J. H.: Multi-model analysis of the Atlantic influence on Southern Amazon rainfall, Atmos. Sci. Lett., 17, 122-127, https://doi.org/10.1002/asl.600, 2016.

Zajac, Z., Revilla-Romero, B., Salamon, P., Burek, P., Hirpa, F. A., and Beck, H.: The impact of lake and reservoir parameterization on global streamflow simulation, J. Hydrol., 548, 552–568, https://doi.org/10.1016/j.jhydrol.2017.03.022, 2017.

Zambrano-Bigiarini, M.: Package hydroGOF. Goodness-of-fit Functions for Comparison of Simulated and Observed Hydrological Time Series, available at: http://www.rforge.net/hydroGOF/ (last access: 25 September 2018), 2017.

Zeng, N., Yoon, J. H., Marengo, J. A., Subramaniam, A., Nobre, C. A., Mariotti, A., and Neelin, J. D.: Causes and impacts of the 2005 Amazon drought, Environ. Res. Lett., 3, 014002, https://doi.org/10.1088/1748-9326/3/1/014002, 2008.

Zhang, C.: Madden–Julian oscillation, Rev. Geophys., 43, RG2003, https://doi.org/10.1029/2004RG000158, 2005.

Zhang, L., and Wang, C.: Multidecadal North Atlantic sea surface temperature and Atlantic meridional overturning circulation variability in CMIP5 historical simulations, J. Geophys. Res.: Oceans, 118, 5772-5791, https://doi.org/10.1002/jgrc.20390, 2013.

Zhang, W., Villarini, G., & Vecchi, G. A.: Impacts of the Pacific meridional mode on June–August precipitation in the Amazon river basin. Q. J. R. Meteorolog. Soc., 143, 1936-1945, https://doi.org/10.1002/qj.3053, 2017.

Zhang, W., Villarini, G., Vecchi, G. A., and Smith, J. A.: Urbanization exacerbated the rainfall and flooding caused by hurricane Harvey in Houston, Nature, 563, 384-388, https://doi.org/10.1038/s41586-018-0676-z, 2018.

Zhang, Y., Wallace, J. M., and Battisti, D. S.: ENSO-like interdecadal variability: 1900–93, J. Clim., 10, 1004-1020, https://doi.org/10.1175/1520-0442(1997)010<1004:ELIV>2.0.CO;2, 1997.

Zhang, Y., Hong, Y., Wang, X., Gourley, J. J., Xue, X., Saharia, M., Ni, G., Wang, G., Huang, Y., Chen, S., and Tang, G.: Hydrometeorological analysis and remote sensing of extremes: Was the July 2012 Beijing flood event detectable and predictable by global satellite observing and global weather modeling systems?, J. Hydrometeorol., 16, 381–395, https://doi.org/10.1175/JHM-D-14-0048.1, 2015.

Zhang, Y., Zheng, H., Chiew, F. H., Arancibia, J. P., and Zhou, X.: Evaluating regional and global hydrological models against streamflow and evapotranspiration measurements, J. Hydrometeorol., 17, 995–1010, https://doi.org/10.1175/JHM-D-15-0107.1, 2016.

Zhao, F., Veldkamp, T. I., Frieler, K., Schewe, J., Ostberg, S., Willner, S., Schauberger, B., Gosling, S. N., Schmied, H. M., Portmann, F. T., Leng, G., Huang, M., Liu, X., Tang, Q., Hanasaki, N., Biemans, H., Gerten, D., Satoh, Y., Pkhrel, Y., Stacke, T., Ciais, P., Chang, J., Ducharne, A., Guimberteau, M., Wada, Y, Kim, H., and Yamazaki, D.: The critical role of the routing scheme in simulating peak river discharge in global hydrological models, Environ. Res. Lett., 12, 075003, https://doi.org/10.1088/1748-9326/aa7250, 2017.

Zsoter, E., Cloke, H., Stephens, E., de Rosnay, P., Muñoz-Sabater, J., Prudhomme, C., and Pappenberger, F.: How well do operational Numerical Weather Prediction configurations represent hydrology?. J. Hydrometeorol., https://doi.org/10.1175/JHM-D-18-0086.1, 2019.

Zulkafli, Z., Buytaert, W., Manz, B., Rosas, C. V., Willems, P., Lavado-Casimiro, W., Guyot, J. L., and Santini, W.: Projected increases in the annual flood pulse of the Western Amazon, Environ. Res. Lett., 11, 014013, https://doi.org/10.1088/1748-9326/11/1/014013, 2016.

# Appendix

This appendix contains the typeset versions of each of the published chapters (i.e. 2, 3, and 4) presented in this thesis. Chapter 5 refers to discussions between anonymous reviewer 2 and the authors which can be found in Appendix 4. For other reviewer comments please see: https://hess.copernicus.org/preprints/hess-2020-580/.

Author contributions statements are provided for A1, A2, and A3 in Chapters 2, 3, and 4 respectively, and are also provided at the end of the typeset versions. All author contributions have been approved by Dr Elisabeth Stephens and Professor Hannah Cloke.

Elisabeth M. Stephens
Hannah L. Cloke

# A1: The attribution of Amazon floods to modes of climate variability: A review

This paper presents the published version of Chapter 2 of this thesis, with the following reference:

Towner, J., Cloke, H. L., Lavado, W., Santini, W., Bazo, J., Coughlan de Perez, E., and Stephens, E. M.: Attribution of Amazon floods to modes of climate variability: A review, Meteorol. Appl., 27, e1949, https://doi.org/10.1002/met.1949, 2020.

# A2: Assessing the performance of global hydrological models for capturing peak river flows in the Amazon basin

This paper presents the published version of Chapter 3 of this thesis, with the following reference:

Towner, J., Cloke, H. L., Zsoter, E., Flamig, Z., Hoch, J. M., Bazo, J., Coughlan de Perez, E., and Stephens, E. M.: Assessing the performance of global hydrological models for capturing peak river flows in the Amazon basin, Hydrol. Earth Syst. Sci., 23, 3057-3080, https://doi.org/10.5194/hess-23-3057-2019, 2019.

# A3: Influence of ENSO and tropical Atlantic climate variability on flood characteristics in the Amazon basin

This paper presents the published version of Chapter 4 of this thesis, with the following reference:

Towner, J., Ficchí, A., Cloke, H. L., Bazo, J., Coughlan de Perez, E., & Stephens, E. M.: Influence of ENSO and tropical Atlantic climate variability on flood characteristics in the Amazon basin, Hydrol and Earth Syst. Sci., 25, 3875-3895, https://doi.org/10.5194/hess-25-3875-2021, 2021.

## A4: Reviewer and author comments

Below are the full set of comments from anonymous reviewer 2 and the authors from Chapter 4. For other reviewer comments please see https://hess.copernicus.org/preprints/hess-2020-580/.